Early Events of SIVsab Mucosal Transmission in African Green Monkeys

by

Kevin David Raehtz

Bachelor of Science, Michigan State University, 2010

Submitted to the Graduate Faculty of

School of Medicine in partial fulfillment

of the requirements for the degree of

Doctor of Philosophy

University of Pittsburgh

2019

UNIVERSITY OF PITTSBURGH

SCHOOL OF MEDICINE

This dissertation was presented

by

Kevin David Raehtz

It was defended on

July 23, 2019

and was evaluated by

Saleem Khan, Professor, Department of Microbiology & Molecular Genetics

Zandrea Ambrose, Associate Professor, Department of Microbiology & Molecular Genetics

Charles Rinaldo Jr., Professor, Department of Pathology

Jacob Estes, Professor, Vaccine and Gene Therapy Institute (VGTI),

Brandon Keele, Principal Investigator & Senior Principal Scientist, AIDS & Cancer Virus Program (ACVP)

Dissertation Director: Cristian Apetrei, Associate Professor, Department of Medicine Infectious Diseases

Early Events of SIVsab Mucosal Transmission in African Green Monkeys

Kevin David Raehtz, PhD

University of Pittsburgh, 2019

Unlike HIV infection in humans, SIV infection is generally nonpathogenic in natural hosts, such as African green monkeys (AGMs), despite high life-long viral replication. Previous research has indicated that key events occurring early during SIV infection of natural hosts may influence the pathogenic outcome of infection. The main objective of this project was to characterize these early events following mucosal transmission in a natural host. To this goal, 29 adult male AGMs were intrarectally infected with SIVsab92018 and serially sacrificed at various stage of acute and early chronic SIV infection. In order to characterize viral spread and replication, an extensive survey of plasma and tissue viral loads was performed. SIV replication and dissemination from the site of inoculation occurred very rapidly, possibly even simultaneously, resulting in a very rapid virus seeding of virtually every tissue compartment. However, immune activation and inflammation in response to infection were limited and largely transient. As control of inflammation is associated with preservation of the integrity of the gut epithelium, which is damaged during acute pathogenic HIV/SIV infections by viral replication in the GALT and bystander effects, a wide variety of markers for immune activation, apoptosis, fibrosis and epithelial integrity were evaluated in the AGM gut. No evidence of disruption of the epithelial barrier in the gut or the translocation of highly inflammatory microbial byproducts from the gut lumen was found. Transcriptomic analysis was performed to evaluate gene expression in the gut of AGMs *versus* rhesus macaques (RMs) intrarectally inoculated with pathogenic SIVmac251. We identified a unique macrophage-mediated wound healing response, which occurred in AGMs and was absent in the RMs which would allow maintenance of the gut mucosa through exquisite repair of virally induced damage during early SIV infection. We concluded that through a combination of repair and low levels of immune activation, AGMs are able to maintain gut

epithelial integrity despite high acute viral replication. As microbial translocation and the resultant chronic inflammation are the major drivers of pathogenesis, prevention of these events by preservation of gut homeostasis are a crucial component to avoiding disease progression in natural hosts.

Table of Contents

List of Tables

List of Figures

Acknowledgements

I would like to thank Drs. Zandrea Ambrose, Jacob Estes, Brandon Keele, Saleem Khan and Charles Rinaldo for all of their assistance and helpful suggestions over the years. I wish to thank my mentor, Dr. Cristian Apetrei, and his long-term collaborator, Dr. Ivona Pandrea, for their support and sticking with me. I would also thank all of my fellow lab members who helped me with this dissertation project. I want to thank my parents, David and Janet Raehtz, and my family for all the years of support during my time as a graduate student. I would also like to thank to Drs. Nancy Miller, John Warren and Allan Schultz of the NIH and Dr. Samuel A. Levine of the University of Pittsburgh, who made this work possible. Finally, I also want to thank the University of Pittsburgh Statistics Consulting Center for their help with verifying the proper statistical methods, and the Center for Biologic Imaging for providing access to the confocal microscope.

This work was funded by grants from the National Institutes of Health/National Center for Research Resources/National Institute of Diabetes and Digestive and Kidney Diseases/National Heart, Lung and Blood Institute/National Institute of Allergy and Infectious Diseases grants R01 RR025781 (CA/IP), R01DK113919 (IP/CA), RO1 HL117715 (IP), R01 AI119346 (CA), R01 HL123096 (IP), the Oregon National Primate Research Center (ONPRC) NIH grant award P51OD011092 (JDE) and in part with Federal funds from the National Cancer Institute, National Institutes of Health, under contract HHSN261200800001E (BFK/JDE). The content of this dissertation does not necessarily reflect the views or policies of the Department of Health and Human Services, nor does mention any trade names, commercial products, or organizations imply endorsement by the U.S. Government. KDR was supported in part by the Pitt AIDS Research Training grant (T32 AI065380) from the National Institute of Allergy and Infectious Diseases. Significant parts of the study were supported by start-up funds from the School of Medicine of the University of Pittsburgh. The funders had no role in the study design, data collection and analysis, or preparation of the dissertation.

Additionally, I would like to thank Michael Katze and Robert Palermo for their input during the early stages of this study. The work done by their groups was supported by the National Institutes of Health, Office of the Director P51OD010425, R24OD011157, and R24OD011172; University of Washington Center for Innate Immunity and Immune Disease; NIAID contract no. HHSN272201300010C; an NIAID Simian Vaccine Evaluation Unit contract with the University of Washington (contract no. N01- AI-60006); NIDDK, NCRR and NHLBI, NIH (R01 DK087625-01. to Q. Li, R24-OD010445 to S. Bosinger and G. Silvestri, RR025781, DK108837, R01HL117715, R01HL123096, R01DK113919, R01AI119346 to I. Pandrea and C. Apetrei); the Preclinical Research & Development Branch, VRP, DAIDS, NIAID, NIH (task order under N01-AI-30018to Q. Li); the DAIDS Reagent Resource Support Program for AIDS Vaccine Development, Quality Biological, Gaithersburg, MD, Division of AIDS (contract no.N01-A30018) and the Swedish Research Council (D0045701) and eSSENCE (to F. Barrenas).

I would also like to acknowledge all those who contributed to this dissertation project, including Fredrik Barrenäs*, Anita Trichel, George H. Richter Cuiling Xu, Dongzhu Ma, Viskam Wijewardana, Claire Deleage, Kathleen Busman-Sahay, Benjamin B. Policicchio, Audrey Valentine, Lynn Law, Egidio Brocca-Cofano, Danielle Piccolo, Jennifer Stock, Richard R. Green, Andrew Nishida, Wuxun Lu, Jianshui Zhang, Matthew J. Thomas, Jean Chang, Elise Smith, Jeffrey M. Weiss, Reem A. Dawoud, Xinxia Peng, Jan Komorowski, Qingsheng Li, Guido Silvestri, Steven E Bosinger, Jacob D. Estes, Brandon F. Keele, Michael Gale, Jr, Cristian Apetrei, and Ivona Pandrea.

1.0 Introduction

A family of primate lentiviruses, collectively referred to as simian immunodeficiency viruses (SIVs), naturally infect a large number of African nonhuman primate (NHP) species. Like other lentiviruses, SIVs possess both RNA and DNA forms of their genome at different stages of their lifecycle. As virions and during production of new viral genomes within the cell, SIVs have RNA genomes. However, upon entering a cell, the RNA is reverse transcribed to DNA, which is then integrated into the host cell DNA (1, 2). Currently, over 40 different SIVs are known to be circulating in wild African NHPs. Unlike like humans infected with HIV or Asian NPHs, which eventually progress to develop acquired immunodeficiency syndrome (AIDS) without treatment, the African NHPs that are natural hosts of SIVs generally do not progress to AIDS, despite chronic, highly active viral replication that is in same range as or even greater than what is typically reported in HIV^+ individuals (2–7). However, there have been some rare cases where AIDS or AIDS-like clinical signs have been reported to occur natural hosts, primarily in captive NHPs that had outlived their normal lifespan of their species in the wild and had been infected and followed for decades (8–11). This clearly indicates that the lack of disease progression in the natural hosts of SIVs is not the result of infection by benign viruses, but rather that these species have adapted to avoid progression to AIDS. Although relatively sparse compared to the body of data on HIV, the research done on the pathogenesis of SIV-infection in natural hosts indicates that the lack of disease progression does not appear to be mediated by a more effective immune response by the host, but rather by a better management of the deleterious consequences of infection (2). These adaptations are undoubtedly the result of long-term coevolution between African hosts and their species-specific SIVs (4, 6, 12–14).

1.1 The evolutionary history of SIVs in Natural Hosts

1.1.1 SIVs naturally infect only wild African NHPs

Before considering the exact features of SIV infection in African NHPs, it is important to understand the long evolutionary relationship that exists between these viruses and their hosts. SIVs have so far been found to infect over 45 species of African NHPs, with 40 genetically distinct SIVs known to be circulating in the wild (2, 6, 15). While most natural hosts are infected by a single species-specific SIV, there are several examples of African NHP species, including mandrills, mustached monkeys, and mantled guerezas, which are infected in the wild by multiple SIVs (3). No SIV has been found yet that naturally infect any wild Asian or New World NHPs in the wild. Therefore, Asian macaques are non-natural hosts of SIV (3, 16, 17). The various SIVmac variants that are used to experimentally infect rhesus macaques (RMs), pigtailed macaques, crabeating macaques and stumptailed macaques in captivity actually represent accidental cross-species transmissions of SIVs from sooty mangabeys (SM), an African NHP species (18). In macaques and other Asian NHPs, SIV infections are pathogenic and lead to the development of AIDS, which is why the RM has become the primary animal model for HIV infection.

From an evolutionary perspective, humans could also be considered to be a non-natural host for HIV, as HIV only appeared in human populations within the last century, when the virus was acquired from chimpanzees/gorillas and sooty mangabeys. The progression to AIDS reflects the poor evolutionary adaptation between HIV and humans. A similar situation exists in chimpanzees, which also acquired SIVcpz from various monkey species through cross-species transmissions and recombination events (19), and then became the source of the SIVgor that infects gorillas (20–24). Like HIV in humans, progression to AIDS has been shown to be a possible outcome of SIVcpz infection in chimpanzees, both in captivity and in the wild, though it is as of yet unclear how prevalent progression to AIDS is amongst wild chimps (25, 26).

1.1.2 African NHPs and SIVs have coexisted for an extremely long period of time

Various studies incorporating biogeology, phylogeny and molecular clock calculations point to very ancient origin of SIV, though the exact estimates vary greatly. Due to the discrepancy with the molecular clock data, it these estimates rely on biogeography that can be used to recalibrate the molecular clocks (12, 27). Through these recalibration, it generally can be surmised that SIVs have been infecting African primates for anywhere between hundreds of thousands to millions of years (12, 28, 29). In fact, it is possible that SIVs have been infecting NHPs since the time of primate speciation, given the complete absence of SIVs in Asian and New World NHPs (7).

While the precise age of SIV infections in their natural hosts may be uncertain, the SIVS and their natural hosts clearly share a long evolutionary history together. One notable example illustrating this relationship can be found in the phylogeny of the various types of SIVagm, which infect different species of African green monkeys (AGMs). AGMs are NHPs belonging to the genus *Chlorocebus*. The genus encompasses four species of AGM: sabaeus, grivet, tantalus, and vervet (2, 3), which were shown to each be infected with a species-specific virus (30). The AGM subspecies are known to have diverged from their common ancestor between 1.5-3 million years ago and then spread out over sub-Saharan Africa, each settling into a different region (31). Although there are several regions where two different species overlap, the SIVagm diversity in the different AGM species follows the host species rather than the geographical location. Furthermore, when different populations of the same species have been separated, the virus diversity follows this geographical segregation (for example, the two different vervet populations on the two sides of the Drakensberg mountains in South Africa, the two mandrill populations at the North or South of the Ogoue River in Gabon), which also indicates long term coevolution between the African NHP hosts and their species-specific SIVs (12, 32).

1.1.3 SIVs are genetically diverse and readily undergo cross-species transmission and recombination

The extensive evolutionary history of SIVs is also reflected in part by their extreme genetic diversity of SIVs and, subsequently, that of the HIVs. Phylogenetic analysis of SIVs has revealed that there have been numerous cross-species transmissions and recombination events in the past, with many SIVs arising after crossing over between two sympatric species (6). There are also multiple examples of cross-species transmission subsequently followed by recombination, including: (i) SIVmnd-2 ; (ii) SIVagm ; (iii) SIVmus, SIVmon, and SIVgsn, three viruses from three different NHP species (mustached monkeys, mona monkeys and greater spot-nosed monkeys) which share genetic and phylogenetic features, suggesting recombination (33–35).

Another notable example is SIVcpz, which shares genetic similarity to both SIVrcm and SIVgsn/mon/mus. Chimpanzees regularly hunt other primates for food and the recombination of these two viruses almost certainly occurred in chimps (19). SIVcpz emergence is most likely a relatively recent event, as is reflected by the reports of 10- to 16- fold increase in mortality and AIDS-like disorders in wild SIVcpz-infected chimpanzees (26, 36, 37). Additionally, expression levels of the SIV coreceptor CCR5 on the surface of chimpanzee $CD4^+$ T cells are intermediate between natural hosts and non-natural hosts. As CCR5 expression levels are generally considered a marker of host adaptation to SIV (38), and are correlated with susceptibility to infection (see 1.3.2) this intermediary CCR5 expression on the $CD4^+$ T cells of chimps suggests a relatively recent cross-species transmission and consequently an incomplete adaptation of the chimpanzee host to the virus (6).

The SIV propensity to readily cross over between species is reflected by the fact that both HIV-1 and HIV-2 originated from multiple cross-species transmissions of SIVs to humans (39). HIV-1 arose from cross-species transmissions from two different primate sources, with HIV Groups M and N being the result of SIVcpz transmission of from chimpanzees to humans in West-Central Africa (23). Conversely, HIV-1

groups O and P emerged in humans as a result of cross-species transmission of SIVgor, which is itself a cross-species transmission of SIVcpz from chimps to gorillas (20, 24, 40, 41). HIV-2, on the other hand, arose in Western Africa from multiple transmission of SIVsmm directly from SMs in Western Africa to humans (22, 39, 42).

1.2 General features of SIV transmission in natural hosts

1.2.1 Most features of SIV infection of natural hosts have been derived from studies on a limited number of species in captivity

Virtually all of the data regarding the characteristics of SIV infection of natural hosts have been derived from studies on a limited number of three animal models (AGMs, SMs and mandrills) in captivity (3, 6). There are several reasons for this. First, most SIVs are only known from their genetic sequences and have never been properly isolated or characterized. SIVagm, SIVsmm, and SIVmnd-1/SIVmnd-2 are among the minority of SIVs that have been studied in detail. Second, the majority of African NHPs are not widely available in primate facilities and importation of NHPs directly from Africa is virtually impossible. Third, many NHPs are endangered and field work on wild animals is exceptionally difficult.

Our lab developed a new model of SIVsab infection in Caribbean AGMs that circumvents most of these problems. The difficulty in importation is averted, as AGMs (sabaeus) from the Caribbean are easy to import. Since the AGMs were brought from Africa to the Caribbean over 300 years ago during the 17th and 18th centuries, they have become well established (43). These animals have been shown to be both free of SIVsab, and genetically indistinguishable from the sabaeus found in Africa, making them ideal for experimental studies (44–46). Finally, neither African nor Caribbean AGMs are endangered, meaning that more invasive methods can be used for the study of SIV pathogenesis in AGMs, including experimental infections, blood draws and tissue sampling and serial necropsies.

1.2.2 SIVs can be highly prevalent in natural hosts in the wild

In many African NHP species and subspecies, SIV infections are very prevalent in the wild. Some examples include: red colobus, AGMs, SMs, red-capped mangabeys, De Brazza monkeys, and mandrills (12, 47–51). The prevalence rates in these species can be uniformly high across the population, as is the case in AGMs, where 80-90% of adult females and 50-60% of adult males in the wild test positive for SIVagm infection (12, 52, 53). However, the picture is less well defined in some other African NHP species. In gorillas and chimpanzees, SIVs tend to be distributed heterogeneously, with high prevalence in certain populations and low prevalence or absence of infection in others (39). There are also several species where the occurrence of SIV infection is quite low, like the greater spot-nosed monkey or the mustached monkey (15). The significance of these features has not yet been established (i.e., it is possible that the low prevalence in some species is the result of high viral pathogenicity).

1.2.3 Horizontal transmission of SIVs in natural hosts is common

Based on the prevalence of SIV-infection of natural hosts in the wild, it can be inferred that horizontal transmission of SIV from one animal to another must be a relatively common event. Horizontal transmission in NHPs has been reported to occur in a variety of ways, including: (i) sexual contact; (ii) biting; (iii) fighting; and (iv) grooming (12, 25, 26, 32, 50, 53–57). Compared to HIV in humans, where urogenital mucosal transmission constitutes the major route of horizontal transmission and oral transmission is remarkably infrequent (apart from transmission during breastfeeding), in NHPs SIV transmission through oral exposure is fairly common (58–61). Consequently, transmission while grooming or cleaning wounds (i.e., oral exposure) most likely represents a significant route of infection in natural hosts. There have also been multiple descriptions of SIV transmission through biting in captive NHPs (56, 62–65). It is important to note that in these cases, whether through grooming or biting, NHPs are being exposed to blood, which typically has a significantly higher viral load than breast milk or sexual secretions.

This may explain in part why horizontal transmission via the oral mucosa is more frequent in NHPs than humans.

1.2.4 Vertical transmission of SIVs in natural hosts is a rare event

Unlike horizontal transmission, vertical transmission, also known as mother-to-infant transmission (MTIT), is exceedingly rare in natural hosts. In humans and macaques, exposure *in utero* or through breastfeeding represent the major routes of MTIT. The rates of MTIT via these routes can be quite high, with 35-40% of infants born to HIV-infected mothers becoming infected, especially if the mothers are acutely infected (66); similarly 40-70% of infant RM become infected with SIV when born to SIVmac-infected dams (67). By comparison, in recent studies of wild vervets in South Africa and Gambia, the rates of MTIT were shown to be only 4-7% (12, 52). Studies of natural hosts housed in various Primate Centers have also found a very low incidence of vertical transmission, supporting the findings of the surveys of animals in the wild (51, 68–71).

1.3 Horizontal SIV transmission in natural hosts

1.3.1 Detailed characterization of mucosal transmission has only been performed in non-natural hosts

Studying the events following mucosal transmission through sexual contact in wild natural hosts is nearly impossible, for the reasons described above. Much of what is currently known about horizontal SIV transmission via the urogenital mucosa originated from studies of intravaginal transmission of SIVmac in RMs (61, 72, 73). More recently, studies also confirmed that the same general events outlined below also occur during penile transmission of SIVmac in RMs (74). While some aspects surrounding mucosal

transmission have been shown to differ between natural and non-natural hosts, characterization of mucosal transmission in RMs should provide a good approximation of the general events (61).

From the RM studies, it appears that the very first phase of transmission occurs when the virus crosses the mucosal epithelium and infects a small 'founder population' of target cells. This can occur at multiple locations throughout the mucosal site of entry, leading to establishment of foci of early virus replication. These foci may appear preferentially where there are higher densities of target cells in the epithelium, though this has only been shown in the RM intravaginal model of transmission (75). The founder $CD4^+$ T-cell populations frequently exhibit markers indicating that they had been previously activated (i.e., still expressing enough CCR5 and transcriptional activators to support SIV infection) but are no longer active or proliferating ($CD69^{neg}CD25^{neg}Ki67^{neg}$), and therefore are referred to as being in a resting state (76).

These resting $CD4^+$ T cells were found to outnumber other resident immune cells types, such as dendritic cells (DCs) and macrophages, at a ratio ranging between 4-5:1 (77). However, mathematical modeling found that the number of these target cells normally present in the mucosa is not sufficient to sustain viral replication alone. In order to expand, the virus needs new target cells to be recruited to the early foci of replication by the innate inflammatory immune response stimulated by the virus. Following the recruitment of the target cells and viral expansion, the virus disseminates to the draining lymph nodes, where there is a high enough concentration of $CD4^+$ T cells to facilitate its rapid expansion. Traveling through the lymphatics, the virus is able to enter the bloodstream through the thoracic duct and spread systemically (61). One implication of this model is that there may be a window of opportunity for intervention prior to recruitment of additional target cells to the site of entry and viral dissemination, when the virus is limited to a relatively small number of target cells.

1.3.2 Target cell availability is reduced at the mucosal sties in natural hosts, but still correlates with the rates of transmission

While most of the detailed knowledge on mucosal transmission comes from the RM intravaginal studies, there has also been significant research done on mucosal sites in natural hosts, particularly at the gastrointestinal tract mucosa. A study of a large cohort of AGMs of varying ages demonstrated that the numbers of $CCR5^+$ $CD4^+$ cells are very low not only in the blood, but also in the gut and jejunum. A strong mathematical correlation was found between increases in levels of gut $CCR5^+$ $CD4^+$ T cells and the rate of SIV mucosal transmission in these animals (52). Another experimental study established that a 10-fold higher dosage of SIVsab was needed to successfully intrarectally and intravaginally inoculate adult AGMs as compared to adult PTMs. This reduced susceptibly was correlated with the number of $CCR5^+$ $CD4^+$ T cells in the rectum, which was shown to be 10-fold lower in the AGMs than PTMs (78).

Considering the extremely high prevalence of SIV infection in the wild, it is apparent that reduction in overall target cell availability at the mucosal sites does not coincide with protection of natural hosts from either transmission or $CD4^+$ T cell depletion in the gut associated lymphatic tissue (GALT, see 1.4.5), though it may render them more resistant to infection (78). Therefore, it can be assumed that there may be an alternative effect of this reduction on the course of infection. One possible explanation is that, as CCR5 is a chemokine receptor, its reduced expression on the surface of $CD4^+$ T cells might decrease homing of effector memory cells to the gut in natural hosts, which in turn could reduce immune activation and inflammation (6).

1.3.3 Reduced target cell availability may protect natural hosts from oral transmission

As natural hosts have reduced availability of $CCR5^+$ $CD4^+$ T cells (i.e., target cells) at the mucosal sites, target cell restriction at the oral mucosa has been proposed as a mechanism of protection from MTIT (70). This is similar to the case of infant RMs, which initially have low populations of $CCR5^+$ $CD4^+$ T cells at

their mucosal sites, yet these levels increase dramatically to nearly the levels seen in adult RMs within the first 6 months postpartum (70). This supports the observation that the virus challenge needed to infect newborn RM infants was 10-fold higher than the dose needed to infect older infants (79). However, a similar an increase in $CCR5^+$ $CD4^+$ T cells could not be observed in AGM infants or juveniles less than 3 years old (52, 70).

A recent study experimentally demonstrated the importance of $CCR5^+$ T cell availability to oral SIV transmission in AGMs. Infant AGMs were orally exposed to high concentrations of SIVagm, while juvenile and adult AGMs were intrarectally inoculated with the same dosage of virus. Following inoculation, none of the infant AGMs became infected, while half of the juveniles and all of the adults were infected. The juveniles that did not become infected were found to have lower levels of $CCR5^+$ $CD4^+$ T cells in blood and mucosal sites than those that did become infected (78).

No study has yet been able to measure the presence of $CCR5^+$ $CD4^+$ T cells at the oral mucosa in wild natural hosts, given the difficulty of invasive sampling in the field. However, in the recent study of wild AGMs in Gambia, the highest frequency of circulating $CD4^+$ T cells expressing CCR5 among the 29 infants tested was observed in the blood of the single infant AGM that was also infected with SIVagm (52).

In the rare instances of MTIT in SMs, the SM infants infected through MTIT exhibited viral loads 2 logs lower than those seen in adults, suggesting that only a low number of $CCR5^+$ $CD4^+$ T cells support viral replication (71). This is in contrast to what has been previously observed in human infants, where viral loads are very high, sometimes exceeding those seen in adults (71). Such an age-related difference in the levels of viral replication was not observed in AGMs (52). These results strongly suggest that target cell restriction at the oral mucosa does act to protect natural hosts from MTIT during breastfeeding and possibly until the age of sexual maturity, when the overall counts of mucosal $CCR5^+$ $CD4^+$ cells increase (70).

1.3.4 A genetic bottleneck is imposed by the mucosal epithelium on the number of transmitted SIV variants

It has been demonstrated that the mucosal barrier acts as a significant obstacle to both SIV and HIV transmission, being difficult for the viruses to cross, particularly in the vagina, where much of the mucosa is covered by durable stratified layers of squamous cell. However, a recent RM-based study demonstrated that transmission is possible at any location along the female reproductive tract (75). On the other hand, the lower intestinal tract mucosa is formed by a simple columnar epithelium shaped into straight tubular crypts, being much thinner than vaginal mucosa and making the target cells more accessible to the virus. Due to these architectural features, the virus can cross the intestinal mucosa more easily than the vaginal mucosa.

There is also a stochastic barrier to infection at the mucosa, as the overall number of target cells initially available to infect is quite low in RMs and even lower in natural hosts. One consequence of these steep impediments to transmission is a 'mucosal bottleneck', where only a small number of transmitted viruses are actually able to go on to establish infection (38, 61, 70).

This genetic bottleneck imposed on transmitted viruses has been documented during mucosal transmission of HIV and SIVmac (80, 81). The same bottleneck was also reported in AGMs, both in the wild and in captivity (52, 78). In a study of AGMs in captivity, following both intravaginal and intrarectal inoculations with SIVsab, only 1-2 viruses were found to have established infection in each animal (78). This agrees with the finding of a more recent study, which found that only a single transmitted viral variant established infection in multiple AGMs in the wild (52). The similarity of the mucosal bottleneck observed in both natural and non-natural hosts implies that there is little difference in the way the mucosal epithelium restricts viral transmission.

1.4 Post-transmission features that may impact SIV pathogenesis in natural hosts

1.4.1 Natural hosts sustain high levels of viral replication without disease progression

There are a number of features that distinguish natural, nonpathogenic hosts from non-natural, pathogenic hosts, like macaques and humans, as shown in Table 1.

Table 1: Pathogenesis of Lentiviral Infections in Natural *versus* Pathogenic Hosts

Feature	Natural hosts	Asian NHPs	Humans
Progression to AIDS	No	Yes	Yes
Acute plasma viremia	+++	+++	+++
Chronic plasma viremia	Stable	Progressive	Progressive
Virus cytopathy	Yes	Yes	Yes
Genetic bottleneck of virus	Yes	Yes	Yes (not IV)
Acute damage to gut epithelium	Yes	Yes	Yes
Microbial Translocation	No	Yes	Yes
Chronic inflammation	No	Yes	Yes
Establishment of acute anti-inflammatory milieu	Yes	No	No
Hypercoagulability	No	Yes	Yes
Comorbidities	Rare	Yes	Yes
Horizontal Transmission	Frequent	Frequent	Frequent
Vertical Transmission	Rare	Frequent	Frequent
Breast milk viral loads	+++	++	++

Of these, the hallmark characteristic of all natural SIV infections are high levels of SIV replication during both the acute and chronic stages of infection (46, 78, 82–95). During the acute infection, the peaks of virus replication in natural hosts are comparable to those seen in untreated HIV-1 and SIVmac infections (12, 46, 52, 78, 82–90, 96–104). During the chronic infection, viral loads in natural hosts tend to be as high as or even slightly higher than the viral loads seen in pathogenic infections (105). Additionally, the chronic viral replication in natural hosts is remarkably stable, whereas it tends to vary widely and increase with disease progression in humans and macaques, thus being predictive of disease progression (6, 7, 88, 96,

97). As viral replication remains virtually unchanged throughout the course of chronic infection in natural hosts, it can be assumed that plasma viremia has no correlation with disease progression. However, in the rare instances where progression to AIDS has occurred in natural hosts, the levels of chronic viral replication were significantly higher (1-2 logs) than normally seen in the majority of naturally SIV-infected animals (6, 11).

Though many studies have examined SIV replication in natural hosts in captivity, very limited information is available regarding the levels of viral replication in the wild. The most comprehensive studies to date on virus replication in the wild were performed using samples collected from several hundred wild-caught vervets from South Africa and sabaeus from Gambia (12, 52). In these animals, plasma viremia ranged between 10^4-10^7 SIVagm RNA copies/mL. Note that these numbers represent an average, as the viral loads in bulk of the animals tested were fairly consistent, measuring between 10^4-10^5 RNA copies/mL. In both AGM species, approximately 10% of animals tested presented with viral loads that were significantly higher (10^6-10^8 RNA copies/mL plasma). The plasma of these animals also tested seronegative for SIV-specific antibodies, suggesting that they were in the Fiebig stage II of acute SIV infection (106), particularly since the levels of viral replication were in the same range of the viral loads observed during acute infection in captive, experimentally infected AGMs (12).

Based on the findings of these studies and on data derived from studies of natural hosts in captivity, it can be reasonably inferred that there is no significant difference in viral replication between wild and captive natural hosts (105). One may argue that the high levels of viral replication observed may be due to a low virus turnover and not necessarily to high levels of virus replication. However, previous experimental studies have shown that virus turnover is high in SIV-infected AGMs and SMs, higher even than in SIVmac infection (88, 107).

The higher levels of chronic viral replication observed in the wild AGMs compared to HIV-1^+ individuals (12, 39, 97), may significantly impact viral transmission in the wild. A plasma viremia of around 1500 RNA copies/mL or higher is associated with significant increase in rates of sexual transmission in

humans (108). This is lower than either the average acute or chronic viral loads in natural hosts. Assuming that similar virus shedding occurs in the body fluids of humans and NHPs, this would support mucosal exposure through sexual contact as the primary route of transmission in the wild (3).

1.4.2 SIV primarily targets CCR5$^+$ CD4$^+$ T cells during mucosal transmission in natural hosts

For most SIVs, the primary viral binding receptor is CD4, while chemokine receptors such as CCR5 serve as coreceptors (109–112). This shared receptor and coreceptor usage indicates that, like HIV, the identity of the primary target cells of SIV are CCR5$^+$ CD4$^+$ T cells (7, 38, 109, 111, 113, 114). However, while HIV can utilize both CCR5 and CXCR4, most SIVs are limited to only CCR5 as a coreceptor. There are some exceptions to this, as several SIV isolates were reported to also use CXCR4, including SIVmnd-1, several SIVsmm strains and SIVagm (91, 115, 116). Very recently, SIVsmm and SIVagm strains were reported to also utilize CXCR6 as a coreceptor (117, 118). It has also been reported that CCR6 and CRK-L3, a natural isoform of CCR6, can act as a coreceptor for both primary HIV and SIVsmm isolates (119, 120). This suggests that some SIVs may have an expanded cell tropism besides CCR5$^+$ CD4$^+$ T cells or an expanded range of potential target cells (117, 118).

One of the major exceptions to the usage of CCR5$^+$ as a coreceptor by SIVs is SIVrcm, which uses CCR2b as a coreceptor instead of CCR5. This appears to be an evolutionary feature born from necessity, as the majority of red-capped mangabeys (RCMs), the natural hosts of SIVrcm, lack CCR5 entirely. This is because approximately 83% of RCMs have a Δ24 deletion that silences transcription of their *CCR5* gene, making them resistant to viral entry using CCR5 as a coreceptor. This is very similar to the situation in humans, where a small number of people exhibit a Δ32 mutation of their *CCR5* gene that renders them resistant to HIV infection (121). Consequently, SIVrcm has adapted to use CCR2 or CCR4 to ensure its continued dissemination throughout the RCM population or persistence upon cross-species transmission (122, 123). The usage of CXCR4, CXCR6 and CCR6 coreceptors by some SIVagm and SIVsmm lineages

suggests that there might have been similar adaption by these viruses to overcome the naturally low availability of $CCR5^+$ $CD4^+$ target cells in natural hosts (see 1.4.4).

1.4.3 Natural hosts maintain peripheral T-cell populations and T-cell function

Despite the high levels of ongoing viral replication during both the acute and chronic infection, another defining feature of SIV-infection of natural hosts is the preservation of peripheral $CD4^+$ T-cell populations during chronic infection (46, 52, 78, 84, 86, 87, 91, 96, 97, 124–127). This is in contrast to pathogenic HIV/SIV infections, where chronic peripheral $CD4^+$ T-cell depletion is associated with disease progression and the development of AIDS (128). However, while natural hosts of SIV share the acute $CD4^+$ T cells depletion with the pathogenic models of infection, the $CD4^+$ T cells are partially restored in natural hosts during the chronic infection, differently from the pathogenic infections, where progressive $CD4^+$ T-cell depletion is a hallmark of infection and one of the defining features of AIDS (see 1.4.5) (6, 7, 76, 129–132).

The fact that natural hosts can undergo even a partial depletion of $CD4^+$ T cells and then maintain high levels of viral replication calls into question how they are able to maintain T-cell function. One possible explanation was derived from studies in SMs, where $CD4^+$ T-cell depletion can occur down to AIDS-associated levels without any clinical consequences (84, 96, 101, 133, 134). This preservation of immune function was reported to be due to populations of $CD4^{neg}$ $CD8^{neg}$ T cells that perform helper cell-like functions following SIV-induced $CD4^+$ T cell depletion (101). These double negative T cells arise through down-regulation of CD4 expression by memory T cells as they enter the memory pool. The double negative T cells were shown to be able to carry out a variety of $CD4^+$ T-cell associated functions (production of IL-2 and IL-17, FoxP3 and CD40 ligand expression, MHCII restriction) and are resistant to SIV infection (135, 136). In HIV^+ individuals, $CD4^{neg}$ $CD8^{neg}$ cells can also arise from down-regulation, but remain susceptible to infection (137).

1.4.4 Natural hosts of SIVs exhibit reduced expression of CCR5 and lower total numbers of $CCR5^+$ $CD4^+$ T cells at mucosal sites

Another defining characteristic of natural hosts of SIV is the low expression levels of the viral coreceptor CCR5 on $CD4^+$ T cells, particularly on those residing in the gut. In comparison, non-natural hosts have high numbers of $CCR5^+$ $CD4^+$ T cells in the gut and other mucosal sites (38, 70). This down-regulation of CCR5 expression specifically occurs for $CD4^+$ T cells, as CCR5 expression on $CD8^+$ T cells remains in the same range as in pathogenic hosts (38). This low levels of expression of CCR5 by the memory $CD4^+$ T- cells occurs even in the absence of SIV-infection in the natural hosts of SIVs (38).

In addition to low expression levels of CCR5, some natural hosts also exhibit a general reduction in the overall $CD4^+$ T-cell counts. While this decrease applies to all tissue compartments, it is even more pronounced at mucosal sites, such as the gut (38, 46, 70, 78). This trend only holds true for some species of African guenons (tribe Cercopithecini), i.e., AGMs, patas and sun-tailed monkeys (46). SMs and mandrills (tribe Papionini) have been reported to have higher $CD4^+$ T-cell counts, similar to those seen in RMs (6).

The observation that natural hosts can have high levels of viral replication, but low levels of $CCR5^+$ $CD4^+$ target cells available to support that replication is one of the major paradoxes of SIV infection in natural hosts. One possible explanation for this is that the level of CCR5 expression by $CD4^+$ T cells does increase in response to infection in natural hosts, but the effect is masked by simultaneous SIV-induced depletion (6). Another potential explanation is that there are other target cells in natural hosts apart from $CCR5^+$ $CD4^+$ T cells, such as macrophages (6). This is somewhat supported by the observation that SIVagm and other SIVs are dual-tropic for CCR5 and CXCR4 (see 1.4.2). The occurrence of giant cell disease in the rare cases of AIDS in natural hosts also supports the infection of monocytes/macrophages during natural infection (11). However, during acute infection, $CD4^+$ T cells are most depleted in the gut, where they more frequently express CCR5. The depletion is more limited in blood and LNs, where a higher fraction of $CD4^+$

T cells express CXCR4. This holds true for infections by both natural (AGMs) and non-natural (RMs and PTMs) hosts, as well as for HIV infections (6, 89, 127), strongly suggesting that even in cases where SIVs can employ other coreceptors for infection, $CD4^+$ T lymphocytes will be preferentially targeted. However, it has been shown that SIVs can employ another coreceptor aside form CCR5 or CXCR4, namely CXCR6. It has been hypothesized that usage of CXCR6 as a coreceptor helps to preserve a functional immune response in natural hosts by redirecting the virus away from the $CCR5^+$ $CD4^+$ T-cell population (117, 138).

Apart from their obvious depletion, $CD4^+$ T cells have been implicated as the major cell type supporting SIV replication by *in situ* hybridization studies showing that SIV RNA colocalizes mostly with $CD3^+$ cells and infrequently with macrophages (88, 107, 139). Furthermore, when natural hosts experimentally receive antiretroviral therapy (ART), the viral decay suggests that the cells predominantly supporting viral replication are short lived, implicating lymphocytes as the principal target cell (88, 107, 139). Additionally, in a study where $CD4^+$ T cells were experimentally depleted in naturally SIVsmm-infected SMs using humanized anti-CD4 mAb, viral loads decreased sharply in blood, rectal biopsies and bronchoalveolar lavages, and returned to baseline levels after the $CD4^+$ populations were replenished (140). Conversely, the $CD4^+$ depletion had no effect on macrophages, T regulatory cell or $CD8^+$ T-cell populations, indicating that $CD4^+$ T cells were the primary cell type supporting viral replication (140).

Yet, when $CD4^+$ T cells are depleted or are resistant to the virus (such as cells defective for CCR5 expression, like in RCMs), SIVs will infect macrophages in both progressive and nonprogressive hosts (100, 141–143). This is best demonstrated by the fact that both progressive and natural hosts that develop AIDS exhibit giant cell disease, a condition characterized by heavy infiltration of tissues by SIV-infected macrophages (9, 11, 144). Macrophage tropism of SIVs is not surprising, since lentiviruses first emerged as macrophage-tropic viruses, as is still the case for lentiviruses infecting other mammal species (Maedi-Visna, equine infectious anemia virus or caprine arthritic encephalitis virus) (7).

1.4.5 Following depletion, peripheral but not the mucosal $CD4^+$ T-cell populations are restored to near preinfection levels in natural hosts

Both natural and non-natural hosts undergo a similar massive depletion of mucosal $CD4^+$ T cells during the acute stage of infection. The primary site of $CD4^+$ T-cell depletion is the gut, specifically the GALT and depletion mainly occurs during the acute stage of infection (76, 84, 89, 129–132, 145, 146). Natural hosts experience this depletion in spite of the reduced level of CCR5 expression or lower total number of $CD4^+$ cells (see 1.4.4) (38, 70).

What sets natural and non-natural hosts apart are the immunological events following depletion of mucosal $CD4^+$ T cells (Table 2)

Table 2: Immunological Features of Lentiviral Infections in Natural *versus* Non-natural Hosts

Feature	Natural Hosts	Asian NHPs	Humans
Primary Target cell	CD4	CD4	CD4
CD4 T-cell CCR5 expression levels	+	+++	+++
Mucosal $CCR5^+$ $CD4^+$ levels	+	+++	+++
Peripheral $CD4^+$ T-cell depletion	Acute only	+++	+++
Mucosal $CD4^+$ T-cell depletion	+++	+++	+++
$CD4^{neg}CD8^{neg}$ resistance to infection	Yes	No	No
T_{scm} depletion	No	Yes	Yes
$CD4^+$ Th17 cell depletion	No	Yes	Yes
$CD8^+$ T-cell response	Yes	Yes	Yes
$CD20^+$ B-cell response	Yes	Yes	Yes
Treg homeostasis	Yes	No	No
γδ T cells anergy	No	Yes	Yes
Chronic immune activation	No	Yes	Yes
Interferon response	Acute only	Yes	Yes
T-cell proliferation	Acute only	Yes	Yes
Inhibitory breast milk factors	Yes	Yes	Yes

In untreated HIV^+ individuals and pathogenic SIV infections, the peripheral $CD4^+$ T-cell populations will eventually decline without intervention, leading to the development of AIDS. The scenario in natural hosts is quite different, with recovery of the peripheral $CD4^+$ T cells population to nearly baseline levels by the chronic infection. Additionally, the GALT-associated $CD4^+$ T cells partially recover, despite the robust chronic viral replication, though GALT $CD4^+$ T cells populations never recover fully to preinfection levels (4, 6, 72, 147). Most of this recovery following acute infection consists of restoration of central memory and naïve T cells, while effector memory T cells remain depleted (89). This partial recovery is possible in natural hosts because of the control of immune activation and apoptosis (see 1.4.6), which prevents excessive depletion of the overall $CD4^+$ T cells population, with the loss due to viral replication being compensated by a normal production of cells (6).

After their restoration, $CD4^+$ central memory T cells are lost in SIVsmm-infected SMs at rates 20 times slower than those of SIV-infected RMs (148). This translates to a half-life of total $CD4^+$ central memory T-cell populations <16 months for RMs, but >17 years for SMs, which is in agreement with the rare cases of AIDS in natural hosts in very old animals. Also, SM $CD4^+$ central memory T-cell proliferation levels are lower than in RMs and the RM $CD4^+$ central memory T-cell proliferation correlates with viral replication (148). Yet, a recent study of mandrills in Gabon found a significant decrease in memory T cells populations that was correlated with the duration of infection (149). However, other studies of the same mandrill cohort did not find similar features (99).

Besides central memory T cells, other cell types are also preserved in natural hosts and show divergent dynamics between SIV-infected RMs and SMs. Notably, memory $CD4^+$ T cells with stem cell-like properties undergo depletion and exhibit increased rates of proliferation and high levels of virus infection in RMs. Conversely, SMs $CD4^+$ stem memory T-cell populations remained stable, showed no marked increase in proliferation, and had very low rates of direct infection. As stem memory T-cell are known to be able to differentiate into central, effector and naïve T cells, their homeostasis could be crucial to restoration of T-cell populations following depletion in natural hosts (150, 151).

1.4.6 Natural hosts control chronic immune activation, proliferation and interferon production

One of the most striking features of the SIV infection in natural hosts is their ability to control their levels of chronic immune cell activation. This is reflected by the expression of HLA-DR and CD69 (both markers of immune cell activation) on T cells, predominately $CD8^+$ T cells, in natural hosts, which increase slightly during acute infection and returns to baseline levels by chronic infection. In pathogenic infections, the expression levels of these activation markers by T cells rise dramatically during the acute infection and are never resolved during the chronic infection, when they continue to increase, being correlated with disease progression (46, 82, 84, 87–89, 91, 97, 125–127, 133, 152). Also, expression of PD-1, a cell surface protein that acts as a negative regulator of the immune activation, was found to be rapidly induced in response to SIV-infection in the lymphatic tissue in SMs. This was associated with resolution of acute immune activation and the preservation of $CD4^+$ T-cell populations and lymphatic tissue structure (153). Resolution of this aberrant, persistent immune activation during the transition from acute-to-chronic infection is therefore thought to be the major mechanism by which natural hosts avoid progression to AIDS (89, 153–157).

Similar to immune cell activation, T-cell proliferation increases only during the acute infection in natural hosts (84, 89, 90, 133, 158). By the chronic phase of infection, proliferation levels return to near their preinfection state (158–160). This can be observed as a transient increase in expression of the proliferation marker Ki-67 during the acute infection and early chronic infection in AGMs, with return to baseline by the transition to chronic infection (76, 89). Conversely, in pathogenic infections, T-cell proliferation continues to increase to the point of excessive cell turnover, likely in an attempt to recover from the depletion of $CD4^+$ T cells (161, 162).

Another point of divergence between natural and non-natural hosts during SIV infection is seen in the production of interferons. A strong and sustained Th1-mediated type I (IFN-α, IFN-β) and type II (IFN-γ) interferon response was observed in the LNs of pigtailed macaques (PTMs) infected with SIVsab, which

is pathogenic in PTMs. In contrast, only a transient type I interferon response occurred in SIVsab-infected AGMs, which was resolved after peak viral replication (163). Furthermore, experimental administration of high concentrations of the type I IFN-α to acutely infected AGMs had no impact on immune activation (164). Taken together, natural hosts seem to possess the ability to maintain homeostasis of their immune cell populations and resolve immune activation, proliferation and IFN production after the acute SIV infection.

1.4.7 $CD8^+$ T cells do not contribute significantly to the prevention of disease progression

The current data indicate that the general $CD8^+$ T-cell populations and their SIV-specific responses are comparable in both infected and uninfected AGMs and RMs (165–168). However, the role that $CD8^+$ T cells play in different natural host species becomes unclear when looking at the dynamics of viral replication following experimental depletion of $CD8^+$ T cells. In chronically SIVmac-infected RMs, experimental $CD8^+$ T-cell depletion results in a 1-3 log increase in plasma viremia (169, 170). In contrast, $CD8^+$ depletion in chronically SIVsmm-infected SMs seem to have very little impact on viral replication, though one study did show an increase in viral loads following $CD8^+$ T-cell depletion (171, 172). Similarly, $CD8^+$ T-cell depletion during acute infection did not increase the peak viral loads in AGMs, but it did lead to a plateau of viral replication following peak infection until the $CD8^+$ T-cell populations were restored. These findings, along with those of other studies on cellular immune responses in natural hosts, indicate that $CD8^+$ T cells do play a role in controlling viral replication to some extent (167, 172, 173). However, none of the *in vivo* depletion experiments had any effect on the actual state of disease progression (171, 174). This is in contrast to $CD8^+$ T-cell depletion in RMs, which results in increased $CD4^+$ T-cell proliferation and rapid disease progression (175). Consequently, it remains unclear what impact, if any, $CD8^+$ T cells play in preventing disease progression in natural hosts.

1.4.8 Natural hosts maintain function of other immune cell populations

Apart from the changes in $CD4^+$ and $CD8^+$ T-cell populations, natural hosts also maintain normal populations and functions of a variety of other immune cell subsets, such as NK cells, Th17 T cells, regulatory T cells (Tregs), γδ T cells and myeloid dendritic cells (mDCs). In contrast, disturbances in these cell populations have been described during pathogenic HIV and SIV infections (161, 176–181). Preservation of these secondary immune cell populations could impact protection from disease progression in natural hosts in a number of ways. For instance, there is evidence to support that maintenance of the Th-17/Treg ratio may be crucial to preventing SIV disease progression and maintaining the integrity of the mucosal barrier during acute infection (177, 178). Moreover, preserving Treg homeostasis might confer protection through production of anti-inflammatory cytokines, such as IL-10, or by prevention of excess $CD4^+$ T-cell proliferation following the initial $CD4^+$ T-cell depletion in the gut (6). Expression of the Treg marker FoxP3 was reported to increase along with anti-inflammatory cytokine production, suggesting that Tregs might play an important role in establishing the anti-inflammatory response (127). Tregs are rapidly depleted in the intestines of neonatal RMs infected with SIVmac, supporting the role of the loss of Tregs in pathogenic models of disease progression (182).

In addition to maintaining Treg homeostasis, preventing dysfunction of γδ T cells may play a crucial role in averting disease progression in natural hosts, as apart from cytokine production, γδ T cells also perform a variety of other functions, including regulation of tissue healing (183, 184). In HIV infection, it has been shown that γδ T cells become anergic and can no longer migrate in response to proinflammatory cytokines (185, 186). In contrast, γδ T cells remain fully functional in SMs (133, 176). It was also shown that γδ T cells in SMs retain their ability to produce the Th1 cytokines TNF-α and INF-γ postinfection, while this capacity was reduced in γδ T cells from HIV-infected subjects, along with the overall numbers of γδ T cells (184). Given the importance of controlling inflammation during primary infection (see 1.4.10

and 1.4.11), preservation of regulatory cell populations like Tregs and γδ T cells likely plays an important role in the prevention of SIV disease progression in natural hosts.

1.4.9 The humoral response plays little to no role in controlling viral replication following mucosal transmission in natural hosts

The humoral response in SIV-infected natural hosts has been shown to be similar to or lower than what has been reported in pathogenic infections (82, 187–189). However, a paucity of SIV Gag-specific antibodies is a shared feature of SIV-infected natural hosts. Oddly, the T-cell response to Gag in natural hosts is comparable to those seen in pathogenic infections, meaning that the absence of anti-Gag antibodies is not due to a lack of Gag-specific T cells (165). Furthermore, some SIVs, like several SIVsmm strains, are actually resistant to antibody neutralization, making it unclear what effect antibodies might have on SIVs (112). Further complicating the situation, experimental depletion of $CD20^+$ B cells had no effect on either viral replication or disease progression in AGMs, even after the depletion was maintained in our studies for over 6 months (166, 187). Similarly, in a pair of studies that sought to suppress the adaptive immune response through simultaneous depletion of $CD8^+$ T cells and $CD20^+$ B cells during primary SIV infection, the depletion caused no alteration in the state of disease progression in AGMs. In contrast, SIVsab-infected PTMs rapidly progressed to AIDS when both $CD8^+$ and $CD20^+$ populations were depleted (166, 168). In summary, these results strongly suggest that the role of the adaptive immune responses are minimally involved in preventing disease progression in natural hosts.

1.4.10 Natural hosts appear to avoid damage to the gut epithelial that is associated with acute pathogenic SIV/HIV infection

Perhaps one of the most important differences between SIV infection in natural and non-natural SIV hosts and the one that might play the key role in preventing persistent immune activation is the lack of

chronic damage to the gut epithelium in natural hosts. In non-natural, pathogenic hosts (i.e., humans and RMs), this damage is a consequence of early viral replication, which causes disruption of the gut epithelium and dysregulation of epithelial cell homeostasis (190). The result is damage to the gut epithelium, which allows leakage of microbes and microbial products from the gut lumen into the surrounding tissue, a process known as microbial translocation. Once outside the lumen, microbial antigens bind to Toll-like receptors, stimulating chronic aberrant immune activation. This, in turn, not only creates more available target cells for the virus, but also functionally exhausts the immune system and its capacity for regeneration (84, 89, 191, 191, 192).

Natural hosts, on the other hand, appear to avoid this vicious cycle of damage and inflammation altogether. This is reflected by the absence of bacterial lipopolysaccharide (LPS) in the plasma during both the acute and chronic stages of SIV infection in AGMs (89). The importance of avoiding microbial translocation was highlighted by two studies where experimentally administration of LPS to AGMs induced general immune activation followed by $CD4^+$ T-cell depletion and an increase in viral loads (though there was ultimately no impact on disease progression) (193, 194). In another study, dextran sulphate, a drug that is directly toxic to intestinal epithelial cells and is known to impair the integrity of the mucosal barrier, was administered to chronically SIVsab-infected AGMs. This resulted in increases in plasma SIV RNA, sCD14 (see below), CRP and LPS levels, along with loss of mucosal $CD4^+$ T cells (195). Conversely, when acutely SIV-infected PTMs were treated with sevelamer, an LPS chelator, in the gut, the treatment resulted in a dramatic reduction in both inflammation and immune activation, directly demonstrating the significance of microbial translocation on SIV pathogenesis (196).

As the bulk of data regarding microbial translocation in natural hosts was derived from studies of animals in captivity, a recent study sought to examine whether or not natural hosts were able to avoid microbial translocation (MT) in the wild. Because direct measurement of mucosal integrity in wild natural hosts would have been virtually impossible, the sCD14 protein was used as a surrogate marker for microbial translocation. CD14 is a coreceptor for LPS expressed by peripheral blood monocytes and tissue

macrophages. After LPS stimulation, $CD14^+$ monocytes/macrophages secrete sCD14 and shed surface CD14, which then bind to LPS (192). There was no observable difference in the plasma sCD14 levels between wild SIV-positive and SIV-negative vervets and sabaeus (12, 52). These results are in agreement with studies of experimentally infected AGMs, where sCD14 levels remained virtually unchanged following SIV infection (78, 78, 89, 105). A separate study of semiwild mandrills in Gabon confirmed these results by showing that plasma levels of sCD14 remained unchanged following SIVmnd1-infection (149).

1.4.11 Maintenance of the gut integrity and prevention of MT primarily hinges on control of apoptosis and establishment of a rapid anti-inflammatory response

The precise means by which natural hosts avoid chronic damage to their gut and the associated MT is still uncertain. $CD4^+$ T-cell apoptosis levels in natural hosts do not increase significantly during acute or chronic infection (89, 126, 197–200). However, transient $CD8^+$ T-cell apoptosis occurs in both natural and pathogenic hosts (200). Lack of increased apoptosis of both gut lymphocytes and epithelial cells may contribute to the preservation of the integrity of the gut epithelium (6).

Another important mechanism reported to contribute to the preservation of the integrity of the gut epithelium is the establishment of an anti-inflammatory milieu early during infection that represses the effects of proinflammatory cytokines. Both natural and non-natural hosts exhibit increased expression levels of proinflammatory cytokines (IFN-γ,TNF-α, IL-1β, IL-12) following infection, albeit at a somewhat lower level in natural hosts. These cytokines are produced by both immune and epithelial cells as part of the innate immune response to viral replication following transmission (6, 201–204). However, this increase is only transient in natural hosts; following acute infection, expression of proinflammatory cytokines return to preinfection levels. In HIV^+ individuals and SIVmac-infected RMs, proinflammatory cytokine production persists into chronic infection, stimulating chronic inflammation and, in turn, immune activation (127, 133, 152). Resolution of this initial proinflammatory response to the virus seems to depend on

establishment of the anti-inflammatory milieu early during infection of the natural host. This is reflected in a rapid increase in expression of the anti-inflammatory cytokines TGF-β and IL-10 following SIVsab infection of AGMs (127). Furthermore, a recent study in RMs established a correlation with internalization of the IL-10 receptor (i.e., lowered responsiveness to IL-10) by mucosal lymphocytes in the gut epithelium with increased levels of apoptosis (205).

2.0 Hypothesis

Previous studies of natural hosts by our lab and others have strongly suggested that events occurring very early during the infection may enable natural hosts to prevent disease progression. Understanding these early events may be crucial to uncovering the mechanisms by which natural hosts avoid progression to AIDS, which in turn could lead to new treatment options for HIV^+ individuals. Specifically, it may help unlock routes to reaching a 'functional cure' (i.e., prevention of progression to AIDS without viral clearance) for HIV^+ individuals and eliminate their dependency on ART. Therefore, the goal of this dissertation study was to characterize the early events of intrarectal transmission of SIVsab in male AGMs. Given that it has been shown that chronic immune activation and inflammation are characteristic of pathogenic HIV/SIV infections, we therefore hypothesized that events occurring during the earliest stages of mucosal transmission contribute to the resolution of the immune activation characteristic of pathogenic lentiviral infection at the passage from acute-to-chronic infection and thus prevent disease progression in nonprogressive hosts. Among the characteristic features of mucosal transmission in natural hosts that are involved in the early events of infection and shape the long-term pathogenic outcome are: (i) lower availability of target cells at the mucosal site(s) of infection; (ii) lower levels of immune activation at the mucosal sites, which result in (iii) reduced recruitment of target cells to mucosal sites of infection and (iv) the establishment of an anti-inflammatory milieu that suppresses the virally induced proinflammatory response. To test this hypothesis, we proposed the following specific aims (SAs):

SA1: Characterize the viral bottleneck and dissemination from the site of infection in AGMs intrarectally (IR) inoculated with SIVsab.

SA2: Examine early changes in the immune cell populations following IR challenge of AGMs with SIVsab.

SA3: Analyze the expression of inflammatory and anti-inflammatory genes following IR SIVsab challenge.

3.0 Acute SIVsab infection of African green monkeys is characterized by rapid viral dissemination and limited immune response at the site of inoculation

3.1 Contributors

Data contributed to the dissertation by several collaborators is included in the following chapter. Drs. Jacob Estes and Claire Deleage contributed the *in situ* hybridization data, the RNAscope data and the fluorescent *in situ* hybridization data. Dr. Brandon Keele contributed the single genome amplification data on the transmitted/founder viruses. Various members of the Apetrei/Pandrea labs contributed to the routine work, including tissue processing, immune cell isolation, flow cytometry, quantitative PCR, and single copy assay for plasma viral loads. The dissertation author managed the serial necropsies and tissue sampling, analyzed the majority of the flow cytometry data, performed the qPCR for the CSF viral loads and all DNA/RNA extractions and qPCR for the tissue viral load quantifications.

3.2 Background

As outlined in 1.0, prior research in African NHPs has indicated that the events that might contribute to the avoidance of disease progression in natural hosts, like the AGM, occur very early on during SIV infection, probably within the first few days following transmission (78, 91, 127, 154, 156, 164). These early events likely occur at the mucosal sites of viral entry or at the initial sites of viral replication. Most of what is known about these initial sites of replication has been derived from studies of intravaginal transmission of SIVmac in RMs and provides a good approximation for transmission at other mucosal sites (see 1.3.1) (61, 72, 206–208). In these studies, it was observed that the virus must first cross the epithelial barrier, which is significant impediment to transmission; this is reflected by the fact that any preexisting

infections, inflammation or microabrasions that might compromise the integrity of the mucosal epithelium significantly increase transmission rates (72, 208–211). After crossing the epithelium, the virus enters the submucosa and infects a small number of target cells. This founder population of cells is comprised of $CD4^+$ T cells, which are typically more numerous than other resident immune cells types (77). However, the initial population of target cells is not large enough to sustain viral replication; therefore, more cells must be recruited to the initial foci of replication by the virus-induced innate and inflammatory immune responses (210). Further viral expansion is facilitated when the virus reaches the draining lymph nodes (LNs), where there is an extremely high concentration of potential target cells. Lymphatic dissemination also allows the virus to move into the bloodstream through the thoracic duct and thereby enter systemic circulation (61, 72). A similar pattern of viral dissemination has been observed in several studies of intrarectal transmission of SIVmac in RMs, supporting this model of early events of mucosal transmission of SIV (212, 213).

The macaque model of mucosal transmission also predicts that the combination of the epithelial barrier, the initially limited availability of resident target cells, and the antiviral immune response imposes a "mucosal bottleneck" (see 1.3.4) on the number of transmitted/founder viral variants that can successfully establish infection (214). The existence of this bottleneck is reflected by the fact that in 80% heterosexual transmission of HIV, only a single transmitted/founder genotype goes on to establish infection (80, 215). Similarly, limited transmitted/founder virus transmission has been observed in experimentally infected AGMs (216); our group demonstrated that in both adult AGMs intravaginally infected with SIVsab, only 1-2 SIV T/F variants had been transmitted (78). This implies that the general features of mucosal transmission of natural hosts like AGMs and pathogenic hosts like RMs and humans are similar.

Nevertheless, there are a number of important characteristics of natural hosts that set them apart from pathogenic hosts that can impact transmission. Foremost amongst these is the fact that AGMs maintain significantly lower levels of $CCR5^+$ $CD4^+$ T cells in blood, LNs and, most importantly, the gut than are seen in humans and RMs. This reduced target cell availability is not sufficient to prevent SIVsab transmission, as discussed in 1.3.2 and 1.3.3. However, this reduction is sufficient to limit transmission, as

we found that infection rates for infant and juvenile AGMs were significantly lower than for adults when inoculated with SIVsab. In the same study we also found that PTMs had higher levels of $CCR5^+$ $CD4^+$ T cells at mucosal sites than AGMs and were infected with a dose of SIVsab 1 log lower than was needed to infect the adult AGMs (78).

Unfortunately, many of these previous studies of early SIVsab infection have been limited by several factors, including being based solely on peripheral blood or LNs, relying on intravenous (IV) inoculations or not encompassing the initial period of viral replication within the first few days of infection. Here, we performed a detailed characterization of the natural history of acute SIVsab infection following intrarectal inoculation in Caribbean AGMs, which we have established as a well-studied and readily available model of natural SIV infection (88, 217). The goal of the studies outlined in this section of the dissertation was to characterize both the virological and immunological parameters of infection immediately surrounding the earliest stages of mucosal transmission in AGMs, particularly at the site of inoculation. To this end, we used PCR analysis of both plasma and tissue sites to both establish the levels of virus and to try to track viral dissemination throughout the body. We also performed additional, more thorough dissection of the site of inoculation itself attempting to identify: (i) the initial sites of viral replication; (ii) the population of founder cells in the mucosa; (iii) any changes in immune activation, immune cell recruitment and cell death; (iv) the mucosal bottleneck of virus transmission by enumerating the transmitted/founder viral variants, should this actually occur.

3.3 Methodology

3.3.1 Ethics Statement

All the animals included in these studies were housed at the RIDC animal facility of the University of Pittsburgh, an AAALAC International facility, as per the regulations outlined in the *Guide for the Care and Use of Laboratory Animals* (218) and the Animal Welfare Act (219). All animal experiments were approved by the University of Pittsburgh Institutional Animal Care and Use Committee (IACUC). Efforts were made to minimize NHP suffering, in agreement with the recommendations in "*The Use of Nonhuman Primates in Research*" (220). The NHP facility was air-conditioned, with an ambient temperature of 21-25°C, a relative humidity of 40-60% and a 12-hour light/dark cycle. AGMs were socially housed in suspended stainless-steel wire-bottomed cages. A variety of environmental enrichment strategies were employed, including providing toys to manipulate and playing entertainment videos in the NHP rooms. The NHPs were observed twice daily and any signs of disease or discomfort were reported to the veterinary staff for evaluation. At the end of the study, the NHPs were euthanized following procedures approved in the IACUC protocol (#1008829).

3.3.2 Animals and infections

Thirty-three adult (4-9 years old) male AGMs (*Chlorocebus sabaeus*) of Caribbean origin were used in these studies. Caribbean AGMs are genetically identical to African AGMs and are much easier to obtain than their African counterparts, making them more practical for all intents and purposes of experimentation (43, 217, 221). The AGMs were intrarectally challenged with infectious plasma originally collected from an acutely infected AGM, diluted to contain 10^7 RNA copies of SIVsab.sab92018 (217). This dosage was established during a preliminary study as a relatively low dose that could reliably infect adult AGMs intrarectally (78). Infectious acute plasma was chosen as an inoculum to better reflect the

natural viral diversity in the wild; it is also more infectious than plasma taken from chronically infected NHPs (222). Male AGMs and the intrarectal route of infection were preferred to avoid the physiological variability of the vaginal mucosa associated with the estrus cycle (75) even though vaginal transmission is far more prevalent in wild NHPs (see 1.2.3).

Given the nature of the study, it was necessary to perform serial necropsies of the animals to obtain the tissues required for proper characterization of site of inoculation, the virus spread throughout the body and a wide-variety of different immune responses. Longitudinal biopsies would have provided neither the quantity nor the diversity of tissues necessary for such an extensive survey.

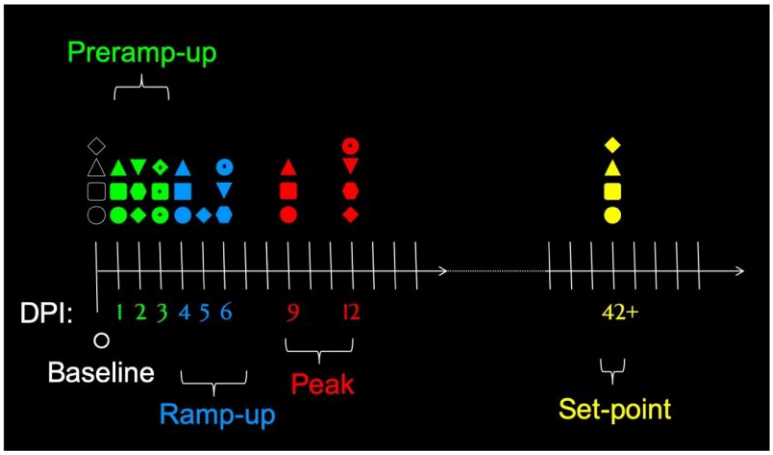

Figure 1: Animal groups for study of the early events of intrarectal SIVsab infection.
Thirty-three African green monkeys (AGMs) were included in this study and exposed intrarectially to SIVsab92018. The AGMs were euthanized throughout the acute and early chronic SIV infection and were divided into the following groups based on their predicted viremic status at the day postinfection (dpi) that the necropsy was performed: (i) preinfection (baseline); (ii) preramp-up (1-3 dpi); (iii) ramp-up (4-6 dpi); (iv) peak (9-12 dpi); (v) set-point (46-55 dpi). Each animal is assigned an individual symbol and color indicating at which stage of infection they were necropsied.

3.3.3 Tissue sampling and isolation of mononuclear cells

Blood, intestinal biopsies and LN biopsies were collected from each animal prior to infection to establish the baseline levels for the tested markers. Then, immediately prior to necropsy, the maximum amount of blood allowed (based on weight) was collected. The bulk of the volume of the blood was collected with EDTA to prevent coagulation, but two separate smaller samples of blood mixed with heparin and sodium citrate were also taken. An extensive tissue sampling was performed during the necropsy. Sections of numerous tissue sites were collected for snap freezing in liquid nitrogen, or fixation in 4% paraformaldehyde. Additional tissue samples were collected for lymphocyte separation from specific tissues of interest, including a variety of regional LNs (colonic, iliac, obturator, mesenteric, axillary, inguinal and submandibular), jejunum, ileum, colon, and rectum. Lymphocytes were separated from whole blood and tissues and used fresh for flow cytometry. Any remaining cells were frozen for later use at -80ºC in freezing medium containing heat-inactivated fetal bovine serum with 10% dimethyl sulfoxide (DMSO).

Special attention was payed to collection of the tissue from the site of inoculation: the rectum and the distal colon. These tissues were removed prior to any other tissue compartment and then sectioned 6 strips each, for a total of 12 strips. These strips were then divided into ~1cm^2 pieces. The pieces were then collected for various purposes, including immunohistochemistry (IHC), RNA sequencing (RNAseq) and DNA/RNA extraction for PCR. As the initial foci of viral replication within the site of inoculation can be widely distributed, the pieces were taken using a rotating collection strategy to maximize the probability of capturing one or more of these foci.

Plasma was separated from whole blood within 1 hour of collection by centrifugation at 2200 rpms for 20 mins, aliquoted and snap frozen at -80ºC. Peripheral blood mononuclear cells (PBMCs) were then isolated by density gradient centrifugation at 2200 rpms using lymphocyte separation media (LSM; MP Biomedicals, Santa Ana, CA), aliquoted and frozen as described (46, 223).

Cells were separated from LNs by first mincing the tissue and then pressing it through a 70 µm nylon filter (Fisher Scientific, Pittsburgh, PA). The cells were then passed through a nylon tissue specimen

bag (ThermoFisher, Waltham, MA) and washed with RPMI media (Lonza, Walkersville, MD) containing 5% heat-inactivated newborn calf serum, 0.01% penicillin-streptomycin, 0.01% L-glutamine, and 0.01% HEPES buffer, as described (89, 193). LN biopsies were also dry frozen at -80ºC for DNA/RNA extraction or fixed in 4% paraformaldehyde for histological processing.

The intestinal biopsies were fixed and frozen in a similar fashion, though they were additionally preserved in RNALater (ThermoFisher) for use in RNAseq. No lymphocytes were separated from the intestinal biopsies due to their small size and the need to prioritize other assays. To isolate lymphocytes from the much larger gut sections taken during the necropsy, they were processed as previously described (78, 114). Briefly, the sections were first trimmed of fat, then opened longitudinally and gently scraped to remove waste. Next, the gut sections were diced into ~1-2mm^2 pieces and then incubated in HBSS (Lonza) with 8 mM EDTA (Fisher Scientific) for 30 mins at 37ºC while shaking at 300 rpms on an orbital shaker/incubator. This was done twice, with fresh HBSS with EDTA added between, before the tissue was thoroughly minced. Then, the tissue was digested twice with RPMI with 0.75% collagenase (Sigma-Aldrich, St. Louis, MO) under the same conditions. Finally, the lymphocytes were separated by density gradient centrifugation at 2200 rpms for 20 mins using 35% and 60% Percoll (Sigma-Aldrich).

3.3.4 Plasma viral RNA extraction and cDNA synthesis

Viral RNA was extracted from plasma using the QIAGEN viral RNA Mini kit (QIAGEN, Germantown, MD). RNA was then eluted and reverse transcription was preformed using the Taqman Gold reverse transcription PCR (RT-PCR) kit and random hexamers (PE, Foster City, CA), as described (217). The RT-PCRs were run in a Gene Amp PCR System 9700 thermocycler (Applied Biosystems, Grand Island, NY).

3.3.5 Plasma viral load quantifications

Plasma viral loads were monitored by real time quantitative PCR (qPCR) based on a 180-bp segment located in the *gag* region (88, 91, 127). Primers and probes (46, 88) were synthesized by Integrated DNA Technologies (Coralville, IA). All qPCRs were run in duplicate and negative controls for the RT-PCR and qPCR were included on each plate. The qPCRs were run on 7900HT Fast Real Time System (Applied Biosystems), as described (88).

qPCR was performed by using TaqMan® Gene Expression Master Mix (PE Applied Biosystems). A set of primers and probe mapping the *gag* sequence was synthesized, as follows: SIV-gag-standard-F (5′-ATA GCA GGG ACC ACT AGC ACA AT-3′), SIV-gag-standard-R (5′-TCT TTG AAT GGT TCC TTG GGT CC-3′), and fluorogenic SIV-gag-standard-Probe (5′-/56-FAM/ATA GCA GGG/ZEN/ACC ACT AGC ACA ATA C/3IABkF/-3′).

Absolute viral RNA (vRNA) copy numbers were calculated relative to amplification of an SIVsab standard, which was subjected to RT-PCR in parallel with the samples being tested. The standard was generated as described (88). The detection limit of this conventional qPCR was 30 vRNA copies/mL of plasma (88).

3.3.6 Single copy assay (SCA)

SCA was originally designed to detect down to one copy of HIV RNA in 7.5 mL of plasma. The assay was previously adapted in our lab for quantification of SIVsab (224), and was performed as previously described (224, 225). Briefly, two sequential rounds of centrifugation (400 g x 10 mins and then 1,350 g x 15 mins) were used to pellet cells and debris in the plasma. The plasma samples were then spiked with an internal control virus derived from avian Rous sarcoma virus (RSV) SR-A strain (RCAS) to assess virion recovery. Virions were then pelleted by ultracentrifugation at 170,000 g for 30 mins, digested with

proteinase K, and homogenized with guanidine thiocyanate (Sigma-Aldrich, St. Louis, MO) supplemented with glycogen (Sigma-Aldrich). The SIV RNA was then precipitated with isopropanol, washed with ethanol and resuspended in 10 mM Tris-HCl pH8.0 supplemented with dithiothreitol and an RNase inhibitor.

RT-PCR was then used to convert vRNA to cDNA and the cDNA was then quantified by qPCR using external standard curves generated from serial dilutions of RNA transcripts synthesized *in vitro*. SIV RNA positive (5 copies/mL) and negative (0 copies/mL) control standards were included in each SCA run to evaluate run-to-run variation and exclude false-positive results. The RCAS internal standard was used to evaluate the efficiency of virion recovery. All samples were run in triplicate on 96-well plates. Any of the samples that returned negative results were retested, as the levels of circulating virus during very early acute infection (primarily during the preramp-up period, 1-3 dpi) were anticipated to be very low (224, 226). For the same reason, when large volumes of plasma were available from the AGMs euthanized at 1-3 dpi, SCA was performed multiple times. Only EDTA or sodium citrate blood was used for SCA, as heparin can interfere with the downstream PCR.

3.3.7 Viral load quantification in the cerebrospinal fluid (CSF)

CSF RNA extraction and PCR were performed with the same basic methodology described in 3.3.4 and 3.3.5 but using slightly different reagents. vRNA was extracted from the CSF with the QIAGEN viral RNA Mini kit, followed by reverse transcription. Instead of the Taqman Gold reverse transcription kit, the M-MLV reverse transcriptase (Thermofisher) was used with random primers (Promega, Madison, WI) and RNasin ribonuclease inhibitor (Promega), as per the manufacturer's specifications.

3.3.8 Single genome amplification for the enumeration of transmitted/founder viruses

SGA was performed as described (52, 78, 80). Briefly, 1X High Fidelity Platinum PCR buffer (ThermoFisher), 2 mM MgSO4, 0.2 mM deoxynucleoside triphosphate, 0.2 μM primer, and 0.025 U/μL Platinum Taq High Fidelity polymerase were combined with cDNA. First-round PCR mixtures were denatured at 94°C for 1 min, followed by 35 cycles of 94°C for 20 sec, 55°C for 30 sec, and 68°C for 1 min per kilobase and terminated with a single 10 min 68°C extension. Next, 1 μL of these products were used for a second-round reaction, which was performed under the same PCR conditions for a total of 45 cycles. Positive secondary PCR products were isolated with gel electrophoresis. Both DNA strands were sequenced, and chromatograms were inspected at every position for double peaks, which would be indicative of a Taq polymerase error in an early cycle or PCR priming from more than one template. Sequences with mixed bases were excluded from further analysis (227, 228).

3.3.9 Tissue DNA/RNA extraction from frozen tissue

DNA/RNA was extracted from the tissue sections that had been snap frozen in liquid nitrogen (-196ºC) in cryogenic vials, one for each tissue section. Prior to thawing, the mass of each tissue section was determined and then used to estimate a volume of TriReagent (Molecular Research Center, Cincinnati, OH) at ratio of 100 mg/1 mL. The snap frozen sections were carefully moved on dry ice from standard cryotubes to SPEX SamplePrep polycarbonate cryotubes. Then, stainless steel ball bearings and hex nuts (MSC, St. Louis, MO) were layered over each tissue before the estimated volume of TriReagent was added. The tissues were homogenized using a SPEX 2010 Geno/Grinder (SPEX SamplePrep, Metuchan, NJ), with a single cycle of agitation at 1,600 rpms for 2 mins. Some tissues that were difficult to break down, such as the heart, received two cycles of agitation. Following homogenization, the tissues were allowed to sit for 15-20 mins in TriReagent to solubilize small tissue particles. Next, 1 mL of tissue lysate was transferred from each sample to 1.5 mL snap cap tube. The RNA was extracted first by adding 100 μL

bromochloropropane (MRC, Cincinnati, OH) to each sample, vortexing for 30 seconds, and then spinning at 14,000 x g for 15 mins at 4ºC. After centrifugation, the upper aqueous phase was removed and transferred to a tube with 12 µL of 20 mg/mL glycogen (Sigma-Aldrich) before being mixed with 500 µL isopropanol. The solution was then spun at 21,000 g for 10 mins at room temperature (RT), the supernatant was removed, and the pellet was washed with 600-800 µL 70% ethanol. Each pellet was allowed to sit under ethanol for 3 days at -20ºC before being dried and either immediately resuspended or stored at -80ºC for future use. The same protocol was repeated for DNA, except with 500 µL DNA Back Extraction solution (4 M GuSCN, 1 M Tris base, 50 mM sodium citrate) instead of BCP.

3.3.10 Total viral load quantification in tissues

Tissue viral loads were quantified by qPCR based on a 180-bp segment located in the *gag* region (88, 91, 127) and the TaqMan® Gene Expression Master Mix (PE Applied Biosystems). Primers and probes (46, 88) were synthesized by Integrated DNA Technologies (Coralville, IA). All qPCRs were run in duplicate and negative controls for the RT-PCR and qPCR were included on each plate. The RT-PCRs were performed in a Gene Amp PCR System 9700 thermocycler (Applied Biosystems). The qPCRs were run on 7900HT Fast Real Time System (Applied Biosystems), as described (88).

qPCR was performed using TaqMan® Gene Expression Master Mix (PE Applied Biosystems). The set of primers and probe mapping the *gag* sequence was synthesized, as follows: SIV-gag-standard-F (5′-ATA GCA GGG ACC ACT AGC ACA AT-3′), SIV-gag-standard-R (5′-TCT TTG AAT GGT TCC TTG GGT CC-3′), and fluorogenic SIV-gag-standard-Probe (5-ATA GCA GGG/ZEN/ACC ACT AGC ACA ATA C-3′).

Absolute vRNA and viral DNA (vDNA) copy numbers were calculated relative to amplification of an SIVsab standard, which was subjected to RT-PCR in parallel with the samples being tested. The standard was generated as described (88). To quantify the number of vRNA/vDNA copies per million somatic cells,

we also ran the samples with primers and probes for RM CCR5, as follows: RM-CCR5-F (5'-CCA-GAA-GAG-CTG-CGA-CAT-CC-3'), RM-CCR5-R (5'-GTT-AAG-GCT-TTT-ACT-CAT-CTC-AGA-AGC-TAA-C-3', RM-CCR5-Probe (5'-CalRed610-TTC-CCC-TAC-AAG-AAA-CTC-TCC-CCG-GTA-AGT-A-BHQ2-3').

3.3.11 RNAScope® *in situ* hybridization for SIVsab

To visualize early virus replication, RNAscope® *in situ* hybridization (Advanced Cell Diagnostics, Newark, CA) was performed to detect SIVsab mRNA transcripts in FFPE tissues using the 2.0 HD RED reagent kit (Advanced Cell Diagnostics) following the manufacturer's instructions (229). Mmu-PPIB (Advanced Cell Diagnostics and DapB (Advanced Cell Diagnostics) were used as positive and negative controls, respectively. Briefly, FFPE sections were baked and deparaffinized. Tissue-specific pretreatment was performed according to the manufacturer's instructions for each tissue type, followed by multiple hybridization steps at 40ºC. The slides were finally counterstained using Gil's Hematoxylin to visualize nuclei. The slides were then imaged at 200X magnification with an Olympus FV10i confocal microscope (Olympus, Central Valley, PA).

3.3.12 Fluorescent *in situ* hybridization (FISH)

To establish the identity of the SIVsab target cells, fluorescent *in situ* hybridization (FISH) was performed as previously described (230). In brief, 5-µm tissue sections were mounted on Superfrost Plus Microscope Slides (Fisher Scientific), heated at 60°C for 1 h, deparaffinized, and then rehydrated. Heat-induced epitope retrieval was performed by placing slides in in 10 mM Citrate (pH 6.0) containing 0.05% Tween-20 or Pretreatment-2 buffer (Advanced Cell Diagnostics) at 100°C for 5 mins followed by immediate immersion into molecular biology-grade H_2O at RT. The slides were then incubated for 5 mins at 37°C in a Tris-buffered solution containing 2 mM $CaCI_2$ and proteinase K (1.25 µg/mL), then washed

in molecular biology-grade H_2O, then acetylated (0.25% acetic anhydride) for 20 mins and placed in 0.1 M triethanolamine (pH 8.0) until hybridization. The slides were then covered with hybridization solution (50% deionized formamide, 10% dextran sulfate, 0.6 M NaCI, 0.4 mg/mL yeast RNA (Ambion Inc, Austin, TX), and 1X Denhardt medium in 20 mM HEPES buffer (pH 7.2, with 1 mM EDTA) containing 100-400 ng/mL pooled SIV riboprobes and hybridized for 18 hrs at 48°C. After hybridization, slides were rinsed with 5X SSC (1X SSC=0.15 M NaCL+0.015 M Sodium Citrate) at 42°C for 20 mins , 2X SSC in 50% formamide at 50°C for 20 mins , and 1X RNA wash buffer (0.1M TRIS-HCL PH 7.5, 0.4M NaCL, 0.05M EDTA PH 8.6) at 37°C with ribonuclease A (25 µg/ml) and T1 (25 U/ml) for 30 mins . After rinsing with RNA wash buffer, 2X SSC, and 0.1X SSC at 37°C for 15 mins each, sections were transferred to 1X Tris-buffered saline (TBS), (Boston BioProducts, Ashland, MA) containing 0.05% Tween-20. Tissues were blocked in TBS with Tween-20 containing 2% donkey serum for 1 hour at RT, then incubated with antibodies specific to the markers of interest in TBS-Tween-20 containing 2% donkey serum overnight at 4°C. Slides were then rinsed in TBS-Tween-20, incubated with donkey anti-goat Alexa594, donkey anti-mouse Alexa488, and donkey anti-rabbit Alexa647 (Invitrogen, Carlsbad, CA) for 1 hour at RT in the dark and then rinsed with TBS-Tween-20. Slides were incubated with 0.1% Sudan Black B in 70% ethanol (ENG Scientific, Clifton, NJ) and 1X TBS for 30 mins at RT to quench autofluorescence then incubated with 300 nM DAPI for 10 mins. Slides were rinsed, mounted with Prolong® Gold (Invitrogen) and imaged on an Olympus FV10i confocal microscope (Olympus) (230). All images were captured at 600X magnification using a 60X phase contrast oil-immersion objective and by imaging using sequential mode to separately capture the fluorescence from the different fluorochromes.

3.3.13 Flow cytometry

Cells were stained for flow cytometry as described (46, 193). Briefly, whole blood was lysed using fluorescence-activated cell sorter (FACS) lysing solution (BD Biosciences, San Jose, CA). Lysed blood

and isolated immune cells from LNs and intestine were incubated at 4°C for 30 mins with monoclonal antibodies (mAbs). Cells were then washed with phosphate-buffered saline (1X PBS) and fixed with a BD stabilizing fixative (BD Bioscience). For intracellular stains, after the surface stain was completed, the lymphocytes were fixed with a 4% paraformaldehyde solution for 20 mins. Cells were then washed with 1X PBS, followed by a wash with 0.1% saponin solution and another mAb incubation. Cells were next washed with 0.1% saponin solution and fixed with a BD stabilizing fixative. The absolute counts of peripheral blood lymphocytes were determined by using Trucount tubes (BD Bioscience) (225, 231). Blood $CD45^+$ cells were quantified using 50 µL whole blood stained with antibodies in the TruCount tubes that contained a predefined number of fluorescent beads to provide internal calibration. The $CD4^+$ and $CD8^+$ T-cell counts were then calculated using the ratio of $CD4^+$ and $CD8^+$ T cells to $CD45^+$ cells in the whole blood at the same time point.

Immunophenotyping of the immune cells isolated from blood, LNs, and intestine was performed using fluorescently conjugated mAbs (Appendix A), chosen to characterize a wide range of immune cell types and markers of activation, proliferation, apoptosis and cellular homing. Live/Dead stains were included only for the innate cell panels (natural killer cells, macrophages, and DCs). For the adaptive cell type panels, dead cells were omitted by gating first for singlets. An example of a gating strategy for primary T-cell populations ($CD3^+$ $CD4^+$, $CD8^+$) and T-cell subsets (effector memory, central memory, naïve) is shown in Appendix B. Data were acquired on an LSR-II flow cytometer (Becton Dickinson, Franklin Lakes, NJ) and analyzed using the Flowjo software version 10.1r5 (Tree Star Inc, Ashland, OR).

3.3.14 Statistical analysis of data

To compare changes in the immune cell populations between preinfection and postinfection time points from the same AGMs, we used the nonparametric two-tailed Wilcoxon matched-pairs signed ranks test, with a $p \leq 0.05$. For comparisons between the flow cytometry results from the control and infected

AGMs, we used the unpaired nonparametric Kruskal-Wallis test, followed by a Dunn's multiple means comparison test to correct for multiple comparisons. The family-wise significance and confidence levels were set at 0.05. All tests were performed using the Graphpad Prism 7 Software (Graphpad Software Inc, La Jolla, CA).

3.4 Experimental results

3.4.1 Intrarectal SIVsab transmission is characterized by rapid establishment of plasma viremia

Viral load testing by RT-PCR and conventional qPCR showed that viremia was established towards the end of the ramp-up period, at 6 dpi. The ramp-up viral loads ranged between 10^3 and 10^4 (geometric mean [GM] 1.25 x 10^4) vRNA copies/mL plasma. Virus remained below the detectable limits of standard qPCR earlier during the ramp-up period, at 4-5 dpi. Following ramp-up, plasma viremia increased sharply by the peak of viral replication, with plasma viral loads rising to 10^5-10^7 (GM 2.01 x 10^6) vRNA copies/mL plasma. These elevated plasma viral loads were maintained for the entirety of the peak period, with similar levels of virus at both 9 dpi and 12 dpi. Entering the early chronic stage of infection, set-point viral loads were established at 10^4-10^5 (GM 3.62 x 10^4) vRNA copies/mL plasma. Note that the animals in the set-point group had additional blood draws at the peak of viral replication. These additional samples were also tested and were found to be within the same range as the peak group animals, as shown in Figure 2.

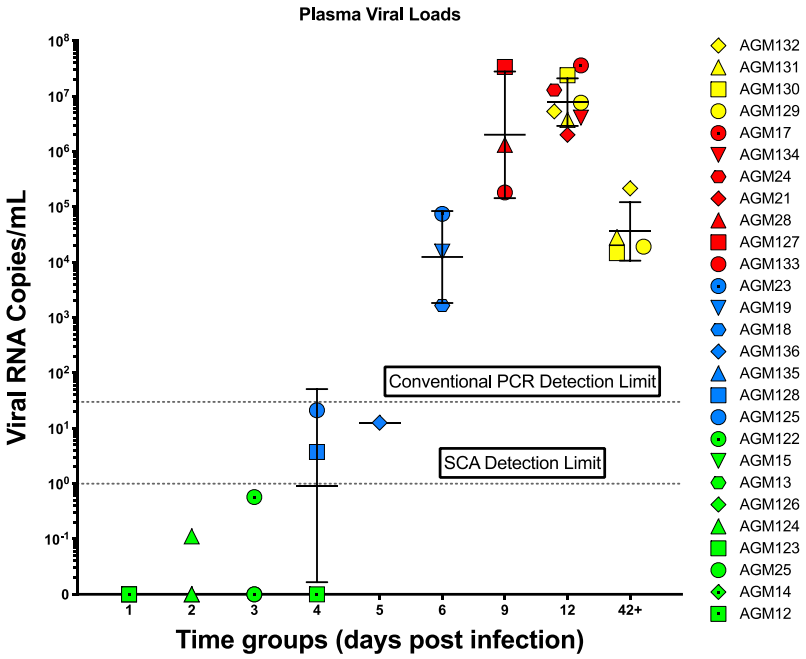

Figure 2: Plasma viral loads in African green monkeys (AGMs) intrarectally-infected with SIVsab90218. The plasma viral loads are shown as $\log_{10}$ values. Each animal is represented by symbol with a unique color and shape combination, as shown in the key to the right. Blood from chronically infected animals were sampled once at acute infection and once during early chronic infection, as indicated by the appearance of the symbols for those animals twice. Limits of detection for conventional and single copy assays are shown by dotted lines. The colors represent the different stages of infection as defined by viral replication status: preramp (green), ramp-up (blue), peak (red) and set-point (yellow). The bars represent the geometric mean and geometric standard deviation of each group. Animals that were negative for viremia are plotted directly on the x-axis.

The conventional qPCR employed for measuring plasma viremia has a detection limit of 30 vRNA copies/mL; therefore, the samples that had tested negative by qPCR (1-5 dpi) were tested with SIV-adapted SCA, which has a theoretical limit of 1 copy/mL (226). By SCA, the ramp-up animals were found to have viral loads within the range of 10^0-10^1 (GM 1.01 x 10^1) vRNA copies/mL plasma (Figure 2). Most of the preamp animals tested negative, even by when tested with SCA. However, two animals did exhibit detectable viremia: AGM122 (3 dpi) and AGM124 (2 dpi). For these animals, AGM122 had a viral load of 5.75 x 10^{-1} viral RNA copies/mL plasma and AGM124 had a viral load of 1.12 x 10^{-1} viral RNA copies/mL plasma (Figure 2). While these values technically fall below the theoretical limit of detection for SCA, the

plasma taken from those animals was retested by SCA two more times and returned positive results both times, so the data was considered potentially valid.

3.4.2 CSF viral loads mirror the plasma viral loads

We next monitored the viral loads in the CSF samples collected at the time of necropsy. CSF was processed in the same manner as plasma using the same methodology (see 3.3.4). By conventional qPCR, we detected virus in several of the ramp-up group animals: AGM125 (4 dpi) at 4.62 x 10^2 vRNA copies/mL and AGM136 (5 dpi) at 4.71E x 10^2 vRNA copies/mL, as shown in Figure 3.

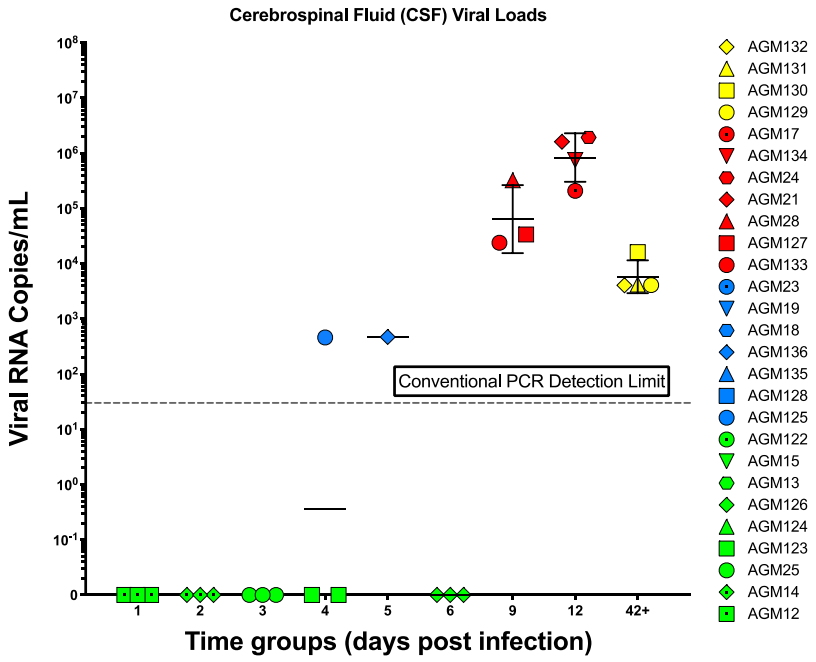

Figure 3: Cerebrospinal fluid (CSF) SIVsab90218 viral loads in African green monkeys (AGMs) during acute and early chornic infection.
The CSF viral loads are shown as $\log_{10}$ values. Each animal is represented by a unique color/shape combination (shown on the right). The limit of detection for conventional qPCR (30 viral RNA copies/mL plasma) is indicated by a dotted line. The colors represent the different stages of infection as defined by viral replication status: preramp (green), ramp-up (blue), peak (red) and set-point (yellow). The bars represent the geometric mean and geometric standard deviation of each group. Animals that were negative for viremia are plotted directly on the x-axis.

However, no virus was detected in any other animals during the ramp-up period of viral replication. Unlike in the plasma, peak CSF viral loads varied significantly from 9 dpi and 12 dpi. The animals sacrificed at 9 dpi exhibited viral loads from 10^4-10^5 (GM 6.41 x 10^4) vRNA copies/mL, while the 12 dpi viral loads ranging from 10^5-10^6 (GM 8.37 x 10^6) vRNA copies/mL (Figure 3). CSF viral loads dropped sharply by establishment of set-point replication, averaging just 10^3-10^4 (GM 8.37 x 10^3) vRNA copies/mL. It should be noted that the volume of CSF obtained was not great enough to facilitate SCA, so testing was limited to conventional qPCR.

3.4.3 SIVsab rapidly disseminates systemically from the site of inoculation

Following extraction and purification of total DNA/RNA from the tissues, vRNA and vDNA was quantified via qPCR utilizing primers specific for SIVsab *gag* and RM CCR5. The first round of tissue viral load testing focused on tissues from the site of inoculation, including: rectum, distal colon, and regional lymph nodes (LNs). By examining these tissues, several of the sections that were collected were identified as potential foci of early viral replication. All of these sections came from AGMs in the preramp-up group (1-3 dpi). Both vRNA and vDNA were measurable in tissues from this group, though the vRNA was somewhat more readily detectable (15 $vRNA^+$ tissues from 1-3 dpi animals $^+$ *versus* 9 $vDNA^+$ tissues from 1-3 dpi animals), as shown in Figure 4 and Figure 5.

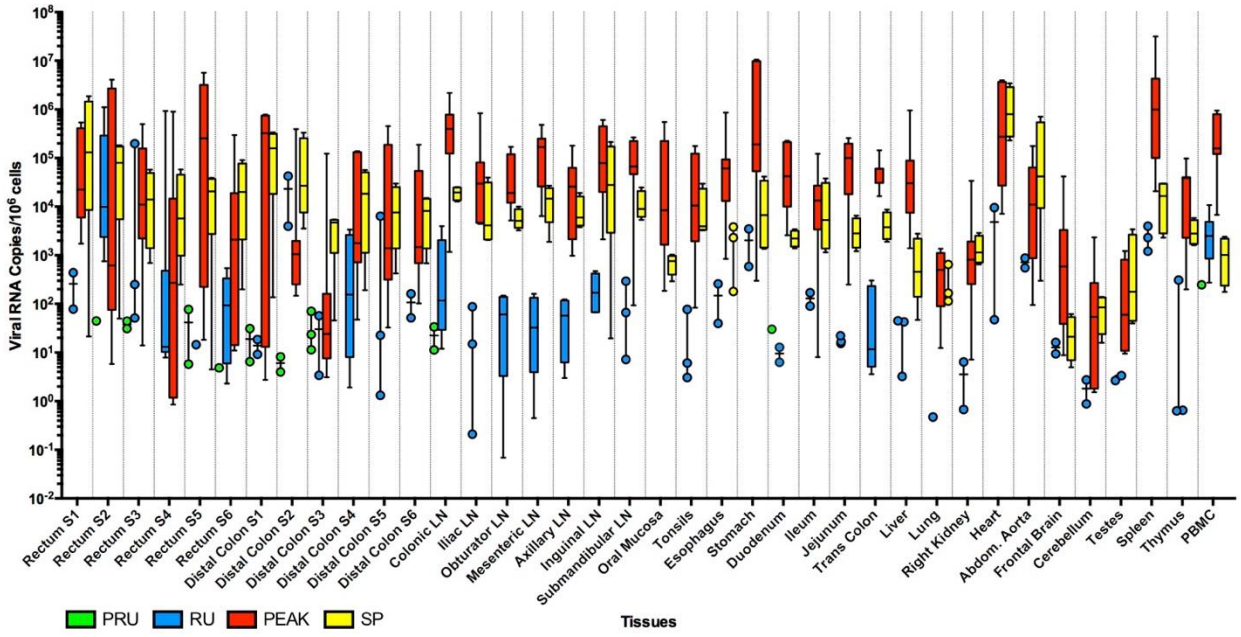

Figure 4: Total viral RNA in tissues of SIVsab-infected African green monkeys (AGMs).

The total viral RNA (i.e, replicative and nonreplicative genomes, cell-associated and cell-free genomes) from each of the 38 tissues tested are shown, with dotted lines delineating each individual tissue. Viral RNA loads are shown on a logarithmic scale and represent the total number of virus RNA genome copies per 106 somatic cells. The names of the tissues are listed below the x-axis. The data are shown as box-whisker plots displaying the median, 1st and 3rd quartiles and the min/max outliers. The colors represent the different stages of infection as defined by viral replication status: preramp (green), ramp-up (blue), peak (red) and set-point (yellow). For the rectum and distal colon, S1-S6 indicates from which strip of tissue the section was taken.

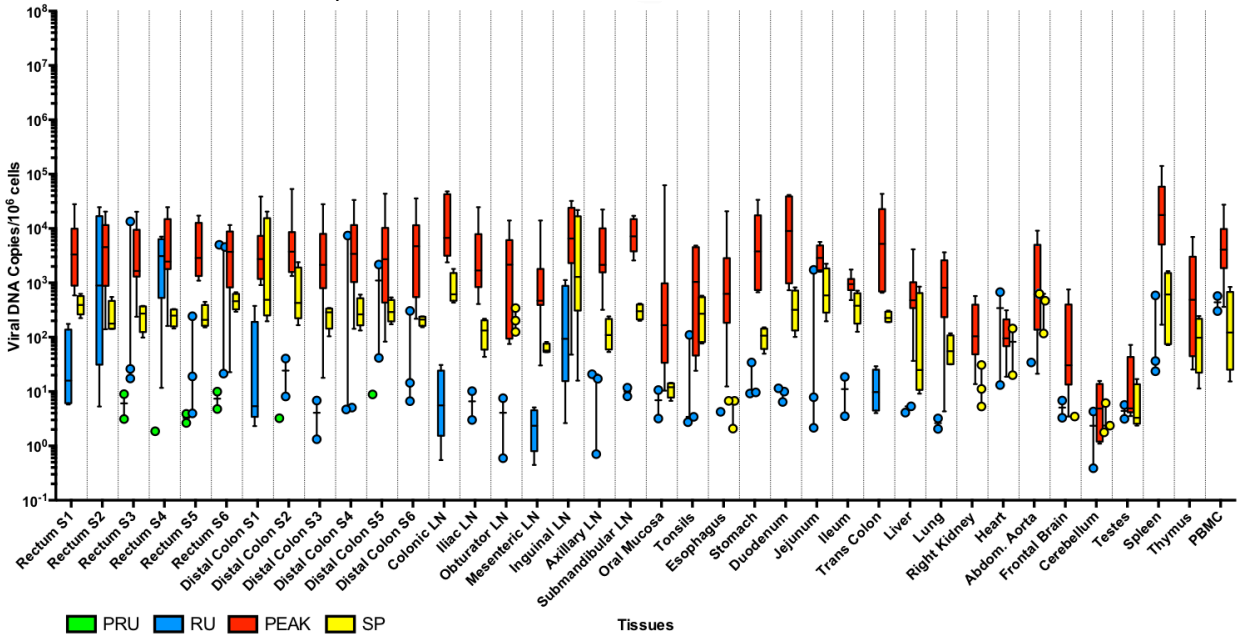

Figure 5: Total viral DNA in tissues of SIVsab-infected African green monkeys (AGMs).

The total viral DNA (i.e., replicative and nonreplicative genomes, cell-associated and cell-free genomes) from each of the 38 tissues tested are shown, with dotted lines delineating each individual tissue. Viral DNA loads are shown on a logarithmic scale and represent the total number of virus DNA genome copies per 10^6 somatic cells. The names of the tissues are listed below the x-axis. The data are shown as box-whisker plots displaying the median, 1st and 3rd quartiles and the min/max outliers. The colors represent the different stages of infection as defined by viral replication status: preramp (green), ramp-up (blue), peak (red) and set-point (yellow). For the rectum and distal colon, S1-S6 indicates from which strip of tissue the section was taken.

Some of the preramp-up animals had multiple sections containing either vRNA or vDNA (AGM25, AGM13, AGM124, AGM122), while others only had one (AGM126). Very early vRNA was additionally detected in the draining (colonic) LN, the duodenum, and the PBMCs, while very early vDNA was found solely at the site of inoculation. Taken as a whole, the viral loads for the tissues from the preramp-up animals were low, ranging from 10^0-10^1 (GM: 2.31 x 10^1) vRNA copies/10^6 somatic cells and only 10^0 (GM: 4.49 x 10^0) vDNA copies/10^6 somatic cells.

After the preramp-up period, of the 38 tissue types tested, 37 had detectable levels of vRNA and 36 had detectable levels of vDNA by the ramp-up period (4-6 dpi); even immunoprivileged sites like the testes and the brain tested positive for both vRNA and vDNA, though they had the lowest viral loads on average. The viral loads were highly variable between tissues, ranging from between 10^{-1}-10^5 vRNA copies/10^6 somatic cells and 10^{-1}-10^4 vDNA copies/10^6 somatic cells. The viral loads at the peak of virus replication, which varied widely amongst the tissues tested, reached from 10^0-10^7 vRNA copies/10^6 somatic cells and 10^0-10^4 vDNA copies/10^6 somatic cells. The early chronic stage of infection (i.e., set-point) also was higher than the ramp-up period, but still lower than the peak on average. At the set-point of SIVsab replication the viral loads alternated between 10^0-10^6 vRNA copies/10^6 somatic cells and 10^0-10^4 vDNA copies/10^6 somatic cells (Figures 4 & 5).

3.4.4 Viral RNA is observable in the mucosa and the lymphoid aggregates in the rectum and distal colon immediately following inoculation

To support the presence of vRNA in the mucosa of rectum and distal colon and the draining LNs, we utilized RNAscope to directly visualize vRNA via microscopy, as shown in Figure 6.

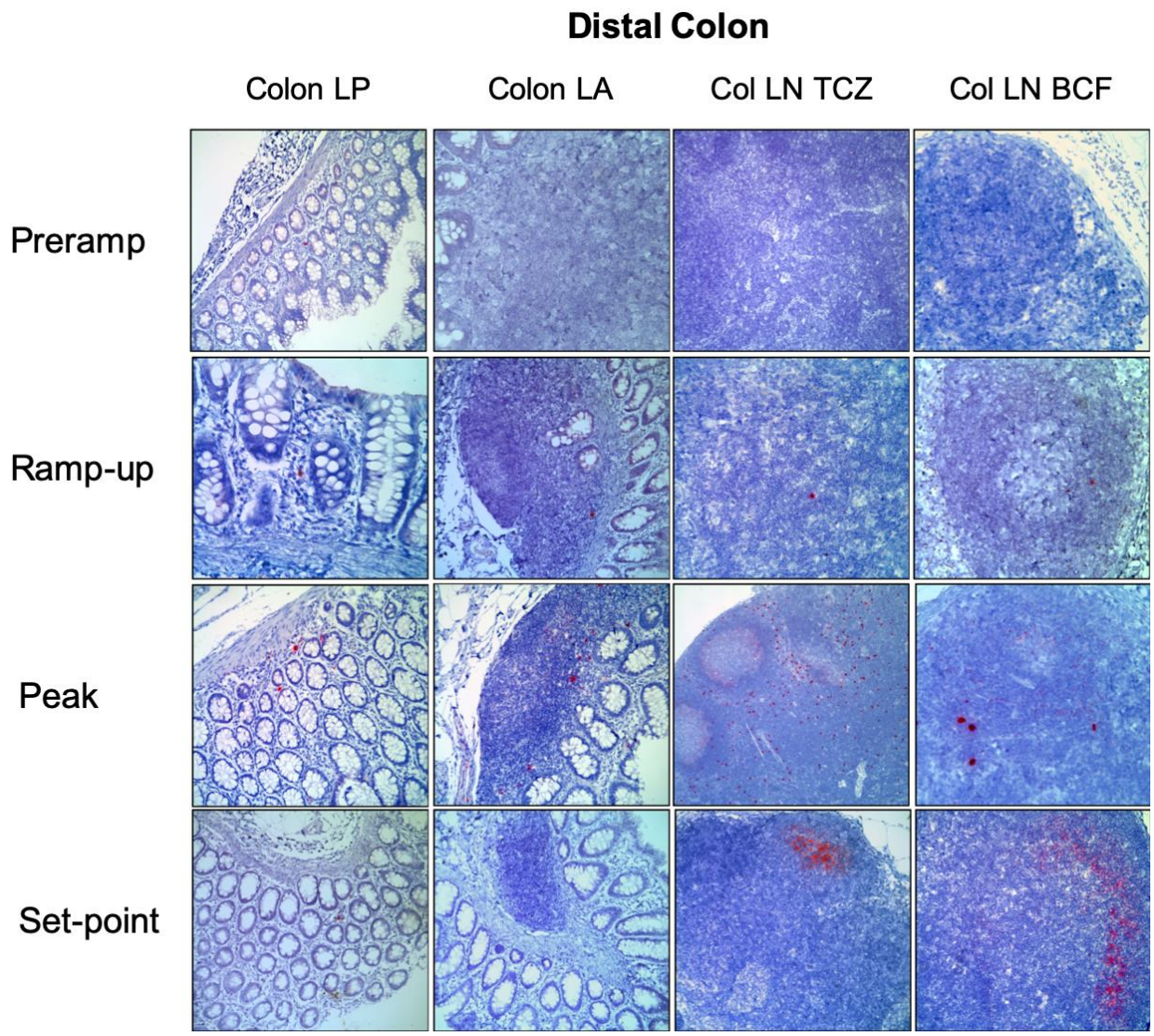

Figure 6: RNAscope for SIVsab RNA at the site of inoculation and in the draining lymphatics.
RNAscope was performed on multiple sections of the rectum and the distal colon, which represent the site of inoculation. Only images from the distal colon are shown for consistency. Viral RNA was stained red, with the surrounding tissue counterstained purple. Each column represents a different tissue type and each row represents a different time group. The following abbreviations were used: (i) LP, lamina propria; (ii) LA, lymphoid aggregate; (iii) TCZ, T-cell zone; (iv) BCF, B cell follicle. All images were captured at 200X magnification with a Olympus FV10i confocal microscope. The time groups are shown on the left side of the figure, reflecting the status of viral replication, with: preramp (1-3 dpi), ramp-up (4-6 dpi), peak (9-12 dpi) and set-point (42 dpi).

In several of the AGMs from the preramp-up group (1-3 dpi), virus was observed in lamina propria of the distal colon, along with the colonic lymphoid aggregates. Virus was also found in the colonic LN from these animals. However, vRNA overall was extremely rare at these time points. Virus was found less frequently in lamina propria and lymphoid aggregates of the colon and more commonly in both the colonic and iliac LN. Within these draining lymphatics, the virus was localized mostly to the T-cell zones, but also found occasionally within the B cell follicles (Figure 6).

These rare occurrences of virus are in contrast to the amount of virus found throughout the site of inoculation and the draining lymphatics later during infection. At the peak of viral replication, SIVsab was frequently found in both the lamina propria and lymphoid aggregates of the colon. There was additionally extensive virus replication in the LNs in the T-cell zones, with extensive trapping of the virus by follicular DCs. Again, virus also present in B cell follicles, though much more frequently than during the early stages of infection. (Figure 6).

Later, by the establishment of set-point viral replication, viral presence has declined to levels similar to early infection. Virus was detected occasionally in the lamina propria, but only rarely in the lymphoid aggregates. In the draining LNs, the majority of virus was trapped by follicular DCs, with little to no vRNA signal in the T-cell zones and B cell follicles (Figure 6). Overall, the presence of SIVsab detected by RNAscope follows the trend in both the plasma and the tissue of the SIV-infected AGMs.

3.4.5 Multiple transmitted/founder viruses established infection in each animal, though a mucosal bottleneck still occurred

Using SGA, we evaluated the total number of transmitted/founder viral variants that established infection in each of the animals that for which viremia was confirmed by conventional qPCR, starting at 6 dpi and extending through the peak and set-point periods. Each animal in these time groups was infected

with multiple transmitted/founder variants, with the total number of transmitted/founder viruses per AGM ranging from 3-10, as shown in Figure 7.

NHP	DPI	Variants
AGM18	6	5
AGM19	6	5
AGM23	6	8
AGM133	9	3
AGM127	9	8
AGM28	9	10
AGM21	12	8
AGM24	12	8
AGM134	12	5
AGM17	12	9
AGM129	12	10
AGM130	12	8
AGM131	12	7
AGM132	12	7

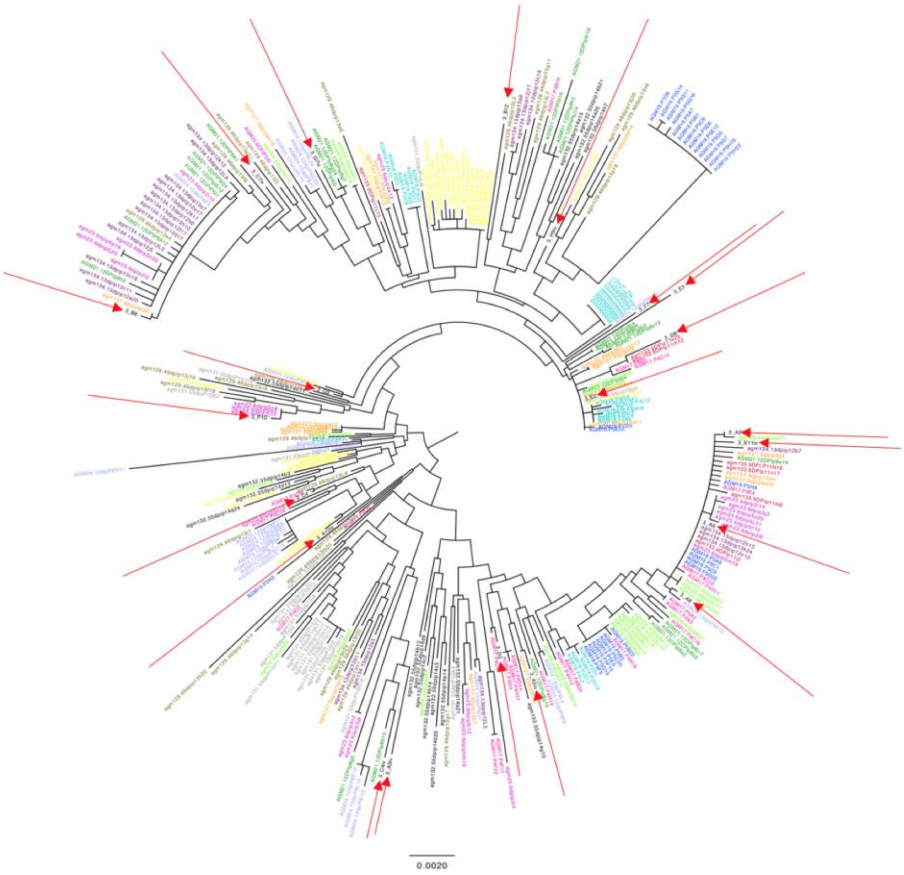

Figure 7: Single genome amplification of SIVsab transmitted/founder (T/F) viruses.
The totality of T/F viruses from the animals listed on the left are shown as a circular phylogenetic tree. The color of the variant name corresponds to the color of the animal name, with the total number of T/F variants per animal listed to the right of the name. Viruses indicated by the red arrows represent the viral species found in the original inoculum used to infect the animals. The set-point animals (AGM129-AGM132) represent viral diversity from blood draws at 12 dpi. All sequences were aligned using MUSCLE Alignment implemented in Geneious (https://www.geneious.com/) and then manually inspected and optimized. Phylogenetic trees were based on nucleotide sequences and constructed using the neighbor-joining method with Tamura-Nei distance model.

Phylogenetic analysis of transmitted/founder viruses from all the animals tested show that the variants lack any clear pattern of relationship to each other. There also appears to be no correlation between the diversity of the transmitted/founder viruses when compared to viruses in the original inoculum (Figure 7, red arrows).

3.4.6 SIVsab target cells at the site of inoculation are of the $CD3^+$ lineage and not of the myeloid lineage

It has been well-established that the primary target cell of both HIV and SIV are $CCR5^+$ $CD4^+$ T cells (7, 38, 109, 111, 113, 114). However, there has been some research to suggest that there might be alternative target cells for SIV, including macrophages, particularly in the case of SIVsab, where macrophages in the CNS of AGMs had previously been shown to support viral replication without disease progression (124). Furthermore, SIVsab is dual-tropic for both CCR5 and CXCR4, as well as the alternative coreceptor CXCR6 (see 1.4.2) (6, 11, 138). To establish the identity of the initial founder population of target cells at the site of inoculation, rectum and colon section were tested with FISH specific for SIVsab vRNA, $CD3^+$ T cells and myeloid lineage cells ($CD68^{neg}$ $CD163^+$ $HAM56^+$) in all the AGMs, as shown in Figure 8.

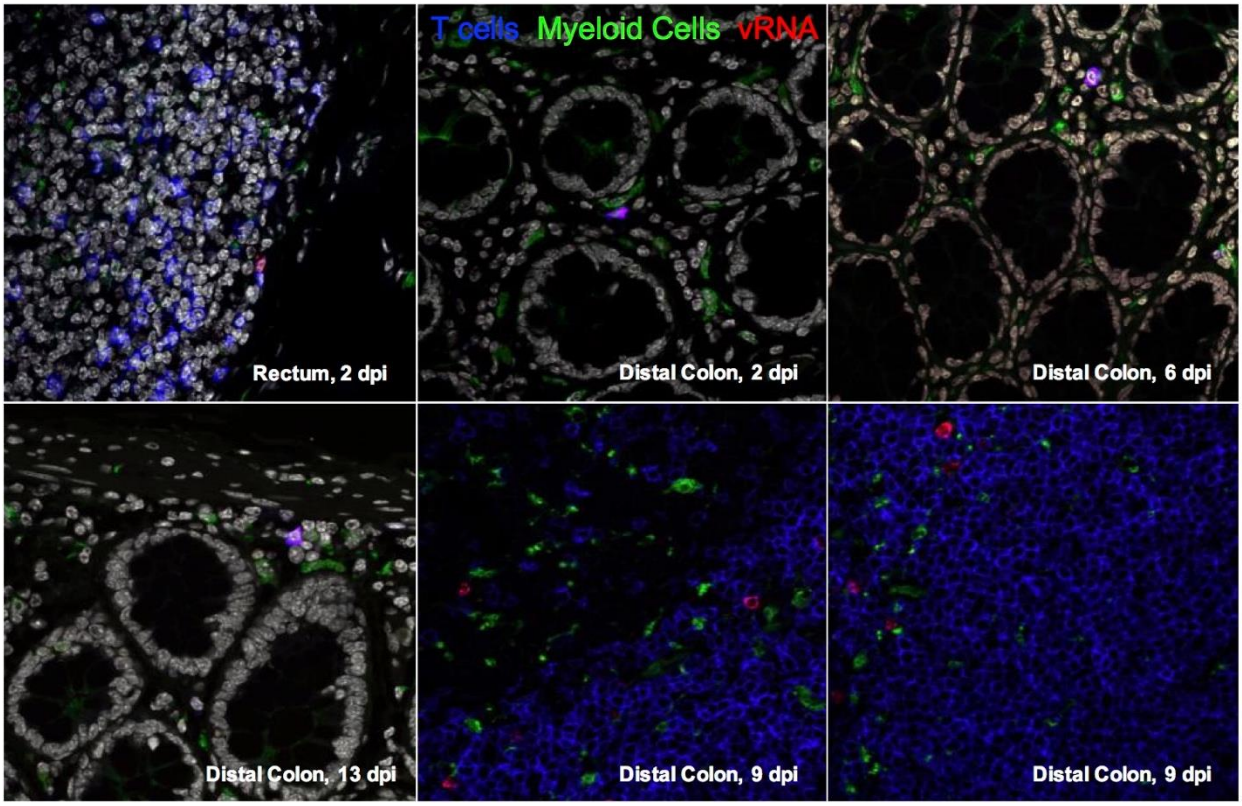

Figure 8: Fluorescent in situ hybridization (FIS) for SIVsab RNA, T cells and myeloid lineage cells. FISH was used to identify with which cells the SIVsab RNA genomes colocalize. Viral RNA copies are shown in red, $CD3^+$ T cells are shown in blue and myeloid lineage cells ($CD68^+$ $CD163^+$) are shown in green. The tissue type and day post infection are shown in white in the lower righthand corner of each image. All images were captured at 600X magnification with an Olympus FV10i confocal microscope using a 60X phase contrast oil-immersion objective and by imaging using sequential mode to separately capture the fluorescence from the different fluorochromes.

FISH showed that vRNA colocalized with $CD3^+$ T cells, but not with any myeloid lineage cells, in all the tissues tested. Moreover, SIVsab vRNA was once again found in both the rectum and distal colon as early as 2 dpi, with virus in lamina propria and the lymphoid aggregates. Even later during the ramp-up and peak periods of viral replication, vRNA consistently colocalized only with T cells, strongly indicating the earliest target cells of SIVsab following intrarectal inoculation are T cells resident to lamina propria of the rectum and distal colon. It should be noted that that images were not quantified, and these results are representative of the general trends observed in the tissues.

3.4.7 $CD4^+$ and $CCR5^+$ $CD4^+$ T-cell populations are not significantly altered at the site of inoculation

Having established that the primary target cells at the site of inoculation are T cells, the populations of $CD4^+$ T cells isolated at the time of necropsy from rectum were analyzed with flow cytometry to measure any changes in cell populations in response to infection, especially any depletion of $CD4^+$ T cells. Here, the overall number of $CD4^+$ T cells (Figure 9A) showed a decline from baseline levels over the course of infection, though this decline lacked significance. In contrast, the number of $CCR5^+$ $CD4^+$ T cells (Figure 9B) actually remained relatively stable, with little variation between the time groups.

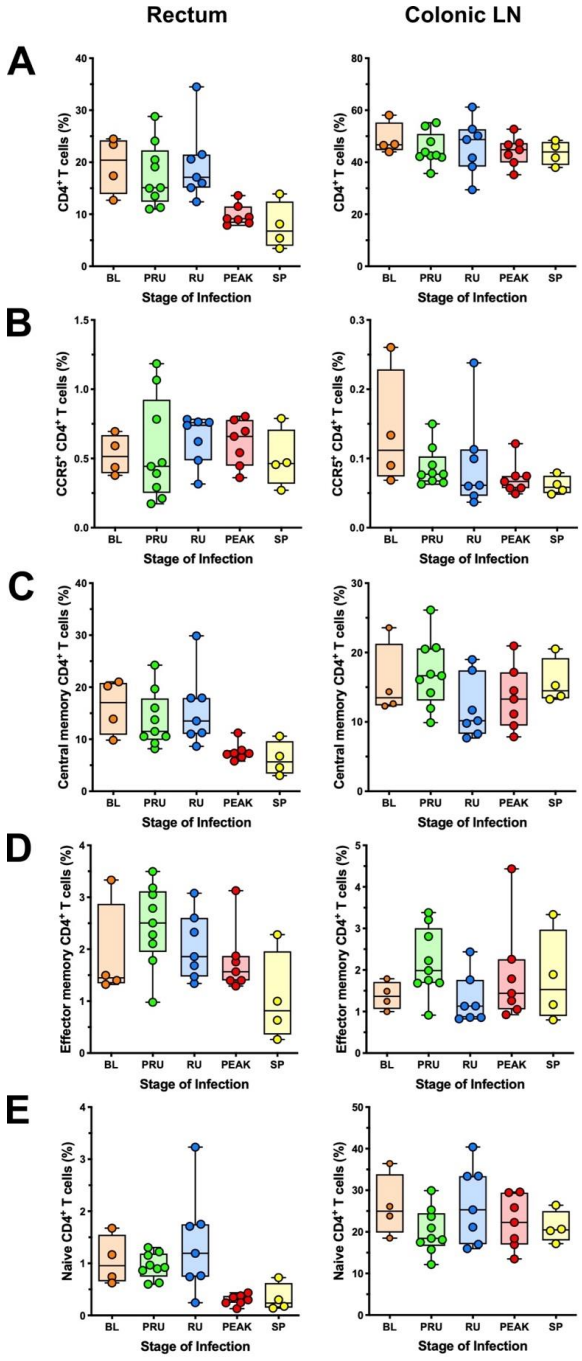

Figure 9: CD4$^+$ T-cell populations and subsets at the site of inoculation in SIVsab-infected AGMs.
Percent populations of total CD4$^+$ T cells (A), CCR5$^+$ CD4$^+$ T cells (B), CD4$^+$ central memory (CD28$^+$ CD95$^+$ CCR7$^+$) (C), effector memory (CD28$^-$ CD95$^+$ CCR7$^-$) (D), and naïve cells (CD28$^+$ CD95$^-$ CCR7$^+$) (E) in the rectum and colonic LN. The data are shown as box-whisker plots displaying the median, 1st and 3rd quartiles and the min/max outliers, with individual points representing each animal. The five groups are based on the days postinfection, with: BL (baseline, preinfection), PRU (preramp, 1-3 dpi), RU (ramp-up, 4-6 dpi), PEAK (peak, 9-12dpi) and SP (set-point, 46-55 dpi). The colors represent the different stages of infection as defined by viral replication status: baseline (orange), preramp (green), ramp-up (blue), peak (red) and set-point (yellow). Asterisks indicates statistical significance when compared to baseline values, with *=$p<0.05$.

In the colonic LN, which is the closest LN to the site of inoculation, the trend was the opposite. Here, the overall $CD4^+$ populations remained relatively unchanged over the course of infection. By comparison, the relative number of $CCR5^+$ $CD4^+$ T cells appeared to decrease somewhat by the peak of infection, though this decrease was also not significant (Figure 9B).

The populations of the various subsets of $CD4^+$ T cells (effector memory, central memory, and naïve) also were not significantly changed at the site of inoculation or in the colonic LN (Figure 9C-E).

3.4.8 $CD8^+$ T-cell populations are not significantly altered at the site of inoculation

In general, the relative number of $CD8^+$ T cells were generally stable over the entire course of the infection in the colonic LN and rectum. The overall $CD8^+$ T-cell population and the memory subsets in the rectum did exhibit a tendency to decrease during the ramp-up period (4-6 dpi) and increase by the establishment of set-point viral replication (46-55 dpi), but these trends were not significant (Figure 10A-D). There were no trends or significant changes in the colonic LN in the general $CD8^+$ T-cell population or the various subsets (Figure 10A-D).

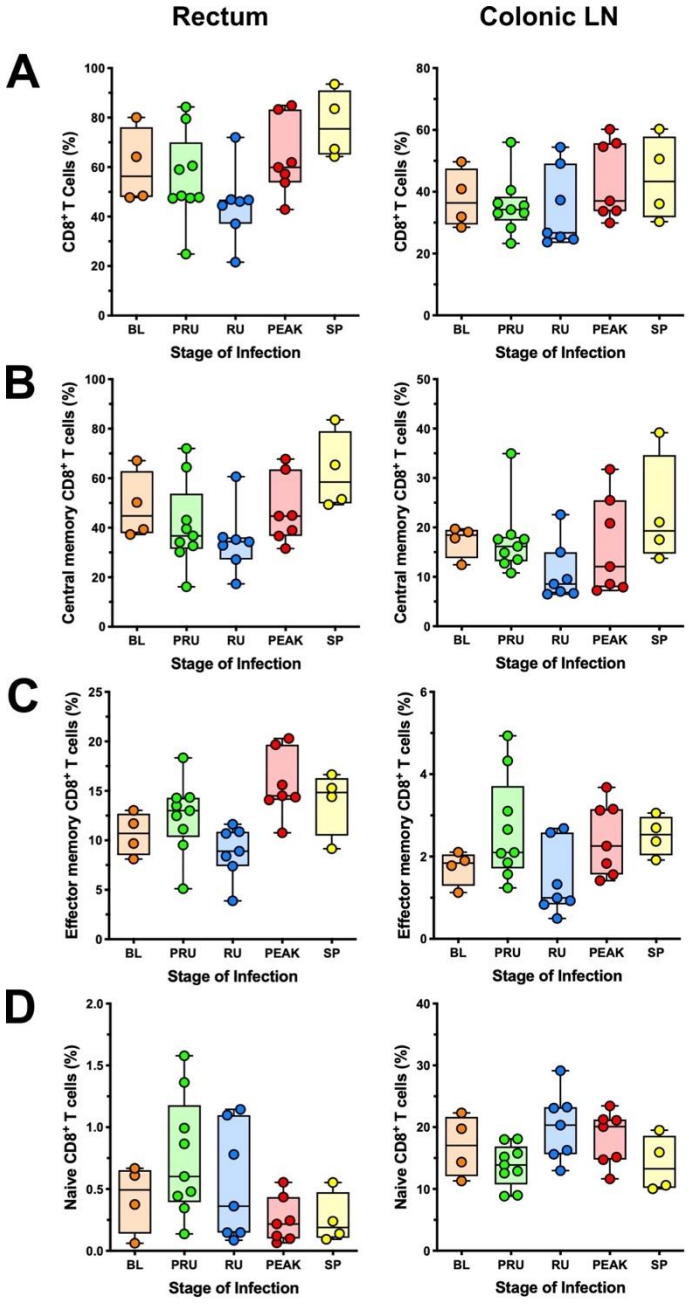

Figure 10: CD8$^+$ T-cell populations and subsets at the site of inoculation in SIVsab-infected AGMs.
Percent populations of general CD8$^+$ T cells (A), CD8$^+$ central memory (CD28$^+$ CD95$^+$ CCR7$^+$) (B), effector memory (CD28$^-$ CD95$^+$ CCR7$^-$) (C), and naïve cells (CD28$^+$ CD95$^-$ CCR7$^+$) (D) in the rectum and colonic LN. The data are shown as box-whisker plots displaying the median, 1st and 3rd quartiles and the min/max outliers, with individual points representing each animal. The five groups are based on the days postinfection, with: BL (baseline, preinfection), PRU (preramp, 1-3 dpi), RU (ramp-up, 4-6 dpi), PEAK (peak, 9-12dpi) and SP (set-point, 46-55 dpi). The colors represent the different stages of infection as defined by viral replication status: baseline (orange), preramp (green), ramp-up (blue), peak (red) and set-point (yellow). Asterisks indicates statistical significance when compared to baseline values, with *=$p<0.05$.

3.4.9 $CD20^+$ cell populations decrease in the rectum, but the innate immune cell types are not significantly altered in response to infection

At the site of inoculation, the levels of $CD20^+$ B cells declined steadily over the course of infection, becoming significantly (*p=0.0435*) decreased from baseline levels by early chronic infection (Figure 11A). This is in contrast to the populations of $CD20^+$ B cells in the colonic LN, which were not significantly altered, even by establishment of set-point viral replication, when a humoral response would have already been established (106).

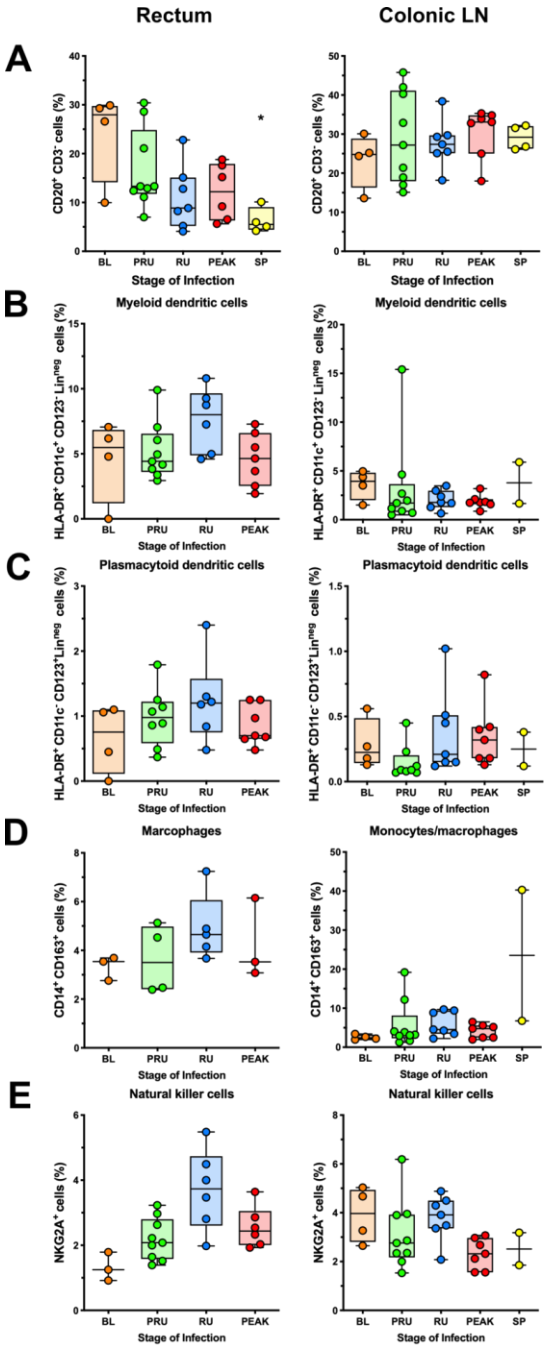

Figure 11: CD20^{+} B cells and innate immune cell populations at the stie of inoculation in SIVsab-infected AGMs.

Percent populations of general CD20^{+} B cells (A), myeloid dendritic cells (HLADR^{+} CD11c^{+} CD123^{-} Lineage^{neg} [CD3^{-} CD20^{-} CD14^{-}]), (B), plasmacytoid dendritic cells (HLADR^{+} CD11c^{-} CD123^{+} Lineage^{neg} [CD3^{-} CD20^{-} CD14^{-}]), (C), and natural killer cells (D) in the rectum and colonic LN. The data are shown as box-whisker plots displaying the median, 1st and 3rd quartiles and the min/max outliers, with individual points representing each animal. The five groups are based on the days postinfection, with: BL (baseline, preinfection), PRU (preramp, 1-3 dpi), RU (ramp-up, 4-6 dpi), PEAK (peak, 9-12dpi) and SP (set-point, 46-55 dpi). The colors represent the different stages of infection as defined by viral replication status: baseline (orange), preramp (green), ramp-up (blue), peak (red) and set-point (yellow). Asterisks indicates statistical significance when compared to baseline values, with *=p<0.05.

The populations of myeloid dendritic cells (mDCs) and plasmacytoid dendritic cells (pDCs), which are lineage negative ($CD3^-CD20^-CD14^-$), $HLADR^+$ cells, remained unchanged throughout the course of acute infection in both the colonic LN, and the rectum (Figure 11B & C). There were also no significant alterations in the levels of monocyte/macrophage and NK cells in the rectum or colonic LN (Figure 11C & D). Unfortunately, our analysis of these populations was limited by the availability of cells from some of the animals, which precluded staining for DCs, monocytes/macrophages and natural killer (NK) cells. It should be noted that this includes the entire set-point group (46-55 dpi), which are therefore absent from the analysis for the rectum. The reason for this discrepancy was that the staining for the T-cell and $CD20^+$ cell populations were given priority, meaning that when there was only a small number of cells available, cells were aliquoted for those stains first. However, for the DC, monocytes/macrophage and NK populations in the colonic LN, only two of the four set-point animals were even stained at all. This was not the result of low cell counts, but due to a technical error with the staining; an attempt was made later to repeat the stains with cryogenically preserved cells from those set-point animals, but the cell viability was too low.

3.4.10 $CD4^+$ and $CD8^+$ T cells are not significantly activated at the site of inoculation

To estimate overall immune cell activation levels, three different activation markers were chosen: HLADR, CD38, and CD69. Examining the total $CD4^+$ T-cell population in the rectum and colonic LN for expression of these markers, we found no significant alteration in the levels of $CD4^+$ cells expressing HLADR and CD38 (Figure 12A) or CD69 (Figure 12B). While again there were no significant alterations, in the colonic LN there was a notable, though not significant, drop at the peak of infection in the level of $CD69^+$ $CD4^+$ T cells.

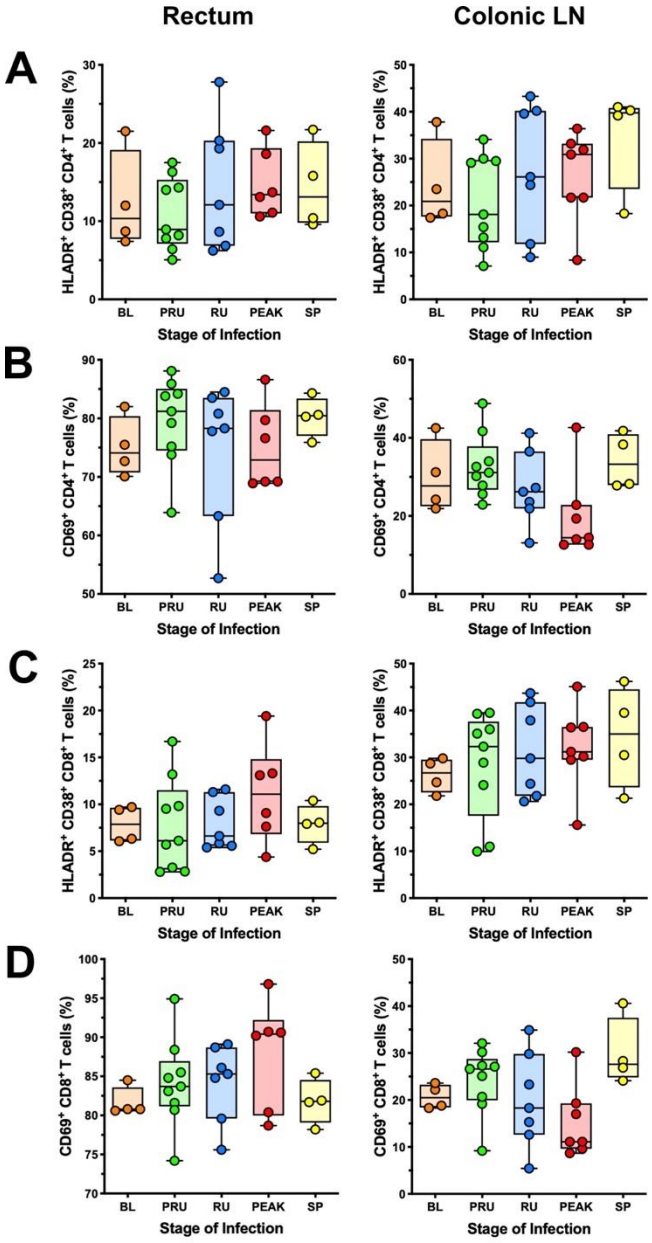

Figure 12: Immune activation of CD4$^+$ and CD8$^+$ T cells at the site of inoculation in SIVsab-infected African green monkeys (AGMs).

The fraction of CD4$^+$ T cells and CD8$^+$ T cells populations of expressing HLADR$^+$ and CD38$^+$ (A & C), and CD69$^+$ (B & D) in the rectum and colonic LN. The data are shown as box-whisker plots displaying the median, 1st and 3rd quartiles and the min/max outliers, with individual points representing each animal. The five groups are based on the days postinfection, with: BL (baseline, preinfection), PRU (preramp, 1-3 dpi), RU (ramp-up, 4-6 dpi), PEAK (peak, 9-12dpi) and SP (set-point, 46-55 dpi). The colors represent the different stages of infection as defined by viral replication status: baseline (orange), preramp (green), ramp-up (blue), peak (red) and set-point (yellow). Asterisks indicates statistical significance when compared to baseline values, with *=$p<0.05$.

In addition to the $CD4^+$ T cells, we also evaluated alterations in the activation and proliferation status of the total $CD8^+$ T-cell population during acute SIV infection of AGMs. As with the $CD4^+$ T-cell, there were no significant alteration in activation status in either the rectum or the colonic LN (Figure 12C & D**)**. Once again, there was a notable, but not significant, drop in CD69 expression at the peak of infection in the colonic LNs. This is different than in RMs, where pathogenesis is characterized by an expansion of $CD69^+$ $CD8^+$ T cells and $HALDR^+$ $CD8^+$ T cells in the LNs (232).

3.5 Discussion

Similar to other natural hosts of SIVs, AGMs are characterized by high levels of viral replication which persists for the remainder of their natural lifespans (8–11), as well as frequent horizontal transmission between adult AGMs (58–61). While AGMs and other natural hosts have certainly evolved a number of adaptions to prevent disease progression (see 1.3), it is clear that they are unable to directly inhibit the lifecycle of SIV during transmission and infection. For this reason, we have previously studied AGMs as model for mucosal HIV transmission, as it approximates all the stages of transmission without progression to AIDS (46, 78, 88). By studying the earliest events of SIV infection in AGMs, we expected to obtain not only insight on how natural hosts like AGMs avert progression to AIDS, but also identify means to better understand the dynamics of early HIV replication during mucosal transmission.

Characterization of the dynamics of SIVsab replication during the early stages of infection began with establishing the appearance of SIVsab in the plasma, after it had entered circulation. When using a conventional qPCR, plasma viremia first became detectable by 6 dpi, which was in agreement with previous studies of SIV-infected AGMs (Figure 2) (46, 78). However, by employing SCA adapted for use with SIVsab.sab92018 (with a limit of detection of 1 copy/mL plasma), we were able to demonstrate a very rapid viral spread, with detectable vRNA in the plasma from 3 out of 4 of the ramp-up animals, at 4-5 dpi (Figure 2). To confirm these findings, the SCA was run in triplicate for each of animals. All the plasma samples

tested positive, documenting the virus presence in circulation. Interestingly, these results are in agreement with a previous study, which demonstrated replicative virus in the PBMCs of *C. sabaeus* as early as 4 dpi, though the animals in that study were inoculated intravenously (85). This study therefore shows that following intrarectal SIVsab transmission in AGMs, the virus is rapidly disseminated in the plasma, within 4 dpi, the same timeframe as intravenous inoculation.

It should be noted that SIVsab RNA was also detected by SCA in the plasma of two of the animals sacrificed even earlier during infection, at 2 dpi (AGM124) and 3 dpi (AGM122) (Figure 2). However, the viral loads for both of these animals were at 10^{-1} vRNA copies/mL plasma, which falls below the technical limit of detection for the SCA. Also, for AGM124, the initial SCA returned only 2 out of 3 positive replicates. However, when the sample was retested, all 3 replicates returned positive. Even so, given the extremely low levels of virus, it can be assumed that this data may not be reliable and should be interpreted with caution. However, the possibility to detect the virus in circulation by 2 dpi would mean that viral replication and dissemination occur nearly simultaneously.

It was also found that during viral dissemination, SIVsab is able to gain access even to immunoprivileged sites, like the brain, as viral RNA was detectable in the CSF as early as 4-5 dpi even through conventional qPCR (Figure 3). While it is unusual that SIVsab was detectable in the CSF prior to virus in the plasma, studies of HIV have suggested that virus localized to the central nervous system may represent a separate, distinct population with different dynamics from the rest of the body (233). However, in terms of concentration, the peak and set-point levels of viral RNA present in the CSF were consistent with the levels found previously in both SIV infected RMs and AGMs, being about 1 log lower than plasma viral loads (124, 234, 235).

After documenting the rapid onset of plasma viremia, we next focused on assessing viral dynamics in tissues. In total, 38 different tissue sites were tested using qPCR of DNA and RNA extracted from snap frozen tissues. Invariably, both SIVsab DNA and RNA genomes were detected in all tissue sites by the peak of viral replication and into the early chronic stage of infection. Even during the ramp-up period of SIV replication at 4-6 dpi, 37 out of 38 tissues returned detectable levels of SIVsab DNA/RNA (Figures 4

& 5). Considering the findings from the plasma viremia analysis, with the virus entering circulation by at least 4 dpi, if not earlier, this likely represents virus seeding throughout the body via the bloodstream. This means that following mucosal transmission, not only is viral dissemination rapid, it is also pervasive.

However, it should be noted that one complicating factor in the survey of the tissue viral loads was the presence of blood within the tissue. The animals were not perfused with saline at the time of necropsy and no special measures were taken (i.e., washing or rinsing) to attempt to remove the blood from the tissue sections after collection and prior to snap freezing. This means that some unknown volume of blood, containing both cell-associated virus and free virus from plasma remained within the tissues and almost certainly contributed to the total number of viral copies measured with qPCR.

Note that the actual volume of the contaminating blood in each sample was likely minimal, as the tissue samples were generally small, 1g or less. However, when examining the total viral RNA in the tissue (Figure 4), some highly vascularized tissues, such as the heart, spleen and stomach, exhibited among the highest viral loads of any tissue during the peak of viral replication. While it is possible that this was due to a larger volume of contaminating blood in these tissues, their viral loads during the ramp-up and set-point of viral replication did not appear to diverge greatly from other tissues. Additionally, some other highly vascular tissues, like the kidney, liver and lung, had relatively low or average viral loads. It is therefore unclear how much contaminating virus was actually quantified. Furthermore, since every tissue surveyed contained at least some blood, the amount of additional virus should have been somewhat homogenously distributed across the samples.

Apart from the systemic spread of the virus, we also sought to characterize the very earliest viral replication directly at the site of inoculation. Immediately after transmission, after crossing the mucosal epithelium, the virus infects resident target cells and forms small foci. These foci have been shown before in pathogenic models of HIV/SIV infection (61, 210), but have never been demonstrated in AGMs. To identify these foci, when collecting tissues for viral load testing, we excised the rectum and distal colon together, before any other tissues were taken. The two segments were then sectioned into strips and divided further into pieces. Each piece was used for a different assay, as assigned on a rotating basis, such that no

two contiguous pieces would be used for the same assay (see 3.3.3). The purpose of this sampling strategy was to capture any of these initial foci of viral replication, when the virus is limited to a small founding population of target cells. In this, we were successful, as we found multiple pieces of the rectum and distal colon that were positive for SIVsab RNA and DNA within 1-3 days following inoculation (Figure 4 & 5). Such early establishment of replication suggests that the population of "founder" cells is infected almost immediately after the virus crosses the mucosal barrier. This is in agreement with previous studies, which also found that viral replication is quickly established following inoculation, both during intrarectal transmission and at transmission at other mucosal sites (212, 236–238).

In addition to the rectum and distal colon, SIVsab RNA was also detectable in the lymph node closest to the site of inoculation, the colonic LN, as early as 3 dpi (Figure 4). The presence of the virus here was shown even earlier, at 2 dpi, when surveying the colonic lymph node with RNAscope (Figure 6). The colonic LNs being the draining lymph nodes for this region, it is not surprising that this would be first tissue to which the virus spreads from the site of inoculation. However, such early presence of the virus in the colonic lymph node also provides a possible explanation for how SIVsab is able to travel so rapidly into circulation. Using the RNAscope, the virus was found only within the T-cell zone, with little to no trapping by follicular DCs occurring until after the ramp-up period (4-6 dpi), at which point the virus had already moved into circulation (Figure 6). This lack of virus trapping by follicular DCs in AGMs has been previously reported (239), and likely enable the virus to circulate unimpeded through the lymphatics, gaining rapid traction to the bloodstream via the thoracic duct.

Another possible explanation for the speed of viral replication and dissemination following intrarectal inoculation of SIVsab is that the rectum provides a somewhat easier route of transmission for the virus (61, 212). The rectal epithelium is relatively thin, being made up of single layer of columnar cells, and is easily crossed compared to other mucosal sites (see 1.3.4), particularly if there are preexisting microabrasions or breakages. Additionally, the mucosa of the rectum and distal colon are densely population with lymphoid aggregates containing many $CD4^+$ T cells, which could serve to facilitate early viral replication, as well as provide more immediate access to the lymphatic system.

However, even if the rectal mucosa is more permissive to transmission than other mucosal sites, such as the vagina or the oral mucosa, it was still restrictive enough to impose a severe genetic bottleneck on the transmitted/founder viruses. In the current study, the original inoculum, which was derived from plasma taken from an acutely infected AGM, was shown to contain a diverse mixture of SIVsab variants, including multiple transmitted-founder strains. In contrast, SGA showed that only 3-10 transmitted-founder viruses in each of the animals surveyed (Figure 8). This indicates that during mucosal transmission, a combination of mucosal epithelium barrier, limited target cell availability and immune responses worked to restrict the number of virus that were able to successfully establish infection, creating a genetic bottleneck.

It should be noted that during the preliminary study that served as groundwork for this dissertation study, the genetic bottleneck was also assessed using SGA following intrarectal and intravaginal transmission in AGMs and only 1-2 transmitted/founder viruses were found in each animal (78); a similar number of viral variants were also found to establish infection in wild AGMs (52) and absolutely similar to the number of transmitted founder viruses reported to occur in both humans and rhesus macaques (80, 81). Given the greater number of transmitted/founder viruses found in the AGMs in this study, it is likely that the concentration of SIVsab in the inoculum was high and the animals were overexposed, resulting in an increased number of transmitted viral variants. However, given the terminal nature of the study, the dosage used for the inoculum (10^7 vRNA copies in 1 mL diluted plasma) was established in an attempt to maximize successful infection, rather than minimize overexposure. Underexposing the AGMs would have resulted in animals being euthanized without becoming infected and a major waste. As it was, even at this dosage, out of the original 29 animals inoculated, only 27 became infected; the remaining two "exposed, uninfected" animals had to be excluded from the study.

To further complete the characterization of SIVsab intrarectal transmission, we sought to establish at least the partial identity of the target cells of the virus immediately following transmission. Using FISH, SIVsab RNA was shown to be associated with $CD3^+$ T cells, but not with myeloid lineage cells ($CD68^+$ $CD163^+$). This was expected, as our stock was generated from diluted plasma taken from an acutely infected

AGM. Thus, it contained largely transmitted-founder viruses, which were reported to exclusively infect lymphocytes and not myeloid cells, unlike the lineages that emerge later during infection (240, 241).

Overall, the characterization of the early events of SIVsab replication and dissemination following transmission showed that, at least upon intrarectal transmission, the virus becomes systemically spread very rapidly. It has a quick egress from the site of inoculation, possibly moving unabated through the draining lymphatics into the bloodstream, where it is disseminated throughout the body. The rapidity with which SIVsab moves after intrarectal transmission is of particular importance to HIV research in relation to interventions to attempt to prevent infection. It has been previously suggested that there exists a "window of opportunity", a period during the eclipse phase of viral replication in HIV which represents the best point at which to target the virus with a vaccine, microbicide or some other intervention to prevent infection. This window was thought to occur only prior to establishment of systemic infection (61, 242). Here, we show that SIVsab replication and dissemination takes place nearly simultaneously, with viral RNA detectable at the site of inoculation and in the draining lymphatics by 1-3 dpi (Figures 4, 5, & 6) and plasma viremia by 2-4 dpi. This means that at least in the case of intrarectal transmission, the window of opportunity to prevent systemic infection may by very short or even nonexistent. As such, these results suggest that future research might focus on measures to prevent transmission altogether, rather than trying to curtail the infection after it might already be too late.

4.0 African green monkeys avoid SIV disease progression by preventing intestinal dysfunction and maintaining mucosal barrier integrity

4.1 Contributors

Data contributed to the dissertation by several collaborators is included in the following section. Drs. Jacob Estes and Kathleen Busman-Sahay contributed the images and the quantitative image analysis data for the chronically SIVmac251-infected RMs. Dr. Frederick Barrenäs contributed the RNAseq analysis and IPA pathway analysis for the genes linked to epithelial damage in the gut, immune cell activation and inflammation. Various members of the Apetrei/Pandrea labs contributed to the routine work, including tissue processing, immune cell isolation, flow cytometry and immunohistochemistry. For the AGMs, the dissertation author managed the serial necropsies and tissue sampling, analyzed the majority of the flow cytometry data, performed the bulk of the immunohistochemistry staining, conducted the image capturing and quantitative analysis, and executed the ELISA assays.

4.2 Background

The vast majority of the studies performed over the last two decades collectively indicate that the main factor behind the lack of disease progression in the natural hosts of SIVs is their ability to actively control chronic immune activation and inflammation (2, 38, 90, 127, 157, 243, 244), which are the main drivers of disease progression and mortality in HIV-infected subjects (191, 245–247). Indeed, AGMs, SMs, and MNDs have the ability to resolve immune activation at the transition from acute-to-chronic SIV infection, and this is the best correlate of the lack of disease progression in these species so far (127, 154, 156, 157, 248).

One of the defining features of African NHPs in preventing chronic immune activation and inflammation during SIV infection is the lack of mucosal dysfunction, which allows them to avert microbial translocation (6, 84, 89, 191), as described in 1.4.10. In pathogenic HIV/SIV infections, microbial translocation occurs as a result of acute viral replication and proinflammatory responses causing extensive damage to the intestinal mucosa (249). These breaches of epithelial integrity allow microbes and microbial byproducts to move from the intestinal lumen into the surrounding tissues and general circulation (176, 192), inducing: (i) recruitment of target cells to the site of viral replication; (ii) exhaustion of major immune cell populations; and (iii) establishment of a chronic inflammatory state which persists indefinitely (191, 192, 249–251). Collectively, these effects perpetuate the destruction of the gut mucosa, triggering further inflammation and T-cell immune activation, which cause even more damage, creating a vicious cycle which is largely self-sustaining. This cycle does not depend on viral replication, as the chronic inflammation and contingent immune activation persist even in individuals on long-term ART (252, 253).

The chronic inflammation induced by microbial translocation is now widely considered to be not only the driving force of the progression to AIDS, but also the cause of numerous AIDS-associated comorbidities, including cardiovascular disease, osteoporosis, neurological disease, liver disease, kidney disease and cancers (191, 194, 196, 245, 254–256). Therefore, understanding the mechanisms leading to the control of systemic inflammation in African NHP hosts of SIV could lead to new strategies to prevent not only HIV disease progression, but also the development of HIV-associated comorbidities.

African NHPs maintain mucosal integrity throughout the chronic infection, as demonstrated by both the lack of microbial translocation during either acute or chronic SIV infection (12, 52, 78, 84, 89, 149) and by cross-sectional analyses of the gut epithelium of chronically SIV-infected SMs, which failed to identify any mucosal lesions (250). Yet, it is unknown whether mucosal integrity observed in chronically SIV-infected African NHP hosts results from their singular ability to repair the injury inflicted to the gut during acute SIV infection, or whether natural hosts can simply prevent loss of gut integrity throughout infection.

Our group has previously demonstrated the importance of a healthy mucosal barrier integrity in natural hosts of SIVs. (see 1.4.10). Through administration of dextran sulfate sodium to chronically SIV-infected AGMs, we experimentally induced colitis that led to increased viral replication and altered key parameters highly predictive of HIV disease progression (195). In contrast, attempts to directly control microbial translocation (196) and/or inflammation (257) in chronically SIV-infected PTMs without reducing the preexisting mucosal damage resulted in only transient positive effects. From this, it appeared that preventing gut dysfunction by maintaining mucosal barrier integrity during the early SIV infection may be the essential element that enables natural hosts to avoid microbial translocation and disease progression.

In order to affirm whether natural hosts can preserve the gut mucosa, an extensive *in situ* analysis of gut integrity was performed in our AGMs, which were serially sacrificed throughout the acute and postacute SIV infection. The gut mucosa was assessed for multiple markers for immune activation, inflammation, apoptosis, disruption of the epithelium and presence of bacterial proteins. When possible, the same parameters were measured in immune cell subsets by flow cytometry. Plasma cytokine levels were tested to monitor the systemic levels of mucosal immune activation and inflammation throughout the follow-up. Finally, RNA transcriptomics was used to evaluate any changes in gene expression in the gut that might be linked to mucosal damage or microbial translocation.

4.3 Methodology

4.3.1 Ethics Statements

As described in 3.3.1.

4.3.2 Animals and infections

As described in 3.3.2 for the AGMs. For the purposes for comparison to a pathogenic SIV infection, we included results from chronically SIVmac-infected adult male RMs sacrificed during chronic infection (127-410 dpi). References for the care and infection strategies used for the RMs are listed below in Appendix A. All data from the chronically infected RMs was provided by Dr. Jacob D. Estes to supplement the original data.

4.3.3 Tissue sampling and isolation of mononuclear cells

As described in 3.3.2 for the AGMs. The tissues from the RMs were collected and processed in a similar manner to the AGMs, as previously described (153, 250). For the AGMs, testing was conducted largely on sections taken from the transverse colon and the jejunum, as opposed to the rectum or distal colon, as: (i) they provided much larger, more intact sections for IHC and other assays; (ii) more cells were isolated from these tissues for flow cytometry, avoiding the issues described in 3.4.10; (iii) only tissues collected from animals sacrificed at 6> dpi or greater were used for IHC, as it was thought that any lesions or damage to the epithelium might be too widely distributed to detect earlier during infection it was also thought that lesions might occur during or after the peak of viral replication. This also represents the point at which the virus is readily detectable in the plasma and has become widely disseminated, reaching sites distant from the site of inoculation (see 3.4.1 and 3.4.3). For this reason, it was decided that by 6 dpi, viral replication would be homogenous throughout the gut, allowing us to employ other compartments apart from the rectum. Additionally, the transverse colon was chosen for testing as it is more structurally similar to the distal colon and the rectum than the jejunum, making for a better approximation.

4.3.4 Tissue DNA/RNA extraction

As described in 3.3.9.

4.3.5 Tissue viral loads quantification

As described in 3.3.10.

4.3.6 Flow cytometry

As described in 3.3.13.

4.3.7 Testing the levels of plasma inflammatory cytokines and chemokines

Systemic changes in chemokines and cytokines were measured using an Invitrogen Monkey Cytokine Magnetic 29-Plex Panel (Invitrogen), as per the manufacturer's instructions using a Bio-Rad Bio-Plex Pro II Wash Station (Bio-Rad, Hercules, CA) and the Bio-Rad Bio-Plex 200 System (Bio-Rad) (194, 257). Briefly, in a 96-well flat bottom plate, 25 µL of magnetic beads coated with antibodies specific for 29 different cytokines and chemokines were added to each well and washed. Washing was done in a Bio-Rad Bio-Plex Pro II Wash Station (Bio-Rad, Hercules, CA) with a magnetic baseplate to retain beads during the wash cycles. Next, 100 µL of negative controls and the serially diluted standard were loaded into the appropriate wells, followed by 100 µL of diluted AGM plasma that had been snap frozen at the time of necropsy into each of the test wells. The plate was then incubated in the dark at RT on an orbital plate shaker for 2 hours, then washed twice. Next, 100 µL diluted Biotinylated Detector Antibody was added to each well and the plate was returned to the shaker to incubate for 1 hour. The plate was washed twice again, and then 100 µL Streptavidin-RPE solution was added before incubating for 30 mins. Finally, the plate was

washed 3 times before the beads were resuspended in 150 µL wash solution and the plate fluorescence was read using a Bio-Rad Bio-Plex 200 System (Bio-Rad, Hercules, CA).

Plasma samples taken from both pre- and postinfection were assayed and used to calculate the total fold change in the plasma chemokine and cytokine levels. These fold change values were then normalized using a $\log_2$ transformation. The transformed data was used to generate a heatmap with the publicly available Morpheus software from the Broad Institute (https://software.broadinstitute.org/morpheus/).

4.3.8 Measuring plasma levels of markers of fibrosis and gut epithelial damage

Systemic levels of intestinal fatty acid binding protein (I-FABP) and hyaluronic acid (HA) were measured by conventional ELISA. I-FABP, a known marker of intestinal damage (258), was assessed using a Monkey I-FABP ELISA kit (MyBioSource, San Diego, CA), as described (223). HA, a prognostic marker of fibrosis (259), was tested using a Monkey Hyaluronic Acid ELISA Kit (MyBioSource).

4.3.9 Immunohistochemical assessment of mucosal tissues

We examined the overall integrity of the gut mucosal barrier with a multifaceted set of markers to assess inflammation in the gut (MX1), epithelial cell proliferation (Ki-67), apoptosis (caspase-3), epithelium continuity (claudin-3) and microbial translocation (LPS-core and *Escherichia coli*). IHC and quantitative image analysis were performed as described (246, 250, 260). Briefly, paraffin fixed tissues mounted on glass slides were deparaffinized by a battery of 3 x 5 min washes in xylene, then rehydrated by 3 x 5 min washes in 100%, 95% and 75% ethanol. Next, the tissues were boiled in diluted Antigen Unmasking buffer (Vector Laboratories, Burlingame, CA) for 25 mins, allowed to cool to RT, then rinsed 5 mins in 1X PBS, and incubated with 3% H_2O_2 for 15 mins. After 2 x 5 min washes in 1X PBS, the tissues were blocked with Protein Block (Dako, Santa Clara, CA) for 30 mins at RT, incubated with primary antibodies (listed in Appendix A) diluted to the appropriate concentration (Dako Antibody Diluent) for at

least 1 hour at RT, rinsed in 1X PBS for 2 x 5 min washes and incubated with diluted Vectastain secondary antibody (Vector Laboratories) for another 30 mins at RT. After 2 x 5 min washes in 1X PBS, the tissues were incubated for 30 mins at RT with Vectastain ABC solution (Vector Laboratories), followed by 2 x 7 mins washes in 1X PBS, and addition of DAB diluted in DAB substrate (Dako) to generate a positive signal, at which point the reaction was quenched in deionized water for 5 mins before being counterstained with haematoxylin. The tissues were then dehydrated with a reverse battery of ethanol and xylene (75%, 95% and 100%) before being coverslipped. The tissues taken from the RMs were processed for IHC and stained in a similar fashion to the AGMs, as previously described (246, 250). Note that this prior study of mucosal integrity served as an experimental framework for the IHC stains outlined in this dissertation.

4.3.10 Assessment of the collagen deposition in the mucosal tissues

We assessed collagen deposition in the tissues using the Chromaview Advanced Testing Masson Trichrome Stain (Thermofisher) as per the manufacturer's instructions, with some modifications. Briefly, tissue slides were deparaffinized as done for IHC, and then incubated overnight in Bouin's fluid. The slides were then washed repeatedly in deionized water until all yellow coloration was removed. The slides were next immersed in Working Weigert's Iron Haematoxylin Stain for 10 mins and then washed again in water for 5-10 mins. The slides were transferred into Bierich's Scarlet-Acid Fuchsin Solution for 5 mins before being rinsed in water for 30 seconds and then incubated for 5 mins with Phosphotungstic-Phosphomolybdic Acid solution. Finally, the slides were fully immersed in Aniline Blue Stain Solution for 30 mins, washed 2 x 2 mins with 1% acetic acid, and then rinsed for 30 seconds in deionized water. The slides were then dehydrated with 2 x 1 min washes in 100% ethanol, followed by 3 x 1 min washes in xylene before coverslipping. The collagen staining for the RMs was done in a similar fashion to the AGMs, as previously described (261).

4.3.11 Quantitative image analysis

Images of IHC stained tissues were captured using an AxioImager M1 brightfield microscope equipped with an AxioCam MRc5 (Zeiss, Oberkochen, Germany) and Axiovision software v.4.7 (Zeiss). To evaluate the levels of immune activation, inflammation and apoptosis markers, images were quantified by measuring the % area of positive signal in multiple images. The quantified regions were randomly selected to minimize bias. In the gut, any lymphoid structures were avoided, as they display distinct immune cell populations compared to the lamina propria. All images were taken at either 100X or 200X magnification, depending on the quantification technique. After image collection, 9-12 images from the same animal were processed by applying the Color Deconvolution function in the FIJI image processing package (version 2.0) (262), splitting the image into 3 separate color channels, one of which isolated the DAB coloration. An intensity threshold was then manually applied to each image to select the DAB signal. The total percent area occupied by the signal above the threshold (i.e., DAB-positive) was measured and averaged for all the images from the same animal. An example of the color deconvolution quantification strategy is shown in Appendix B.

Quantification of tissue collagen was accomplished in a similar fashion, but by applying a threshold to isolate a particular range of color within the spectrum instead of preset color. This was accomplished by using the Color Threshold function in FIJI to manually set the maximum and minimum range based on the color hue. A range was selected that isolated as much of the blue coloration of the collagen while minimizing selection of background color. Note that the blue stain was also partially taken up by the goblet cells in the mucosal epithelium of the gut, so some background signal was unavoidable. However, we feel that this does not create a significant error, as goblet cells were present in all images of the lamina propria, therefore their contribution to the background should have been similar across all images. After the hue selection range was set, the image was converted to black and white, removing all non-selected regions from the image. A standard threshold was then applied to measure the total area of the positive collagen

signal (now black) in the image. An example of the color threshold-based quantification strategy is shown in Appendix B.

To quantify enterocyte proliferation, we measured the proportion of the villi length with Ki-67$^+$ epithelial cells, as previously published (246). As epithelial proliferation is localized to the base of the crypts, we measured both the total length of the crypt and the length of the crypt with Ki-67$^+$ epithelial cells. Any increase in epithelial cell proliferation results in an increase in the total number of Ki-67$^+$ cells along the crypt. In brief, this was done by manually drawing a black line through the middle of the villi from the base to the luminal end, then bifurcating the line based on the position of the Ki-67$^+$ epithelial cells and measuring the two segments with the FIJI Wand tool. This allowed us to quantify the fraction of proliferating and activated mucosal epithelial cells. An example of this strategy is shown in Appendix B.

To quantify the proliferation of cells specific to the lamina propria, we used FIJI to manually exclude the epithelium from the images, allowing us to quantify the total % area of the positive signal in the lamina propria alone. This was accomplished by overlaying white coloration on each of the individual sections of the crypts containing epithelial cells. Both transverse and longitudinal crypt sections were excluded, but images featuring primarily transverse sections were preferentially chosen due to the more consistent distribution of the epithelium. After excluding the epithelium, the images were quantified using the standard color deconvolution technique described above. An example of the exclusion technique is shown in Appendix B.

To quantify the percent of the GI tract epithelial barrier that is damaged, we took multiple overlapping images of the gut epithelium stained for claudin-3 and used them to create large composite images of the GI tract with the Image Stitching plugin (263) in the FIJI software (262, 264). Once the composite image was generated, we first traced the length of the intact epithelium with a green line and then traced any regions lacking claudin-3 staining (i.e., damaged or discontinuous epithelium) with red line. The lines were drawn freehand at a constant width of 10 pixels. The total lengths of the two lines were then measured using the FIJI Wand tool to establish the length of intact *versus* broken epithelium, as previously described (250). For each animal, 3-4 composite images were quantified to establish an average. Similar

methodologies were used for quantification of the IHC stains for the RMs, as previously described (250). All AGM quantifications were done using the open-source FIJI software, v.1.0 (262, 264).

4.3.12 RNAseq transcriptomics for differential gene expression

RNAseq and the subsequent bioinformatic analysis was performed as described (265). Briefly, rectal tissues were immediately perfused in RNAlater and stored at -80°C until further processing. Whole transcriptome libraries were constructed using the TruSeqStranded Total RNA with Ribo-Zero Gold (Illumina, San Diego, CA) as per the manufacturer's instructions. Libraries were quality controlled and quantitated using the BioAnalzyer 2100 system (Kapa Biosystems, Woburn, MA) and qPCR. The resulting libraries were then sequenced on a HiSeq 2000 using HiSeq v3 sequencing reagents, with read number finishing using a Genome Analyzer IIx using GA v5 sequencing reagents, both of which generated paired end reads of 100 nucleotides. The libraries were clonally amplified on a cluster generation station using Illumina HiSeq version 3 and GA version 4 cluster generation reagents to achieve a target density of approximately 700,000 (700K)/mm^2 in a single channel of a flow cell. Image analysis, base calling, and error estimation were performed using Illumina Analysis Pipeline (version 2.8).

4.3.13 Statistical analysis

To compare changes in the immune cell populations between preinfection and postinfection time points from the same AGMs, we used the nonparametric two-tailed Wilcoxon matched-pairs signed ranks test, with a $p \leq 0.05$. For comparisons between control and infected AGMs, which included both the flow cytometry results and the IHC quantifications, we used the unpaired nonparametric Kruskal-Wallis test, followed by a Dunn's multiple means comparison test to correct for multiple comparisons between the time groups. A Mann-Whitney *U* test was used to test differences between the set-point AGMs and the

chronically infected RMs. The family-wise significance and confidence levels were set at 0.05. All tests were performed using the Graphpad Prism 7 Software (Graphpad Software Inc.)

4.4 Experimental results

4.4.1 SIVsab replicates to high levels in the jejunum, transverse gut and axillary LN during the early stages of infection

As damage to the gut is triggered initially by inflammation driven by local viral replication (see 1.4.10), we sought to assess the timing and magnitude of the viral replication in the gut and axillary LNs. We extracted DNA and RNA from the whole snap frozen tissue samples and quantified the total vDNA and vRNA SIVsab genomes in the transverse colon, jejunum and axillary LNs, as shown in Figure 4 and Figure 5 of 3.4.3.

In the transverse colon and jejunum, vRNA first became detectable between 4-6 dpi, at 10^1-10^2 (GM: 1.25±0.08 log vRNA copies/10^6 cells) and 0-3 logs (GM: 1.29±0.83 log vRNA copies/10^6 cells), respectively. Similarly, vDNA became detectable between 4-6 dpi, at 0-1 log (GM: 1.49±1.54 log vDNA copies/10^6 cells) and 0-2 logs (GM: 0.95±0.46 log vDNA copies/10^6 cells), for jejunum and colon, respectively. The viral loads then rose sharply reaching peak between 9-12 dpi, at 4-5 log for both jejunum and colon (GM: 4.61±1.05 log vRNA copies/10^6 cells and 4.66±0.32 log vRNA copies/10^6 cells, respectively); at the same time points, vDNA levels ranged between 3-4 log (GM: 3.45±0.23 log vDNA copies/10^6 cells) in the jejunum and 2-4 log (GM: 3.61±0.76 log vDNA copies/10^6 cells) in the colon. At the transition to chronic infection (46-55 dpi), vRNA levels ranged between 3-4 log in both jejunum and colon (GMs: 3.44±0.31 log vRNA copies/10^6 cells and 3.59±0.28 log vRNA copies/10^6 cells, respectively), with vDNA showing only a slight decrease from peak levels, to 2-4 log (GM: 2.80±0.43 log vDNA copies/10^6 cells) in the jejunum, and 2-3 log (GM: 2.37±0.10 log vDNA/10^6 cells) in the colon.

In the axillary LNs, vDNA (but not vRNA) became detectable by 4-6 dpi, at 0-2 log (GM: 1.44±0.75 log vRNA copies/10^6 cells) for vRNA and 1-2 log (GM: 1.54±0.31 log vDNA copies/10^6 cells) for vDNA.). This was similar to the jejunum and the colon, but not as early as the colonic LN, which drains the site of inoculation. The axillary LN viral loads peaked at 9-12 dpi, at 3-5 log (GM: 4.27±0.82 vRNA copies/10^6 cells) for vRNA, and 2-4 log (GM: 3.50±0.46 log vDNA copies/10^6 cells) for vDNA. The set-point viral loads at the transition to chronic infection in the axillary LNs were 3-4 log (GM: 3.85±0.31 log vRNA copies/10^6 cells) for vRNA and 1-2 log (GM: 2.04±0.29 log vDNA copies/10^6 cells) for vDNA.

4.4.2 Circulating $CD4^+$ T cells transiently decrease, but $CD4^+$ T cells remain relatively stable in other tissues

$CD4^+$ T cells are the primary target cells for SIVs, and are massively depleted during the acute infection, particularly in the lamina propria of the GI tract (61, 109, 114, 149, 193) (see 1.4.5). A significant depletion of the peripheral blood $CD4^+$ T cells occurred early during SIV infection in AGMs and persisted throughout the acute stage of infection. Thus, circulating $CD4^+$ T cells counts were significantly decreased during the preramp-up period (*p=0.0039*), the ramp-up period (*p=0.0156*), and the peak of viral replication (*p=0.0156*), as shown in Figure 13A.

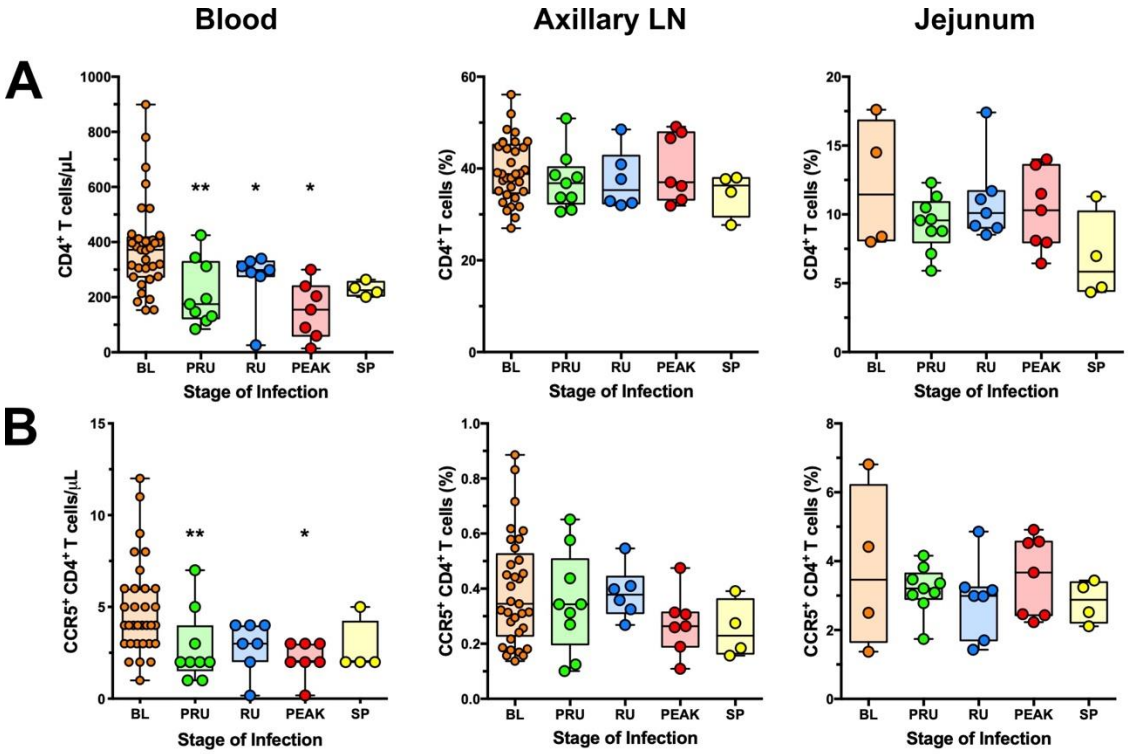

Figure 13: Total CD4$^+$ and CCR5-expressing CD4$^+$ T-cell populations in the blood, jejunum and axillary lymph nodes of SIVsab-infected African green monkeys (AGMs).

Total populations of (A) CD4$^+$ T cells; (B) CCR5$^+$ CD4$^+$ T cells isolated from blood, axillary LN and jejunum. The values for blood represent absolute cell counts, while the values in the jejunum and axillary LN represent percent populations. The five groups are based on the days postinfection, with: BL (baseline, preinfection), PRU (preramp, 1-3 dpi), RU (ramp-up, 4-6 dpi), PEAK (peak, 9-12dpi) and SP (set-point, 46-55 dpi). Each group is assigned a corresponding color: orange (baseline), green (preramp), blue (ramp-up), red (peak) and yellow (set-point). Asterisks indicates statistical significance when compared to baseline values, with *=$p<0.05$; **=$p<0.01$.

By the onset of chronic infection, CD4$^+$ T cells were partially restored in the blood, albeit below the preinfection levels.

However, this trend was not reflected in other tissues. Thus, CD4$^+$ T cells remained stable in the LNs, with little to no variation at any point during infection. In the jejunum, CD4$^+$ T cells were not significantly decreased from baseline and remained mostly unchanged over the course of the acute stage of infection. The only exception was an appreciable drop in CD4$^+$ T cells in the jejunum by the set-point of viral replication, though without reaching significance (Figure 12A). This trend was very similar to the what was observed for CD4$^+$ T-cell populations in the rectum (Figure 9A).

We also examined the levels of CCR5-expressing $CD4^+$ T cells in blood, jejunum and axillary LNs. Circulating CCR5-expressing $CD4^+$ T cells displayed a similar pattern as the total $CD4^+$ T-cell population, with significant decreases during the preramp-up (*p=0.0156*) and peak of viral replication (*p=0.0312*). However, the levels of $CCR5^+$ $CD4^+$ T cells did not undergo any significant alterations in the axillary LNs or the jejunum (Figure 13B) at any point during the course of infection; again, this mirrors the trends seen in the colonic LN (Figure 9B).

4.4.3 $CD8^+$ T cells and $CD20^+$ B cells transiently decreased in circulation but are largely unaltered in other tissues.

In the blood, the $CD8^+$ T cells underwent a slight decrease during preramp-up and throughout the acute stage of infection. $CD8^+$ T cells then returned to preinfection levels or greater by the time of the chronic infection. By comparison, the levels of $CD8^+$ T cells in the axillary LNs were largely unchanged, with no significant alterations baseline levels at any point during the infection. In the jejunum, $CD8^+$ T cells were also relatively stable, with only a slight decrease during ramp-up and a slight increase at the set-point, none of these reaching significance (Figure 14A), similar to what was seen for the $CD8^+$ T-cell populations in the rectum (Figure 10A).

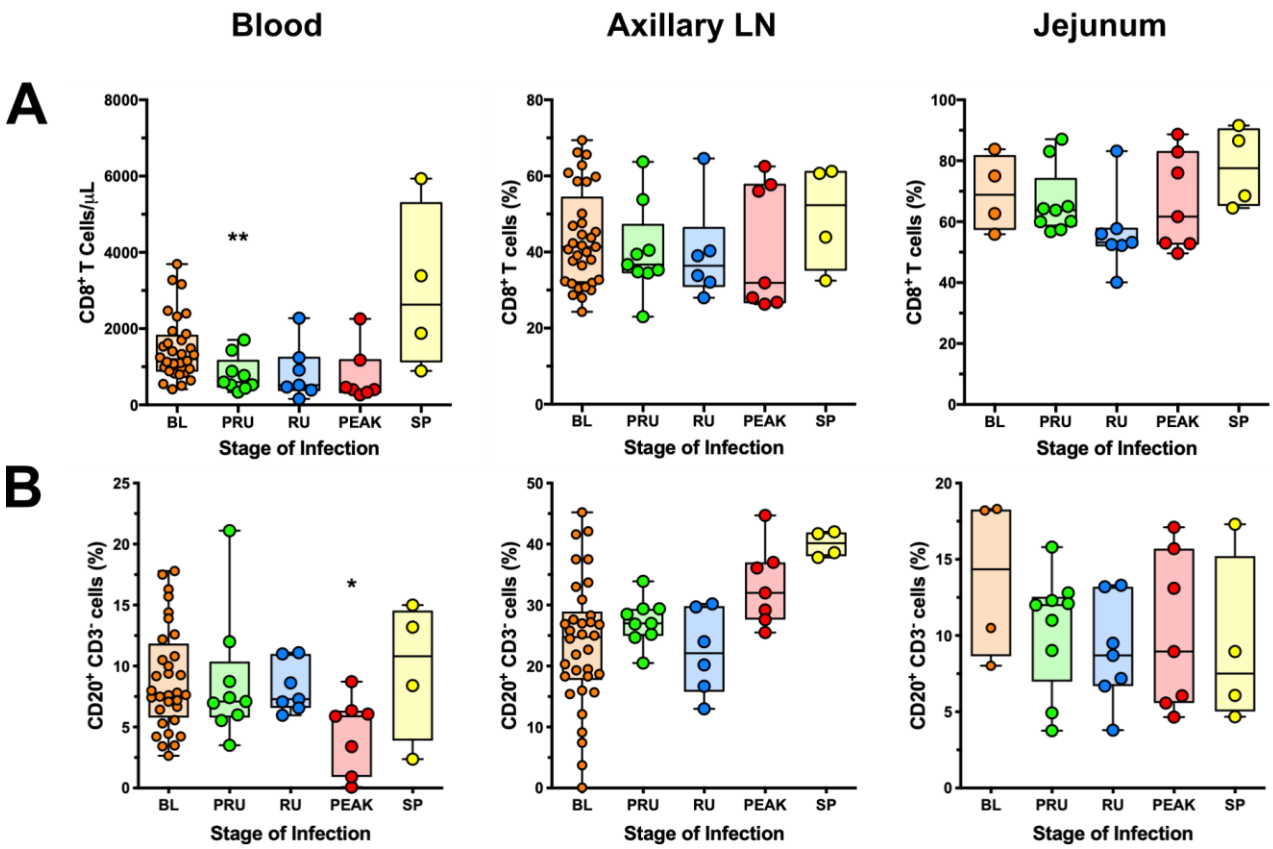

Figure 14: CD8$^+$ T-cell and CD20$^+$ cell populations in blood, jejunum and axillary lymph nodes of SIVsab-infected African green monkeys (AGMs).

Total populations of (A) CD8$^+$ T cells; and (B) CD20$^+$ B cells isolated from blood, axillary LN and jejunum. The values for blood represent absolute counts, while the values in the jejunum and LN represent percent populations. The five groups are based on the days postinfection, with: BL (baseline, preinfection), PRU (preramp, 1-3 dpi) RU (ramp-up, 4-6 dpi), PEAK (peak, 9-12dpi) and SP (set-point, 46-55 dpi). Each group is assigned a corresponding color: orange (baseline), green (preramp), blue (ramp-up), red (peak) and yellow (set-point). Asterisks indicates statistical significance when compared to baseline values, with *=p<0.05; **=p<0.01.

A significant decrease ($p=0.0312$) in the absolute counts of peripheral blood CD20$^+$ B cells occurred by the peak of viral replication followed by rapid restoration to preinfection levels or higher by the time of early chronic infection. Conversely, CD20$^+$ B cells expanded in the axillary LNs by the transition to chronic infection, though this expansion lacked significance, similar to the colonic LN (Figure 11A) While widely variable, the overall CD20$^+$ B cell population remained relatively stable throughout infection in the jejunum (Figure 14B), unlike in the rectum, where CD20$^+$ B cell populations were significantly decreased by early chronic infection (Figure 11A).

4.4.4 Dendritic cells, monocytes/macrophages and natural killer cells are not significantly altered in the blood, axillary LN and jejunum

Since innate immune responses are mounted very early during infection and can drive inflammation in tissues, we thoroughly monitored the changes in different populations of innate immune effector cells. Both the mDCs or pDCs were slightly increased in the blood, axillary LN or jejunum during acute SIVsab infection in AGMs, but these increases did not reach significance, as shown in Figure 15A & B.

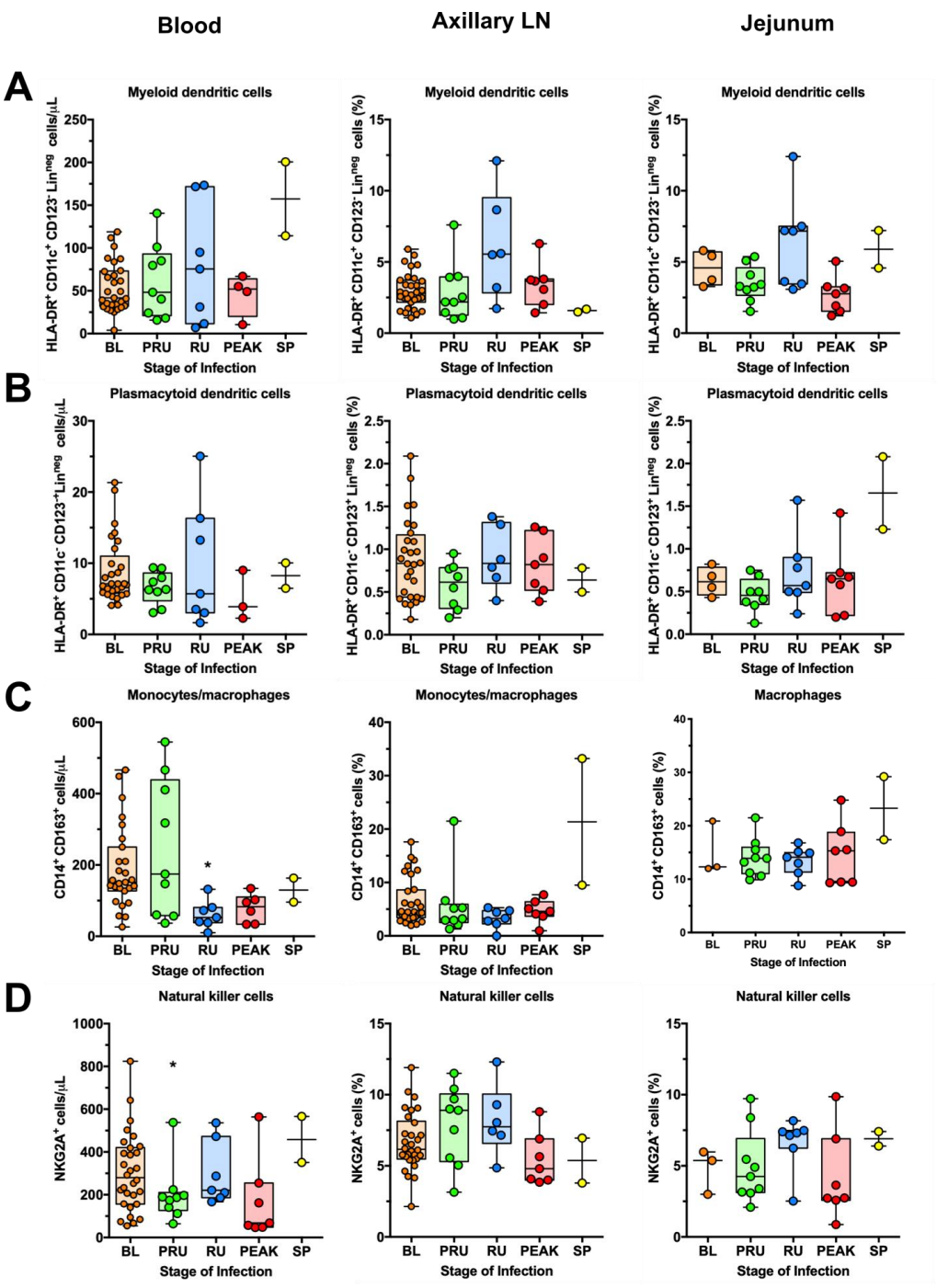

Figure 15: Changes in innate immune cell populations in blood, jejunum and axillary lymph nodes in SIVsab-infected African green monkeys (AGMs).

The flow cytometry analysis encompassed multiple immune cell subtypes, including: (A) myeloid dendritic cells; (B) plasmacytoid dendritic cells; (C) monocytes/macrophages ($CD14^+$ $CD163^+$); and (D) natural killer cells ($NKG2A^+$). These cells were isolated from a variety of different tissues, including blood, jejunum and axillary LN. The five different time groups are based on the days postinfection, with: BL (baseline, preinfection), PRU (preramp, 1-3 dpi) RU (ramp-up, 4-6 dpi), PEAK (peak, 9-12dpi) and SP (set-point, 46-55 dpi). Each time group is assigned a corresponding color: orange (baseline), green (preramp), blue (ramp-up), red (peak) and yellow (set-point). Asterisks indicates statistical significance when compared to baseline values, with *=$p<0.05$.

The monocyte/macrophage populations also showed no significant changes in the axillary LNs or the gut (Figure 15C) yet, a significant, transient decrease in the absolute counts of circulating monocytes occurred at the ramp-up, with return to baseline or greater levels by set-point. Also, the average populations of blood monocytes decreased between baseline and ramp-up regardless of the identifying monocyte markers used to survey the population ($CD14^+$, $CD163^+$, $CD14^+$ $CD163^+$). Finally, the absolute NK cell counts decreased slightly, but significantly (*p=0.0273*) in circulation during preramp-up. No significant changes of the NK cell populations in the LNs were observed throughout course of infection. The gut NK cells mirrored the changes observed for circulating NK cells, with a modest preramp-up decrease, followed by rebound during ramp-up and another decline at the peak (Figure 15D). The lack of significant changes in the jejunum and axillary LN somewhat parallels the lack of alterations in the rectum and colonic LN (Figure 11). It should be noted that only two of the four animals euthanized at set-point (46-55 dpi) were stained for DCs, monocytes/macrophages, and NK cells, as described in 3.4.9, despite attempts to restain the missing animals later.

4.4.5 AGMs exhibit minimal and transient T-cell and B cell immune activation and proliferation in the blood, axillary LN and jejunum

One of the key features of SIV infection in the natural hosts is the control of inflammation, immune activation and proliferation during the transition from acute-to-chronic SIV infection (2, 6, 127, 156, 168, 248). Therefore, using Ki-67 as a cellular proliferation marker, we monitored changes in these parameters for $CD4^+$ and $CD8^+$ T cells from blood, LNs and intestine via flow cytometry. The Ki-67^+ $CD4^+$ T-cell fraction showed nonsignificant minimal alterations at all these three sites (Figure 16A).

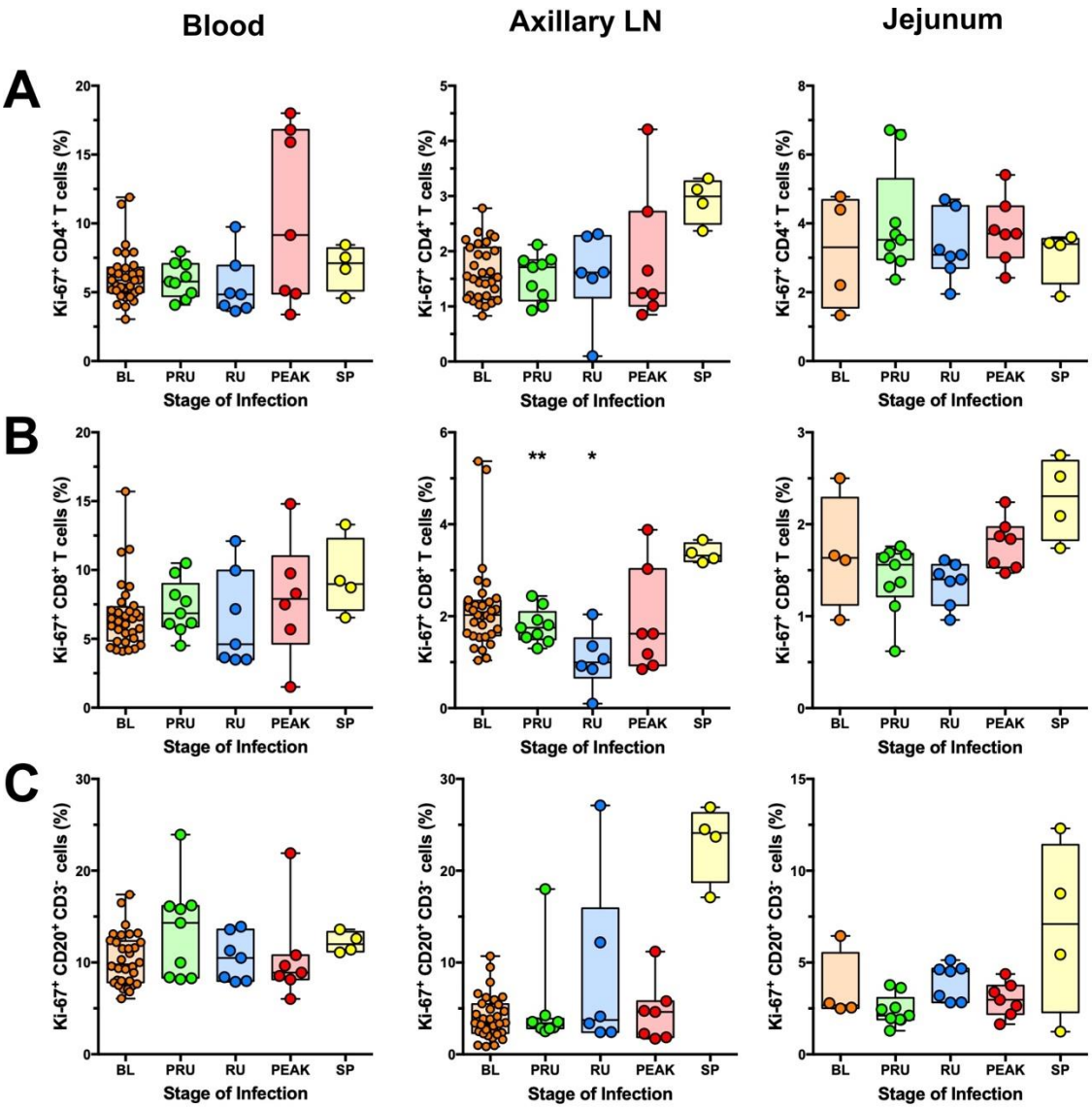

Figure 16: General immune activation and proliferation in blood, jejunum and axillary lymph nodes in SIVsab-infected African green monkeys (AGMs).

Ki-67 expression on (A) $CD4^+$ T cells; (B) $CD8^+$ T cells; and (C) $CD20^+$ B cells isolated from a variety of different tissues, including blood, jejunum and axillary LN. The five groups are based on the days postinfection, with: BL (baseline, preinfection), PRU (preramp, 1-3 dpi) RU (ramp-up, 4-6 dpi), PEAK (peak, 9-12dpi) and SP (set-point, 46-55 dpi). Each group is assigned a corresponding color: orange (baseline), green (preramp), blue (ramp-up), red (peak) and yellow (set-point). Asterisks indicates statistical significance when compared to baseline values, with *=$p<0.05$; **=$p<0.01$.

There was a transient drop in the frequency of the Ki-67$^+$ CD8$^+$ T cells in the axillary LNs during the preramp-up (*p=0.0078*) and ramp-up periods (*p=0.0312*), with full restoration to baseline levels by the peak (Figure 16B). Ki-67$^+$ CD8$^+$ T cells then slightly increased at the set-point in the axillary LNs and, to a less extent, the jejunum, but did not reach significance.

As pathogenic SIV infections are associated with B cell dysfunction (266), we next assessed the fate of CD20$^+$ B cell populations during the earliest stages of SIVsab infection of AGMs, and found that Ki-67$^+$ CD20$^+$ B cells remained relatively unchanged during acute infection in blood, LNs or jejunum, but increased in LNs by the early chronic stage of infection, though this increase lacked significance. In the jejunum, there were no significant alterations of the CD20$^+$ B cell activation or proliferation status, though some animals exhibited elevated levels by early chronic infection (Figure 16C).

4.4.6 Transient increases of systemic inflammation occur during the acute infection

Plasma levels of a wide variety of cytokines and chemokines measured to assess systemic inflammation in acutely SIVsab-infected AGMs showed increases in two-waves, at 3-4 dpi and 9-12 dpi, with the second wave coinciding with the peak of viral replication. As the experimental design only encompassed the acute and postacute infection, four chronically infected historic controls were included for this analysis. These AGMs were also infected intrarectally, using the same SIVsab stock at the same infectious dose, but were euthanized much later in infection, at 180 dpi (78). In these controls, all plasma cytokines and chemokines were found to be at nearly baseline levels, as shown in Figure 17.

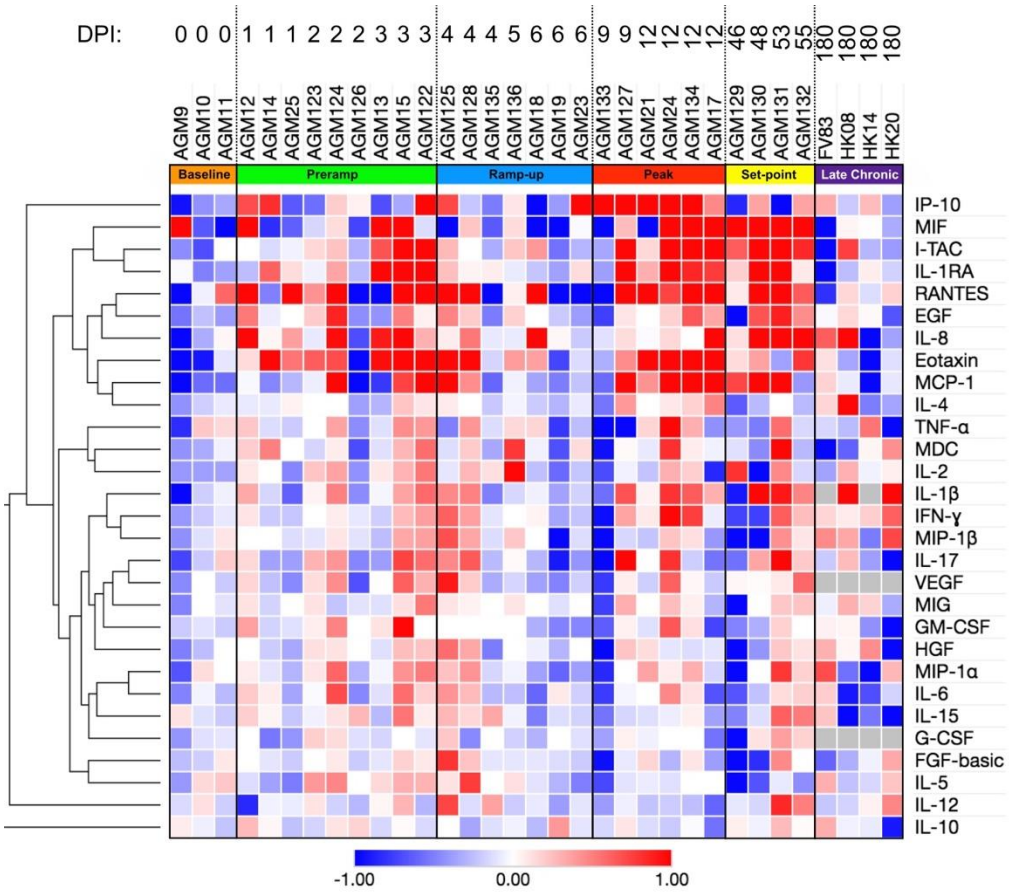

Figure 17: Heatmap of cytokine fold changes from baseline following SIVsab infection.
Colors represent the fold change from preinfection to postinfection of the cytokines for each of the AGMs. Red indicates a positive fold change, while blue represents a negative fold change, with color intensity being proportional to the magnitude of the fold change, as shown below the heatmap. Animal numbers are shown above the heatmap along with dpi, with the colors below the numbers highlighting their time groups: orange (baseline), green (preramp), blue (ramp-up), red (peak), yellow (set-point), purple (AGM historical controls, late chronic). Cytokines and chemokines are listed on the right side of the heatmap. The results are clustered using a Spearman correlation, with the dendrogram showing relationship displayed on the left. The fold changes for the cytokines and chemokine levels were normalized with a $\log_2$ transformation. The heatmap was generated using the publicly available Morpheus software (Broad Institute).

Several soluble markers of inflammation were increased during the acute SIVsab and early chronic infection in AGMs [i.e., eotaxin (CCL11), IL-1RA (IL1RN), IL-8 (CXCL8), IP-10 (CXCL10), I-TAC (CXCL11), MCP-1 (CCL2), MIF (GIF), RANTES (CCL5)] (Figure 17). Together, these results point to a robust, but relatively limited and transient increase of systemic inflammation during the acute infection of AGMs, in agreement with previous studies on SIV natural hosts (2, 6, 127, 156, 168, 248). This is in stark

contrast with pathogenic HIV/SIV infections, where rampant levels of inflammation persist throughout the chronic stage of SIV-infection and are strong predictors of progression to AIDS and death (6, 76, 153, 247, 267, 268).

In addition to the systemic inflammation, we also surveyed markers of T-cell immune activation by measuring expression levels of CD69, HLA-DR and CD38 (114, 269). The levels of circulating and LN $CD69^+$ $CD4^+$ T cells increased significantly either at preramp-up (axillary LN $p= 0.0391$) or peak (blood $p=0.0156$), but transiently, with $CD69^+$ T cells back to baseline level by viral set-point. Conversely, no significant increase in $CD69^+$ $CD4^+$ T cells was observed in the jejunum (Figure 18A), as was also the case with the rectum (Figure 12A).

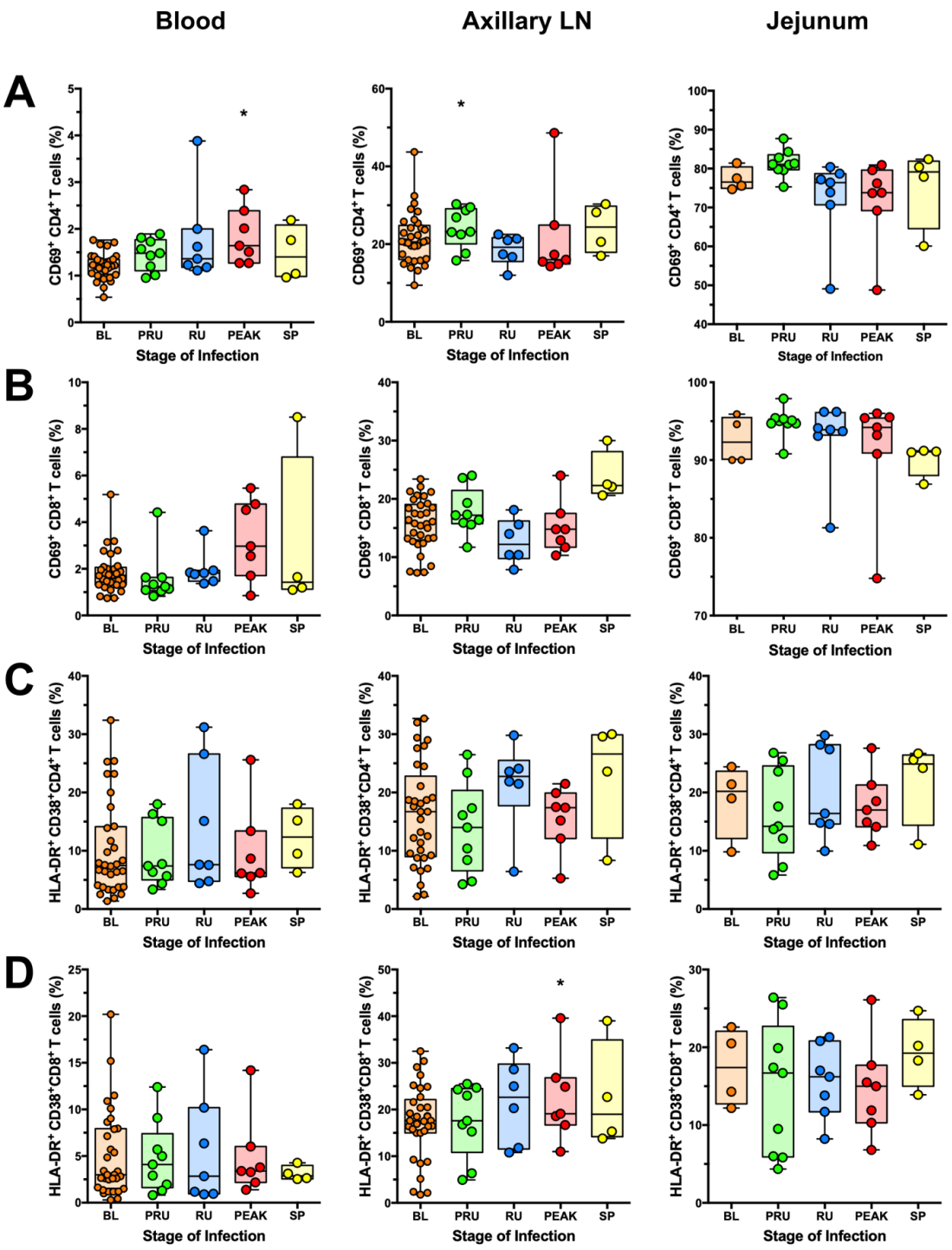

Figure 18: Immune cell activation in blood, jejunum and lymph nodes in SIVsab-infected African green monkeys (AGMs).

CD69 expression on (A) $CD4^+$ T cells; (B) $CD8^+$ T cells; and HLA-DR^+ $CD38^+$ expression on (C) $CD4^+$ T cells and (D) $CD8^+$ T cells isolated from a variety of different tissues, including blood, jejunum and axillary LN. The five groups are based on the days postinfection, with: BL (baseline, preinfection), PRU (preramp, 1-3 dpi) RU (ramp-up, 4-6 dpi), PEAK (peak, 9-12dpi) and SP (set-point, 46-55 dpi). Each group is assigned a corresponding color: orange (baseline), green (preramp), blue (ramp-up), red (peak) and yellow (set-point). Asterisks indicates statistical significance when compared to baseline values, with *=$p<0.05$.

Furthermore, the frequency of $CD4^+$ T cells expressing HLA-DR^+ and $CD38^+$ did not change significantly in any tissue at any time during acute or early chronic infection (Figure 18C), however, the HLA-DR^+ and $CD38^+$ expression by $CD4^+$ T cells were extremely variable across all groups. The levels of $CD69^+$ $CD8^+$ T cells showed no significant changes in the blood, axillary LN or jejunum at any point during the follow-up (Figure 18B). While we did observe a significant increase in the HLA-DR^+ $CD38^+$ $CD8^+$ T-cell levels at the peak of infection in the axillary LNs ($p= 0.0156$), $CD8^+$ T-cell activation was back to baseline level by the set-point of viral replication (Figure 18D).

4.4.7 Only a transient mucosal inflammation and interferon-stimulated response occurs in AGMs

In progressive HIV/SIV infection, mucosal inflammation and extensive cell death during the acute infection trigger multiple alterations to the gut integrity and microbial translocation, as well as systemic inflammation and immune activation, setting the stage for later disease progression (191, 196, 270, 271). Since significant, but only transient systemic inflammation and immune activation occur during SIVsab infection of AGMs, we next investigated whether gut mucosal pathologies associated with pathogenic HIV/SIV infections are likewise resolved in the natural hosts or prevented altogether. Using IHC, we directly examined expression of three markers of mucosal immune activation/inflammation: (i) Ki-67; (ii) MPO, a major component of azurophilic granules, a defining attribute of neutrophils (272); and (iii) MX1, an antiviral protein, directly linked to stimulation by type I (IFN-α, IFN-β) and type II (IFN-γ) interferons (248, 273, 274). We stained for these immunological markers from several of the primary sites of viral replication and $CD4^+$ T-cell depletion during the early stages of SIV infection: the transverse colon, jejunum and superficial LNs (61, 76, 84, 89, 114). There was no significant increase in the fraction of Ki-67 expressing cells in the lamina propria or the epithelium of the transverse colon epithelium, as shown in Figure 19 A & C.

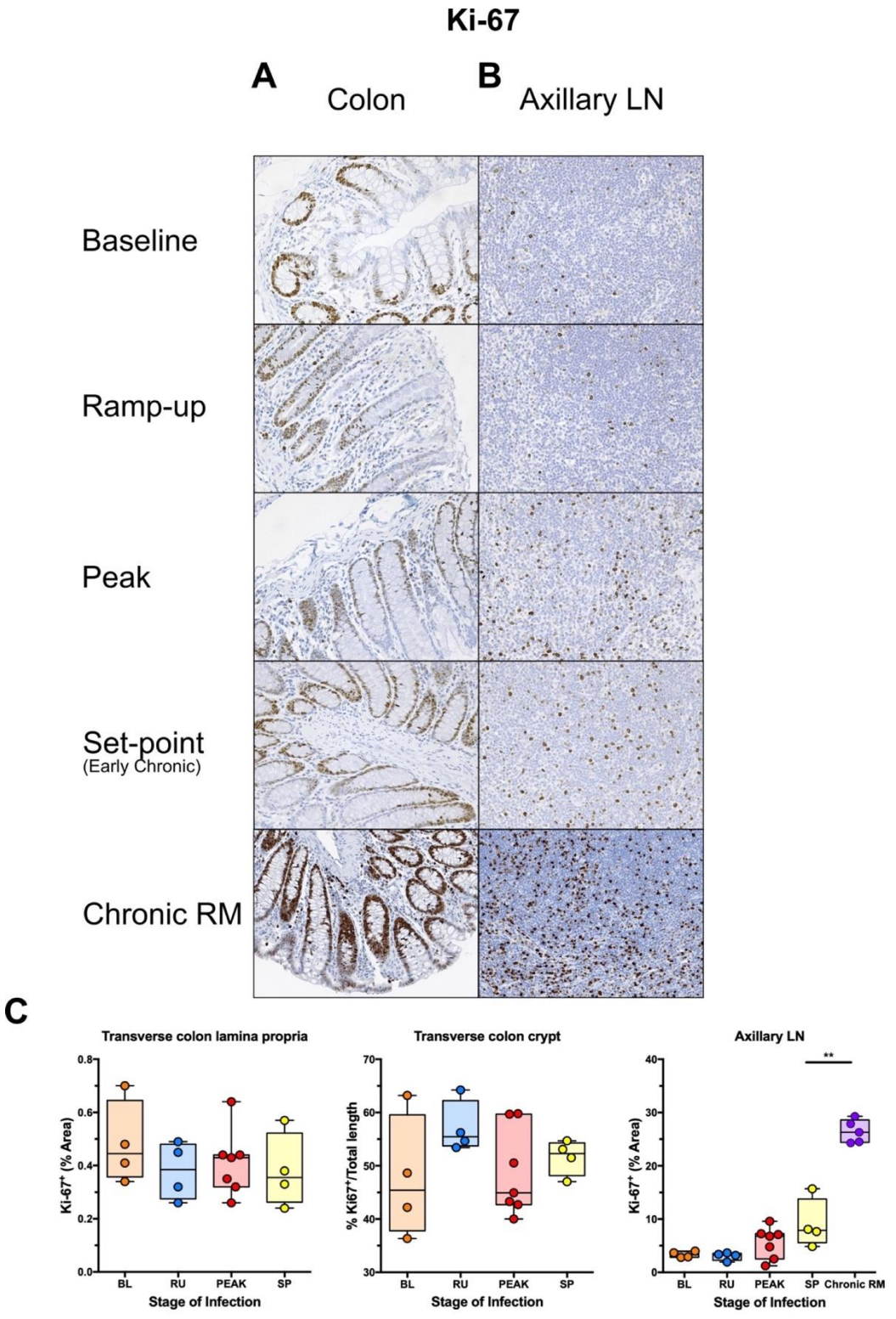

Figure 19: Immunohistochemistry (IHC) for immune activation and proliferation in SIVsab-infected African green monkeys (AGMs).

DAB-based IHC for Ki-67 in the (A) transverse colon, (B) axillary LN of AGMs and chronically SIV-infected RMs. In all the images, positive DAB signal is shown in brown, with the remaining tissue counterstained blue. The representative images of the gut display longitude cuts of the villi to better show the localization of proliferating

epithelial cells in the crypts. Representative images of the axillary LN are taken from the T-cell area, to avoid the dense clustering of proliferating cells in the B cell follicles. Below are shown image quantifications (C) of proliferation in the gut and gut mucosa. For the colon, the ratio of the length of Ki-67 epithelial cells along the colonic crypts vs the total crypt length was used to estimate epithelial cell proliferation, while exclusion of the epithelium from the images was used to measure Ki-67 in the lamina propria alone. The quantification for each animal represents the average of the values from 9-12 individual image quantifications. The four different time groups are based on the days postinfection, with: BL (baseline, preinfection), RU (ramp-up, 4-6 dpi), PEAK (peak, 9-12dpi) and SP (set-point, 46-55 dpi). Each time group is assigned a corresponding color based on the stage of viral replication: orange (baseline), blue (ramp-up), red (peak) and yellow (set-point). The chronic RMs are shown in purple. All AGM quantifications were performed using FIJI version 1.0. Asterisks indicate statistical significance, with **=$p<0.01$. All AGM images were captured at 200X magnification using an AxioImager M1 bright-field microscope equipped with an AxioCam MRc5.

Conversely, in the LNs, Ki-67 expression was slightly increased at the peak and remained elevated into early chronic infection (Figure 19B). By comparison, during pathogenic infection in RMs, the expression of Ki-67 remains highly elevated throughout the chronic infection in both the lamina propria and the mucosal epithelium (Figure 19A) of the gut, with large numbers of proliferating cells. This preponderance of Ki-67 is also reflected in the LNs, where there are far more Ki-67$^+$ cells throughout the T-cell zone, as demonstrated by quantitative analysis (Figures 19B & C). We also did not observe any significant alteration in the total number of Ki-67$^+$ cells in the jejunum (Appendix C)

As immune activation and inflammation is normally associated with recruitment of neutrophils, tissue was stained for MPO, which is a component of the azurophilic granules found in neutrophils. There was a statistically significant (*$p=0.0153$*), but transient increase in the frequency of MPO-positive neutrophils in the transverse colon during the ramp-up period (Figures 20A & C), that returned to baseline level by peak, with no significant changes in the number of MPO-expressing neutrophils in any of the other tissues studied , as shown in Figure 20A-C.

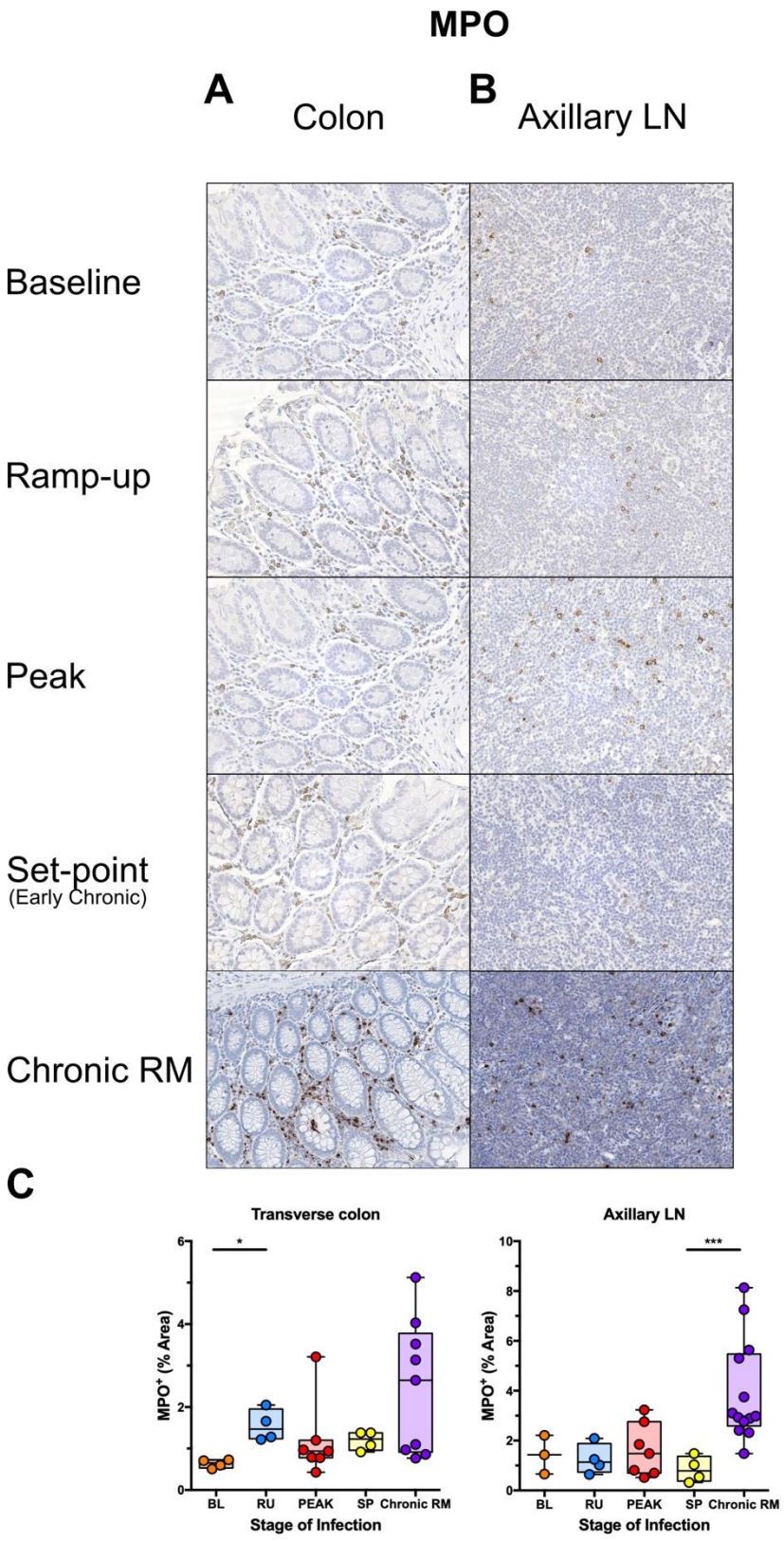

Figure 20: Immunohistochemistry (IHC) for neutrophil infiltration and activation in SIVsab-infected African green monkeys (AGMs).

DAB-based IHC for MPO in the (A) transverse colon, and (B) axillary LN of AGMs and chronically SIV-infected RMs. In all the images, positive DAB signal is shown in brown, with the remaining tissue counterstained blue. The representative images of the gut display lateral cuts of the crypts to demonstrate the presence of neutrophils in the surrounding lamina propria. Below are shown image quantifications (C) of the percent area of the total positive DAB signal. The quantification for each animal represents the average of the values from 9-12 individual image quantifications. The four different time groups are based on the days postinfection, with: BL (baseline, preinfection), RU (ramp-up, 4-6 dpi), PEAK (peak, 9-12 dpi) and SP (set-point, 46-55 dpi). Each time group is assigned a corresponding color based on the stage of viral replication: orange (baseline), blue (ramp-up), red (peak) and yellow (set-point). The chronic RMs are shown in purple. All AGM quantifications were performed using FIJI version 1.0. Asterisks indicate statistical significance, with *=$p<0.05$ and ***=$p<0.001$. All AGM images were captured at 200X magnification using an AxioImager M1 bright-field microscope equipped with an AxioCam MRc5.

Interestingly, uninfected AGMs already had a significantly larger number of MPO-positive neutrophils present in the gut at the baseline, especially compared to normal SIV-infected RMs, which have only rare MPO-positive neutrophils present in the lamina propria (195). Indeed, the overall levels of MPO-positive neutrophils present in the colon of AGMs preinfection are not dissimilar to those found in RMs during the chronic stage of infection, though in the LNs AGMs have significantly less neutrophils than RMs by the transition to chronic infection (Figures 20A & C). We also did not observe any significant change in the number of MPO^+ cells in the jejunum (Appendix C)

Conversely, any changes in MX1 were only transient, with expression increasing sharply at the peak and a full return to baseline level at the transition to chronic SIV infection, as seen in Figures 21A-C and Appendix C.

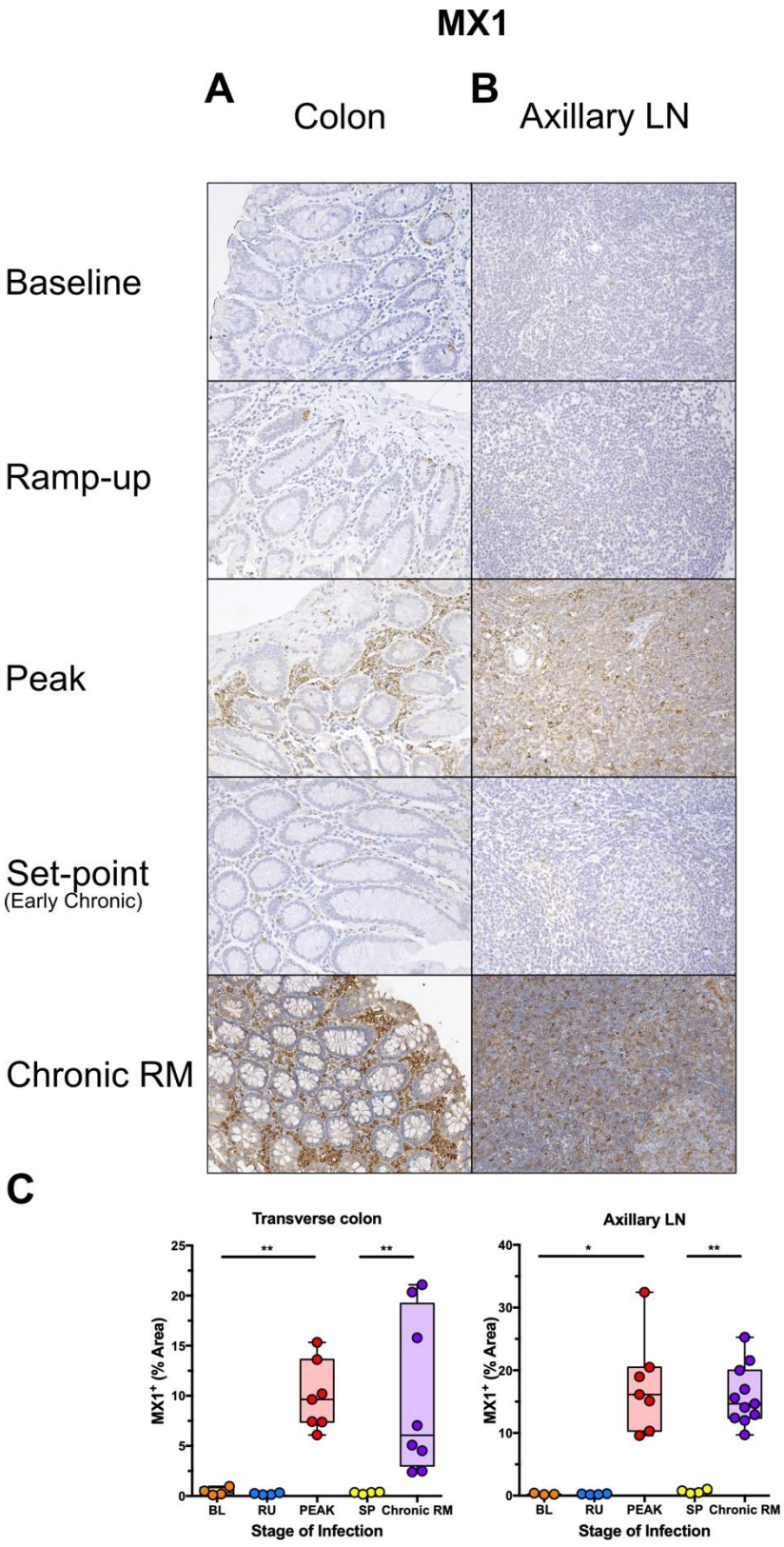

Figure 21: Immunohistochemistry (IHC) to inteferon-based responses to infection in SIVsab-infected African green monkeys (AGMs).

DAB-based IHC for MX1 in the (A) transverse colon, and (B) axillary LN of AGMs and chronically SIV-infected RMs. In all the images, positive DAB signal is shown in brown, with the remaining tissue counterstained blue. Below are shown quantifications (C) of the percent area of the total positive DAB signal. The quantification for each animal represents the average of the values from 9-12 individual image quantifications. The crypts were included in the quantification and the crypt enterocytes may have contributed to the overall % area of positive. The four time groups are based on the days postinfection, with: BL (baseline, preinfection), RU (ramp-up, 4-6 dpi), PEAK (peak, 9-12dpi) and SP (set-point, 46-55 dpi). Each time group is assigned a corresponding color based on the stage of viral replication: orange (baseline), blue (ramp-up), red (peak) and yellow (set-point). The chronic RMs are shown in purple. All AGM quantifications were performed using FIJI version 1.0. Asterisks indicate statistical significance, with *=$p<0.05$ and **=$p<0.01$. All AGM images were captured at 200X magnification using an AxioImager M1 bright-field microscope equipped with an AxioCam MRc5.

Notably, the MX1 expression during peak infection in AGMs is in the same range as during chronic pathogenic SIV infection in RMs in both the gut and LNs (Figures 21A-C). However, as MX1 expression is nearly absent by the set-point of infection, this likely reflects the fact that while there is an initial antiviral response, it is rapidly resolved in AGMs while being sustained in RMs; indeed, the chronically SIV-infected RMs have a significantly higher level of MX1 than AGMs by establishment of chronic infection (Figure 21C). These responses parallel viral replication, suggesting that the interferon-based changes observed during the acute SIV infection are strictly determined by direct viral effects.

4.4.8 AGMs show limited expression of genes associated with immune activation and epithelial damage in response to infection

A transcriptomic profiling of gut tissues taken during necropsy (265) was performed (see 5.0) with the goal to assess changes in genes associated with epithelial damage and adaptive and innate immune responses , as shown in Figure 22.

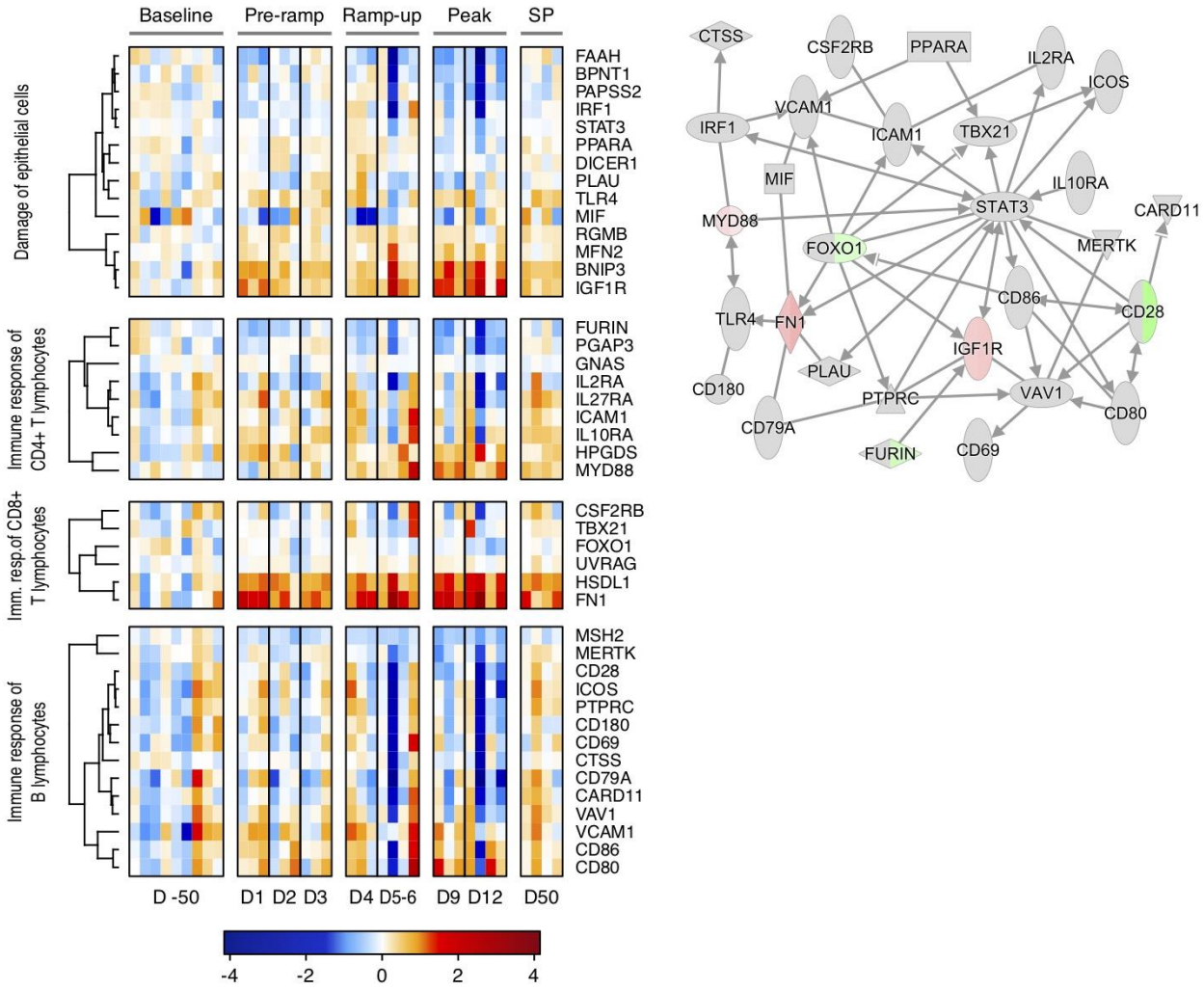

Figure 22: Heatmap & network of changes in gene expression in the gut over course of SIV infection in African green monkeys (AGMs).

RNAseq data from AGM gut tissue displayed as: (A) a heatmap showing gene expression changes in genes associated with biological processes related to SIVsab infection, immune responses and damage to the gut epithelium; (B) a network showing direct interactions between genes in SIV related processes at the peak of infection (9-12 dpi). For the heatmap, the level of alteration of gene expression is shown in blue (downregulation) and red (upregulation), with genes clustered using a Spearman correlation, with the dendrogram showing relationship displayed on the left. For the pathway, each gene is shown as a node and the arrows between nodes indicate direct gene interactions. Red nodes indicate upregulation of gene expression, green nodes indicate downregulation. In split nodes, the left and right node sections correspond to 9 dpi and 12 dpi, respectively.

Most of the genes surveyed showed limited alterations. Notable exceptions include several $CD4^+$ T cell-associated genes (including HPGDS and MYD88), which were transiently up-regulated during the ramp-up and peak stages of infection. While HPGDS can be linked to proinflammatory Th2 $CD4^+$ T cells, this primarily occurs in eosinophil-driven allergic responses in the gut (275). As an essential TLR signal transducer, MYD88 has been shown to be important for regulation of $CD4^+$ T cells, including in promoting activation in the murine inflammatory bowel model (276). As such, MYD88 could potentially be directly associated with an antimicrobial response and microbial translocation. However, MYD88 has also been linked to promotion of normal wound healing response through TLR signaling (277, 278).

Two genes linked to $CD8^+$ T-cell regulation (including HSDL1 and FN1) were more widely up-regulated during peak SIVsab infection. The HSDL1 enzyme itself is largely considered to be nonfunctional (279), but FN1 can activate degranulation of $CD8^+$ T cells (280). However, as described in 5.4.5, we showed that FN1 is a key part of unique wound healing pathway in AGMs. Repair of any damage caused by early viral replication could play an important role in the resolution of inflammation, preventing establishment of chronic inflammation later on.

Genes linked to $CD20^+$ B cell regulation were also analyzed, with no clear expression patterns being apparent and any variation appeared most likely to be due to inter-animal variability (Figure 22A).

We next established whether there were any interactions between these genes and their respective pathways. To this end, we linked established protein interactions between all included genes from the IPA database (see 5.3.4). The resulting network (Figure 22B) showed a central role for STAT3, a transcription factor associated with epithelial damage. However, most of the genes, including STAT3, did not show any significant alteration in expression from baseline. Furthermore, while STAT3 has been linked to both inflammatory cytokines and chemokines, it has been shown to be critical to signaling necessary for repair of damage to the gut (281–283).

Finally, the gene expression analysis also showed that in AGMs the strong antiviral response at the peak of infection is reflected by changes in gene expression levels. This is seen primarily through the highly increased expression of the interferon-induced genes CXCL10 and CXCL11, which promote immune cell activation and migration, and MX1, as shown in Figure 23.

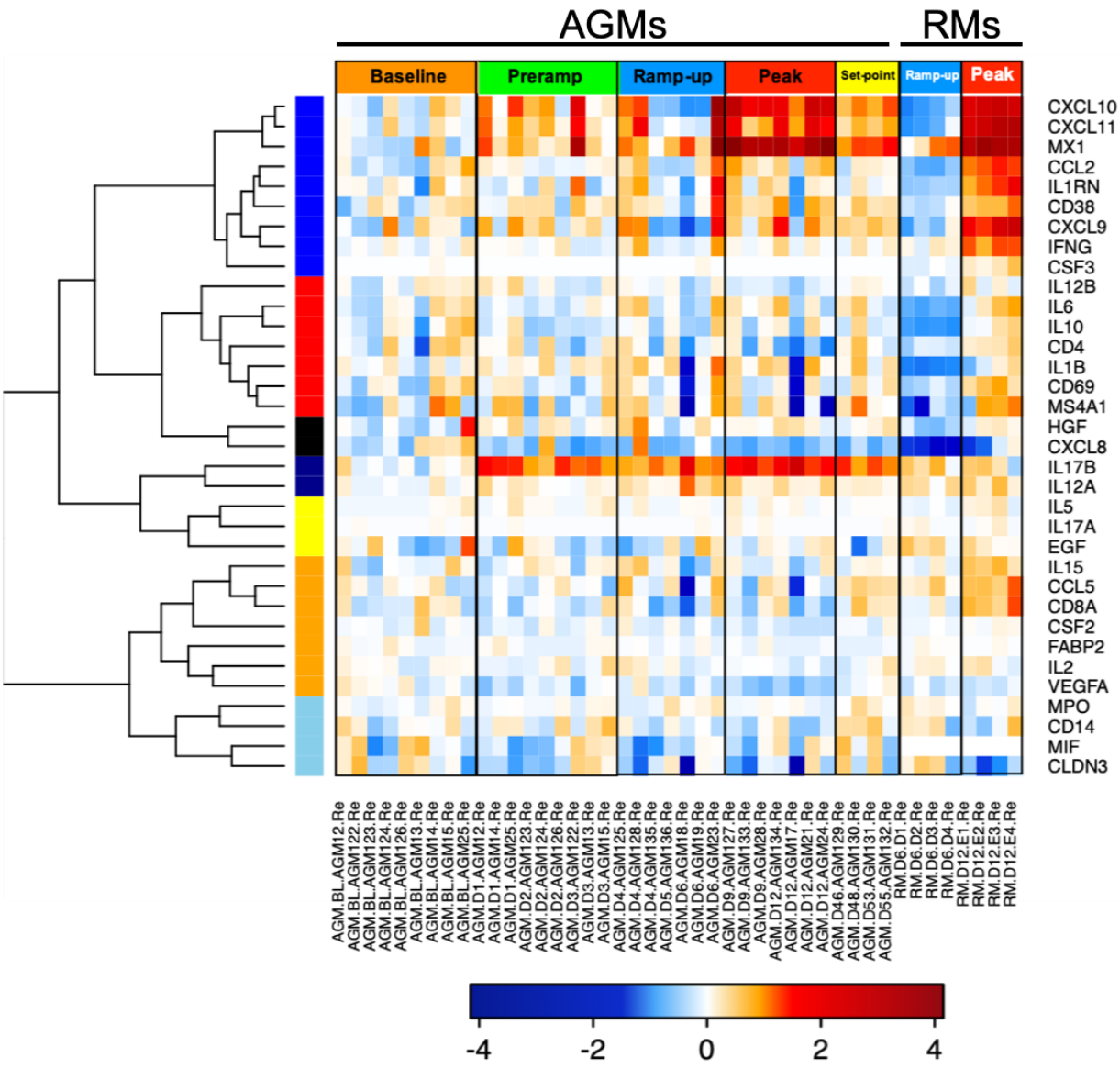

Figure 23: Comparative changes in gene expression in the gut over the course of SIV infection in African green monkeys (AGMs) and rhesus macaques (RMs).

RNAseq data from AGM and RM gut tissue displayed as a heatmap showing gene expression changes in specific genes of interest associated with biological processes related to SIV-infection and the host immune response. The level of alteration of gene expression is shown in blue (downregulation) and red (upregulation), with genes clustered using a Spearman correlation, with the dendrogram showing relationship dispalyed on the left. Animal numbers are shown below the heatmap along with dpi, while the time groups are shown above the heatmap, with the colors indicating the groups: orange (BL, baseline), green (PRU, preramp), blue (RU, ramp-up), red (peak), yellow (SP, set-point). The data for the time groups of the AGMs are listed in black text on the left, while the data from the equivalent RM time groups are listed in white text on the right.

The increase in MX1 at the peak of infection mirrors the increases we observed *in situ* in the AGMs and RMs (Figure 21). It also mirrors the increase in interferon regulated genes seen in SIV-infected RMs at the peak of viral replication (Figure 23)

However, the AGMs alone showed strong, sustained upregulation of IL-17B expression starting immediately postinfection (Figure 23). Part of the IL-17 family, IL-17B has been demonstrated to have an anti-inflammatory effect during acute colon inflammation, suggesting that it may promote control of inflammation in the AGMs (284).

4.4.9 Little to no apoptosis occurs in the gut lamina propria or epithelium during SIVsab infection

Given the central role of microbial translocation in driving disease progression and that one of the main causes of microbial translocation is the "leaky gut", we assessed the capacity of AGMs to maintain the integrity of their gut mucosal barrier (6, 61). Mucosal barrier integrity was examined by for three different conditions associated with gut damage: apoptosis, fibrosis and loss of tight junctions between epithelial cells (285–288). Apoptosis was measured in the gut and LNs by assessing the levels of active caspase-3, a central component of both the extrinsic and intrinsic apoptosis pathways (289). Relatively few cells expressed active caspase-3 in all tissues surveyed, especially the axillary LNs (Figures 24A & B & Appendix C).

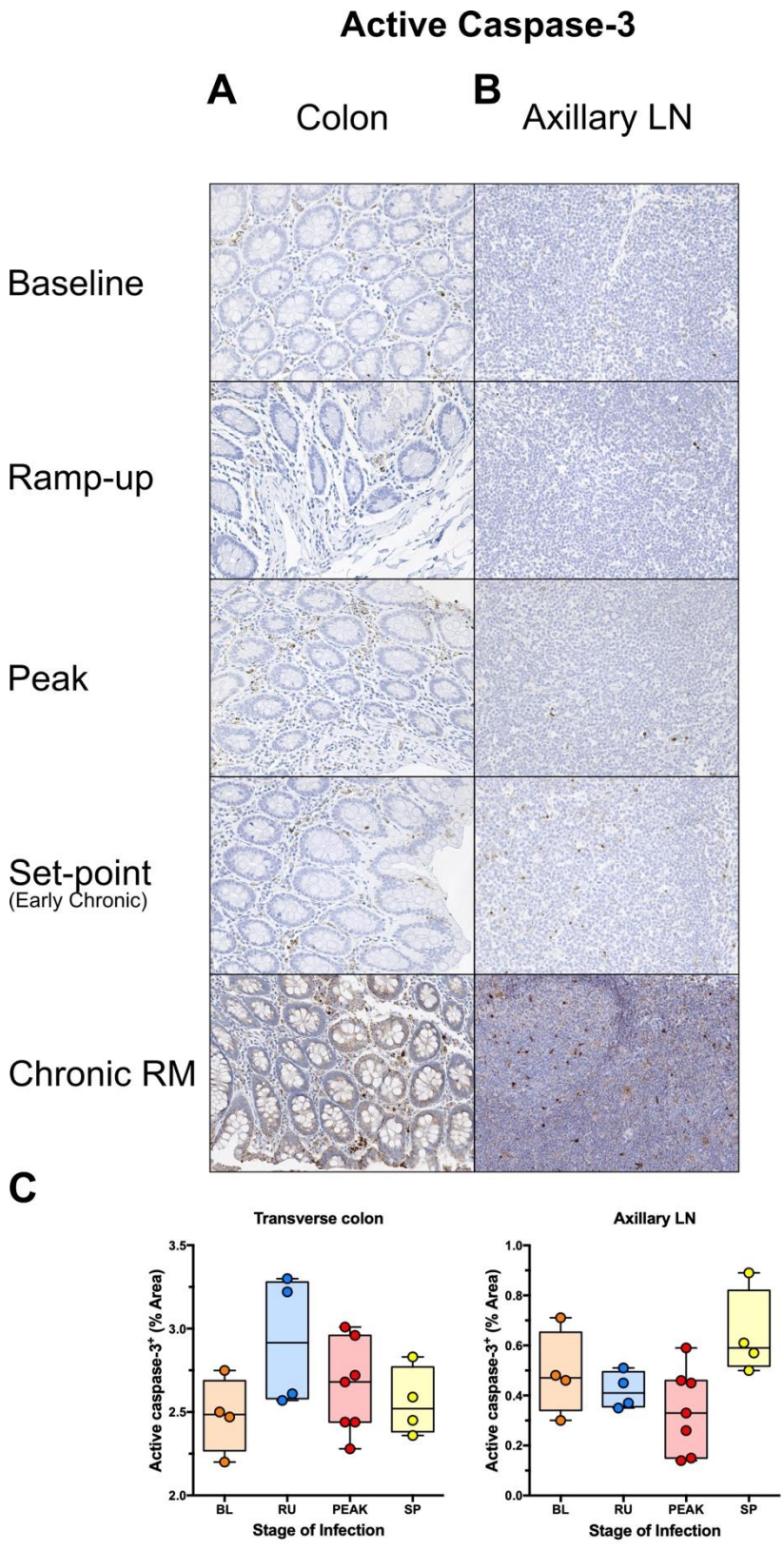

Figure 24: Immunohistochemistry (IHC) for apoptosis in SIVsab-infected African green monkeys (AGMs).

DAB-based IHC for active caspase-3 in the (A) transverse colon, and (B) axillary LN of AGMs and chronically SIV-infected rhesus macaques (RMs). In all the images, positive DAB signal is shown in brown, with the remaining tissue counterstained blue. The representative images display lateral cuts of the crypts to show apoptosis in both the epithelium and lamina propria. Below are shown image quantifications (C) of the percent area of the total positive DAB signal. The quantification for each animal represents the average of the values from 9-12 individual image quantifications. The four time groups are based on the days postinfection, with: BL (baseline, preinfection), RU (ramp-up, 4-6 dpi), PEAK (peak, 9-12dpi) and SP (set-point, 46-55 dpi). Each time group is assigned a corresponding color based on the stage of viral replication: orange (baseline), blue (ramp-up), red (peak) and yellow (set-point). All AGM quantifications were performed using FIJI version 1.0. Asterisks indicate statistical significance, with *=$p<0.05$. All AGM images were captured at 200X magnification using an AxioImager M1 bright-field microscope equipped with an AxioCam MRc5.

Using quantitative image analysis, we found a slight increase of the levels of active capase-3 in the transverse colon during the ramp-up, which did not reach significance and rapidly returned to baseline (Figure 24B), similar to the transient increase in neutrophils in the colon (Figure 20). In the jejunum and axillary LN, active caspase-3 levels remained largely unaltered, with slight tendencies to increase by the early chronic infection in jejunum and to decrease during the early stages of infection in the LNs (Figures 24B & Appendix C). Finally, active caspase-3 was expressed almost exclusively in the lamina propria of the gut with few, if any, of the enterocytes of the gut epithelium staining positive for active caspase-3 (Figures 24A & Appendix C). In contrast, a large number of enterocytes expressed high levels of active caspase-3 in chronically SIV-infected RMs (Figure 24A), reflecting the apoptosis of these cells due to chronic inflammation. The LNs of the RMs also had higher levels of active capase-3 expression than in the AGMs in both the T-cell zones and B cell follicles (Figure 24B).

4.4.10 Gut epithelial integrity is maintained throughout the course of SIV infection in AGMs

The lack of epithelial cell death was confirmed by staining for claudin-3, a principal component protein of cellular tight junctions in the gut. Tight junctions are vital not only for cell-to-cell adhesion, but also for regulating paracellular permeability and allowing small molecules and ions to move across the epithelial barrier (290). Any loss of claudin-3 due to cell death or internalization *via* endocytosis in response

to infection would be indicative of a loss of mucosal integrity (192). Importantly, no such loss was observed in the mucosal epithelium of the transverse colon, as shown in Figure 25A-B.

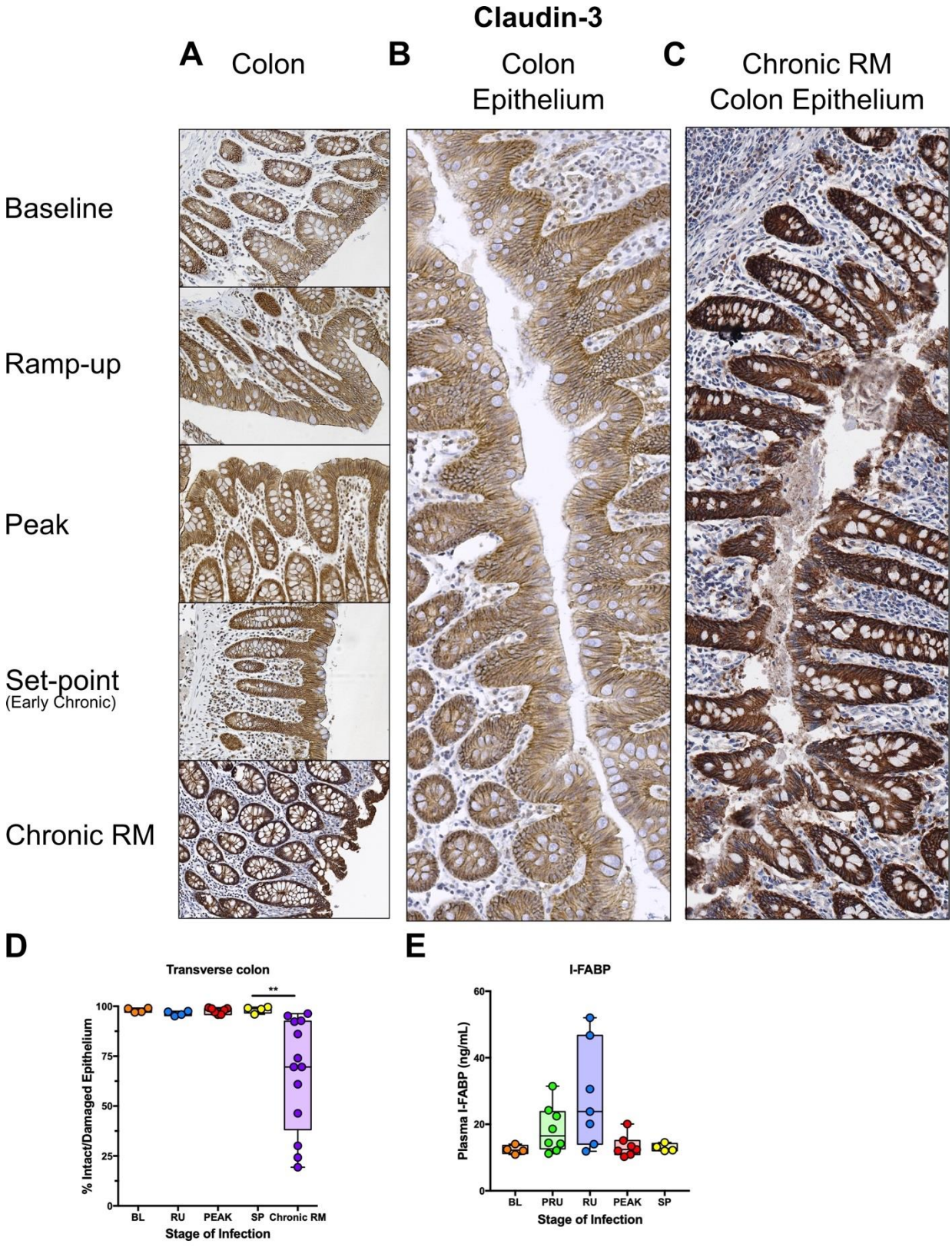

Figure 25: Immunohistochemistry (IHC) for mucosal integrity and continuity in SIVsab-infected African green monkeys (AGMs).

DAB-based IHC for claudin-3 in the transverse colon of AGMs and chronically SIV-infected rhesus macaques (RMs). In all images, positive DAB signal is shown in brown, with the remaining tissue counterstained blue. The representative images of the gut display longitude cuts of the villi to show continuity of the epithelial barrier (A). (B) Composite image of continuous transverse colon epithelium from an AGM during peak acute viral replication. (C) Image of continuous transverse colon epithelium from an RM during late chronic viral replication. (D) The percent area of the total positive DAB signal and the ratio of damaged/total epithelium. (E) Plasma concentrations in ng/μL of I-FABP, a marker of epithelial damage in the gut. The images were stitched together to form a composite image using the Stitching plugin for FIJI version 1.0. Overall continuity of the mucosal epithelium was estimated by tracing the length intact vs damaged epithelium and quantifying their relative areas. The total DAB quantifications for the AGMs represent the average of the values from 9-12 individual image quantifications, while the epithelial damage quantifications represent 3-4 composite images. The four different time groups are based on the days post infection, with: BL (baseline, preinfection), RU (ramp-up, 4-6 dpi), PEAK (peak, 9-12dpi) and SP (set-point, 46-55 dpi). Each time group is assigned a corresponding color based on the stage of viral replication: orange (baseline), blue (ramp-up), red (peak) and yellow (set-point). The chronic RMs are shown in purple. All AGM quantifications were performed using FIJI version 1.0. Asterisks indicate statistical significance, with **=$p<0.01$. All AGM individual images were captured at 200X magnification using an AxioImager M1 bright-field microscope equipped with an AxioCam MRc5. For the composite images, each individual image was captured at 100X magnification.

Measurement of the ratio of intact/damaged epithelium in the colon showed that the percent of damaged epithelium did not significantly change during SIV infection of AGMs. This is a very different scenario than in the chronically SIV-infected RMs, where the percent of damaged epithelial barrier was quite extensive and is easily observable (Figures 25C-D), consistent with previous reports (250).

To further confirm that the gut epithelium did not sustain any significant injury during early SIVsab infection, we monitored the plasma levels of I-FABP. This protein was recently established as a marker of gut damage, as it is highly expressed by mucosal epithelial cells in the small intestinal and is rapidly released upon injury (291). While the I-FABP levels (measured by ELISA) increased slightly in some animals during the preramp-up and ramp-up periods, this did not reach statistical significance and it quickly returned to baseline by the peak and remained at these levels during the early chronic infection (Figure 25E).

The jejunum was also stained for claudin-3 and, while integrity of the continuous epithelial was not quantified as was done with the transverse colon, we did not observe any noticeable loss of mucosal integrity (Appendix C).

4.4.11 Acute SIVsab infection does not induce fibrosis of the gut or LNs of AGMs

A hallmark of pathogenic HIV/SIV infections is the loss of structure and fibrotic damage of lymphoid tissues (292); therefore, we assessed whether SIV infection of AGMs is also associated with early gut and lymph node fibrosis, similar to pathogenic HIV/SIV infections (285). Collagen levels in the transverse colon, jejunum and axillary LNs did not significantly change during SIV infection of AGMs (Figures 26 & Appendix C), in contrast to the significant amount of collagen deposition in the LNs of chronically SIV-infected RMs (Figures 26B & C).

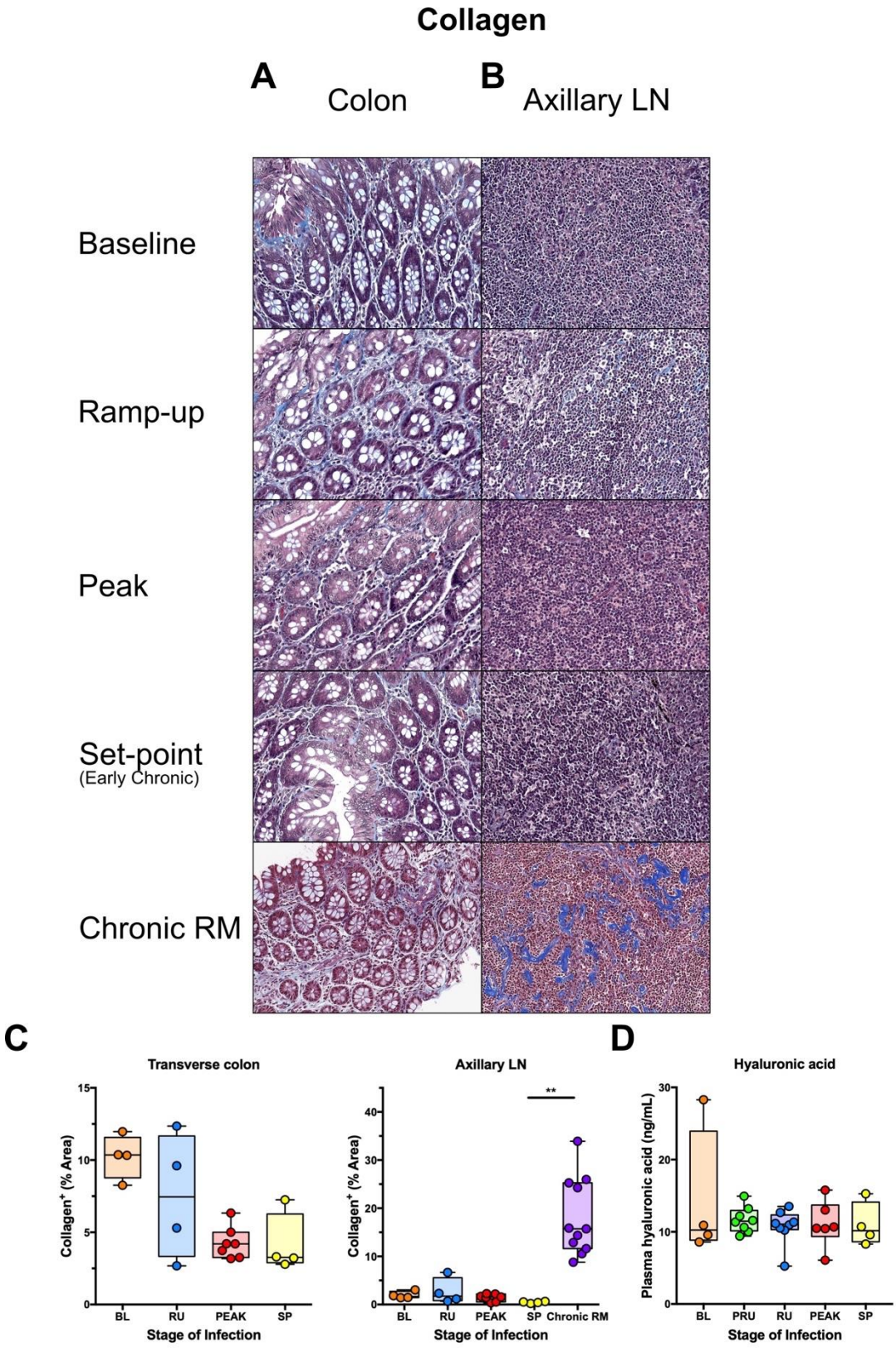

Figure 26: Immunohistochemistry (IHC) for collagen deposition and fibrosis in SIVsab-infected African green monkeys (AGMs).

Masson's trichrome stain for collagen in the (A) transverse colon, and (B) axillary LN of AGMs and chronically SIV-infected rhesus macaques (RMs). For the trichrome stain, red/pink are myosin fibers and cytoplasm, black is nuclei, and blue is collagen. The representative images of the gut display longitude cuts of the villi to better show the presence of collagen in the lamina propria. Below are shown image quantifications (C) of the percent area of the total blue signal indicating collagen. (D) Plasma concentrations in ng/μL of hyaluronic acid, a marker of fibrosis. The quantification for each animal represents the average of the values from 9-12 individual image quantifications. The four different time groups are based on the days post infection, with: BL (baseline, preinfection), RU (ramp-up, 4-6 dpi), PEAK (peak, 9-12dpi) and SP (set-point, 46-55 dpi). Each time group is assigned a corresponding color based on the stage of viral replication: orange (baseline), blue (ramp-up), red (peak) and yellow (set-point). The chronic RMs are shown in purple. All AGM quantifications were performed using FIJI version 1.0. Asterisks indicate statistical significance, with **=$p<0.01$. All AGM images were captured at 200X magnification using an AxioImager M1 bright-field microscope equipped with an AxioCam MRc5.

As limiting fibrosis and maintaining the LN architecture has been shown to be critical in preserving $CD4^+$ T-cell populations (261) during pathogenic SIV infection, avoiding early fibrosis in the LNs could contribute to prevention of disease progression in AGMs.

To further confirm the lack of fibrosis in SIVsab-infected AGMs, we monitored the plasma levels of hyaluronic acid, a biomarker of liver fibrosis (259). Our results showed no perceptible changes in hyaluronic acid levels at any point of acute SIV infection, even at the peak of viral replication, with the exception of a few outliers (Figure 26D). Together, our results demonstrate that acute SIV infection of AGMs, a natural, nonprogressive host of SIVs, is associated with no increase in intestinal epithelial apoptosis, fibrosis, or breakage of the mucosal epithelium, supporting that the overall integrity of the intestinal epithelium is maintained throughout the course of SIV infection.

4.4.12 No increased microbial translocation during early SIV infection in AGMs

To confirm the maintenance of mucosal integrity and prevention of microbial translocation in acutely SIV-infected AGMs, we performed quantitative IHC using: (i) a monoclonal antibody to the core region of lipopolysaccharide (LPS), a highly immunogenic endotoxin found in the outer membrane of Gram-negative bacteria (293); and (ii) a polyclonal anti-*Escherichia coli* antibody that cross-reacts with numerous enterobacteria species and that have previously been used as a markers of microbial translocation

in pathogenic SIV infections (250). Interestingly, prior to SIV infection, AGMs had LPS-core already present in the transverse colon, largely localized to the lamina propria. The LPS-core levels did not increase in the colon postinfection though, indicating that the observed levels of LPS are independent of SIV infection, as shown in Figure 27.

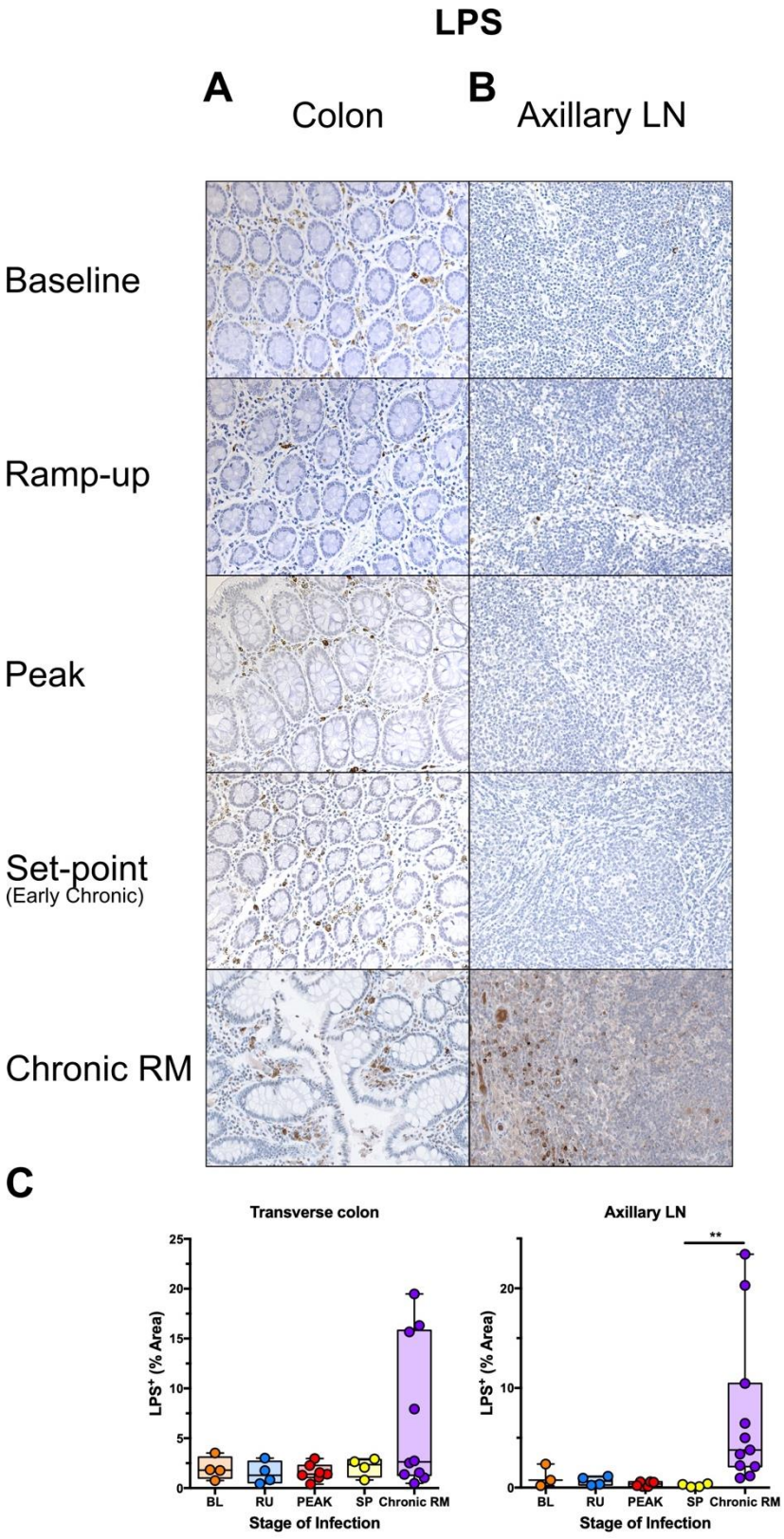

Figure 27: Immunohistochemistry (IHC) for the translocation of LPS in SIVsab-infected African green monkeys (AGMs).

DAB-based IHC for LPS-core protein in the (A) transverse colon, and (B) axillary LN of AGMs and chronically SIV-infected rhesus macaques (RMs). In all the images, positive DAB signal is shown in brown, with the remaining tissue counterstained blue. Below are shown image quantifications (C) of the percent area of the total positive DAB signal. The quantification for each animal represents the average of the values from 9-12 individual image quantifications. The four time groups are based on the days postinfection, with: BL (baseline, preinfection), RU (ramp-up, 4-6 dpi), PEAK (peak, 9-12dpi) and SP (set-point, 46-55 dpi). Each time group is assigned a corresponding color based on the stage of viral replication: orange (baseline), blue (ramp-up), red (peak) and yellow (set-point). The chronic RMs are shown in purple. All AGM quantifications were performed using FIJI version 1.0. Asterisks indicate statistical significance, with **=$p<0.01$. All AGM images were captured at 200X magnification using an AxioImager M1 bright-field microscope equipped with an AxioCam MRc5.

Quantitative image analyses of the LPS-core levels in the lamina propria at different stages of SIVsab infection in the colon revealed no significant change from baseline level (Figure 27C). Likewise, LPS-core levels were very low in the jejunum and axillary LNs and did not significantly change during SIV infection of AGMs (Figures 27B & Appendix C). In contrast, chronically SIV-infected RMs had abundant levels LPS-core present both beneath the epithelium in the gut (Figures 27A & C) and throughout the parenchyma of peripheral LNs (Figures 27B & C). It is worth noting that the presence of LPS-core in the RM peripheral LNs is extensive and contrasts sharply with the almost complete absence of LPS-core in AGM axillary LNs. This indicates that the LPS found in the lamina propria of the colon in AGMs is retained within the GI tract and not systemically disseminated, in contrast to SIV-infected RMs.

Using the additional stain to measure microbial translocation, we found that *E. coli* was present only very sparsely within the gut lamina propria (Figures 28A & Appendix C), and at very low levels in the axillary LNs throughout the course of infection (Figure 28B).

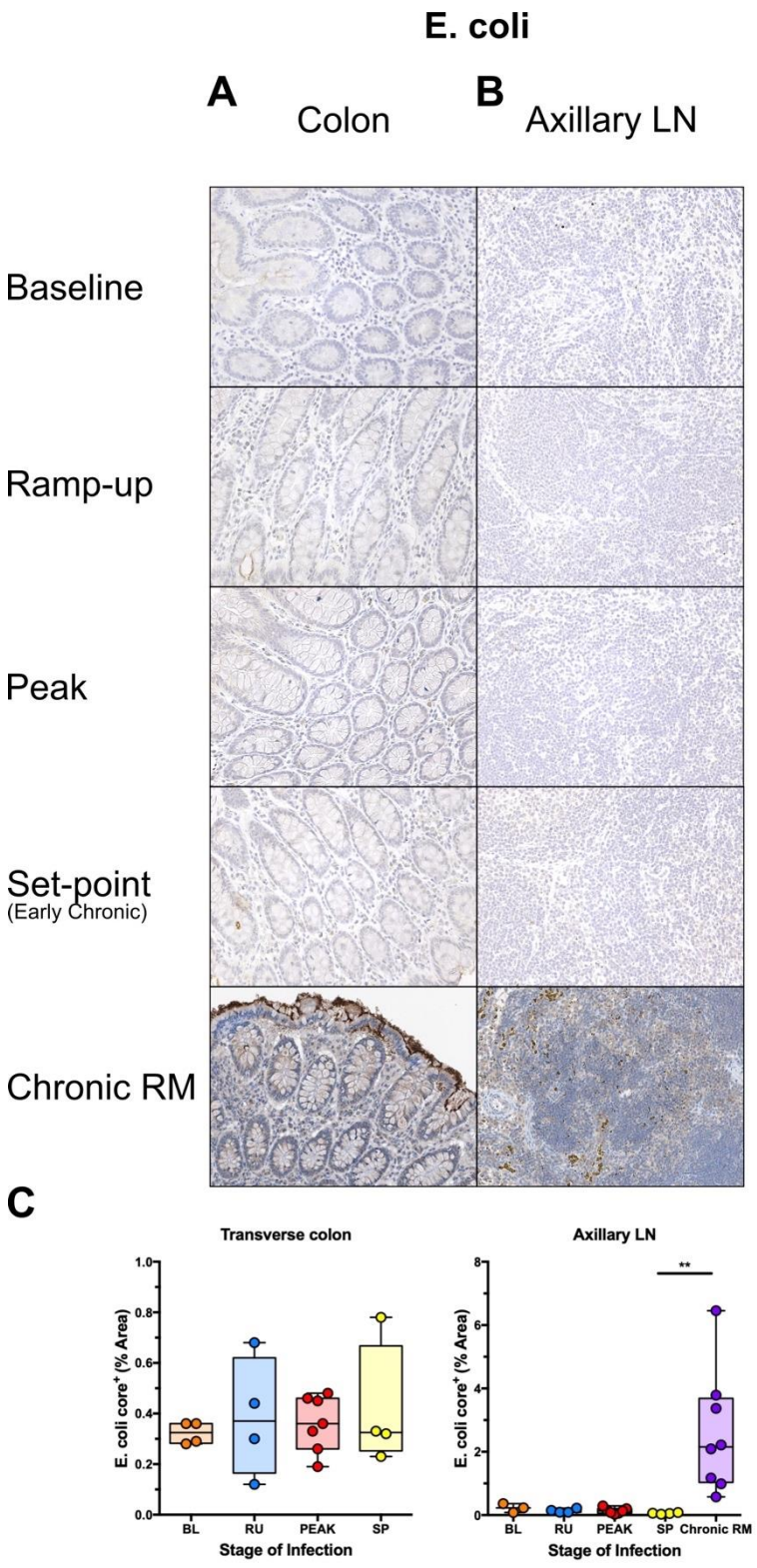

Figure 28: Immunohistochemistry (IHC) for translocation of *E. coli* in SIVsab-infected African green monkeys (AGMs).

DAB-based IHC for *E. coli* in the (A) transverse colon, and (B) axillary LN of AGMs and chronically SIV-infected rhesus macaques (RMs). In all the images, positive DAB signal is shown in brown, with the remaining tissue counterstained blue. Below are shown image quantifications (C) of the percent area of the total positive DAB signal. The quantification for each animal represents the average of the values from 9-12 individual image quantifications. The four different time groups are based on the days post infection, with: BL (baseline, preinfection), RU (ramp-up, 4-6 dpi), PEAK (peak, 9-12dpi) and SP (set-point, 46-55 dpi). Each time group is assigned a corresponding color based on the stage of viral replication: orange (baseline), blue (ramp-up), red (peak) and yellow (set-point). The chronic RMs are shown in purple. All AGM quantifications were performed using FIJI version 1.0. Asterisks indicate statistical significance, with **=$p<0.01$. All AGM images were captured at 200X magnification using an AxioImager M1 bright-field microscope equipped with an AxioCam MRc5.

Quantitative image analysis demonstrated that none of the tissues displayed any significant changes in the *E. coli* levels during the course of SIV infection in AGMs. In contrast and, as with LPS, abundant levels of *E. coli* were present in both the gut lamina propria and peripheral LNs of the chronically SIV-infected RMs, with significantly higher levels of *E. coli* in the LNs than early chronic AGMs (Figures 28A-C). In summary, AGMs are able to maintain gut mucosal integrity throughout all stages of SIV infection, thereby preventing the translocation of microbes or microbial products from the lumen to surrounding tissues and, as such, preventing chronic inflammation and disease progression.

4.5 Discussion

African NHPs that are natural hosts of SIVs avert disease progression despite sustaining high levels of SIV replication by mechanisms only partially understood. It is widely acknowledged that understanding these mechanisms has the potential to generate new strategies for preventing HIV disease progression in humans (46, 78, 88, 96, 97, 124–127, 135, 156, 243, 248, 294), and could help alleviate the social and financial burden of HIV infection and long-term ART (294, 295).

Here, we thoroughly assessed the impact of acute SIVsab infection in AGMs at the mucosal sites to understand if their ability to avoid disease progression stems from maintenance of a healthy gut throughout infection, or an exquisite capacity to rapidly resolve the effects of viral replication and T-cell

depletion at mucosal sites. In progressive lentiviral infections (i.e., SIV infection of macaques and HIV infection of humans), the majority of gut $CD4^+$ T cells are initially killed by direct viral cytopathic effects due to ongoing viral replication, which drives apoptosis of epithelial enterocytes, immune activation in the gut, recruitment of innate immune cells and inflammation, leading to further damage the gut epithelium fueling destruction of the gut mucosal barrier and MT that trigger chronic systemic immune activation and inflammation (253, 254, 296).

Given the importance of the initial virus-host interactions and viral cytopathic effects in establishing this vicious cycle, we assessed the dynamics of viral replication in the GI tract after intrarectal challenge and found high levels of viral replication starting as early as 4-6 dpi in the gut and even earlier in the draining LNs. We anticipated that these high levels of viral replication would be paralleled by depletion of $CD4^+$ T cells, the major cellular targets of SIVsab. However, in spite of the high levels of virus replication in both the gut and LNs (Figures 4 & 5), the overall levels of $CD4^+$ T cells were relatively stable during the early stages of infection (Figures 13), in contrast to previous reports of significant mucosal $CD4^+$ T-cell depletion in AGMs during acute and early chronic infection (46, 78, 88).

One possible explanation for this discrepancy is that while the previous studies have largely relied on longitudinal blood and tissue sampling from the same animal, our cross-sectional study mostly compared data between different animals; thus, individual variations between animals (which can be very large in AGMs) may have partially obfuscated the $CD4^+$ depletion. Indeed, for the blood and LNs, where preinfection samples were available for all the animals, allowing for direct pre- *versus* postinfection comparison, we were able to document $CD4^+$ T-cell depletion (Figure 13).

As the early viral replication induces high levels of immune activation in pathogenic infections (61), we assessed the levels of immune activation in early SIVsab infection of AGMs. As a marker of activation *via* proliferation, Ki-67 expression by $CD4^+$and $CD8^+$ T cells or $CD20^+$ B cells did not significantly increase in either the gut or the LNs at any time, by either flow cytometry (Figure 14) or IHC (Figures 18). While low levels of immune activation by establishment of chronic infection is in agreement with previous studies of natural hosts (78, 88, 89, 126, 159), sooty mangabeys previously showed increased

markers of T-cell activation in the LNs during acute infection (153). This suggests that reduced early immune activation may be a unique feature of AGMs as a natural host of SIV.

In contrast, Ki-67 expression increased in the gut and LNs of pathogenically infected RMs (Figures 18 & Appendix C) Our observation of low levels of immune activation was also supported by our finding that there were few alterations in gene expression that would indicate a major uptick in $CD4^+$ or $CD8^+$ T-cell activation during acute infection and essentially no major alteration to $CD20^+$ linked genes (Figure 22 & Figures 23). The most notable alterations were linked to interferon-stimulated genes (ISGs), with highly elevated gene expression around the peak of infection. This is similar to what was previously observed, though our study only examined gene expression in gut tissue and didn't follow the animals into late chronic infection (156).

As T-cell immune activation is usually accompanied by an innate immune response, we assessed neutrophil recruitment to the gut and found little to no neutrophil accumulation in the gut mucosa and superficial LNs (Figure 20 and Appendix C). These results are in stark contrast with the large scale recruitment of MPO-positive neutrophils to the gut epithelium in chronically SIV-infected RMs, both in our study (Figure 23) and previous studies (249), as well as in HIV-infected subjects (245), or in other pathological conditions associated with gut inflammation and MT, such as IBD (297). We also saw no major change in MPO gene expression levels in the AGMs at any time during infection (Figure 23) supporting the lack of sustained alteration to neutrophil populations in response to SIV infection in AGMs, though the expression levels of MPO do not necessarily correlate with the number of neutrophils in the gut.

Interestingly, the AGMs actually had similar levels of neutrophils in the gut to some of the chronically infected RMs (Figure 23C) and to RMs during early acute infection (249). Historically, it has been shown that both uninfected RMs (195) and HIV^{neg} individuals (245, 298) tend to have very small numbers of neutrophils resident in the gut, so their presence in AGMs suggests some role in responding to SIV infection. One possible explanation is that the resident gut neutrophils respond immediately to any possible leakage, no matter how minimal, from the gut lumen during the acute infection, through mechanisms like phagocytosis and the release of NETs. Indeed, we do see a significant increase in the

number of MPO-positive cells in the colon only during the ramp-up period (Figure 23C), possibly indicating a transient increase of neutrophils during the earliest period following infection. However, any activity by neutrophils would have to be carefully controlled to minimize collateral damage to the epithelium, as occurs in many inflammatory mucosal disorders (299). Another possible explanation for their presence is that the resident gut neutrophils in AGMs play a nontraditional role and contributing directly to maintaining the epithelial barrier, though the vast majority of evidence supports neutrophils having net negative impact on tissue homeostasis (300).

Populations of other immune cell types typically involved with the initial innate response and the subsequent inflammation, including DCs, macrophages and NK cells (Figure 15) were also virtually unchanged from baseline in acutely SIVsab-infected AGMs. Together with the lack of sustained MPO-positive neutrophil infiltration, this suggests a limited recruitment of innate response effectors to the major site of early viral replication, which may help dampen the early proinflammatory responses in AGMs.

Previous research has shown that in both pathogenic and nonpathogenic hosts, activated immune cells and epithelial cells exhibit increased production of proinflammatory cytokines in response to HIV/SIV infection (6, 202–204, 249). However, in pathogenic hosts, this increase is sustained chronically, while nonpathogenic hosts resolve their inflammation by establishment of an anti-inflammatory milieu early during infection (127). Supporting this trend, we found that there were only transient increases in a limited set of immune-linked cytokines/chemokines (Figure 22) that were mostly resolved by chronic infection. Additionally, we observed that almost immediately following infection the AGMs exhibited increased expression of the gene encoding IL-17B (Figure 23), which is a T cell-derived cytokine with potential anti-inflammatory effects in the gut (283).

However, control of inflammation does not mean lack of response by the host, as demonstrated in previous studies by the ability of the natural hosts to mount robust innate immune responses during acute infection (154, 156, 157, 163), particularly the type 1 ISGs genes (ISGs), including MX1, MX2 and IP-10. These responses are then rapidly resolved at the transition to chronic infection, as we observed here with MX1 in our AGMs (Figures 21 & 23). In contrast, SIV-infected RMs exhibit strong innate immune

activation and ISG upregulation throughout the entire course of SIV infection (154, 156, 157, 163), as reflected by the high levels of MX1 in our chronically infected RMs (Figures 21 & S23). Persistence of IFN-based responses in pathogenic SIV infections eventually induces IFN desensitization and decreased ISG expression, resulting in increased SIV reservoir size and $CD4^+$ T-cell loss (272).

Interestingly, while some acute SIV infection studies observed upregulation of MX1 and other ISGs as early as 1 and 6 dpi (156), here the tissue protein levels of MX1 did not increase prior to the peak, at 9-12 dpi (Figure 21). This discrepancy may be due to the route of inoculation (mucosal *versus* IV), that could shift the acute infection towards later time points (78). Additionally, some of the individual AGMs did exhibit increased expression levels of ISGs, including MX1, earlier during infection (Figure 23). This suggests that the early virus replication might be sufficient in some cases to induce a response that is both transient and of a far lesser magnitude than seen at the peak of virus replication.

Going hand-in-hand with the greater levels of immune activation, pathogenic SIV infections are also differentiated from nonpathogenic infections by the massive increase in apoptosis of both the $CD4^+$ T cells in the lamina propria and the mucosal epithelial cells in the gut (76, 285), as we observed in our chronically SIV-infected RMs (Figure 24). This drives the mucosal epithelium into a compensatory state of regeneration, with high levels of proliferation and turnover, as reflected by a significant, simultaneous increase in both Ki-67^+ and active caspase-3-positive epithelial cells (285). We found no increase of either of these markers in SIV-infected AGMs (Figures 18 & 24), despite the sustained high levels of viral replication in the gut (Figure 4 & 5), in agreement with previous studies (198).

Epithelial cell death and loss of mucosal barrier integrity is also reflected by degradation of the tight cell junctions, resulting in breaks in the gut epithelial layer (249, 301). In SIV-infected RMs, claudin-3 staining has been used to measure the breakdown in mucosal epithelium continuity, while expression of claudin-encoding genes (i.e., *CLDN3*) has been shown to be downregulated as early as 3 dpi (302), similar to what was also observed in rats during experimentally-induced IBD (287). Importantly, at no timepoint post SIVsab infection in AGMs did we find that the mucosal epithelium integrity was significantly damaged, nor were the levels of claudin-3 gene (CLDN3) expression in the gut altered, in stark contrast

with reduced mucosal epithelium integrity in chronically infected RMs (Figures 25A,B,&D & Appendix C). These histologic data were supported by the finding of relatively stable levels of plasma I-FABP in the SIVsab infected AGMs (Figure 25E). We also observed upregulation of several genes linked to wound healing and repair of epithelial damage (Figures 22 & 23), suggesting that the lack of damage might be connected to maintenance of the gut epithelium itself, as shown in 5.0 (264). The importance of maintenance of the gut barrier in natural hosts was shown when experimental colitis induced in AGMs recapitulated many of the features of pathogenic SIV infections, including higher levels of plasma SIV RNA, sCD14, LPS, C-reactive protein and an increased rate of mucosal $CD4^+$ T-cell loss (195).

Apart from loss of gut mucosal integrity, increased collagen deposition is also a hallmark of pathogenic HIV/SIV infections and impaired immune recovery in the gut (284, 303). It has also long been known that destruction of LN architecture and the subsequent fibrosis is characteristic of chronic HIV-infection in humans and SIV-infection in RMs (Figures 26B & C) (304, 305). In keeping with the lack of chronic inflammation, we found no evidence of increased fibrosis (i.e., collagen deposition) in either the gut or LNs of SIVsab-infected AGMs (Figures 26 & Appendix C), and we confirmed this result by showing stable levels of hyaluronic acid in the plasma throughout the follow-up (Figure 26D).

Finally, we directly assessed the levels of MT in SIVsab-infected AGMs by measuring LPS-core and *E. coli* in the lamina propria and LNs by quantitative IHC. None of these markers showed significant increases during either acute or postacute SIVsab infection (Figures 27 & 28 & Appendix C), in contrast with chronically SIV-infected RMs (Figures 27 & 28). This is also unlike the results seen in SIV-infected AGMs that were treated to induce experimental colitis (191, 195, 248, 249, 269).

Interestingly, the uninfected AGMs did have higher levels of LPS, but not of *E. coli*, in the lamina propria of the transverse colon compared to uninfected RMs, though these levels were stable even after infection and lower than those seen in the chronic RMs (Figures 27 & 28). It is possible that gut resident phagocytic cells in AGMs, such as neutrophils, macrophages or DCs, take up LPS from the colonic lumen, but actively attenuate inflammatory responses. It has been shown that human colonic macrophages are highly anergic to LPS as a proinflammatory stimuli, possibly through interaction with the commensal

colonic flora (306, 307), making it plausible that an analogous form of anergy to LPS may exist in AGMs. This may even contribute to dampening the early inflammatory response induced by MT following SIV infection. Indeed, a study in SMs, another natural SIV host, showed an alteration to the TLR4 gene associated with a blunted response to TLR4 ligands (308). As LPS is one of the most important TLR4 ligands, a similar LPS anergy in AGMs could promote an attenuated SIV pathogenesis.

As such, our results showed that in the absence of mucosal damage, the transient increases in inflammatory responses observed in natural SIV infection do not have any major pathogenic consequences. It follows that any interventions to prevent or modulate intestinal mucosal damage during HIV/SIV pathogenic infection may result in a lack of disease progression, even in the presence of active viral replication. A similar situation has been observed with viremic nonprogressor HIV-infected subjects, where limited immune activation and inflammation are associated with lack of disease progression (309, 310). Our study therefore suggests that early interventions aimed at repairing or preventing gut epithelial damage may represent a viable alternative to the current interventions intended to curb the deleterious consequences of HIV infection.

5.0 Macrophage associated wound healing contributes to control of SIV pathogenesis in African green monkeys

5.1 Contributors

Data contributed to the dissertation by several collaborators is included in the following section. Notably, all work related to the RNAseq, including design and implantation of the bioinformatic analyses, was done by Dr. Frederick Barrenäs. Because of this, Dr. Barrenäs is cofirst author on the associated publication, along with the dissertation author. Dr. Qingsheng Li contributed the immunohistochemistry staining, imaging and image analysis for the fibronectin. Drs. Guido Silvestri and Steve Bosinger contributed to the macrophage sorting. The dissertation author managed the serial necropsies and tissue sampling, performed all the immunofluorescence stains and the confocal microscopy, and conducted immunohistochemistry staining, imaging and image analysis for the tissue macrophages.

5.2 Background

As described in 1.4.6, one of the defining trait of the natural hosts of SIV is lack of persistent immune activation (97, 126, 127, 154). In non-natural hosts like humans and macaques, sustained expression of markers of immune activation are strong indicators of mortality (311). Some of the immunological mechanisms linked to the control of immune activation in natural hosts include: (i) alterations in sequence or expression of CD4 or CCR5 (38, 135, 312) on target cells, restricting infection; (2) resolution of viral induced interferon signaling and activation of innate immune cells (see 4.4.7) (154, 156, 177); (3) preservation of the maintenance of mucosal integrity (see 4.410) (89, 135, 177, 191, 249).

Transcriptomic analyses of RMs acutely infected with SIVmac have found that genes associated with activation of NK cells, monocytes and T cells in rectal tissues are strongly up-regulated (313). The intestinal tract also has a dramatic decrease in the expression of tight junction protein during the acute stage of pathogenic SIV infection in RMs (302). This allows microbial components to penetrate the epithelial barrier, leading to microbial translocation and setting up the chronic inflammatory responses crucial to driving the development of AIDS (249).

In contrast, $CD4^+$ T cells of SIV-infected AGMs actually mount interferon responses earlier than in RMs, but resolve them after the acute stage of infection; resolution of this early innate immune response could potentially have a major effect on preventing a pathogenic outcome of infection (156, 163, 177). Likewise, both the colon and lymph nodes show strong but transient immune activation, along with polarization of naïve T cells into Th1 cells and progenitor cell regeneration during acute infection in AGMs (163). Myeloid DCs also show diminished immune activation and apoptosis during acute SIV infection in AGMs, compared to pathogenic hosts (180). Taken together, these factors demonstrate the importance in natural hosts of regulating immune responses in such a way to minimize the deleterious impact of viral replication and help maintain homeostasis, both of immune function, as well as mucosal integrity.

To define the gene expression signatures of acute SIV/HIV infection that link the immune response at the site of inoculation with systemic immune regulation, we simultaneously examined alterations in gene expression and the associated tissue responses after intrarectal SIV inoculation of both AGMs and RMs with their respective SIVs. Using total RNAseq, bioinformatics, viral load testing and IHC, we found highly dissimilar gene expression dynamics between AGMs and RMs postinfection.

To fully investigate these differences, a novel systems biology approach was developed, referred to as conserved gene signature analysis (CGSA). This approach operates by correlating gene expression signatures from acutely SIV-infected animals with multiple informative transcriptomic datasets from the public domain. These datasets encompassed relevant tissue, such as immune cell subsets, mucosal tissue, and epithelial cells, along with related conditions, like tissue damage, immune activation and cytokine stimulation. The data sets were also derived from a variety of different species. This enabled CGSA to

perform a data-driven, unbiased investigation of novel pathogenic or protective mechanisms of SIV disease progression in both natural and non-natural hosts.

5.3 Methodology

5.3.1 Animals and infections

For the AGMs, as described in 3.3.1 and 3.3.2. The RMs were housed at the Washington National Primate Research Center according to guidelines approved by the University of Washington Environmental Health and Safety Committee, the Occupational Health Administration, and the Primate Center Research Review Committee. Experiments were approved by the Institutional Animal Care and Use Committees (IACUCs) of the University of Washington (#214207), and Emory University (#2002173). Each RM was intrarectally inoculated with 1 ml of inoculum containing 6000 $TCID_{50}$s (50% tissue culture infectious doses) of SIVmac251.

The RMs were serially euthanized over the course of acute and early chronic SIV infection and were divided into the following groups based on their predicted viremic status at the time of sacrifice: (i) preinfection (baseline); (ii) preramp-up (1-3 days postinfection (dpi); (iii) ramp-up (6 dpi); (iv) peak (12 dpi); (v) set-point (84 dpi), as outlined in Figure 29. This design paralleled the one used for the AGMs (Figure 1). It should be noted that the uninfected RMs in the baseline group were only used for histological surveys, as gene expression baselines were established from samples collected prior to infection, as described below.

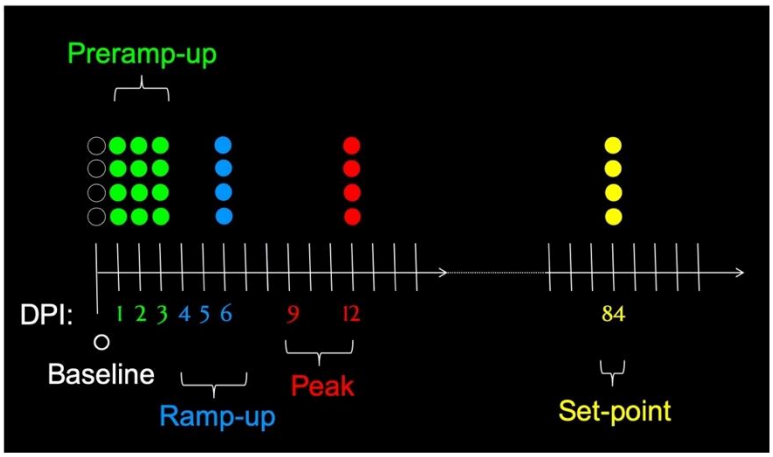

Figure 29: Rhesus macaque (RM) groups for study of intrarectal SIVmac251 infecton.
The RMs were euthanized throughout the acute and early chronic SIV infection and were divided into the following groups based on their predicted viremic status at the day post infection (dpi) that the necropsy was performed: (i) preinfection (baseline); (ii) preramp-up (1-3 dpi); (iii) ramp-up (4-6 dpi); (iv) peak (9-12 dpi); (v) set-point (46-55 dpi).

5.3.2 Tissue processing and isolation of mononuclear cells

Tissues were collected and processed for the RMs similarly to the AGMs, as described in 3.3.3. To create baseline transcriptomic profiles, pinch biopsies were taken from the rectum 50 days prior to inoculation for the AGMs and 14 days prior to inoculation for the RMs. At the time of necropsy, all rectal tissue samples were taken using the method outlined in 3.3.3 and at a depth of 25 mm from the anus, corresponding to the depth at which the inocula were deposited. During necropsy, blood draws and other tissues were taken from the RMs for viral load measurement, cell separation and histology, as was done with the AGMs. Sections of the rectum and distal colon were immediately perfused in RNAlater, and then stored at -80°C until extraction of genomic material later.

5.3.3 Rectal tissue transcriptomic profiling

As described in 4.3.12. The full rectal sequencing data, including gene counts, can be found in Gene Expression Omnibus (GSE111077).

5.3.4 Bioinformatic analysis

Differentially expressed (DE) genes were identified using the edgeR library and defined as having an adjusted p-value (*false discovery rate*) less than 0.05 and absolute fold change greater than1.5.

For CGSA co-expression network construction, the log counts per million (CPM) from RM/SIVmac251 and AGM/SIVsab92081 were combined into one matrix, creating a single row for the RM and AGM homologues of each human gene, respectively. To focus the analysis on the response to SIV inoculation (and not on differences between the species) the average baseline expression value for the RM and AGM data was subtracted from their respective time series, resulting in log CPM fold change values (i.e. positive values where genes show above-baseline expression and negative values where genes show below-baseline expression).

The Acute SIV Co-expression Network was created from the pool of DE genes using rank-based network construction (302), with midweight bicorrelation (bicor) (314) as distance metric. The only parameter for this method is the number (*d*) of interactions to assign each gene, which was selected using gene ontology (GO) biological process similarity (315). We found that *d* values of 1 and 2 added interactions with high biological relevance, compared to when *d* was increased to 3 and above. We therefore selected to use a *d* value of 2.

Transcriptomic datasets from Gene Expression Omnibus were included based on four criteria: (1) relevance for the biological process in which the DE genes were enriched, as shown below in Figure 30C; (2) that data was obtained from relevant tissue, such as epithelial cells or colon biopsies, based on enriched GO terms; (3) a high number of samples, for statistical power; (4) the data described a time series similar

to the time course of acute SIV infection, or was from a large clinical study. Each interaction between two genes (termed *a* and *b*) was given a weight, defined as a weighted mean between the bicor values in acute SIV infection and the 23 reference datasets:

$$W_{a,b} = \frac{A_{a,b} * 1 + R_{a,b} * 5.75}{1 + 5.75}$$

Where $A_{a,b}$ is the bicor value between gene *a* and *b* in the acute infection data; $R_{a,b}$ is the bicor provided by the reference datasets. In reference datasets from mouse, rat and axolotl, probe IDs were mapped to ensemble gene IDs, and to their human orthologue when one-to-one orthologues were available. Otherwise, they were excluded from the rest of the analysis. The weight (5.75) was selected to optimize GO term similarity values in the resulting network:

$$R_{a,b} = \frac{\sum_{i=1}^{23} D_{a,b,i} * u_i}{\sum_{i=1}^{23} u_i}$$

Where $D_{g1,g2,i}$ is the bicor value between *g1* and *g2* in reference dataset *i*. Given that the datasets can be of varying size and quality, the datasets were given individual weights (*u*), defined as the Spearman correlation coefficient between the vector of bicor values for the dataset (*D*) and the similarity values of the corresponding GO term. Biological modules were identified in the network using a modularity optimization algorithm (316).

The complete R code and more details about the methods and the analytical pipeline used are available from Dr. Barrenäs (fredrik.barrenas@icm.uu.se) upon request.

5.3.5 Immunohistochemistry

Samples of rectal tissue were collected from animals euthanized at baseline, at 1 dpi and at 3 dpi. The samples were fixed in SafeFix II (RMs) (cat# 23-042-600, Fisher Scientific) or paraformaldehyde (AGMs, see 3.3.3) and later embedded in paraffin. Antibodies against fibronectin (FN) (1:5,000 dilution; cat# 3776-1, Epitomics Inc.) and HAM56 (1:100 dilution, cat# 14-6548-93, eBioscience) were used for IHC as previously described (193). The IHC for FN was performed by Li et al. (School of Biological Sciences, University of Nebraska-Lincoln). and the HAM56 IHC was performed in our lab.

Whole FN stained slides were scanned and digitized using an Aperio ScanScope slide scanner (Leica, Buffalo Grove, IL). For quantitative image analysis, the slide scans were imported into Aperio ImageScope software (Leica). Regions of the rectal lamina propria and epithelium were selected using the ImageScope drawing tools. FN expression was quantified using a positive pixel count algorithm in the Spectrum Plus analysis program (version 9.1). The parameters of the algorithm were manually tuned to accurately match the FN^+ markup image over the background DAB stain. Once the parameters were set, the algorithm was applied automatically to all images to measure FN^+ signals by area.

Quantitative image analysis was also performed for HAM56 using the methodology described in 4.3.11. Additionally, given that variable structure and cell distribution within the rectal lamina propria, the initial quantification was verified by performing additional imaging for the entire lamina propria from the epithelium to the underlying muscularis mucosa, when possible. To isolate the lamina propria alone for quantification, for each image the luminal space and all the surrounding tissue were manually excluded. Then, the standard color deconvolution technique was applied, with manual thresholding to isolate the DAB signal. Examples of this technique are shown in Appendix C.

5.3.6 Immunofluorescence

We histologically examined fibronectin expression by macrophages in the gut by performing a double immunofluorescence (IF) stain for FN and HAM56, as described previously (317). Briefly, the paraffin tissue sections were deparaffinized by a battery of three 5 min washes in xylene and then rehydrated by 3-5 min sequential washes in 100%, 95% and 75% ethanol. Next, the slides were boiled in diluted Antigen Unmasking buffer (Vector Laboratories, Burlingame, CA) for 20-23 mins before being allowed to cool to RT. The slides were then washed three times in 1X PBS for 5 mins. The slides were then blocked with Protein Block (Dako, Santa Clara, CA) for 30 mins. The blocking solution was dumped off and the slides were incubated with the FN antibody (mouse IgG, ThermoFisher, clone FBN11, ref# MA5-11981) diluted to 1:100 with Antibody Diluent (Dako, Santa Clara, CA) for 1 hour at RT. After incubation with the first primary antibody, the slides were again washed three times in 1X PBS before incubating with the corresponding secondary antibody (donkey anti-mouse IgG, Abcam, Alexa Fluor® 488, ref# A-21121) diluted to 1:100 with Antibody Diluent for 30 mins. The slides were then washed three times in 1X PBS and incubated with the HAM56 antibody (mouse IgM, ThermoFisher, clone HAM56, ref# 14-6548-93) diluted to 1:100 with Antibody Diluent for another 60 mins. Following three more washes in 1X PBS, the slides were incubated with the corresponding secondary antibody (goat anti-mouse IgM, ThermoFisher, polyclonal, Alexa Fluor® 633, ref# A-21046) diluted to 1:100 with Antibody Diluent for 30 mins. The slides were then washed three more times in 1X PBS and incubated for 5 mins with DAPI (MilliporeSigma, Burlington, MA) at 1:5000 dilution in 1X PBS and then washed again. To reduce lipofuscin autofluorescence, the slides were incubated for 30-60 seconds with TrueBlack autofluorescence quencher (Biotium, Fremont, CA) and then washed in 1X PBS. Finally, the slides were washed for 5 mins in dH2O and then coverslipped using Fluorescence Mounting Medium (Dako). After staining, the slides were stored in the dark at 4°C until they were visualized with an Olympus Fluoview 1000 Confocal microscope (Olympus) housed at the Center for Biologic Imaging (University of Pittsburgh, Pittsburgh PA). All images were taken at 200X magnification. Maximum intensity projections (IPs) were generated from image z-

stacks of 11-28 images using NIS Elements 5.20.00 (https://www.lim.cz/). Each image in the z-stack was taken 1.87 μm apart, with a resolution of 0.321 μm/pixel. The maximum IPs were processed and edited using FIJI version 2.069 (https://fiji.sc/). Editing includes adjustment of color channel brightness for clarity and application of the built-in FIJI Despeckle median filter to reduce noise.

5.3.7 Monocyte sorting and RNA sequencing

To obtain monocytes for sorting, AGM and RM PBMCs were isolated from whole blood with EDTA diluted in sterile phosphate-buffered saline (PBS) and centrifuged for 30 mins at 1850 RPMs at 25°C layered over Ficoll-Paque gradient separation media (Lonza) at a 3:2 ratio. The isolated buffy coat was washed with 1X PBS and any contaminating red blood cells lysed using an ammonium-chloride-potassium lysing buffer (Lonza) for 10 mins before washing and pelleting the cells in 1X PBS (10 mins, 1800 RPM, 25°C). Cells were counted using a LIVE/DEAD® Aqua Dead Cell Stain Kit (Life Technologies), stained with antibodies against CD14 and CD16 (Beckman Coulter) and incubated for 30 mins at RT before washing with FACS buffer (PBS + 2% FBS). Samples were sorted using a FACS ARIA II (BD Immunocytometry) and analyzed using FlowJo software. Collected monocytes (~50,000 cells/sample) were stored in RLT. RNA was isolated using RNeasy MicroKit (Qiagen) including DNase Digestion (Qiagen, cat# 74004 and 79254). The RNA quality and quantity were determined using a Bioanalyzer RNA Pico chip (Agilent, #5067-1513). The SMARTer Ultra Low Input RNA Kit for Sequencing-v3 (Clontech/TAKARA, #634851) was used for first-strand cDNA synthesis and cDNA amplification (14 cycles) starting with ~2 ng of total RNA. The amplified cDNA was cleaned using DNA Clean & Concentrato-5 kit (Zymo, D4014) and quantified using Qubit dsDNA High Sensitivity kit (Thermo, Q32854). Using the resulting purified cDNA (500 pg/library), the library construction was completed using three steps from the Illumina Nextera XT Library Prep (Illumina, FC-131-1096) workflow (Tagment DNA, Amplify Tagmented DNA, and Clean Up Amplified DNA). The resulting libraries were quantified (Qubit dsDNA High Sensitivity Kit) and sizes confirmed using a Bioanalyzer High Sensitivity DNA Chip Kit

(Agilent, 5067-4626). The gene libraries were sequenced to a depth of ~ 25 million raw reads/sample using a NextSeq 500, and 150 cycle, NextSeq 500/550 High Output v2 kits (Illumina, FC-404-2002). The rectal sequencing data, including gene counts, can be found in Gene Expression Omnibus (GSE111233).

5.4 Experimental results

5.4.1 Principal component analysis reveals differentially expressed genes between AGMs and RMs

To identify the host responses that determine pathogenic outcomes in natural and non-natural hosts, 28 AGMs and 24 RMs were intrarectal inoculated with two genetically diverse swarm stocks (SIVsab92081 and SIVmac251) previously shown to have comparable infection kinetics (127, 267).

As such, in both the AGMs and the RMs, peak viral load occurred at 9-12 dpi, with 1.39 x 10^7 vRNA copies/mL plasma in AGMs, and 2.48 x 10^7 vRNA copies/mL in RMs, as shown in Figure 30A. Here, the data are given as $\log_{10}$ values, with the AGMs shown in teal and the RMs shown in pink. There was a statically significant difference ($p<0.05$) between the plasma viral loads of the AGMs and the RMs at D50, as indicated by the asterisk. In Figure 30B, the principal component analysis of the 7420 differentially expressed genes is shown, with the number on the axis to indicate the percentage of the total genetic variation explained. In Figure 30C, a heatmap displays representative genes sets derived by the principal component analysis. Genes with the strongest contribution to the genetic variation in proportional numbers are shown, taken from the top six principal components. The top enriched biological functions for each set of genes is listed on the right side of the heatmap.

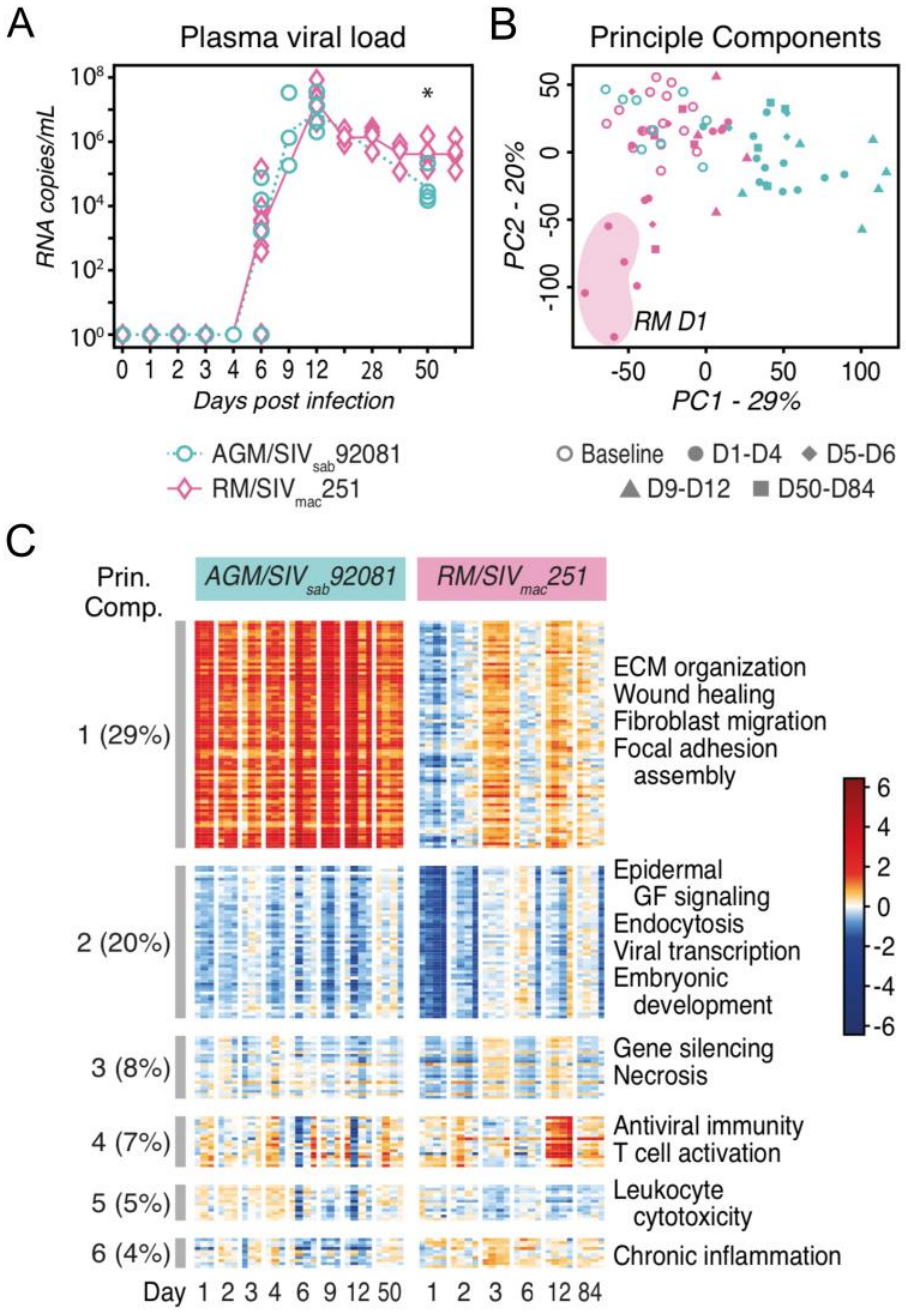

Figure 30: Plasma viral loads, principle component analysis and differentially expressed genes of African green monkeys (AGMs) *versus* rhesus macaques (RMs).

(A) Plasma viral loads in AGMs (teal) and RMs (pink), given as $\log_{10}$ values. Asterisks indicate statistical significance, with *=p<0.05. (B) Principle component (PC) analysis of the 7420 differentially expressed genes between the AGMs and RMs that showed the greatest divergence over time. The numbers on the axis indicate the percentage of total variation between the two species explained by the PC. (C) A heatmap showing the representative gene sets generated by the PC analysis. The genes with the strongest contribution to variation within the top six PCs are shown. A functional enrichment test was applied to these genes sets, with the top biological functions listed on the right side of the heatmap.

At the set-point, the AGMs had plasma viral loads approximately one log lower than RMs (6.95 x 10^4 vRNA copies/mL and 5.69 x 10^5 vRNA copies/mL, respectively, $p<0.05$). However, in the rectum samples, the viral loads were comparable between the AGMs and RMs (data not shown).

The transcriptomic profiling showed highly divergent responses to acute SIV infection between AGMs and RMs. The rectal tissues collected during pre- and during the necropsy underwent total RNAseq profiling. The resulting sequence reads were mapped to the AGM and RM genomes for differential expression (DE) and other bioinformatic analyses. Direct comparisons between the two species utilized genes for which there were human ENSEMBL one-to-one orthologues for both the RMs and the AGMs. DE analysis was conducted in two ways: (i) for each time point, preinfection pinch biopsies taken from the rectum were used as baseline to compare with the rectal necropsy samples, resulting in hundreds of DE genes at each time point, with fewer than 10% being shared between the species at most time points (Table 3); (ii) to avoid any potential bias due to utilizing different tissue sample type for baseline *versus* postinfection, pairwise comparisons were done between all the time points tested (all-to-all comparisons) for each animal model, which resulted in a union of 7420 DE genes between the two species (Table 3).

Table 3: Results of DE Analysis of AGMs and RMs

	AGM/SIVsab92081			RM/SIVmac251			Intersection	
Time point	*n*=	Up-regulated	Down-regulated	*n*=	Up-regulated	Down-regulated	Up-regulated	Downregulated
1 dpi	3	1703	687	4	903	2058	117	270
2 dpi	3	690	71	4	231	893	41	17
3 dpi	3	535	40	4	651	241	197	1
4 dpi	3	1035	422	4	NA	NA	NA	NA
5-6 dpi	4	2241	525	4	28	195	25	9
9 dpi	3	2265	1063	4	NA	NA	NA	NA
12 dpi	4	1707	526	4	729	575	299	77
46-55/ 84 dpi	4	905	82	4	180	267	93	7
All-in-all genes		6033			4294			4294

The principle component (PC) analysis (Figure 30B & C) demonstrated that many genes in AGMs were persistently up-regulated early during SIV infection (first PC). Conversely, the response from 1-4 dpi in the RMs was transient, subsequently returning to baseline gene expression levels (second PC). Gene Ontology (GO) enrichment revealed that the first PC (AGMs) showed up-regulation of genes linked to extracellular matrix organization, wound healing, fibroblast migration and focal adhesion assembly. The second PC (RMs) showed transient down-regulation of genes linked to epidermal growth factor signaling, endocytosis, viral transcription and embryonic development. The PCs enriched for typical immune responses (the fourth, fifth and sixth PCs) comprised only 16% of the total variability in the dataset. These gene sets were associated with antiviral immunity, T and B cell activation and chronic inflammation. The fourth PC (antiviral immunity, T-cell activation) was strongly induced at 12 dpi in RMs, which corresponds to the peak of viral replication. (Figure 30C).

5.4.2 Systems biology approach defines distinctly different gene signatures across biological processes between pathogenic and nonpathogenic models

As the initial analysis identified thousands of genes with divergent time kinetics between the AGMs and the RMs, we reasoned that the infection outcome is affected by specific cellular responses, occurring at different times following SIV infection. To understand the impact of these responses, the CGSA was devised as a systems biology approach for correlating acute SIV infection data with informative time series datasets from the public domain.

This data-driven approach adds time dimensions to documented, static gene functions, avoids false positive gene-gene interactions and increases statistical robustness. To develop CGSA, we collected transcriptomic datasets (reference datasets) pertaining to GO Biological Processes enriched amongst the genes identified during the PC analysis, resulting in a catalogue describing four biological processes: wound healing (from skin or mucosal tissues samples collected post-wounding), experimental colitis (from colon tissues sampled post-oral dextran sulfate sodium or dinitrobenzene sulfonic acid administration), *in vitro*

cytokine stimulation of epithelial cells, and microbial colonization (from colon tissues collected from germ-free mice after introduction of normal intestinal microbiota). Datasets from large-scale clinical studies of colon cancer and inflammatory bowel diseases were also included. These six biological processes encompassed 23 reference datasets, representing a total of 2438 microarray samples (Appendix A). We also constructed a co-expression network (the Acute SIV Co-expression Network) using our acute SIV infection RNAseq data, thereby identifying gene pairs that were co-expressed in both species.

To determine if transcriptomic signatures from the reference datasets could produce the differences in gene expression between the AGMs and the RMs, we examined CGSA on a whole genome scale. Specifically, we calculated the Pearson correlation coefficient between the gene expression log fold change (logFC) values from acute SIV infection in each species at each time point, to each reference dataset (Figure 31).

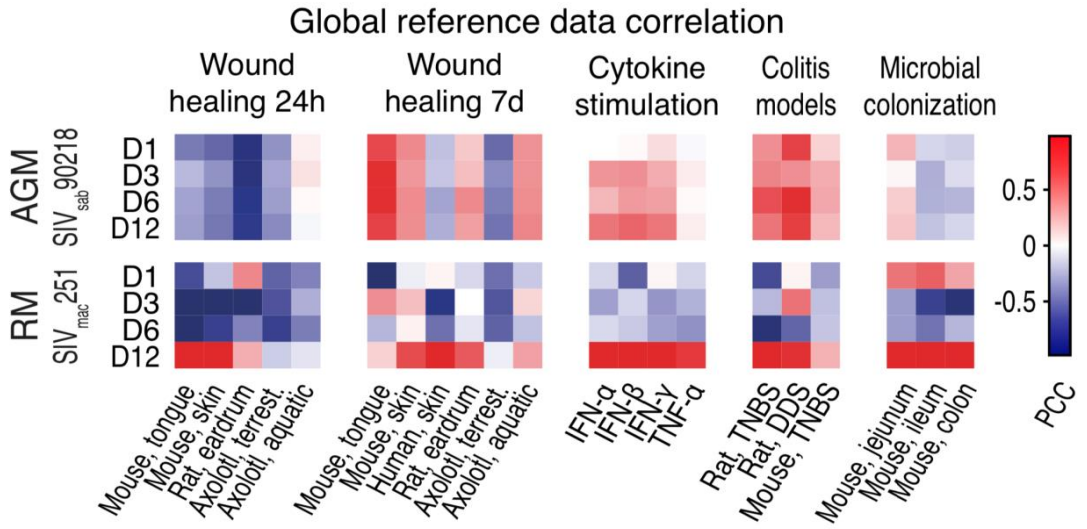

Figure 31: Whole geneome correlations between acute SIV infection of African green monkeys (AGMs) *versus* rhesus macaques (RMs) and gene reference datasets.
Colors in the heatmaps represent the Pearson correlation coefficient between the log fold change values of gene expression during acute SIV-infection in the AGMs and RMs and the reference datasets for each of the timepoints listed on the left. The associated biological functions are listed above, and the specific species are listed below. For the wound healing response, datasets for wound healing at two time points post wounding, 24 hours and 7 days, are shown. For cytokine stimulation, changes in genes linked to interferon response at 12 hours post-stimulation and *TNF-α* at 6 hours post-stimulation, are shown. Similarly, the colitis model dataset represents 7 days following chemical induction of colitis and the microbial colonization dataset represents 16 days post colonization of germ-free mice by normal intestinal flora.

This revealed that at the peak of viral replication, the transcriptional profile in RMs was correlated with microbial colonization, cytokine stimulation and, perhaps most importantly, tissue damage. These genes were associated with a variety of biological conditions included: the inflammatory stage of wound healing (Figure 31, Wound healing 24h), a period of strong neutrophil and M1 macrophage activation (318), and chemically induced colitis (Figure 31, colitis models). In contrast, the gene expression profile in the AGMs only moderately correlated to colitis models and cytokine stimulation (including type I (IFN-α, IFN-β) and type II (IFN-γ), but not TNF-α) starting from the previremic (i.e., preramp-up) stage and then throughout the course of infection. However, any correlations to inflammatory wound healing and microbial colonization were negligible or negative. This suggests that AGMs upregulate certain immune pathways during the previremic (preramp-up) stage, but even during peak viremia, immune activation and tissue damage are limited. AGMs also showed stronger correlation to late stage wound healing (day 7) in the reference datasets. By day 7, the inflammatory stage of wound healing is normally resolved, and tissues are undergoing re-epithelization, angiogenesis and remodeling (319).

5.4.3 Absence of microbial translocation signatures in AGM innate immune response

The genome-wide comparison between acute SIV and reference datasets showed a stronger association between for RMs than AGMs with inflammatory tissue damage at peak viremia. To identify the genes responsible for this discrepancy, we systematically removed each of the 23 gene modules from the Acute SIV Co-Expression Network and re-calculated the correlation to the reference datasets in the AGMs and RMs separately. The module removal analysis suggested that in AGMs, the genes in the interferon module were specifically activated by innate immune signaling ("Cytokine stimulation"), while in RMs the module was also affected by bacterial PAMPs and tissue damage ("Wound healing 24h" and "Microbial colonization"). To confirm this independently, we used Ingenuity Pathway Analysis (IPA), which is based on manual curation of scientific publications, to identify upstream regulators of DE genes from both the

AGMs and the RMs. We performed Fisher's exact tests between targets of each IPA upstream regulator, and DE genes in AGMs and RMs, using the interferon module as background (Figure 32A).

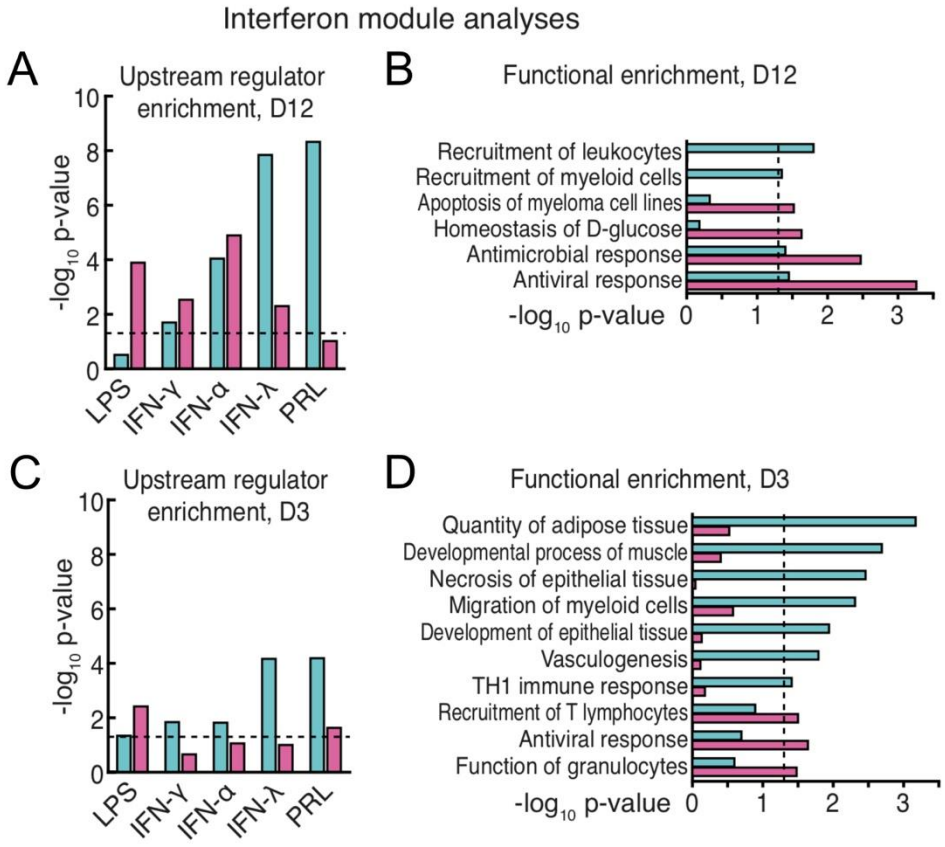

Figure 32: Enrichment tests for biological functions of differentially expressed genes linked to inteferons during acute SIV infection.

Enrichment of differentially expressed genes from African green monkeys (AGMs) (teal) and rhesus macaques (RMs) (pink) linked to upstream regulator targets (A & C) and biological functions (B & D) compared to all genes in the interferon gene module. The enrichment tests were performed for gene expression at 3 dpi and 12 dpi and the $-\log_{10}$ of the p-value are shown on the axis, with dashed lines indicating that p=0.05. The p-values were determined using Fisher's exact tests between the targets of the IPA upstream regulators and the differentially expressed genes.

This interferon-based analysis supported a regulator role for bacterial LPS in RMs, but not AGMs, supporting the possible anergy to LPS observed in 4.4.12. However, both interferon-γ (*IFN-γ*) and interferon-α (*IFN-α*) type interferons had similar p-values for the two model systems. The AGM immune

response showed stronger enrichment for interferon-λ (*IFN-λ*), a potent antiviral cytokine (320), and growth factor prolactin (*PRL*) which shows elevated levels in individuals with HIV (321). We repeated the enrichment analysis on biological functions, confirming stronger activation of antiviral and antimicrobial immune responses in RMs, while only the AGMs showed activation of leukocyte and myeloid cell recruitment genes (Figure 32B). This outcome agrees with the upstream regulator analysis, as several myeloid cell types, including macrophages and DCs, produce high levels of IFN-λ in response to viral infection (322). IFN-λ is known to inhibit HIV infection of macrophages, potentially contributing to the low rates of SIV infection of macrophages in natural hosts (323).

Before the viremic (ramp-up) stage, there was little genome-wide correlation between inflammatory processes in the reference datasets (such as acute wounding, cytokine stimulation, colitis, microbial colonization) and SIV infection. However, several events that contribute to pathogenesis are previremic, including reduction of tight junction protein expression at 3 dpi (302). We therefore performed an upstream regulator analysis on the interferon module to determine if there was a gene expression indicating the presence of LPS at day 3 in RMs (Figure 32C). While the LPS signature was present (*p=0.0038*), there was no enrichment of any of the *IFN-α*, *IFN-γ* or *IFN-λ* targets. AGMs, by contrast, showed a stronger enrichment for targets of *IFN-α*, *IFN-γ*, *IFN-λ* and *PRL* without the presence of LPS, thus supporting an early antiviral response in the absence of microbial translocation. The functional categories at day 3 (Figure 32D) showed that AGMs were already expressing genes associated with myeloid cell migration. In addition, even though the genes encompassed by the interferon module are specifically regulated by interferons, the AGM DE genes within this module were also associated with tissue development (adipose, epithelial and muscle tissue).

5.4.4 Dominant signatures of noninflammatory wound healing occur early in host response to infection in AGMs but not RMs

The genome-wide analysis showed an inflammatory tissue damage signature in RMs, while AGMs activated a signature similar to those seen during the later stages of wound healing. These observations suggested that unlike RMs, AGMs can limit tissue disruption of the gut epithelium during acute infection by rapidly repairing SIV-induced damage before it results in a colitis-like state and microbial translocation. The end result of this would be the prevention of the chronic inflammation associated with microbial translocation and maintenance of mucosal T-cell homeostasis (195). To investigate the gene signatures linked to these outcomes, we explored wound healing mechanisms in the Acute SIV Co-Expression Network and reference datasets.

The six wound healing datasets included genes expression signatures from biopsies of healing skin or mucosal tissue in human, mouse or rat, as well as axolotl (*Ambystoma mexicanum*). Different from wound healing response in the majority of animal species, aquatic axolotl wound healing is non-inflammatory and results in fully functional, scar-free tissue (324). The genome of the terrestrial axolotl species was used as comparison, as they exhibit a more mammal-like wound healing process (325). Using this data, we created a unique resource of wound healing signatures from different species, and different time points and tissues during acute SIV infection. The resulting network, referred to as the Wound Healing Network, contained 191 interactions between 166 genes.

Using CGSA further revealed that the genes in the Wound Healing Network also showed consistent gene expression dynamics for wound healing across all reference datasets, except for the aquatic axolotl. For this species, the dynamics entailed down-regulation during the first 24-72 hours post-wounding, corresponding approximately to the inflammatory stage of normal mammalian wound healing, followed by up-regulation of genes during the later tissue remodeling and re-epithelization stage (326), as shown in Figure 33A.

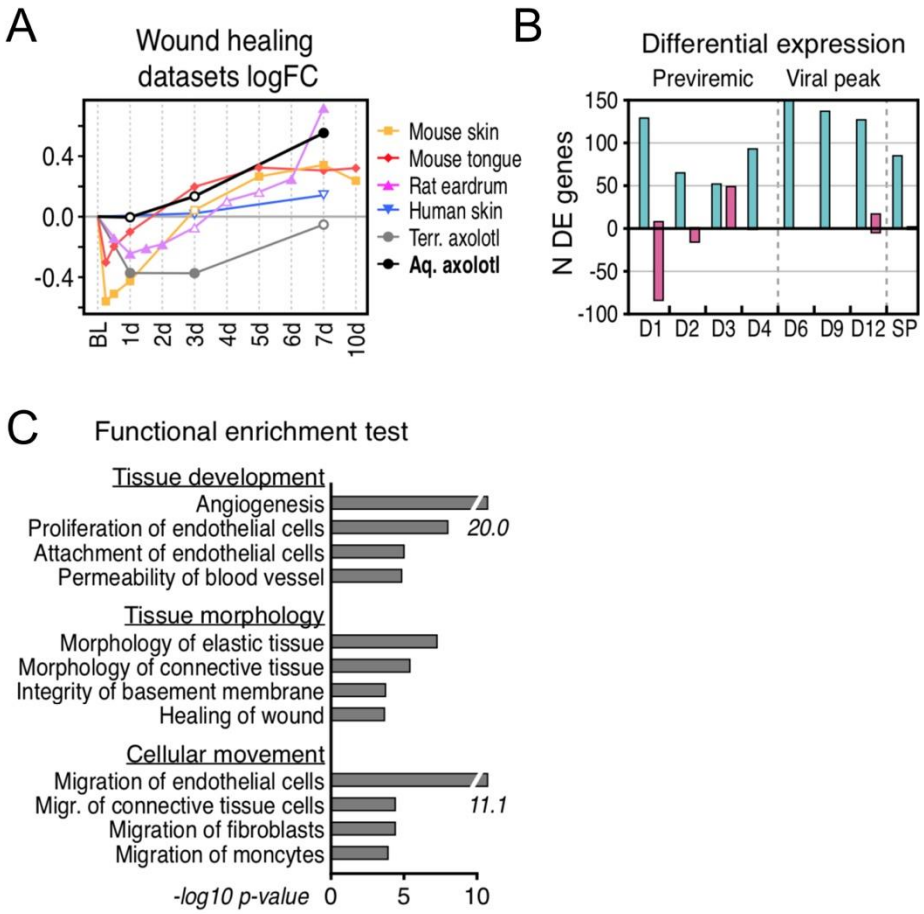

Figure 33: Fold change, total number of genes and functional enrichment of differentially expressed genes within the Wound Healing Network.

(A) The average log fold change values of the Wound Healing Network genes from each wound healing reference dataset, with day post wounding shown on the x-axis and log fold change shown on the y-axis. Filled circles indicate a significant change from baseline values, while empty circles indicate a lack of significance. (B) The number of up-regulated and down-regulated genes in the Wound Healing Network at each time point during acute and early chronic SIV-infection in African green monkeys (AGMs) (teal) and rhesus macaques (RMs) (pink). (C) Functional enrichment analysis of the Wound Healing Network genes differentially expressed in the AGMs divided into three biological categories.

In the aquatic axolotl, the Wound Healing Network genes stayed near baseline expression level during the mammalian inflammatory stage but showed strong up-regulation during remodeling at day 7. In RMs, the Wound Healing Network genes were down-regulated during the first days post infection, and then returned to baseline expression levels. This pattern suggests that the RM host response to acute SIV infection involves the inflammatory stage of wound healing, but not the tissue remodeling (Figure 33B). In

stark contrast, AGMs showed up-regulation of the Wound Healing Network genes at all time points, suggesting that they immediately activate late stage wound healing processes and, like the aquatic axolotl, bypassing the inflammatory stage of wound healing. Functional enrichment of the genes emphasized wound healing mechanisms critical for axolotl wound repair, including blood vessel development (327) (angiogenesis, proliferation/attachment of endothelial cells), tissue density (325) (permeability of blood vessel, integrity of basement membrane) and cell migration (328) (endothelial cells, fibroblasts and monocytes) in the Wound Healing Network (Figure 33C).

5.4.5 Role of fibronectin in maintenance of AGM epithelial integrity

In the Wound Healing Network, the contrast between the early response to SIV infection between the AGMs and RMs was similar to the contrast between early axolotl and mammalian wound repair gene signatures. To identify which specific axolotl-like repair mechanisms were present in the AGM SIV model, we examined what biological functions were up-regulated at day 1 of axolotl wound healing by calculating the Pearson correlation coefficient between membership in each IPA biological category (0 for non-members, 1 for members), and the log fold change values of the genes. Six functional categories were found to be positively correlated with day 1 of axolotl wound repair, including known wound healing mechanisms (fibroblast development, infiltration of cells), but also tissue formation (adiposity, fibrous tissue development, tissue branching, colony formation), as shown to the right of the heatmap in Figure 34A.

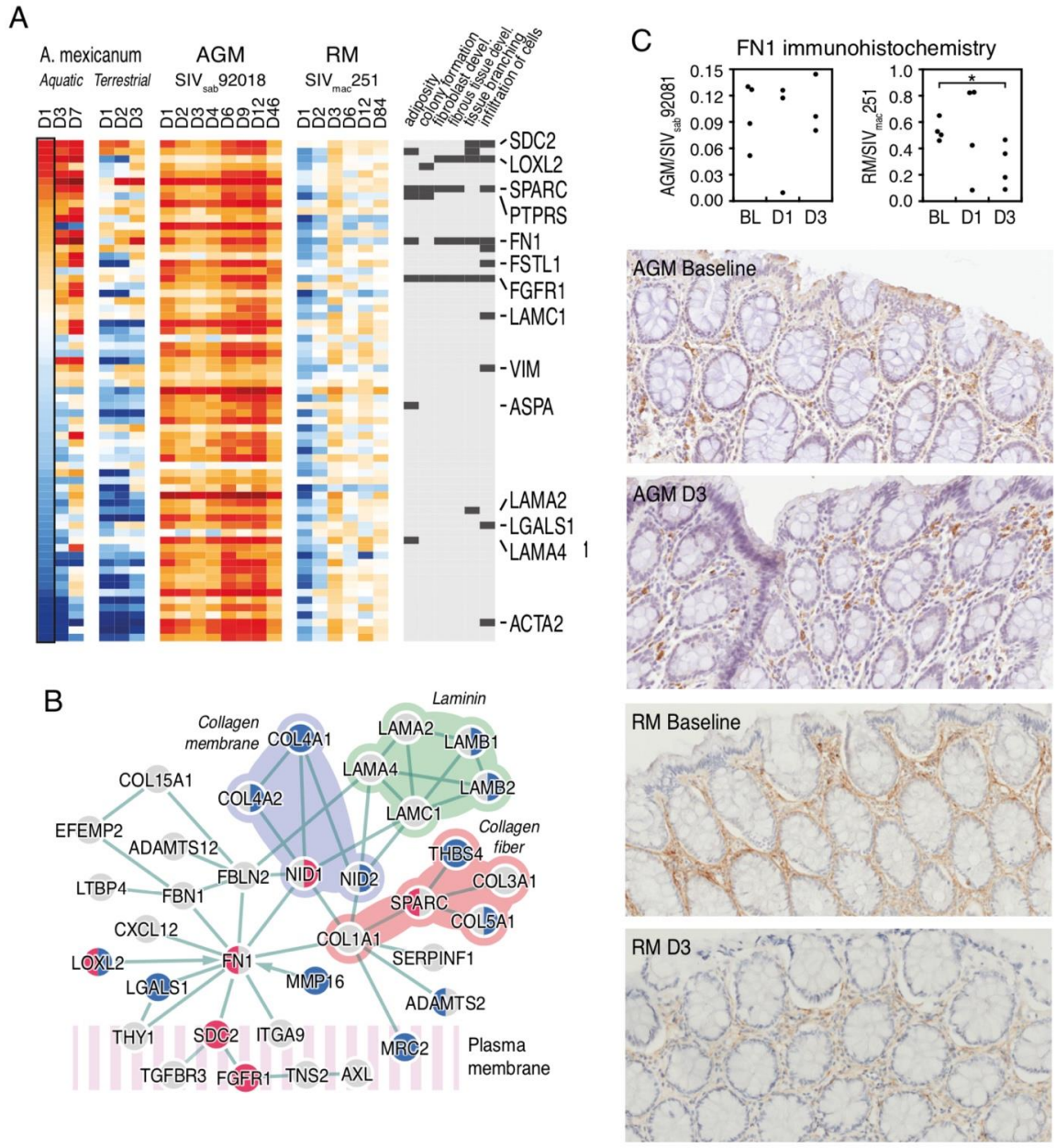

Figure 34: Axolotl wound healing genes and immunohistochemistry for fibronectin in the rectal mucosa. (A) A heatmap of Wound Healing Network genes in axolotl wound repair and acute SIV infection. The genes are ordered based on the gene expression during day 1 of aquatic axolotl wound repair, with the most up-regulated genes at the top and the most down-regulated genes at the bottom. Six of the biological functions with a positive Pearson correlation coefficient with day 1 wound repair in the aquatic axolotl are shown to the right of the heatmap, along with their associated genes. (B) A IPA network showing the interactions of various proteins encoded by genes in the Wound Healing Network. At each of the nodes, red indicates up-regulation and blue indicates down-regulation at day 1 post wounding, with the aquatic axolotl on the left side of the node and the terrestrial axolotl on the right. (C) Immunohistochemistry staining for fibronectin in the rectum lamina propria at 1 dpi and 3 dpi in the African green monkeys (AGMs) and the rhesus macaques (RMs). At the top are shown the results of image-based quantification of fibronectin by pixel density. Asterisks indicating statistical significance, with *=p<0.05. Representative images of the immunohistochemistry staining for fibronectin are shown below, with the AGMs shown on top and the RMs shown on the bottom.

As genes frequently encode proteins that have a wide variety of functions and protein-protein interactions, we constructed a new network between the Wound Healing Network genes using protein interactions from IPA (329) (Figure 34B). The resulting network consisted mainly of ECM and cellular membrane proteins. The up-regulated genes at day 1 of axolotl wound repair (FN1, SDC2, FGFR1, LOXL2 and SPARC) were all associated with cell migration, and most were critical for network connectivity. Many of the contacts between ECM components and cell surface proteins were mediated by FN1, through SDC2 and FGFR1, while SPARC mediated connections between fibrous collagen proteins. These observations imply the wound healing mechanism in AGMs uses an axolotl-like repair process entailing FN1 mediated recruitment of endothelial cells, fibroblasts and monocytes. To confirm the role of the FN1 protein, fibronectin (FN), in maintenance of AGM tissue integrity, we performed IHC staining in rectal tissue at baseline, 1 dpi, and 3 dpi post SIV inoculation, for both the AGMs and the RMs. Quantification of FN expression showed down-regulation ($p < 0.05$, t-test) by day 3 in RMs, consistent with observations from the RNAseq, albeit delayed (Figure 34C). During SIV infection in both species, FN was primarily expressed in the lamina propria. However, in RMs FN showed more fibrillar structure than in AGMs, where the FN was more localized to the ECM (Figure 34C).

5.4.6 AGM monocytes show overexpressed wound repair genes and transforming growth factor β

Normal wound healing requires that every growth factor, cytokine and cell type is activated within a precise timeframe (318). Monocytes participate in both early and later stages of the process, as they can differentiate into inflammatory M1 macrophages or regulatory M2 macrophages. The M2 macrophages orchestrate later stages of mammalian wound repair and have been shown to be essential for axolotl wound healing (330, 331).

Thus, we examined if macrophages support the wound healing mechanisms found in AGMs by conducting double IF staining for the macrophage marker HAM56 and the wound healing protein FN, as shown in Figure 35 & Appendix C.

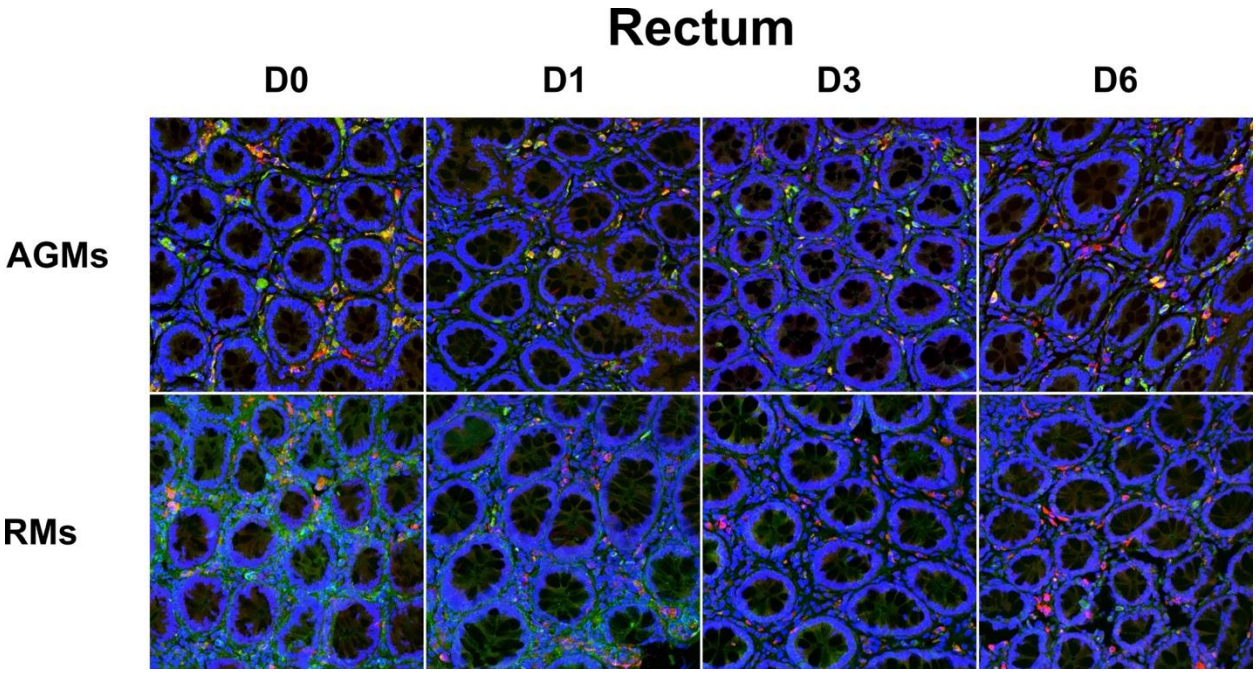

Figure 35: Immunofluorescent staining for HAM56/FN in rectum lamina propria of African green monkeys (AGMs) *versus* rhesus macaques (RMs).

Rectum from AGMs (top) and RMs (bottom) was doubled stained for HAM56 (red) and FN (green), with a DAPI stain (blue) to visualize nuclei. Colocalization, if any, appears as yellow. From left to right, representative images are shown from 0-6 days post infection. All images are at 200X magnification and were captured with an Olympus Fluoview 1000 Confocal Microscope housed at the Center for Biologic Imaging, Pittsburgh, PA. Each image represents a maximum intensity projection form a z-stack of 11-28 images at 1.78 μm per step. The resolution of every image is 0.321 μm/pixel. Maximum intensity projections were created with NIS Elements 5.20.00 (https://www.lim.cz/). All image editing was performed using FIJI version 2.0 (https://fiji.sc/). Editing includes adjustment of color channel brightness for clarity and application of the built-in FIJI Despeckle median filter to reduce noise.

This showed while many $HAM56^+$ cells were also FN^+ in AGMs, most $HAM56^+$ cells were FN^- in RMs. Single HAM56 IHC staining did show any difference in the numbers of macrophages in the AGMs compared to the RMs (Figure 36 & Appendix C).

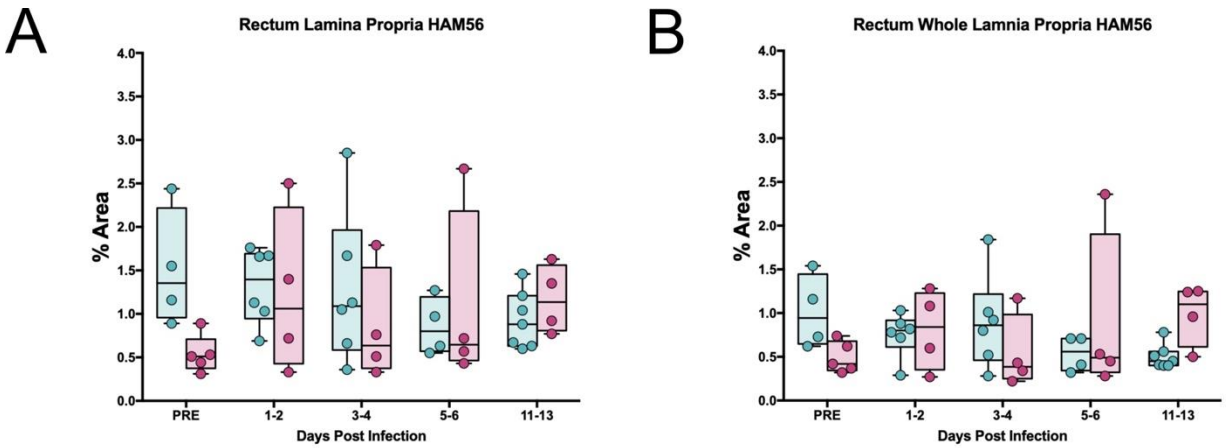

Figure 36: Quantification of immunohistochemistry for HAM56$^+$ macrophages in African green monkeys (AGM) rectum lamina propria.

Image based quantitative analysis was performed to measure the total positive DAB signal as percent area in the rectal lamina propria of AGMs (teal) and rhesus macaques (RMs) (pink). (A) For each animal, a total of 9-12 individual images of the lamina propria were quantified and averaged. Selection of image regions was randomized to minimize bias. (B) However, given the variable structure and cell distribution within the lamina propria, the initial quantification was verified by performing additional imaging of the entire lamina propria from the underlying muscularis mucosa to the epithelium, when possible. For each animal, 5 of these images of the whole lamina propria were quantified and averaged.

These results strongly suggested that while the numbers of macrophages were similar in the two species, they exhibit a stronger wound healing phenotype in AGMs than in RMs.

To test this hypothesis, we performed deep mRNAseq on M1 (CD14$^+$) and M2 (CD14$^-$/CD16$^+$) monocytes isolated from blood samples taken at 7, 14, and 28 dpi from a different group of animals than used for the rest of the transcriptomics; this study group included two AGMs and four RMs. Due to the small number of animals, we avoided DE analysis, and leveraged the genome-wide dataset by a PC analysis analyzing the 1000 genes with the highest variance. The first PC allowed for separation of the AGM and RM monocytes, while the second PC delineated the M1 from M2 subtypes, including in samples taken before SIV inoculation, as shown in Figure 37A.

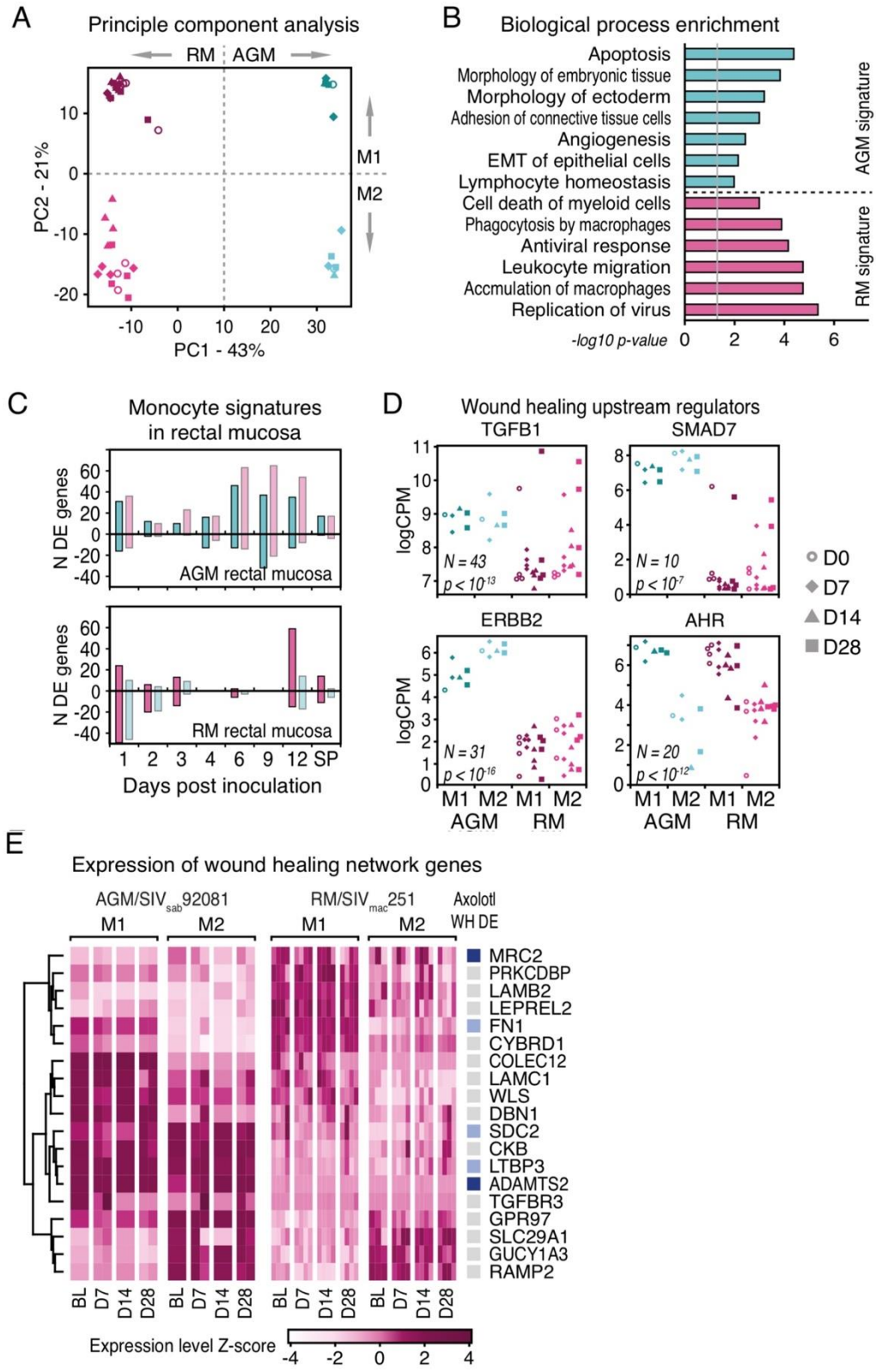

Figure 37: Genetic profiling of monocytes from African green monkeys (AGMs) and rhesus macauqes (RMs).

Monocytes were isolated from tissue collected from a set of AGMs and RMs not included in the original study and were used for RNAseq. (A) Principal component (PC) analysis of the 1000 most variable genes between the AGMs (teal) and RMs (pink). The shapes of the symbols representing each animal indicate the day postinfection: baseline (circle), 7 dpi (diamond), 14 dpi (triangle), 28 dpi (square). Dark colored symbols indicate M1 macrophages, while light colored symbols indicate M2 macrophages. (B) Functional enrichment of the monocytes transcriptomic signatures from the AGMs and the RMs. The biological functions represent the 300 genes with the strongest positive and negative correlation with PC1 shown in (A). (C) The number of up-regulated and down-regulated genes from the rectum of the AGMs and RMs that overlapped with the genes in the AGM or RM monocyte signatures. (D) Expression levels for predicted upstream regulators of the Wound Healing Network genes in the AGM and RMs peripheral blood monocytes. Number ("N") indicates the number of genes in the Wound Healing Network linked to that regulator and p-values are for the corresponding enrichment test. The symbol shapes and colors used are the same as in (A). (E) A heatmap of the expression of Wound Healing Network genes in the AGM and RM monocytes. As the greatest contribution to variation here was introduced by the species and monocyte subset, not the time postinfection, expression Z-scores are shown instead of log fold change values. The column to the right of the heatmap shows genes that are significantly up-regulated in the axolotl wound healing response. Genes that are up-regulated at 1 day post-wounding are marked in dark blue, while genes that are up-regulated at 7 days post-wounding are marked in light blue.

These results clearly demonstrate that for both AGM and RM monocytes, the M1 and M2 monocytes had distinct transcriptomic profiles, both before and after SIV infection. Functional enrichment tests revealed that the 300 genes most over-expressed in AGMs (i.e., the AGM monocyte signature) was associated with embryonic tissue development (abnormal morphology of embryonic tissue, morphology of ectoderm) and epithelial-mesenchymal transition (EMT) of epithelial cells (Figure 37B). These gene signatures suggested that AGM monocytes have stem cell-like properties and greater differentiation potential than normal monocytes, in keeping with axolotl-like tissues. In contrast, the corresponding RM monocyte signature was primarily enriched for macrophage mediated antiviral immunity (Figure 37B).

As the monocytes and rectal tissues analyzed here were obtained from different sets of animals, we evaluated the overlap between the genes in the AGM or RM monocyte signatures to the DE genes from the rectal tissue data (where most monocytes are differentiated into tissue macrophages). In AGM rectal tissues, genes from both the determined AGM and RM monocyte signatures were differentially expressed throughout the course of infection (Fig 38C). On the other hand, in the RMs both the AGM and RM monocyte signatures are predominantly down-regulated during the previremic stage of infection (1-4 dpi). Only at 12 dpi was the immune-associated RM signature up-regulated.

Thus, AGM tissue macrophages showed a wider range of monocyte responses, encompassing both tissue development and immune activation. RM tissue macrophages, by contrast, lack the wound healing profile of AGM macrophages, and produce a primarily inflammatory monocyte response to SIV infection.

To investigate how the monocytes contribute to wound healing in AGM rectal tissue, we examined the expression of predicted upstream regulators of the Wound Healing Network from IPA, in both the AGM and the RM peripheral blood monocytes. Out of the all the wound healing regulators that were expressed in the monocytes, three (TGFB1, ERBB2, and SMAD7) showed higher average expression levels in AGM monocytes (both M1 and M2) compared to RM monocytes. One, AHR, had comparable levels of expression in the two models, as shown in Figure 37D. Here, the number of regulator target genes in the Wound Healing Network and the p-values pertain to the corresponding enrichment test are shown, with the colors and symbols matching Figure 37A.

It is known that during axolotl limb regeneration, macrophages secrete *TGF-β* to supply the growing tissue with new cells through influx and proliferation (332). The remaining regulators encoded an epidermal growth factor receptor (ERBB2), nuclear receptor (AHR) and transcription factor (SMAD7), that presumably regulate gene expression in the monocytes themselves. We therefore examined the Wound Healing Network genes that were over-expressed in AGM peripheral blood monocytes. Among the 1000 most variable genes in the monocyte dataset, 19 were Wound Healing Network genes (Figure 37E). Since most of the variation within the genes was introduced by species and monocyte subset and not time point, we show expression Z-score instead of log FC values. Three of the 19 genes were up-regulated at day 1 of axolotl wound repair, as shown by the dark blue marks on the column to the right of the heatmap (the light blue marks indicate genes up-regulated at 7 dpi): FN1, *TGF-β* release factor LTBP3 and cellular receptor SDC2, a mediator of *TGF-β* signaling (333). The PCA analysis also included WLS, a mediator of wnt secretion, which was elevated in AGMs. Wnt is another major meditator in tissue regeneration pathways in several different species, including the aquatic axolotl (334).

5.5 Discussion

Natural hosts of SIV, such as the AGM, avoid disease progression and maintain immune cell homeostasis following SIV infection and in the face of persistent viral replication. Additionally, natural hosts are characterized by a lack of the chronic inflammation that is typical of pathogenic SIV/HIV infections. By studying how natural hosts control pathogenesis, new avenues for the development of therapies to prevent both AIDS and chronic inflammatory diseases. To help determine the mechanisms by which AGMs are able to avert progression to AIDS, a transcriptomic analysis was performed to study differential gene expression over the course of infection in a nonpathogenic (AGM) and pathogenic (RM) SIV host. By using tissue samples, including the site of inoculation, collected during acute SIV infection into early chronic infection, this study complements previous transcriptomic studies, which have focused only on later time points during infection or immune cells from peripheral blood (156, 163).

However, one of the major issues during transcriptomic profiling of whole tissues is that it lacks biological resolution, being unable to differentiation factors like individual cell types. To help circumvent this, CGSA was developed, which is a unique bioinformatic pipeline that integrates curated transcriptomic reference data from a diverse set of species to interpret gene expression signatures. By drawing from a large and varied body of reference data, CGSA avoids some of the limitations in preexisting knowledge. The large amount of CGSA reference data also adds statistical robustness to the analysis and reduces the false gene-gene associations that are common in co-expression analysis, as biologically relevant interactions tend to be conserved (335).

Following SIV challenge, the transcriptomic analysis revealed thousands of differentially expressed genes in rectal tissue samples taken from the AGMs and the RMs (Figure 30). A major feature of the AGM response to infection was a unique regenerative wound healing signature facilitated by blood monocytes and tissue macrophages. This tissue repair process was associated with preservation of mucosal integrity and absence of the inflammatory phenotype of tissue damage in progressive HIV/SIV infections. Thus, the wound healing signature in AGMs could be critical for the maintenance of mucosal integrity and

preservation of mucosal immunity, which, in turn, may contribute to the prevention of disease progression in SIV/HIV infections. While this response seems to be spearheaded by monocytes and macrophages, it is likely that other immune cells types are involved and should be investigated in future studies.

The AGM wound healing signature was identified by CGSA using reference data from a Mexican salamander species, the aquatic axolotl. Unlike their terrestrial cousins, aquatic axolotls never fully mature from their tadpole-like form, and possess semi-undifferentiated, almost fetal-like tissues. This enables the axolotl to accomplish healing in a fashion similar to embryonic development, totally bypassing the inflammatory stage of healing. After wounding, axolotl epithelial cells and keratinocytes migrate rapidly across the wound to restore the external barrier, then initiate basement membrane regeneration and tissue remodeling (328). This produces scar-free, fully functional new tissue (325). Outside of restoring functioning tissue, limiting tissue damage without killing the pathogen is known strategy for achieving immune tolerance and avoiding inflammatory responses to microbial infections (336). As such, the AGM wound healing phenotype links with protection against disease progression in SIV infection.

In addition, several recently reported genetic factors can support the wound healing profile AGMs. These include accelerated evolution of genes that viral interactions with host cells and growth factor signaling (337), as well as variant of TLR4 that can limit LPS responses in natural hosts, possibly limiting the amount of tissue damage caused by events such as MT (308).

In AGMs, the wound healing response includes several constituents of the basement membrane, which is a collagen-rich sheet separating the intestinal epithelium from the lamina propria; it is also one of the first tissue structures to regenerate after limb amputation in salamanders (338). Normal basement membrane proteins involved in wound healing include: (i) collagens, which are major structural proteins; (ii) laminins, which anchor cells to basement membrane (339); (iii) nidogens, which tether collagen to laminin (339); and (iv) fibrillin, which improves ECM elasticity (340). Collagen deposition in axolotl wound healing is minimal, similar to the lack of collagen formation that we observed in the AGMs postinfection (see 4.4.11) However, various other ECM proteins are transiently expressed at the margin of the wound, including fibronectin. Fibronectin is a large ECM protein, crucial for both early and late wound

healing stages (341) and expressed in the basement membrane of regenerating axolotl limbs (342). Formation of the fibronectin matrix starts at cellular surfaces, where α5β1 integrin binds soluble fibronectin to create complexes, that are then stretched into fibrils through cellular contractions. Here, IHC and IF (Figures 34 & 35) showed that in AGMs, the fibronectin was concentrated to the ECM, were it would be primed to initiate the wound healing response (341) and thus accelerate the tissue repair process.

The axolotl regeneration ability is based on their embryonic maturation state and entails a distinct immune cell profile, characterized by low neutrophil infiltration, as we observed in the IHC of the gut (see 4.4.7). It is also involves the specific recruitment of TGF-β secreting M2 macrophages (332). Although mammalian wound healing is also associated with M2 macrophages, both M1 and M2 AGM monocytes showed a distinct embryonic tissue development profile, including the TGF-β gene. Thus, CGSA has expanded the wound healing/M2 macrophage paradigm to protection and will be used in future studies to explore for other immune cells that might regulate the wound healing response.

The transcriptomic analysis showed that the embryonic development signature (Figure 37) and fibronectin tissue localization (Figures 34 & 35) were present in the monocytes/macrophages of the AGMs prior to infection. This implies that the intestinal mucosa of AGMs, a natural host of SIV, is constitutively poised to mount a protective wound healing response to infection. In a similar fashion, axolotl keratinocytes are constantly poised to migrate into any fresh wounds or injuries, due to their constitutive integrin expression (343). It is possible that the noninflammatory wound healing response in AGMs (and possibly other natural hosts) is an evolutionary adaption developed over many generations (see 1.1) to prevent loss of gut integrity and the subsequent establishment of the highly deleterious chronic inflammation that follows. This supports the conclusion that the tissue repair phenotype in AGMs is dynamic and directed by monocytes in general as a feature of protection against SIV pathogenesis (177).

Given the critical role of the wound healing response in preventing pathogenesis in SIV infected AGMs, development of therapeutic strategies that could replicate this response to at least some degree in humans might serve to help suppress and control HIV disease progression. In an era of widespread antiviral therapy, even without achieving viral clearance, relieving the financial and social burden of long-term

treatment to prevent progression to AIDS would be a great boon to millions of HIV^+ individuals around the world. Already, some therapies, such as the administration of IL33 to cutaneous wounds, have shown beneficial effects in accelerating wound healing, enhancing re-epithelization, activating M2 macrophages and increasing fibronectin expression in mice. (344)

6.0 Conclusions

6.1 Site of inoculation

6.1.1 SIVsab replication is established immediately at the site of entry following rectal inoculation

We identified sections of the rectum and distal colon that might represent the original foci of viral replication, with detectable levels of virus DNA/RNA in the tissue by 1-3 dpi (Figure 4 & 5). Using RNAscope, we were able to confirm these findings by visualizing SIVsab RNA in the lamina propria of the distal colon during the same preramp-up period (Figure 6), with rare instances of viral RNA as early as 1 dpi.

6.1.2 The virus enters into circulation very rapidly following infection

Using standard qPCR, SIVsab RNA was first detectable in the plasma by 6 dpi, (Figure 2). This standard qPCR method has a limited sensitivity though, being only able to detect down to 30 RNA copies/mL plasma. Viral concentrations lower than this limit of detection are not quantifiable. We bypassed this limitation by employing an adapted version of the SCA, which has a limit of detection of 1 RNA copy/mL plasma. By SCA, we found that most of the animals that had been previous detectable earlier during the ramp-up period, at 4-5 dpi, had viral loads between 10^0-10^1 RNA copy/mL plasma (Figure 2). SIVsab RNA was also detected by SCA in the plasma AGMs at 2 dpi and 3 dpi (Figure 2), though the level of virus in these animals technically fell below the limit of detection.

6.1.3 SIVsab is disseminated through the lymphatics early during infection

Apart from the rectum and distal colon, one of the other tissue compartments that SIVsab first became detectable in was the colonic LN (Figure 4). Viral RNA was found in the colonic LNs, which drain the site of inoculation, as early as 1-3 dpi. Detection of SIVsab very early in the draining LNs, followed by establishment of plasma viremia by 4-6 dpi, indicates that the virus disseminates rapidly from the site of inoculation to the lymphatics and then through the lymphatics into the bloodstream.

6.1.4 Viral spread during acute SIVsab infection is highly pervasive

Not only is the dissemination of SIVsab from the site of inoculation extremely rapid, it is also highly pervasive. Out of 38 tissue compartments that were surveyed, 37 of them were positive for vRNA by 4-6 dpi and all became positive for vRNA by the peak of viral replication. The virus even rapidly crossed the blood brain barrier, as was reflected not only by the tissue viral loads, but also the levels of virus in the CSF. In fact, in some cases, the virus became detectable by qPCR in the CSF early during the infection, when the virus was undetectable in the plasma without the use of SCA (Figure 3).

6.1.5 A partial bottleneck of transmitted/founder viruses occurs during SIVsab intrarectal transmission

In the preliminary study, it was demonstrated with SGA that infection was established by a single transmitted/founder virus in in both intravaginally and intrarectally infected AGMs (78). However, the observed number of transmitted/founder viruses per AGM in this study ranged from 3-10 variants (Figure 7). However, the original inoculum was highly diverse, meaning that the number of viruses that went on to successfully establish infection was severely reduced by the genetic bottleneck imposed by the mucosal epithelium.

6.1.6 $CD3^+$ T cells are the primary target cell of SIVsab

Using FISH, SIVsab was shown to infect $CD3^+$ T cells in both the rectum and the distal colon, reinforcing these cells as the primary target cells supporting viral replication following transmission. This was true in both the lamina propria, as well as in the lymphoid aggregates. The virus did not appear to infect myeloid lineage cells at the site of entry, with no viral RNA association with the myeloid cell types. This is expected of transmitted/founder viruses, as discussed in 1.4.4 and in agreement with previous studies (88, 107, 139) (Figure 8).

6.1.7 There were minimal alterations to primary and innate immune cell populations at the site of entry, with little to no immune activation

While transmission and viral dissemination from the site of inoculation were rapid in AGMs, SIVsab infection appears to have had very little impact on both primary and secondary immune cell populations in the rectum or the draining LN (Figures 9-12). In general, the levels of various immune cells at the site of inoculation, including $CD4^+$ and $CD8^+$ T cells, $CD20^+$ B cells, DCs, monocytes/macrophages, and natural killer cells, did not change during acute or early chronic SIVsab infection. These same populations also showed little to no alteration in activation status, as measured by activation markers such as HLADR, CD38 and CD69. Any changes that did occur either lacked significance or were transient, with return to baseline levels by the set-point of viral replication. This was similar to the low levels of immune activation observed elsewhere in the tissues more distal to the site of inoculation, including other sections of the gut and peripheral LNs (see 6.2.1).

6.2 Mucosal integrity

6.2.1 $CD4^+$ T-cell populations are relatively stable in the gut despite high levels of viral replication

Following intrarectal challenge with SIVsab, we found high levels of viral replication starting as early as 4-6 dpi in sites distal from the site of inoculation, including the jejunum, transverse colon and axillary LN. We identified both viral DNA and viral RNA in these tissues (Figures 4 & 5). Appearance of virus in these distal tissues matched establishment of plasma viremia levels detectable by qPCR, indicating that this likely represents seeding of the tissues by plasma virus (Figure 2). Virus replication in the jejunum, transverse colon and axillary LNs (Figures 4 & 5) was not associated with significant loss of target cells, with $CD4^+$ T cells populations being unaltered during the early stages of infection (Figure 13), as was also the case in the rectum and colonic LN (Figure 9). However, there was a significant depletion of $CD4^+$ T cells in the blood during the acute stage of SIVsab infection. This depletion was only transient, with loss of significance by early chronic infection, though this may have been due to smaller number of animals in that time group.

6.2.2 AGMs also exhibit low levels of immune activation in tissue distal to the site of inoculation

Used as a maker of immune cell activation and proliferation, Ki-67 expression levels by $CD4^+$and $CD8^+$ T cells or $CD20^+$ B cells did not significantly increase in either the gut or the LNs at any point during acute SIVsab infection, by either flow cytometry (Figure 16) or IHC (Figure 19 & Appendix C). In contrast, Ki-67 expression increased in both the gut and LNs of chronically SIVmac-infected RMs (Figures 19A-C). There was also little to no alteration of expression of activation markers such as HLADR, CD38 and CD69 by either the $CD4^+$or $CD8^+$ T cells (Figure 18), as was also observed at the site of inoculation (Figure 12). Additionally, RNAseq revealed little to no change in gene expression related to immune activation that would indicate $CD4^+$and $CD8^+$ T cells or $CD20^+$ B cell activation during acute infection (Figures 22 & 23).

6.2.3 Alterations in plasma cytokine and chemokine levels in response to infection are limited and transient, with two distinct waves of expression

We observed that several soluble markers of inflammation were increased during the acute SIVsab and early chronic infection in AGMs: (i) eotaxin (CCL11), a chemokine for eosinophils and possibly resting T cells and neutrophils (345), was strongly increased at both 3-4 dpi and 9-12 dpi; (ii) IL-1RA (IL1RN), an antagonist of the inflammatory IL-1 receptor (346), was also increased in plasma during acute infection and remained elevated at the set-point, but fell to baseline levels during the chronic infection; (iii) IL-8 (CXCL8), a neutrophil chemotactic factor also shown to be a chemoattractant for T-cell and basophils (347, 348), was increased throughout the acute and postacute infection, but returned to the baseline levels during late chronic infection; (iv) IP-10 (CXCL10), a chemoattractant for monocytes and T cells associated with HIV disease progression (266, 349, 350), exhibited very large increases (>100x) in some AGMs, particularly around the viral load peak, but was already normalized by the set-point of infection; a similar increase was observed in the levels of I-TAC (CXCL11), a T-cell chemokine strongly induced by IFN-γ along with IP-10 (351). Apart from these, MCP-1 (CCL2), a chemoattractant for monocytes, memory T cells and DCs (352), MIF (GIF), a proinflammatory cytokine associated with HIV infection (353, 354) and RANTES (CCL5), a T-cell chemotactic chemokine and possible $CD8^+$-mediated HIV suppressor (355, 356) were all increased in the majority of 3-4 dpi AGMs, and in all 9-12 dpi and 46-55 dpi animals, but returned to preinfection levels in the chronically SIV-infected historic controls (Figure 17).

6.2.4 AGMs have little to no recruitment of neutrophils to the gut despite having relatively large populations of resident neutrophils

As T-cell immune activation is usually accompanied by an innate immune response and recruitment of neutrophils, we assessed neutrophil populations and found little to no neutrophil accumulation in the gut

mucosa or the superficial LNs (Figure 20 & Appendix C). In comparison, the chronically SIV-infected RMs had large numbers of neutrophils recruited to the gut. (Figures 20A & C). We also saw no major change in MPO gene expression levels in the AGMs at any time during infection (Figure 23), suggesting that neutrophil activation and MPO expression is not altered during acute SIVsab infection.

6.2.5 There are few alterations to macrophage, dendritic cell, and natural killer cell populations in the gut

The overall levels of innate immune cells types, including DCs, monocytes/macrophages and NK cells (Figure 15) remained relatively stable in the distal tissues during acute SIVsab infection. This is in-line with the same populations at the site of inoculation (Figure 11), and in agreement with the lack of neutrophil recruitment during acute and early chronic SIV infection. It should be noted that there were significant decreases in the levels of monocytes/macrophages and natural killer cells in the blood during the preramp and ramp-up periods of acute infection, but these changes were only transient, with a loss of significance at the peak of viral replication (Figure 15).

6.2.6 AGMs exhibit a strong interferon-linked response to infection

The SIVsab-infected AGMs exhibited a significant anti-viral response in both the gut and the LNs, observed here as a large increase in production of MX1 at the peak of viral replication (Figure 21 & Appendix C). However, this response was only transient, with a total return to baseline levels by the early chronic stage of infection. Inversely, the RMs had high levels of MX1 expression into chronic stage of SIV infection (Figures 21). The magnitude of the MX1 present in the tissues was similar at the peak of SIVsab infection in the AGMs and during chronic SIVmac infection in the RMs, which was reflected in the RNAseq analysis of gene expression in both species (Figure 23), where MX1 and the interferon-linked CXCL10 and CXCL11 showed strong up-regulation.

6.2.7 There is little to no increase in the fraction of apoptotic immune cells in response to SIV infection

Despite the high levels of viral replication, we found no significant increase in the levels of active caspase-3 in the tissues (Figures 24) at any time-point during acute or early chronic infection in SIVsab-infected AGMs, as was seen in previous studies (198). This is in contrast our findings in the SIV-infected RMs, where we observed high levels of active caspase-3 during the chronic stage of infection (Figure 24). The lack of apoptosis in the AGMs mirrors the lack of immune activation, proliferation and inflammation in response to infection (Figures 13-23)

6.2.8 AGMs maintain the homeostasis and integrity of the gut epithelium during acute and chronic SIVsab infection

In line with the lack of apoptosis in the gut, staining for the tight junction protein claudin-3 showed that AGMs sustain no major cell death or damage to the gut epithelial during SIVsab-infection, even during the peak of viral replication (Figures 25A, B & D & Appendix C). By comparison, there were numerous lesions and breakages in the gut in the chronically infected RMs (Figure 25C & D). The constancy of the gut mucosa in AGMs in the face of SIVsab-infection was also reflected by the lack of significant alterations in the plasma levels of I-FABP, a marker of enteropathy (Figure 25E).

Preservation of the gut architecture in the AGMs was also observed by total lack of fibrosis, both in the gut and the LNs (Figures 26 & Appendix C), with none of the build-up of collagen associated with fibrosis in pathogenic infections (284, 303–305). This is unlike the chronically infected RMs, where large amounts of collagen were present, particularly in the LNs, indicating extensive fibrosis. To support these results, we tested for plasma levels of a hyaluronic acid, a marker of fibrosis, and found that hyaluronic acid in the plasma was not significantly altered throughout the follow-up (Figure 26D).

6.2.9 No microbial translocation occurs during acute SIVsab infection in AGMs

Maintenance of the mucosal integrity in the AGMs would result in lack of MT and, indeed, we found no increase in the amount of LPS-core or the number of *E. coli* in the lamina propria and LNs of our SIVsab-infected AGMs. None of these markers showed significant increases during either acute or postacute SIVsab infection (Figures 27 & 28 & Appendix C), in contrast with the chronically SIV-infected RMs, which had high levels of LPS and *E. coli* (Figures 27 & 28). Furthermore, quantitative image analysis revealed that these two markers of MT were significantly higher in the LNs of the RMs during chronic SIVmac infection than in the AGMs during early chronic SIVsab infection.

6.3 Epithelial wound healing response

6.3.1 AGMs exhibit a unique wound healing response mediated by macrophages and monocytes

Following intrarectal inoculation with SIVmac251 in RMs and SIVsab92018 in AGMs, respectively, we found highly divergent patterns of gene expression. This schism included thousands of genes which were differentially expressed in response to infection (Figure 30). From this set of DE genes, a unique regenerative wound healing signature was identified in AGMs, which was wholly absent in the RMs. This wound healing response was activated by monocytes in the peripheral blood and then further propagated by tissue macrophages resident to the site of inoculation (Figure 37). The AGM-specific wound healing was linked with preservation of mucosal integrity and the absence of the inflammatory phenotype typically associated with the normal wound healing response following injury (Figure 31) and matches the observations made of the AGM gut during SIV infection, as described in 4.0.

6.3.2 The AGM wound healing response is scar-free and is not associated with inflammation

AGM wound healing signature was discovered by CGSA to be similar to gene expression in a primitive species of Mexican salamander, the axolotl. Axolotls are able to accomplish wound healing via a noninflammatory pathway that bypasses the early inflammatory stage of wound healing (Figures 33 & 34). This enables the axolotl to avoid the immune activation and tissue damage that accompany the inflammation that occurs post wounding. Given that acute SIV-infection is already associated with limited immune activation and inflammation (see 3.0 and 4.0), the AGM wound healing phenotype could contribute to protection against both inflammation and disease progression during SIVsab infection.

6.3.3 Fibronectin plays a critical role in the wound healing response in the AGM gut epithelium

Here, IHC and IF imaging for fibronectin (Figures 34 & 35) showed that in AGM mucosal tissue, fibronectin, a scaffolding protein that is critical for organization of proteins necessary for the wound healing (Figure 34B), was concentrated to at the ECM, where fibronectin polymerization is initiated during wound repair (341). In RMs, fibronectin was predominantly present at low levels or as diffuse extracellular fibrils. This cellular localization of fibronectin in AGMs could potentially accelerate wound healing compared to RMs.

6.3.4 Fibronectin is strongly associated with macrophages in AGM.

Using IF staining and imaging, we found that fibronectin frequently colocalized with macrophages, which were delineated using HAM56, a marker specific to mature macrophages (Figure 35 & Appendix C). This colocalization occurred both prior to inoculation and during the early stages of acute SIVsab-infection. In the RMs, colocalization of fibronectin with the macrophages was rare to nonexistent. This

suggests that in AGMs the macrophages play an integral role production and assembly of fibronectin and therefore facilitate formation of the entire complex of wound healing proteins.

6.3.5 AGM macrophages exhibit a distinct wound healing phenotype

Normally, wound healing is predominantly associated with M2 macrophages and not with inflammatory M1 macrophages. However, the wound healing gene expression signatures observed in both classically activated M1 and alternatively activated M2 monocytes in AGMs (Figures 37 & 38). Both the M1 and M2 macrophages in the AGMs also were found to express several upstream regulators of the wound healing response, including TGF-β, SMAD7, and ERBB2. Similarly, the AGM macrophages, but not the RM macrophages, expressed key genes upregulated during the early axolotl wound healing response, including *FN1*, *MRC2*, *ADAMTS2* and *SCD2* (Figure 37).

6.3.6 The AGM gut epithelium is already primed for wound healing prior to SIVsab infection

When examining gene expression linked to wound healing in AGMs, both the embryonic development signature and fibronectin tissue localization were present in AGM monocytes pre-inoculation, as shown by both the transcriptomics and IF imaging (Figures 34B, 35 & Appendix C). The upstream regulators of wound healing and the axolotl wound healing genes were also already upregulated in the baseline AGMs, prior to SIV infection (Figure 37). This shows that in AGMs, the wound healing response is already primed for activation before the infection even begins.

6.4 Future Directions

6.4.1 Assessing the ability of AGM macrophages to repair damage in an epithelial wounding model

As shown in 5.4, one of the defining characteristics of AGMs is their unique wound healing process, which is similar to that of the aquatic axolotl. This type of wound healing is nonfibrotic, forming new, fully functional, scar-free tissue. It is also noninflammatory, having a similar gene expression profile immediately post wounding that other species would have much later, at 7 days post wounding (Figures 31 & 33). The transcriptomic analysis identified that at least one of the major mediators of the AGM wound healing response are monocytes/macrophages, with AGM peripheral blood monocytes exhibit similar wound healing signature to the axolotl (Figure 37). Macrophages were also shown to be strongly associated with the wound healing related-linked protein fibronectin in AGMs, but not RMs, using IF (Figure 35 & Appendix C)

However, this singular capacity of AGM monocytes/macrophages to facilitate tissue repair was not demonstrated functionally. To show this, one possible experiment would be to use an *in vitro* model of epithelial wounding. Recently, a new model for studying epithelial wound healing has been described. Compared to previous models which relied on undifferentiated monolayers of epithelial cells, this model uses stratified human corneal epithelial cells, which exhibit proper cellular differentiation and polarization. Even more importantly, these cells demonstrated normal wound healing response, with epithelial cell migration and restoration of the transcellular barrier and apical intercellular junctions (357).

Using this model, it would be possible to test the wound healing capacity of AGM macrophages by introducing them in culture and inducing wounding of the epithelial cells. The macrophages would need to be isolated from a tissue, likely from the blood, as was done in this study (see 5.3.7), before being added to the epithelial cell culture. Several factors would need to be addressed, including: (i) assessing the viability of the AGM macrophage in culture with human epithelial cells; (ii) testing macrophages from AGMs *versus* RMs: (iii) ascertaining if the macrophages require additional activation to stimulate repair.

6.4.2 Functional characterization of M1 and M2 macrophages from AGMs and RMs

The transcriptomic analysis of the monocytes/macrophages from the AGMs and RMs was extended to differentiate M1 and M2 macrophages. Generally, M1 macrophages are "kill" macrophages are involved in the immune responses against infection and stimulate inflammation and immune activation. M2 macrophages are the "heal" macrophages, producing growth factors, reducing inflammation and helping to clear cellular debris (358). Here, we found that the M1 and M2 monocytes/macrophages from AGMs had distinct genetic signatures and phenotypes compared to the RMs; here, both M1 and M2 macrophages expressed genes linked to wound healing. Some of these same genes were also associated with the wound healing response in the axolotl.

Not only is this phenotype crucial to the AGM wound healing response, it is also highly unusual in a more general sense. However, it has traditionally be difficult to separate due to lack of specific cell markers and, consequently, M1 and M2 macrophages are frequently generated by differentiation in culture (359). Recently, two new markers have been described to delineate M1 (CD38) and M2 (Egr2) macrophages. Using these markers, it may be possible to separate the M1 and M2 monocytes/macrophages from peripheral blood taken from AGMs and RMs. Functional studies could then be performed to characterize the macrophages and determine if the M1 and M2 cells from AGMs exhibit similar functions related to wound healing, such as production of TGF-β. It would also be informative to attempt to introduce the M1 and M2 cells from the AGMs and RMs separately into the epithelial wound healing model described in 6.4.1.

6.4.3 Depletion of macrophages in AGMs prior to SIVsab infection

A studies from our group showed that depletion of $CD8^+$ T cells (174) and $CD20^+$ B cells (187) had no lasting impact on SIVsab-infection in chronically infected AGMs. That being said, the essential role that monocytes/macrophages in facilitating the wound healing response in AGMs that was demonstrated

by this study suggests that removing them from the equation might impact disease progression. The problem is that there is little to no work done on depleting monocytes/macrophages in nonhuman primates. In mice, monocyte/macrophage depletion is often accomplished through injection of liposome-encapsulated clodronate (360, 361). However, this treatment has not been adapted to NHPs due to a narrow therapeutic window, poor tolerability and liver toxicity (362).

A relatively recent study demonstrated a novel method for monocyte/macrophage depletion; after failing to deplete using a CD14-depelting antibody, rhesus macaques were treated with liposomal bisphosphonate alendronate, resulting in consistent depletion of the monocytes in the blood and macrophages in the tissues and an increased frequency of monocytes in the bone marrow. The treatment had no adverse clinical effects or significant alterations in serum chemistry, making it viable method for monocyte/macrophage depletion in NHPs (362).

6.4.4 Surveying other immune cell types involved in immune response with CGSA

While monocytes/macrophages were the most prominent cell type to be associated with the wound healing pathway using CGSA, they aren't the only cell type associated with wound healing. Other cells, including neutrophils, fibroblasts, and myofibroblasts, play roles in the wound healing response, and could be potential targets of interest for future CGSA. Of particular interest are the neutrophils, as we found that the AGMs in this study had relatively high levels of neutrophils present in the gut prior to infection, which remained unchanged following infection (Figure 20). Neutrophils are traditionally associated with inflammation and tissue damage, but their presence prior to SIV infection makes them a potential cell type of interest. Additionally, the current CGSA analysis revealed a unique genetic signature in the gut of the AGMs for eosinophils and subsequent IHC for major basic protein, a core protein of eosinophilic granules, showed a large number of eosinophils in the lamina propria (data not shown). The role of eosinophils in wound healing is unclear (363), although there is some evidence to suggest that they might facilitate wound healing during ulcerative colitis (364), so further investigation may be warranted.

6.4.5 Promoting macrophage-mediated wound healing response in chronically SIV-infected RMs

The importance of gut damage in driving disease progression was clearly shown in a previous study, where colitis was induced in uninfected RMs through treatment with dextran sodium sulfate (DSS). Experimental administration of DSS to the RMs resulted in inflammation and immune activation similar to pathogenic SIV-infection. Additionally, DSS treated AGMs exhibited increased viral loads and markers of disease progression, though these changes were only transient (195). The return to homeostasis by the AGMs is particularly notable in the context of this study in regard to the macrophage-mediated wound healing response.

This is because the majority of HIV-infected persons represent chronic stages of infection, with the associated levels of chronic inflammation. The DSS treatment of the AGMs demonstrated their wound healing response was sufficient to restore normal gut function following the insult imposed by the treatment. This implies that if a treatment or strategy induced a similar response in individuals chronically infected with HIV, the wound healing may be able to reduce or suppress the chronic inflammation and restore gut integrity.

Recently, several studies have linked improved wound healing and macrophage survival with IL-33 (344) and IL-35 (365) in mice. In a future study, it would be highly informative to attempt treatment of chronically SIVmac-infected RMs with IL-33 or IL-35 or another agent designed to stimulate the macrophage-mediated wound healing response and evaluate any changes in inflammation status, immune activation, epithelial integrity and disease progression.

6.4.6 Treating chronically SIV-infected RMs to minimize loss of mucosal integrity in the gut

As the findings of this study reinforce the importance of maintenance of gut integrity in preventing disease progression, a future study might focus on the impact of reducing the amount of damage to the gut epithelium in pathogenic SIV infection. This could be done readily in RMs infected with SIV and would

need to address: (i) whether minimizing gut damage during acute pathogenic infection effects later disease progression: (ii) whether reducing gut damage during chronic infection impacts further disease progression or chronic inflammation. There are numerous potential candidates for testing; in just the past year, baicalein (366), PAP-1(367), syringic acid (368), and several strains of the probiotic bacterium *Akkermansia muciniphila* (369) were all shown to lessen the impact of DSS-induced colitis.

7.0 Summary

At the start of this dissertation project, the following core hypothesis was proposed: that events occurring during the earliest stages of mucosal transmission may contribute to the resolution of the immune activation characteristic of pathogenic lentiviral infection at the passage from acute-to-chronic infection and thus prevent disease progression in nonprogressive hosts (see 2.0). To test this hypothesis, the three following specific aims were proposed:

7.1 SA1: Characterize the viral bottleneck and dissemination from the site of infection in AGMs intrarectally (IR) inoculated with SIVsab

To address this specific aim, we intrarectally inoculated 29 adult male AGMs with SIVsab92018 and then performed serially necropsies on them. Each AGM was euthanized at a specific point in time, corresponding to the predicted state of the plasma viremia (Figure 1). The viremic state was later confirmed by either qPCR or SCA (Figure 2). From each animal, samples were collected from a wide variety of tissues, snap frozen and, later, total DNA/RNA was extracted from each specimen. By testing the total number of vRNA and vDNA copies in over 38 tissues (Figures 4 & 5), it was established that all tissues were seeded with SIVsab92018 by the peak of viral replication, at 9-12 dpi. With only a few exceptions, such as in the oral mucosa, virus was already present by 4-6 dpi. This corresponded with the establishment of reliably detectable plasma viremia, as measured with qPCR and SCA, indicating that by this time, the virus had already reached the blood stream through the lymphatics and been distributed systemically. Virus was only detectable early, at 1-3 dpi, in tissues taken from the site of inoculation (rectum, distal colon) and the draining colonic LN. Therefore, enough SIVsab92018 to establish systemic infection was transmitted from the rectal site of inoculation through the lymphatics to the thoracic duct and into the blood stream within 3

dpi. This timeframe for viral spread was supported by RNAscope (Figure 6) and FISH (Figure 8), which revealed the presence of virus within the lamina propria of the rectum and distal colon as early as 1-3 dpi.

Despite the more permissive nature of the rectal mucosa to infection, viral transmission itself was not unrestricted, as SGA revealed there was a genetic bottleneck of the transmitted/founder during intrarectal inoculation, with 3-10 transmitted/founder viruses generating infection in each animal tested (Figure 7). While this number was higher than expected, possibly due to overdosing during inoculation, it still reflected restriction of virus in the original inoculum.

7.2 SA2: Examine early changes in the immune cell populations following IR challenge of AGMs with SIVsab

At the time of necropsy, apart from the tissues used for viral load quantification, multiple tissues were collected to use for cell separation (see 3.3.3). These included the site of inoculation (rectum, distal colon), other sections of the lower and upper intestinal tract (transverse colon, jejunum, and ileum), draining LNs (colonic, iliac, obturator) and LNs progressively more distant from the site of inoculation (mesenteric, axillary, inguinal and submandibular). Cells were isolated from many of these tissues and stained for flow cytometry to analyze any changes in immune cell populations or activation status (Figures 9-12 & 13-15). However, in the majority of these tissues, including those collected from the site of inoculation, there were few, if any, significant alterations of the primary $CD4^+$ and $CD8^+$ populations or their subsets (central and effector memory, naïve). Other immune cell populations, including $CD20^+$ cells, monocytes and macrophage, dendritic cells and natural killer cells, also were largely unaffected in response to SIVsab92018 infection. Any significant changes were mostly transient.

Immune cell populations were also surveyed through extensive IHC testing for expression of a number of different markers, including: Ki-67 (Figure 19), myeloperoxidase (Figure 20), MX1 (Figure 21), and active capase-3 (Figure 24). The relative levels of markers in each tissue (transverse colon, axillary LN,

and jejunum) were measured using quantitative image analysis (see 4.3.11). However, it was found that, as shown by flow cytometry, immune cell activation and proliferation (Ki-67) remained largely unchanged in response to infection, both in the lamina propria and the epithelium of the gut. Likewise, there was little to no increase in apoptosis (caspase-3) and any recruitment of neutrophils (MPO) in response to infection was only transient. There was also a transient, but significant, increase in the interferon-linked antiviral response (MX1) in both the gut and the lymph nodes, but only during the peak of viral replication.

These trends were reflected by the gene expression patterns in the AGM gut. Transcriptomic analysis revealed few, if any, alterations to genes linked to immune response of $CD4^+$ and $CD8^+$ T cells or $CD20^+$ B cells (Figure 22). Genes associated with the interferon response to viral infection, including MX1 and the interferon-induced genes CXCL10 and CXCL11, were highly upregulated at the peak of viral replication (Figure 23). These increases in CXCL10//CXCL11 were also observed in the plasma at the peak of viral replication (Figure 17).

7.3 SA3: Analyze the expression of inflammatory and anti-inflammatory genes following IR SIVsab challenge.

During tissue collection, samples taken from the rectum and distal colon were preserved in RNAlater specifically to be used for RNAseq and transcriptomics. The transcriptomics was performed in tandem with RMs that had been intrarectally infected with SIVmac251, which is pathogenic in RMs. This allowed for direct comparison between gene expression profiles in pathogenic and nonpathogenic infections. The initial analysis reveal that AGMs lacked up-regulation of genes associated with chronic inflammation (Figure 30C); they also expressed more of the anti-inflammatory cytokine IL-17B almost immediately postinfection (Figure 23). Additionally, the AGMs exhibited increased expression of a number of genes potentially related to the wound healing response.

It is known that during acute HIV/SIV infection, viral replication within the GALT drives inflammation and damage of gut epithelium, leading to microbial translocation from the gut lumen. This, in turns, leads to establishment of chronic inflammation. By avoiding or repairing damage to the gut epithelium, AGMs would prevent both microbial translocation and the subsequent inflammation.

Indeed, when examined on a whole genome scale, a correlation was found in AGMs with late stage (noninflammatory) wound healing response (Figure 31A), while lacking any gene expression signatures associated with the presence of LPS at 3 dpi (i.e., microbial translocation) (Figure 32C). The AGMs were shown to have pattern of up-regulation of gene linked to wound healing very similar to those found in aquatic axolotl (Figures 33 & 34A). A primate species of salamander, the axolotl is able to conduct wound healing without inflammation or scar tissue formation. Like the axolotl, the AGMs appear to bypass the inflammatory stage of wound healing in the gut. Doing so would not only enable them to repair virally induced damage to the epithelium, but also maintain lower levels of inflammation overall. Analysis of the protein interactions associated with specific gene pathways revealed that axolotl-like wound healing in AGMs was mediated by the ECM protein fibronectin (Figure 34B).

IHC quantification of fibronectin in the rectum of the AGMs revealed that it was strongly localized to the ECM, a phenotype normally associated with wound healing (Figure 34C). Immunofluorescence staining for fibronectin and the macrophage marker HAM56 revealed that many macrophages in the rectal lamina propria of AGMs, but not RMs, were strongly positive for fibronectin (Figures 35 & 36). Deep mRNAseq showed that in AGMs, both M1 and M2 macrophages exhibited gene expression patterns associated with wound healing (Figure 37)

The findings from the transcriptomics were confirmed by IHC staining for makers associated with loss of epithelial integrity (claudin-3, Figure 25), fibrosis (collagen, Figure 26) and microbial translocation (LPS-core and *E. coli*, Figures 27 & 28). By measuring the ratio of intact versus damaged gut epithelium stained for claudin-3 (see 4.3.11 & Appendix C), it was established that AGMs exhibit little to no loss of mucosal integrity in the gut following infection. They also exhibited no evidence for the fibrosis that would follow any significant damage to the gut. This lack of disruption to the gut epithelium was accompanied by

no significant alterations to LPS or *E. coli* levels, showing that no microbial translocation occurs following SIVsab infection.

7.4 Final conclusion

Taken together, we believe that these results have largely addressed the 3 original specific aims of this project. Therefore, we can confirm our original hypothesis, with a caveat. It was initially proposed that prevention of disease progression would hinge on: (i) lower availability of target cells at the mucosal site(s) of infection; (ii) lower levels of immune activation at the mucosal sites, which result in (iii) reduced recruitment of target cells to mucosal sites of infection and (iv) the establishment of an anti-inflammatory milieu that suppresses the virally induced proinflammatory response While we did demonstrate lower levels of immune activation at the mucosal sites following SIV-transmission and a lack of target-cell recruitment, we did not find a strong anti-inflammatory milieu following infection.

Instead, our findings suggest prevention of inflammation in the gut may depend on preservation of gut integrity through a unique wound healing mechanism. It is probable that none of the elements are separate, with the low levels of immune activation and the anti-inflammatory response following infection limiting the rate of damage to the gut enough to allow for repair of the mucosal barrier, thereby preventing further disease progression in natural hosts.

However, more research is needed to better understand these protective responses in AGMs, particularly in regard to the macrophage-mediated wound healing response. Better understanding of these mechanisms could prove invaluable to the development of new strategies to reduce inflammation and preserve or restore the gut integrity in HIV^+ individuals. Eventually, this could advance progress towards a functional cure to prevent progression to AIDS, potentially allowing cessation of ART treatment without the threat of disease progression. This research could also open up paths towards reducing the impact of the

comorbidities associated with the chronic systemic inflammation triggered by HIV/SIV infection, leading to a better quality of life and long-term pathogenic outcome for ART-treated HIV^+ individuals.

Appendix A Reference Information

Table 4: Chronically SIVmac-Infected RMs Reference Information

Animal ID	SIV Isolate	Weeks Post Infection or Disease Stage	Reference	DOI
55I	SIVmac239	24	(249)	10.1371/journal.ppat.1001052
83I	SIVmac239	24	"	"
AD09	SIVmac239	23	"	"
AY25	SIVmac239	39	"	"
AY44	SIVmac239	39	"	"
AY99	SIVmac239	30	"	"
DBB8	SIVmac239	12	(370)	10.1093/infdis/jis643
DBEH	SIVmac239	12	“	"
DBGE	SIVmac239	12	“	"
DEMD	SIVmac239M	34	NA	NA
F57	SIVmac239	105	NA	NA
FZ2	SIVmac239	105	NA	NA
P383	SIVmac251	86	NA	NA
P436	SIVmac251	58	NA	NA
P735	SIVmac251	70	NA	NA
P787	SIVmac251	66	NA	NA
P857	SIVmac251	65	NA	NA
R268	SIVsmmE660	8	(249)	10.1371/journal.ppat.1001052
R365	SIVmac251	8	NA	NA
R366	SIVmac251	8	NA	NA
R367	SIVmac251	8	NA	NA
R406	SIVmac251	8	NA	NA
R410	SIVmac251	8	NA	NA
R437	SIVsmmE660	26	(249)	10.1371/journal.ppat.1001052
R443	SIVmac239	56	“	"
R451	SIVmac239	21	“	"
R453	SIVmac239	37	(157)	10.1128/JVI.02612-09
R457	SIVmac239	57	(249)	10.1371/journal.ppat.1001052
R462	SIVmac239	57	"	"
R475	SIVmac239	28	"	"

Table 4 (continued)				
R533	SIVmac251	8	NA	NA
R694	SIVmac251	8	NA	NA
R695	SIVmac251	8	NA	NA
R696	SIVmac251	8	NA	NA
RH594	SIVsmmE543	39	(93)	10.1182/blood-2012-06-437608
RH767	SIVsmmE543	23	“	
RHk8	SIVmac239	50	“	
RJi9	SIVmac239	32	“	
ROu8	SIVmac239	Chronic	(153)	10.4049/jimmunol.180.10.6798
RWu8	SIVmac239	Chronic	(153, 157)	10.4049/jimmunol.180.10.6798, 10.1128/JVI.02612-09

Table 5: Flow Cytometry Panels Showing Target Markers and Fluorochromes

	FITC	PE	PE-TxR	PE-Cy7	APC-H7	APC	APC-Cy7	V450	Qdot565(SA/Biotin)	PerCP	PE-Cy5	Alexa 700
SS1	CD95	CCR5	CD8a/b	CD28	CCR7	CD4		CD3	CCR7			
SS2	CD3	Beta 7	CD8a/b	CXCR3		CD4		CCR4	CCR6			
SS3	CD38	CD25	CD8a/b	HLA-DR		CD4	CD69	CD3				
ICS1	Ki-67	CD95	CD8a/b	CD28		CD4	CD20	CD3				
TruCount					CD20	CD4		CD3		CD45		
DC Surface	CD95	Lineage		CD123		CD11C	HLADR	CD80	CD86	CD45		
DC ICS	Ki-67	Lineage		CD123		CD11C	HLADR	Caspase-3	CCR7	CCR5		
Macrophage	Ki-67	CD163		CD80		CD14	HLADR	Caspase-3	CD86	CCR5		
NK ICS1	Perforin	Granzyme B		CD56	CD16	NKG2A		CD3			CD69	CD8a
NK ICS2	Ki-67	NKP30		CD56	CD16	NKG2A		CD3			NKP46	CD8a

Table 6: Product Information for Flow Cytometry Antibodies

Antibody	Clone	Catalogue #	Company	Antibody	Clone	Catalogue #	Company
CD3e-FITC	SP34	556611	BD Pharm	CD16 APC-H7	3G8	560195	BD
CD38-FITC	AT-1	60131FI	Stem Cell	CD20-APC-H7	2H7	560853	BD Pharm
CD95-FITC	DX2	555673	BD Pharm	CD4-APC	L200	551980	BD Pharm
Ki-67-FITC	B56	556026	BD Pharm	CD11c-APC	S-HCL-3	340544	BD BioSci
Perforin-FITC	PF-344	3465-7	Mabtech AB	CD14-APC	M5E2	555399	BD Pharm
CD3-PE	SP34-2	552127	BD Pharm	NKG2A-APC	Z199.1	A60797	Beckman Coulter
CD14-PE	M5E2	555398	BD Pharm	CD20-APC-Cy7	L27	335794	BD BioSci
CD20-PE	2H7	556633	BD Pharm	CD69-APC-Cy7	FN50	557756	BD Pharm
CD25-PE	2A3	341009	BD Pharm	HLA-DR-APC-Cy7	L243	335796	BD BioSci
CD95-PE	DX2	555674	BD Pharm	CD3-V450	SP34-2	560351	BD Pharm
CD163-PE	GHI/61	556018	BD Pharm	CD80-V450	L307.4	560442	BD Horizon
CCR5-PE (CD195-PE)	3A9	556042	BD Pharm	CCR4-V450 (CD194)	1G1	561123	BD Pharm
Granzyme B-PE	GB11	561142	BD Pharm	Caspase-3-V450	C92-605	560627	BD Horizon
Integrin b7-PE	FIB504	555945	BD Pharm	Streptavidin Q. Dot 565		Q10131MP	Invitrogen
NKp30-PE (CD337)	Z25	IM3709	IOTest	CD86-Biotin	2331(FUN-1)	555656	BD Pharm
CD8 α/b -PE Texas Red	3B5	MHCD0817	Invitrogen	CCR6-Biotin (CD196)	11A9	559561	BD Pharm
CD28-PE-Cy7	CD28.2	560684	BD Pharm	CCR7-Biotin	3D12	552174	eBioscience
CD56-PE-Cy7	NCAM16.2	335791	BD BioSci	CD45-PerCP	D058-1283	558411	BD Pharm
CD80-PE-Cy7	L307.4	561135	BD Pharm	NKp46 Purified	9 E2	331901	Biolegend
CD123-PE-Cy7	7G3	560826	BD Pharm				
HLA-DR-PE-Cy7	L243	335813	BD BioSci				
CXCR3-PE-Cy7 (CD183)	1C6/CXCR3	560831	BD Pharm				

Table 7: Immunohistochemistry Antibodies Information

Target Marker	Antibody	Manufacturer	Clone	Reference #	Dilution	Incubation Time
Ki-67	mouse IgG	Dako	MIB-1	M7240	1:100	5 min
MPO	rabbit IgG	Dako	polyclonal	A0398	1:800	30 sec-2 min
MX1	rabbit IgG	Abcam	polyclonal	ab95926	1:800	3 min
Caspase-3	rabbit IgG	Abcam	polyclonal	ab2302	1:50	5-15 min
Claudin-3	rabbit IgG	ThermoFisher	polyclonal	RB-9251-P1	1:100	<60 sec
LPS	mouse IgG	Hycult	WM1 222-5	HM6011	1:100	2-3 min
E.coli	rabbit IgG	Dako	polyclonal	B0357	1:500	2 min

Table 8: Reference Datasets for Biological Processes

GSE	Description	Species	Tissue	*n*=	PMID
GSE23006	Wound healing	Mouse	Skin	24	20704739
GSE23006	Wound healing	Mouse	Tongue	24	20704739
GSE28914	Wound healing	Human	Skin	25	23082929
GSE17698	Wound healing	Rat	Eardrum	40	21919009
GSE35255	Wound healing	Axolotl, aquatic	Skin	16	22485136
GSE35255	Wound healing	Axolotl, terrestrial	Skin	16	22485136
GSE9293	Colitis by TNBS	Rat	Colon	18	NA
GSE9281	Colitis by DSS	Rat	Colon	42	NA
GSE35609	Colitis by TNBS	Mouse	Colon	34	23226271
GSE19392	IFN-β stimulation	Human	Airway epithelial cells	169	20064372
GSE19182	Cytokine stimulation	Human	HNEC cells	21	22005912
GSE27870	TNF-α a stimulation	Human	Endothelial cells	24	22121215
GSE32513	Microbial colonization	Mouse	Jejunum	48	22617837
GSE32513	Microbial colonization	Mouse	Ileum	48	22617837
GSE32513	Microbial colonization	Mouse	Colon	48	22617837
GSE51269	TLR knock-out	Mouse	Colon	20	25210121
GSE39582	Colon cancer	Human	Colon	585	23700391
GSE26253	Colon cancer	Human	Colon	432	24598828
GSE44076	Colon cancer	Human	Colon	246	25215506
GSE17536	Colon cancer	Human	Colon	177	19914252
GSE11223	Ulcerative colitis	Human	Colon	202	18523026
GSE20881	Crohn's disease	Human	Colon	172	20848455
GSE48634	Ulcerative colitis	Human	Colon	171	25171508

Appendix B : Methods

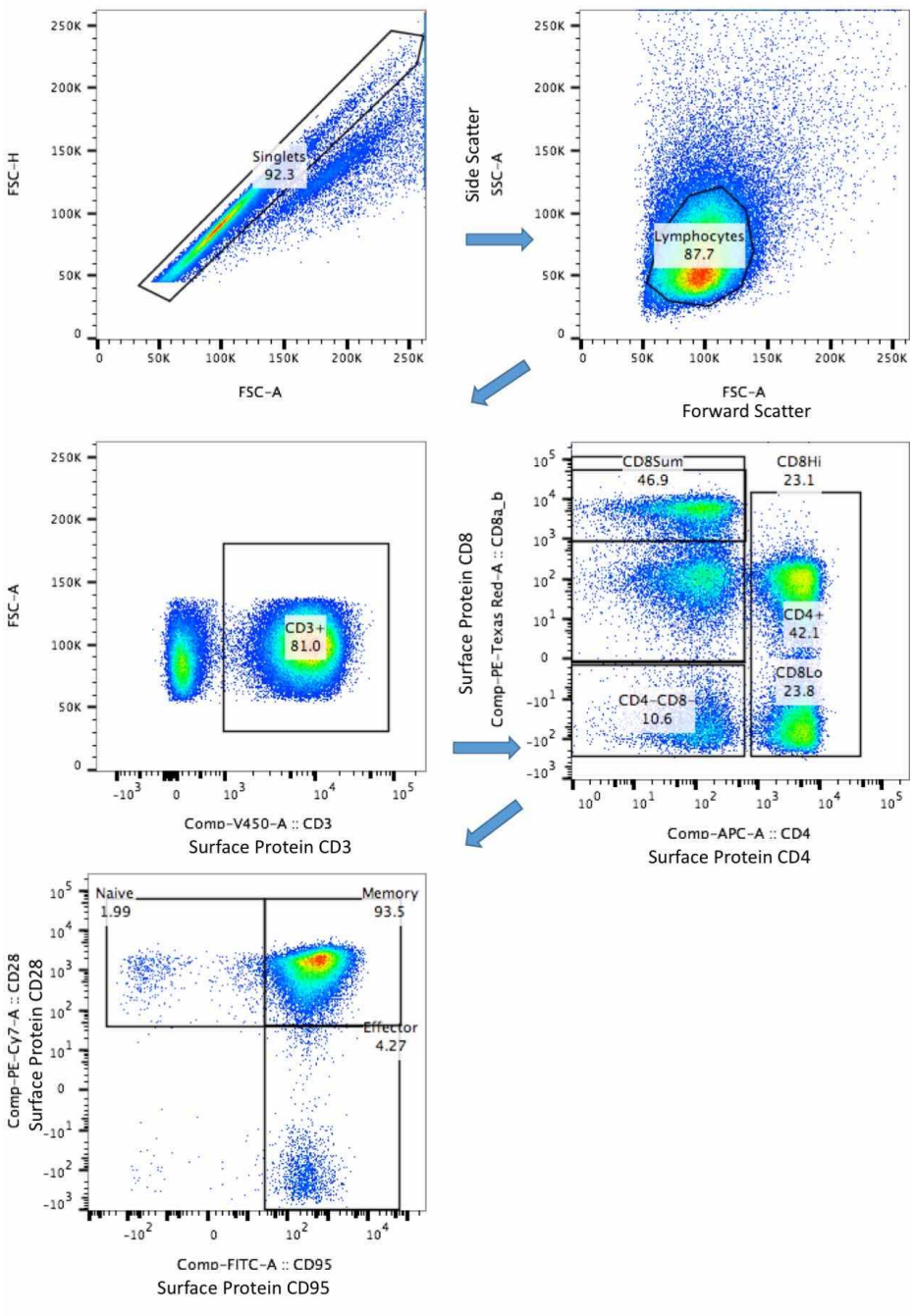

Figure 38: Flow cytometry gating strategy for CD4$^+$ and CD8$^+$ populations.
Gating strategy used to delineate primary T-cell populations (CD3$^+$, CD4$^+$, CD8$^+$) and secondary T-cell populations (EM, CM and naïve). All gates were generated using Flowjo software version 10.1r5 (Tree Star Inc, Ashland, OR).

Figure 39: Method for quantification of positive DAB signal based on color deconvolution.
To quantify the DAB stain, each raw image (A) was processed using the Color Deconvolution 1.7 plugin for FIJI v.1.0. The preset DAB settings were selected, and the software separated the image into 3 color channels, with the brown channel representing the positive DAB signal (B). A threshold was then manually applied to the brown channel image to remove background coloration (C). Finally, the area of each image representing the DAB signal above threshold was measured as a percentage of the total area of the image. All images were captured at 200X magnification using an AxioImager M1 brightfield microscope equipped with an AxioCam MRc5. All image manipulations and measurements were done with FIJI v.1.0.

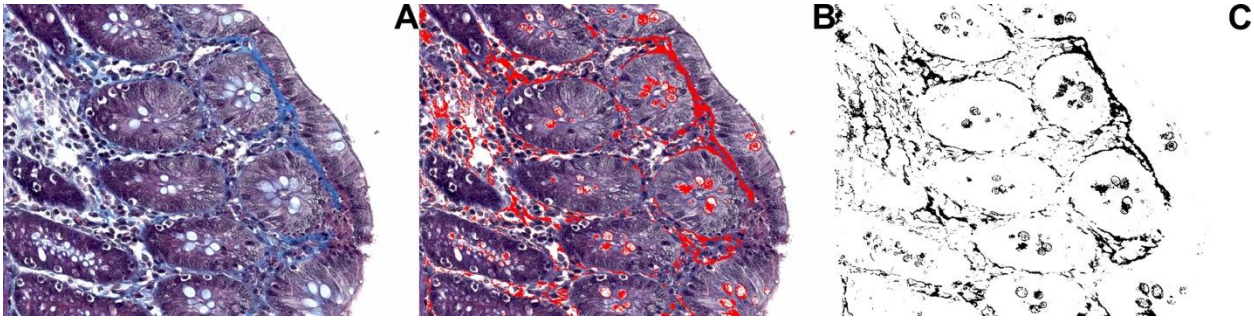

Figure 40: Method for quantification of tissue collagen based on color thresholds.
To quantify the amount of collagen in each tissue, each raw image (A) was processed with the built-in Color Threshold function in FIJI v.1.0. Using this feature, first the collagen was isolated from the rest of the image by adjusting the Hue value of the Color Threshold function to only encompass the blue of the collagen (B). It should be noted that the blue dye was also partially taken up by the goblet cells in the mucosal epithelium. After setting the Color Threshold, all background colors were removed, and the image was transformed into black and white (C). This eliminates all area of the image that is not blue coloration, which then can be measured by setting an intensity threshold to select all black area in the image. All images were captured at 200X magnification using an AxioImager M1 brightfield microscope equipped with an AxioCam MRc5. All image manipulations and measurements were done with FIJI v.1.0.

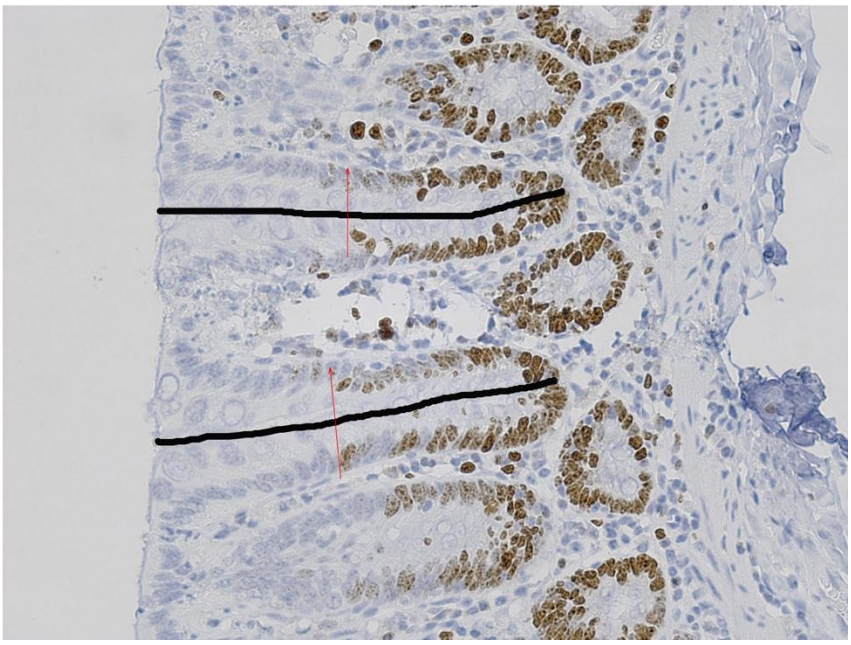

Figure 41: Approximation of epithelial proliferation in colonic crypts.
To generate an approximation of the levels of on-going proliferation in the gut epithelium, we captured images of individual crypts in tissue sections stained with Ki-67. As epithelial proliferation is localized to the base of the crypts, we measured both the total length of the crypt (total black line) and the length of the crypt with Ki-67^{+} epithelial cells (black line below the bisecting green arrow). Since increased levels of proliferation should result in an increase in the total number of Ki-67^{+} cells along the crypt, taking the ratio of the areas of the line allowed us to normalize proliferation across multiple crypts. All individual images were captured at 200X magnification using an AxioImager M1 brightfield microscope equipped with an AxioCam MRc5. All image manipulations and measurements were done with FIJI v.1.0.

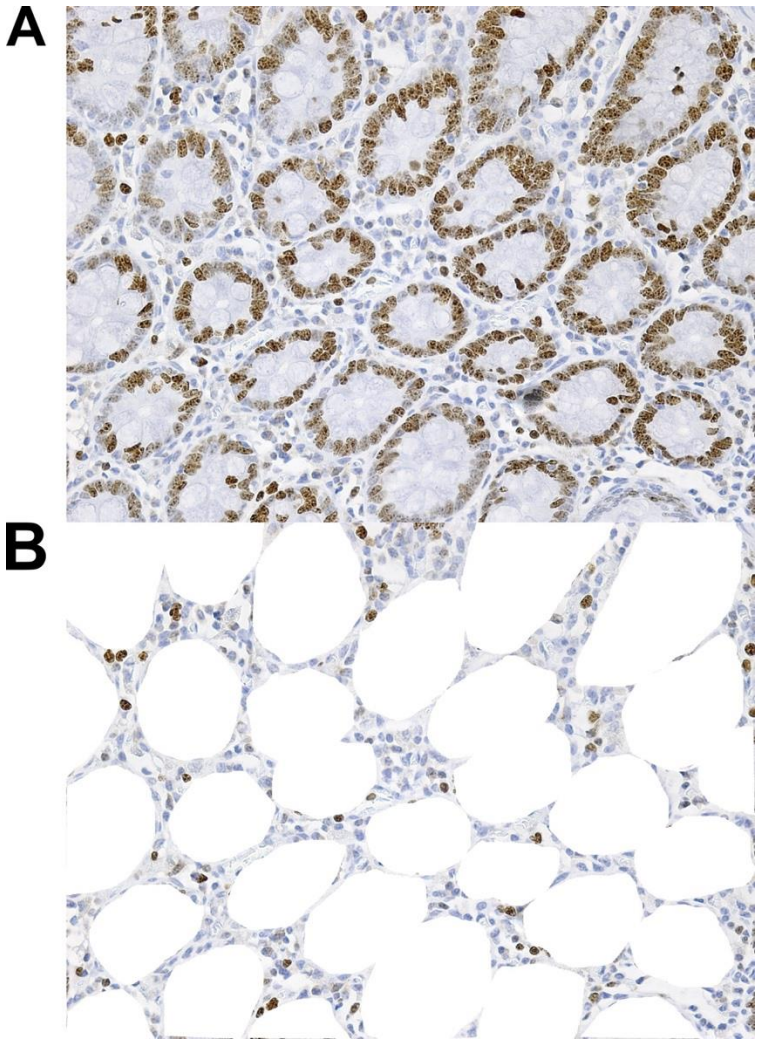

Figure 42: Exclusion of epithelium to isolate cells in the lamina propria.
To measure the Ki-67 expression by cells in the lamina propria, all the epithelial cells were manually removed from the images. By overlaying white coloration on the epithelial sections of the crypts, they were excluded from the thresholding for positive DAB signal (Figure 39). Then, a threshold could be applied to the area within the lamina propria alone and the total DAB signal measured as normal. All individual images were captured at 200X magnification using an AxioImager M1 brightfield microscope equipped with an AxioCam MRc5. All image manipulations and measurements were done with FIJI v.1.0.

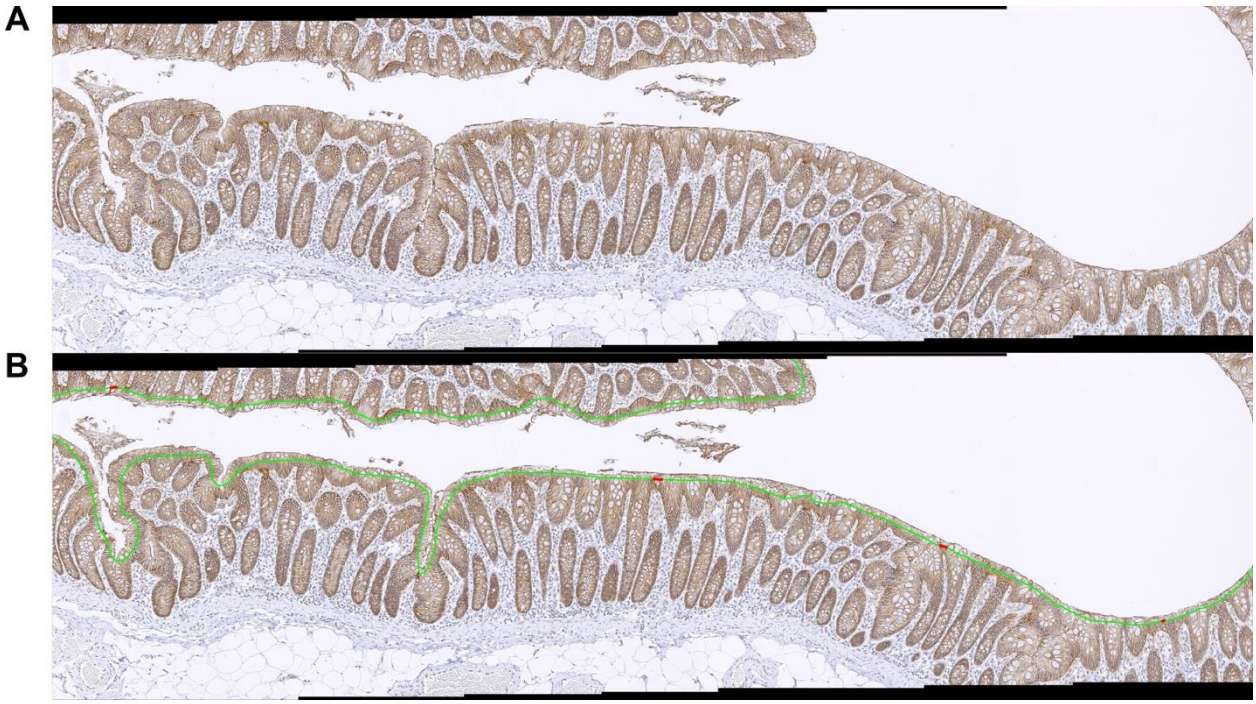

Figure 43: Measurement of intact *versus* damaged transverse colon epithelium.
To determine the relative proportion of intact colon mucosal epithelium compared to damaged epithelium, multiple contiguous images of a section of colonic mucosa were obtained. The length of the epithelium shown in the generated composite image was then traced using FIJI v.1.0; here, green lines represents intact, continuous epithelium, while red lines indicates broken, discontinuous epithelium. The lines were drawn freehand at a constant width of 10 pixels. Following tracing, the area of the line segments was measured with FIJI and these areas were used to establish a ratio representing of intact *versus* broken epithelium. All individual images were captured at 100X magnification using an AxioImager M1 brightfield microscope equipped with an AxioCam MRc5. After collection, the images were stitched together to form a composite using the Stitching plugin for FIJI version 1.0.

Appendix C : Supplemental data

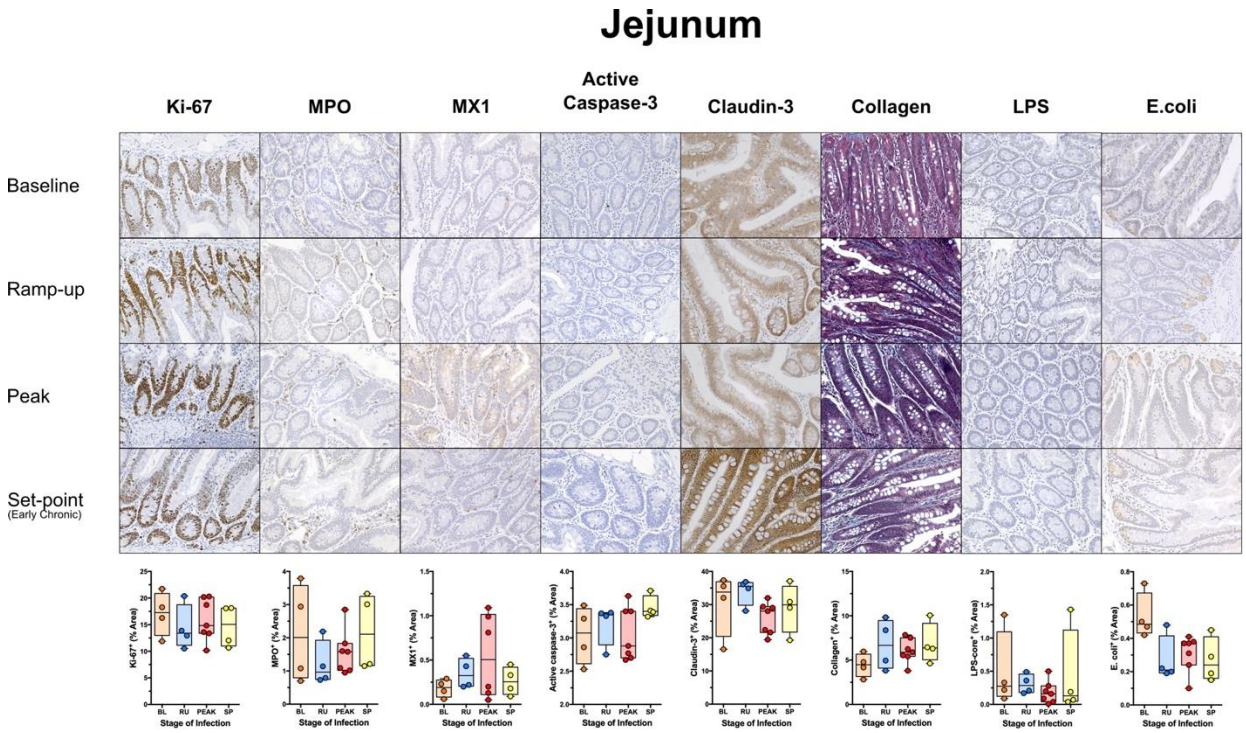

Figure 44: Immunohistochemistries (IHC) of the jejunum in SIVsab-infected African green monkeys (AGMs).

DAB-based IHC for the same array of markers that were used for the colon and axillary LN. In all the images, positive DAB signal is shown in brown, with the remaining tissue counterstained blue. Below are shown quantifications of positive signal within the image. The quantification for each animal represents the average of the values from 9-12 individual image quantifications. Villi enterocytes were included in all quantifications. The four different time groups are based on the days postinfection, with: BL (baseline, preinfection), RU (ramp-up, 4-6 dpi), PEAK (peak, 9-12dpi) and SP (set-point, 46-55 dpi). Each time group is assigned a corresponding color based on stage of viral replication: orange (baseline), blue (ramp-up), red (peak) and yellow (set-point). All quantifications were performed using FIJI version --1.0. Asterisks indicate statistical significance $p<0.05$. All images were captured at 200X magnification using an AxioImager M1 bright-field microscope equipped with an AxioCam MRc5.

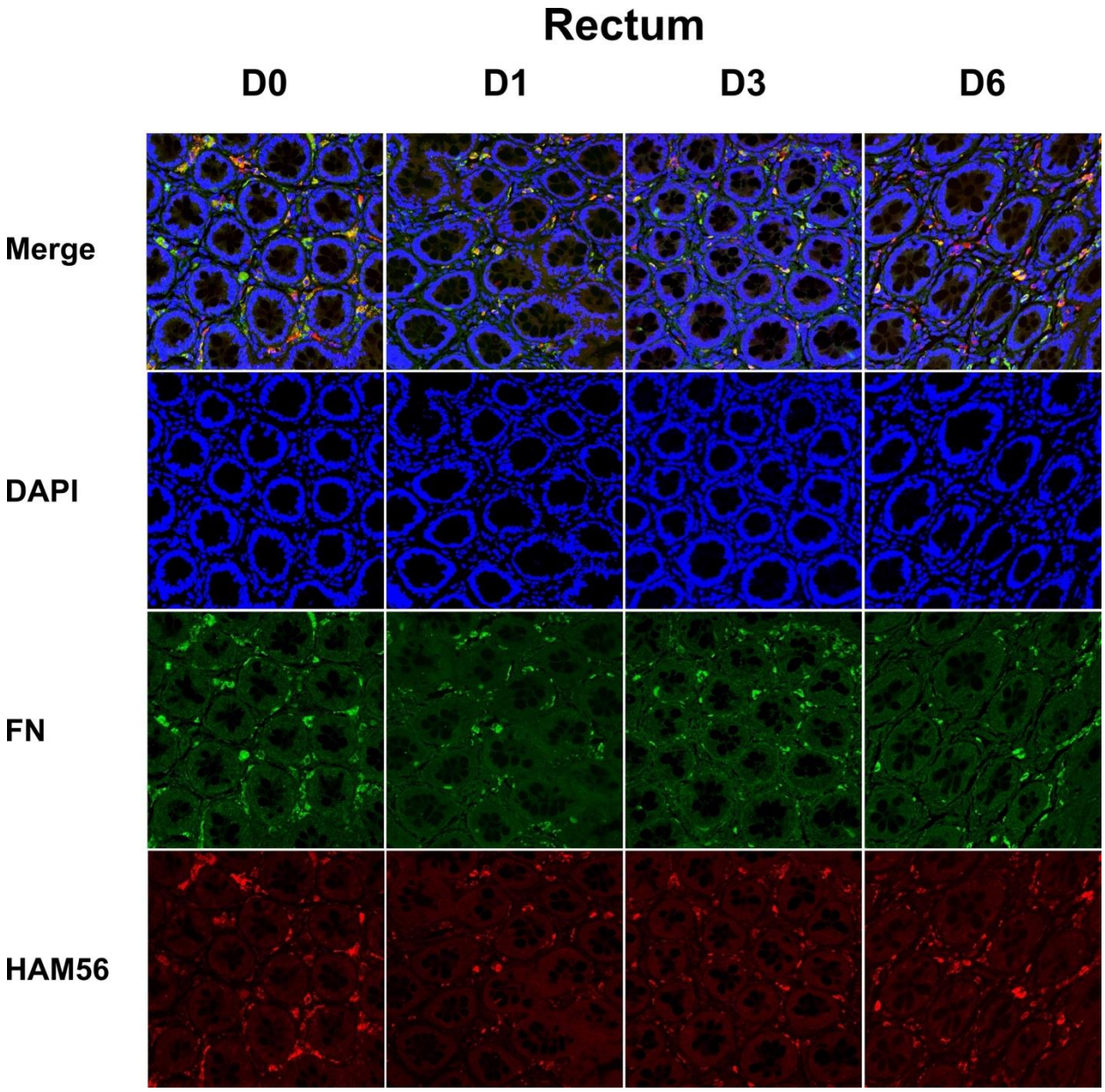

Figure 45: Immunofluorescent (IF) staining for HAM56/FN in rectum lamina propria of African green monkeys (AGMs) with separate color channels.

Rectum from AGMs were doubled stained for HAM56 (red) and FN (green), with a DAPI stain (blue) to visualize nuclei. Colocalization, if any, appears as yellow. From top to bottom are shown the composite images and then the DAPI, FN and HAM56 color channels. From left to right, representative images are shown from 0-6 days post infection. All images are at 200X magnification and were captured with an Olympus Fluoview 1000 Confocal Microscope housed at the Center for Biologic Imaging, Pittsburgh, PA. Each image represents a maximum intensity projection form a z-stack of 11-28 images at 1.78 μm per step. The resolution of every image is 0.321 μm/pixel. Maximum intensity projections were created with NIS Elements 5.20.00 (https://www.lim.cz/). All image editing was performed using FIJI version 2.0 (https://fiji.sc/). Editing includes adjustment of color channel brightness for clarity and application of the built-in FIJI Despeckle median filter to reduce noise.

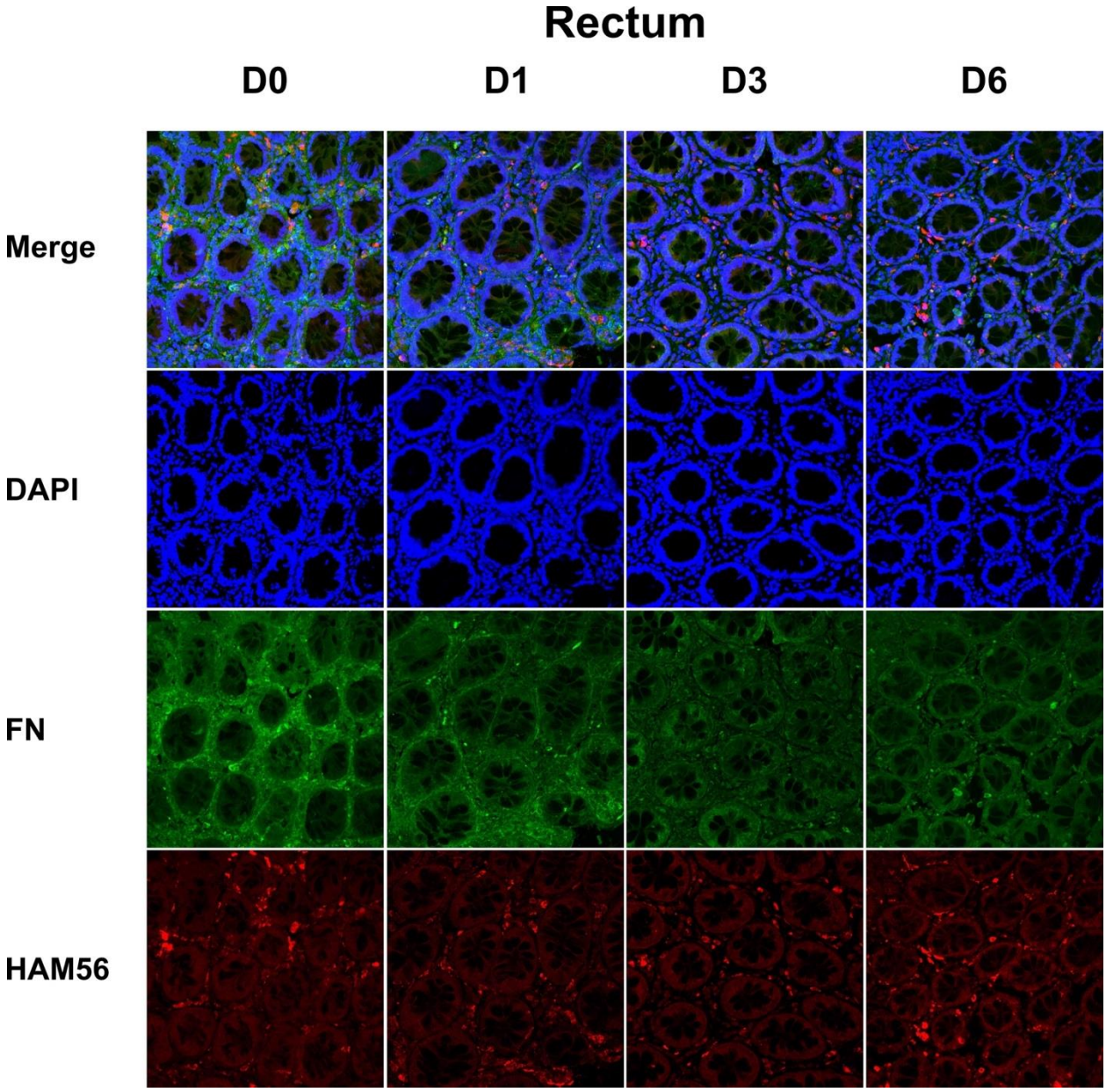

Figure 46: Immunofluorescent (IF) staining for HAM56/FN in rectum lamina propria of rhesus macaques (RMs) with separate color channels.

Rectum from RMs were doubled stained for HAM56 (red) and FN (green), with a DAPI stain (blue) to visualize nuclei. Colocalization, if any, appears as yellow. From top to bottom are shown the composite image and then the DAPI, FN and HAM56 color channels. From left to right, representative images are shown from 0-6 days post infection. All images are at 200X magnification and were captured with an Olympus Fluoview 1000 Confocal Microscope housed at the Center for Biologic Imaging, Pittsburgh, PA. Each image represents a maximum intensity projection form a z-stack of 11-28 images at 1.78 μm per step. The resolution of every image is 0.321 μm/pixel. Maximum intensity projections were created with NIS Elements 5.20.00 (https://www.lim.cz/). All image editing was performed using FIJI version 2.0 (https://fiji.sc/). Editing includes adjustment of color channel brightness for clarity and application of the built-in FIJI Despeckle median filter to reduce noise.

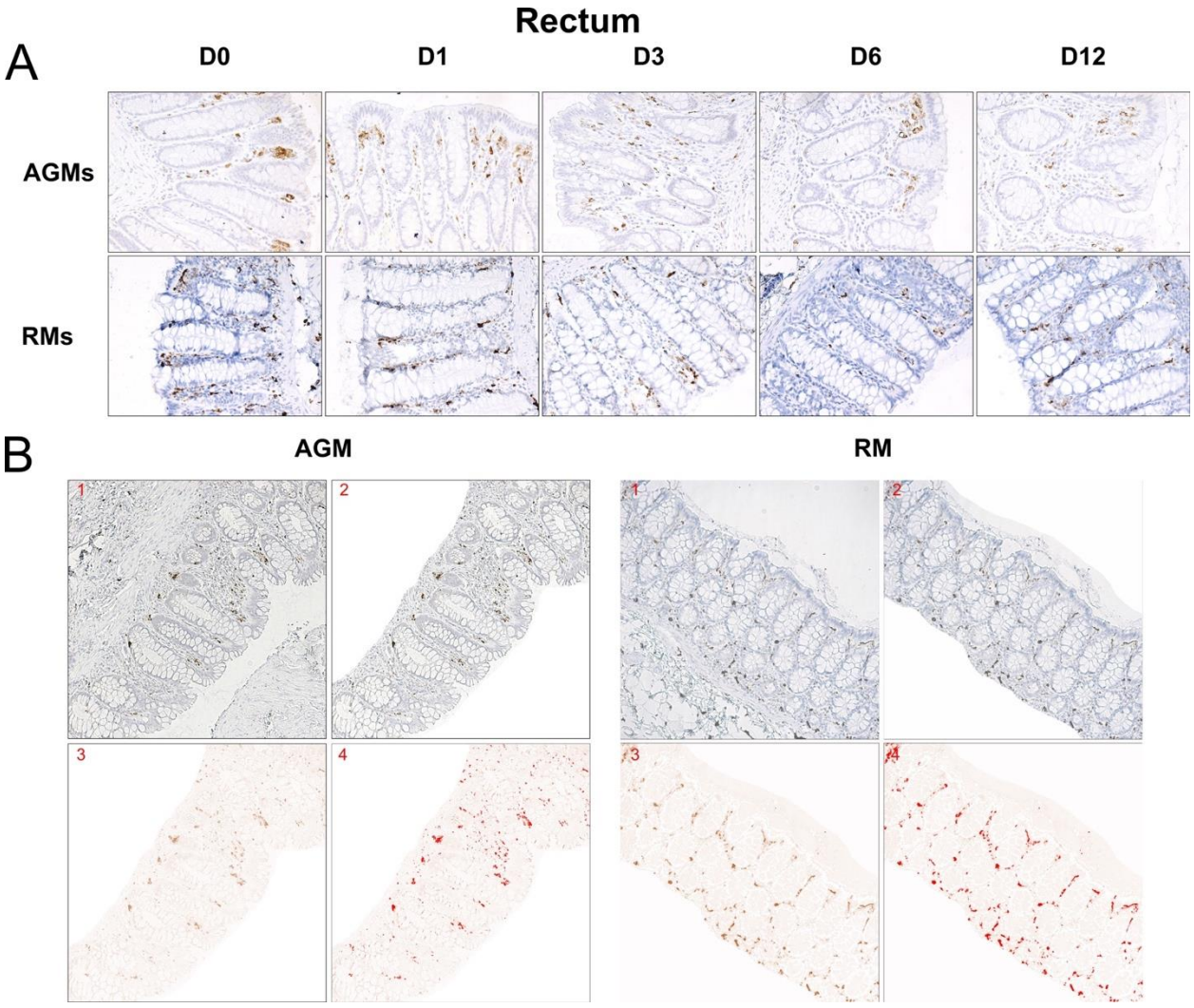

Figure 47: Example images for HAM56 immunohistochemistry and quantification.
DAB-based IHC for HAM56 in the rectums of African green monkeys (AGMs) and rhesus macaques (RMs), from 0-12 days post infection (A). In all images, positive DAB signal is shown in brown, with the remaining tissue counterstained blue. (B) The strategy to isolate the lamina propria for quantification is shown for the AGMs (left) and RMs (right). For each raw image (1), the luminal space and all surrounding tissue were manually excluded from the image (2), color deconvolution was used to separate the DAB coloration (3), and a threshold for color intensity was manually set to isolate the DAB signal (4). All image quantifications and editing were performed using FIJI version 2.0 (https://fiji.sc/). All images were captured at either 200X or 100X (for whole lamina propria) magnification using a Zeiss AxioImager M1 bright-field microscope equipped with an AxioCam MRc5.

Bibliography

1. Kraus G, Behr E, Baier M, Konig H, Kurth R. Simian immunodeficiency virus reverse transcriptase. Purification and partial characterization. *European Journal of Biochemistry* 1990;192(1):207–213.

2. Pandrea I, Sodora DL, Silvestri G, Apetrei C. Into the Wild: Simian Immunodeficiency Virus (SIV) Infection in Natural Hosts. *Trends Immunol* 2008;29(9):419–428.

3. Ansari AA, Silvestri G. *Natural hosts of SIV: implication in AIDS*. Amsterdam ; Boston: Elsevier : Academic Press; 2014:

4. Chahroudi A, Bosinger SE, Vanderford TH, Paiardini M, Silvestri G. Natural SIV Hosts: Showing AIDS the Door. *Science* 2012;335(6073):1188–1193.

5. Locatelli S, McKean KA, Clee PRS, Gonder MK. The Evolution of Resistance to Simian Immunodeficiency Virus (SIV): A Review. *Int J Primatol* 2014;35(2):349–375.

6. Pandrea I, Apetrei C. Where the Wild Things Are: Pathogenesis of SIV Infection in African Nonhuman Primate Hosts. *Current HIV/AIDS Reports* 2010;7(1):28–36.

7. VandeWoude S, Apetrei C. Going Wild: Lessons from Naturally Occurring T-Lymphotropic Lentiviruses. *Clinical Microbiology Reviews* 2006;19(4):728–762.

8. Apetrei C et al. Direct Inoculation of Simian Immunodeficiency Virus from Sooty Mangabeys in Black Mangabeys (Lophocebus aterrimus): First Evidence of AIDS in a Heterologous African Species and Different Pathologic Outcomes of Experimental Infection. *J. Virol.* 2004;78(21):11506–11518.

9. Ling B et al. Classic AIDS in a Sooty Mangabey after an 18-Year Natural Infection. *J. Virol.* 2004;78(16):8902–8908.

10. Pandrea I et al. Chronic SIV infection ultimately causes immunodeficiency in African non-human primates. *AIDS* 2001;15(18):2461–2462.

11. Pandrea I, Silvestri G, Apetrei C. AIDS in african nonhuman primate hosts of SIVs: a new paradigm of SIV infection. *Curr. HIV Res.* 2009;7(1):57–72.

12. Ma D et al. SIVagm Infection in Wild African Green Monkeys from South Africa: Epidemiology, Natural History, and Evolutionary Considerations. *PLOS Pathog* 2013;9(1):e1003011.

13. Kobayashi T et al. Characterization of red-capped mangabey tetherin: implication for the co-evolution of primates and their lentiviruses [Internet]. *Sci Rep* 2014;4. doi:10.1038/srep05529

14. Fischer W et al. Distinct Evolutionary Pressures Underlie Diversity in Simian Immunodeficiency Virus and Human Immunodeficiency Virus Lineages. *J. Virol.* 2012;86(24):13217–13231.

15. Aghokeng AF et al. Extensive survey on the prevalence and genetic diversity of SIVs in primate bushmeat provide insights into risks for potential new cross-species transmissions. *Infect Genet Evol* 2010;10(3):386–396.

16. Lowenstine LJ et al. Seroepidemiologic survey of captive Old-World primates for antibodies to human and simian retroviruses, and isolation of a lentivirus from sooty mangabeys (Cercocebus atys). *Int. J. Cancer* 1986;38(4):563–574.

17. Ohta Y et al. Isolation of simian immunodeficiency virus from african green monkeys and seroepidemiologic survey of the virus in various non-human primates. *Int. J. Cancer* 1988;41(1):115–122.

18. Apetrei C et al. Molecular Epidemiology of Simian Immunodeficiency Virus SIVsm in U.S. Primate Centers Unravels the Origin of SIVmac and SIVstm. *J. Virol.* 2005;79(14):8991–9005.

19. Bailes E et al. Hybrid Origin of SIV in Chimpanzees. *Science* 2003;300(5626):1713–1713.

20. D'arc M et al. Origin of the HIV-1 group O epidemic in western lowland gorillas. *PNAS* 2015;112(11):E1343–E1352.

21. Faria NR et al. The early spread and epidemic ignition of HIV-1 in human populations. *Science* 2014;346(6205):56–61.

22. Hirsch VM, Olmsted RA, Murphey-Corb M, Purcell RH, Johnson PR. An African primate lentivirus (SIVsm) closely related to HIV-2. *Nature* 1989;339(6223):389–392.

23. Keele BF et al. Chimpanzee Reservoirs of Pandemic and Nonpandemic HIV-1. *Science* 2006;313(5786):523–526.

24. Van Heuverswyn F et al. Human immunodeficiency viruses: SIV infection in wild gorillas. *Nature* 2006;444(7116):164–164.

25. Etienne L et al. Noninvasive Follow-Up of Simian Immunodeficiency Virus Infection in Wild-Living Nonhabituated Western Lowland Gorillas in Cameroon. *J. Virol.* 2012;86(18):9760–9772.

26. Keele BF et al. Increased mortality and AIDS-like immunopathology in wild chimpanzees infected with SIVcpz. *Nature* 2009;460(7254):515–519.

27. Worobey M et al. Island Biogeography Reveals the Deep History of SIV. *Science* 2010;329(5998):1487–1487.

28. Gifford RJ et al. A transitional endogenous lentivirus from the genome of a basal primate and implications for lentivirus evolution. *PNAS* 2008;105(51):20362–20367.

29. Compton AA, Emerman M. Convergence and Divergence in the Evolution of the APOBEC3G-Vif Interaction Reveal Ancient Origins of Simian Immunodeficiency Viruses. *PLOS Pathog* 2013;9(1):e1003135.

30. Allan JS et al. Species-specific diversity among simian immunodeficiency viruses from African green monkeys.. *J. Virol.* 1991;65(6):2816–2828.

31. Xing J et al. A mobile element-based evolutionary history of guenons (tribe Cercopithecini). *BMC Biology* 2007;5:5.

32. Souquière S et al. Wild Mandrillus sphinx Are Carriers of Two Types of Lentivirus. *J. Virol.* 2001;75(15):7086–7096.

33. Takemura T, Hayami M. Phylogenetic analysis of SIV derived from mandrill and drill. *Front. Biosci.* 2004;9:513–520.

34. Jin MJ et al. Mosaic genome structure of simian immunodeficiency virus from west African green monkeys.. *EMBO J* 1994;13(12):2935–2947.

35. Liégeois F et al. Full-Length Genome Analyses of Two New Simian Immunodeficiency Virus (SIV) Strains from Mustached Monkeys (C. Cephus) in Gabon Illustrate a Complex Evolutionary History among the SIVmus/mon/gsn Lineage. *Viruses* 2014;6(7):2880–2898.

36. Rudicell RS et al. Impact of Simian Immunodeficiency Virus Infection on Chimpanzee Population Dynamics. *PLOS Pathog* 2010;6(9):e1001116.

37. Etienne L et al. Characterization of a new simian immunodeficiency virus strain in a naturally infected Pan troglodytes troglodytes chimpanzee with AIDS related symptoms. *Retrovirology* 2011;8:4.

38. Pandrea I et al. Paucity of CD4+CCR5+ T cells is a typical feature of natural SIV hosts. *Blood* 2007;109(3):1069–1076.

39. Sharp PM, Hahn BH. Origins of HIV and the AIDS Pandemic. *Cold Spring Harbor Perspectives in Medicine* 2011;1(1):a006841–a006841.

40. Plantier J-C et al. A new human immunodeficiency virus derived from gorillas. *Nat Med* 2009;15(8):871–872.

41. Takehisa J et al. Origin and Biology of Simian Immunodeficiency Virus in Wild-Living Western Gorillas. *J. Virol.* 2009;83(4):1635–1648.

42. Ayouba A et al. Evidence for continuing cross-species transmission of SIVsmm to humans: characterization of a new HIV-2 lineage in rural Côte d'Ivoire [Internet]. *AIDS* 2013;27(15). doi:10.1097/01.aids.0000432443.22684.50

43. Denham W. History of green monkeys in West Indies: migration from Africa. *J BHMS* 1981;36:210–29.

44. Daniel MD et al. Prevalence of antibodies to 3 retroviruses in a captive colony of macaque monkeys. *Int. J. Cancer* 1988;41(4):601–608.

45. Hendry RM et al. Antibodies to simian immunodeficiency virus in African green monkeys in Africa in 1957-62. *Lancet* 1986;2(8504):455.

46. Pandrea I et al. Simian Immunodeficiency Virus SIVagm.sab Infection of Caribbean African Green Monkeys: a New Model for the Study of SIV Pathogenesis in Natural Hosts. *J. Virol.* 2006;80(10):4858–4867.

47. Locatelli S, Peeters M. Cross-species transmission of simian retroviruses: how and why they could lead to the emergence of new diseases in the human population. *AIDS* 2012;26(6):659–673.

48. Leendertz SAJ et al. High Prevalence, Coinfection Rate, and Genetic Diversity of Retroviruses in Wild Red Colobus Monkeys (Piliocolobus badius badius) in Taï National Park, Côte d'Ivoire. *J. Virol.* 2010;84(15):7427–7436.

49. Bibollet-Ruche F et al. New Simian Immunodeficiency Virus Infecting De Brazza's Monkeys (Cercopithecus neglectus): Evidence for a Cercopithecus Monkey Virus Clade. *J Virol* 2004;78(14):7748–7762.

50. Estaquier J et al. Prevalence and transmission of simian immunodeficiency virus and simian T-cell leukemia virus in a semi-free-range breeding colony of mandrills in Gabon. *AIDS* 1991;5(11):1385–1386.

51. Fouchet D et al. Natural simian immunodeficiency virus transmission in mandrills: a family affair?. *Proceedings of the Royal Society of London B: Biological Sciences* 2012;279(1742):3426–3435.

52. Ma D et al. Factors Associated with Siman Immunodeficiency Virus Transmission in a Natural African Nonhuman Primate Host in the Wild. *J. Virol.* 2014;88(10):5687–5705.

53. Otsyula MG et al. Apparent lack of vertical transmission of simian immunodeficiency virus (SIV) in naturally infected African green monkeys, Cercopithecus aethiops. *Ann Trop Med Parasitol* 1995;89(5):573–576.

54. Rudicell RS et al. High Prevalence of Simian Immunodeficiency Virus Infection in a Community of Savanna Chimpanzees. *J. Virol.* 2011;85(19):9918–9928.

55. Santiago ML et al. Simian Immunodeficiency Virus Infection in Free-Ranging Sooty Mangabeys (Cercocebus atys atys) from the Taï Forest, Côte d'Ivoire: Implications for the Origin of Epidemic Human Immunodeficiency Virus Type 2. *J. Virol.* 2005;79(19):12515–12527.

56. Phillips-Conroy JE, Jolly CJ, Petros B, Allan JS, Desrosiers RC. Sexual transmission of SIVagm in wild grivet monkeys. *J. Med. Primatol.* 1994;23(1):1–7.

57. Cooper R, Feistner A, Evans S, Tsujimoto H, Hayami M. A lack of evidence of sexual transmission of a simian immunodeficiency agent in a semifree-ranging group of mandrills. *AIDS* 1989;3(11):764.

58. Baggaley RF, White RG, Boily M-C. Systematic review of orogenital HIV-1 transmission probabilities. *Int J Epidemiol* 2008;37(6):1255–1265.

59. Ruprecht RM et al. Oral Transmission of Primate Lentiviruses. *J Infect Dis.* 1999;179(Supplement 3):S408–S412.

60. Chenine AL et al. Relative Transmissibility of an R5 Clade C Simian- Human Immunodeficiency Virus Across Different Mucosae in Macaques Parallels the Relative Risks of Sexual HIV-1 Transmission in Humans via Different Routes. *J Infect Dis.* 2010;201(8):1155–1163.

61. Haase AT. Early Events in Sexual Transmission of HIV and SIV and Opportunities for Interventions. *Annual Review of Medicine* 2011;62(1):127–139.

62. Rey-Cuillé M-A et al. Simian Immunodeficiency Virus Replicates to High Levels in Sooty Mangabeys without Inducing Disease. *J. Virol.* 1998;72(5):3872–3886.

63. Corbet S et al. env Sequences of Simian Immunodeficiency Viruses from Chimpanzees in Cameroon Are Strongly Related to Those of Human Immunodeficiency Virus Group N from the Same Geographic Area. *J. Virol.* 2000;74(1):529–534.

64. Lowenstine LJ et al. Evidence for a lentiviral etiology in an epizootic of immune deficiency and lymphoma in stump-tailed macaques (Macaca arctoides). *J. Med. Primatol.* 1992;21(1):1–14.

65. Nerrienet E et al. Phylogenetic analysis of SIV and STLV type I in mandrills (Mandrillus sphinx): indications that intracolony transmissions are predominantly the result of male-to-male aggressive contacts. *AIDS Res. Hum. Retroviruses* 1998;14(9):785–796.

66. Aldrovandi GM, Kuhn L. What babies and breasts can teach us about natural protection from HIV infection. *J Infect Dis* 2010;202(S3):S366–S370.

67. Amedee AM, Rychert J, Lacour N, Fresh L, Ratterree M. Viral and immunological factors associated with breast milk transmission of SIV in rhesus macaques. *Retrovirology* 2004;1:17.

68. Ogino T et al. Increased Th17-Inducing Activity of CD14+ CD163low Myeloid Cells in Intestinal Lamina Propria of Patients With Crohn's Disease. *Gastroenterology* 2013;145(6):1380-1391.e1.

69. Fultz PN, Gordon TP, Anderson DC, McClure HM. Prevalence of natural infection with simian immunodeficiency virus and simian T-cell leukemia virus type I in a breeding colony of sooty mangabey monkeys. *AIDS* 1990;4(7):619–625.

70. Pandrea I et al. Paucity of CD4+ CCR5+ T Cells May Prevent Transmission of Simian Immunodeficiency Virus in Natural Nonhuman Primate Hosts by Breast-Feeding. *Journal of Virology* 2008;82(11):5501–5509.

71. Chahroudi A et al. Mother-to-Infant Transmission of Simian Immunodeficiency Virus Is Rare in Sooty Mangabeys and Is Associated with Low Viremia ▿ . *J Virol* 2011;85(12):5757–5763.

72. Haase AT. Targeting early infection to prevent HIV-1 mucosal transmission. *Nature* 2010;464(7286):217–223.

73. Cohen MS, Shaw GM, McMichael AJ, Haynes BF. Acute HIV-1 infection. *New England Journal of Medicine* 2011;364(20):1943–1954.

74. Ma Z-M, Dutra J, Fritts L, Miller CJ. Lymphatic Dissemination of Simian Immunodeficiency Virus after Penile Inoculation. *J. Virol.* 2016;90(8):4093–4104.

75. Stieh DJ et al. Vaginal Challenge with an SIV-Based Dual Reporter System Reveals That Infection Can Occur throughout the Upper and Lower Female Reproductive Tract. *PLOS Pathog* 2014;10(10):e1004440.

76. Li Q et al. Peak SIV replication in resting memory CD4+ T cells depletes gut lamina propria CD4+ T cells. *Nature* 2005;434(7037):1148–1152.

77. Zhang Z-Q et al. Roles of substrate availability and infection of resting and activated CD4+ T cells in transmission and acute simian immunodeficiency virus infection. *PNAS* 2004;101(15):5640–5645.

78. Pandrea I et al. Mucosal Simian Immunodeficiency Virus Transmission in African Green Monkeys: Susceptibility to Infection Is Proportional to Target Cell Availability at Mucosal Sites. *J. Virol.* 2012;86(8):4158–4168.

79. Chenine A-L et al. Older Rhesus Macaque Infants Are More Susceptible to Oral Infection with Simian-Human Immunodeficiency Virus 89.6P than Neonates. *J. Virol.* 2005;79(2):1333–1336.

80. Keele BF et al. Identification and characterization of transmitted and early founder virus envelopes in primary HIV-1 infection. *Proceedings of the National Academy of Sciences* 2008;105(21):7552–7557.

81. Keele BF et al. Low-dose rectal inoculation of rhesus macaques by SIVsmE660 or SIVmac251 recapitulates human mucosal infection by HIV-1. *J Exp Med* 2009;206(5):1117–1134.

82. Souquière S et al. Simian immunodeficiency virus types 1 and 2 (SIV mnd 1 and 2) have different pathogenic potentials in rhesus macaques upon experimental cross-species transmission. *Journal of General Virology* 2009;90(2):488–499.

83. Diop OM et al. High Levels of Viral Replication during Primary Simian Immunodeficiency Virus SIVagm Infection Are Rapidly and Strongly Controlled in African Green Monkeys. *J. Virol.* 2000;74(16):7538–7547.

84. Gordon SN et al. Severe Depletion of Mucosal CD4+ T Cells in AIDS-Free Simian Immunodeficiency Virus-Infected Sooty Mangabeys. *J Immunol* 2007;179(5):3026–3034.

85. Gueye A et al. Viral load in tissues during the early and chronic phase of non-pathogenic SIVagm infection. *Journal of Medical Primatology* 2004;33(2):83–97.

86. Onanga R et al. High Levels of Viral Replication Contrast with Only Transient Changes in CD4+ and CD8+ Cell Numbers during the Early Phase of Experimental Infection with Simian Immunodeficiency Virus SIVmnd-1 in Mandrillus sphinx. *J. Virol.* 2002;76(20):10256–10263.

87. Onanga R et al. Primary Simian Immunodeficiency Virus SIVmnd-2 Infection in Mandrills (Mandrillus sphinx). *J. Virol.* 2006;80(7):3301–3309.

88. Pandrea I et al. Simian Immunodeficiency Virus SIVagm Dynamics in African Green Monkeys. *Journal of Virology* 2008;82(7):3713–3724.

89. Pandrea IV et al. Acute loss of intestinal CD4+ T cells is not predictive of simian immunodeficiency virus virulence. *The Journal of Immunology* 2007;179(5):3035–3046.

90. Silvestri G et al. Divergent Host Responses during Primary Simian Immunodeficiency Virus SIVsm Infection of Natural Sooty Mangabey and Nonnatural Rhesus Macaque Hosts. *J. Virol.* 2005;79(7):4043–4054.

91. Pandrea I et al. Impact of Viral Factors on Very Early In Vivo Replication Profiles in Simian Immunodeficiency Virus SIVagm-Infected African Green Monkeys. *Journal of Virology* 2005;79(10):6249–6259.

92. Goldstein S et al. Comparison of Simian Immunodeficiency Virus SIVagmVer Replication and CD4+ T-Cell Dynamics in Vervet and Sabaeus African Green Monkeys. *J. Virol.* 2006;80(10):4868–4877.

93. Brenchley JM et al. Differential infection patterns of CD4+ T cells and lymphoid tissue viral burden distinguish progressive and nonprogressive lentiviral infections. *Blood* 2012;120(20):4172–4181.

94. Wilks AB et al. High Cell-Free Virus Load and Robust Autologous Humoral Immune Responses in Breast Milk of Simian Immunodeficiency Virus-Infected African Green Monkeys. *J. Virol.* 2011;85(18):9517–9526.

95. Kouyos RD, Gordon SN, Staprans SI, Silvestri G, Regoes RR. Similar Impact of CD8+ T Cell Responses on Early Virus Dynamics during SIV Infections of Rhesus Macaques and Sooty Mangabeys. *PLOS Comput Biol* 2010;6(8):e1000901.

96. Apetrei C et al. Virus Subtype-Specific Features of Natural Simian Immunodeficiency Virus SIVsmm Infection in Sooty Mangabeys. *J. Virol.* 2007;81(15):7913–7923.

97. Pandrea I et al. High levels of SIVmnd-1 replication in chronically infected Mandrillus sphinx. *Virology* 2003;317(1):119–127.

98. Goldstein S et al. Wide Range of Viral Load in Healthy African Green Monkeys Naturally Infected with Simian Immunodeficiency Virus. *J. Virol.* 2000;74(24):11744–11753.

99. Apetrei C et al. Immunovirological Analyses of Chronically Simian Immunodeficiency Virus SIVmnd-1- and SIVmnd-2-Infected Mandrills (Mandrillus sphinx). *J. Virol.* 2011;85(24):13077–13087.

100. Mir KD et al. Reduced Simian Immunodeficiency Virus Replication in Macrophages of Sooty Mangabeys Is Associated with Increased Expression of Host Restriction Factors. *J. Virol.* 2015;89(20):10136–10144.

101. Milush JM et al. Lack of clinical AIDS in SIV-infected sooty mangabeys with significant CD4+ T cell loss is associated with double-negative T cells. *J Clin Invest* 2011;121(3):1102–1110.

102. Schmitz JE et al. Memory CD4+ T Lymphocytes in the Gastrointestinal Tract Are a Major Source of Cell-Associated Simian Immunodeficiency Virus in Chronic Nonpathogenic Infection of African Green Monkeys. *J. Virol.* 2012;86(20):11380–11385.

103. Mir KD et al. Simian Immunodeficiency Virus-Induced Alterations in Monocyte Production of Tumor Necrosis Factor Alpha Contribute to Reduced Immune Activation in Sooty Mangabeys. *J. Virol.* 2012;86(14):7605–7615.

104. Vanderford TH et al. Treatment of SIV-infected sooty mangabeys with a type-I IFN agonist results in decreased virus replication without inducing hyperimmune activation. *Blood* 2012;119(24):5750–5757.

105. Pandrea I et al. Simian immunodeficiency viruses replication dynamics in African non-human primate hosts: common patterns and species-specific differences. *Journal of Medical Primatology* 2006;35(4–5):194–201.

106. Fiebig EW et al. Dynamics of HIV viremia and antibody seroconversion in plasma donors: implications for diagnosis and staging of primary HIV infection. *Aids* 2003;17(13):1871–1879.

107. Gordon SN et al. Short-Lived Infected Cells Support Virus Replication in Sooty Mangabeys Naturally Infected with Simian Immunodeficiency Virus: Implications for AIDS Pathogenesis. *J. Virol.* 2008;82(7):3725–3735.

108. Watkins DI, Burton DR, Kallas EG, Moore JP, Koff WC. Nonhuman primate models and the failure of the Merck HIV-1 vaccine in humans. *Nat Med* 2008;14(6):617–621.

109. Chen Z, Zhou P, Ho DD, Landau NR, Marx PA. Genetically divergent strains of simian immunodeficiency virus use CCR5 as a coreceptor for entry.. *J. Virol.* 1997;71(4):2705–2714.

110. Zhang Y et al. Use of Inhibitors To Evaluate Coreceptor Usage by Simian and Simian/Human Immunodeficiency Viruses and Human Immunodeficiency Virus Type 2 in Primary Cells. *J. Virol.* 2000;74(15):6893–6910.

111. Moore JP, Kitchen SG, Pugach P, Zack JA. The CCR5 and CXCR4 Coreceptors—Central to Understanding the Transmission and Pathogenesis of Human Immunodeficiency Virus Type 1 Infection. *AIDS Research and Human Retroviruses* 2004;20(1):111–126.

112. Gautam R et al. In vitro Characterization of Primary SIVsmm Isolates Belonging to Different Lineages. In Vitro growth on Rhesus Macaque Cells is Not Predictive for In Vivo Replication in Rhesus Macaques. *Virology* 2007;362(2):257–270.

113. Chen Z, Gettie A, Ho DD, Marx PA. Primary SIVsm Isolates Use the CCR5 Coreceptor from Sooty Mangabeys Naturally Infected in West Africa: A Comparison of Coreceptor Usage of Primary SIVsm, HIV-2, and SIVmac. *Virology* 1998;246(1):113–124.

114. Veazey RS et al. Identifying the target cell in primary simian immunodeficiency virus (SIV) infection: highly activated memory CD4+ T cells are rapidly eliminated in early SIV infection in vivo. *Journal of virology* 2000;74(1):57–64.

115. Owen SM et al. Simian Immunodeficiency Viruses of Diverse Origin Can Use CXCR4 as a Coreceptor for Entry into Human Cells. *J. Virol.* 2000;74(12):5702–5708.

116. Schols D, De Clercq E. The simian immunodeficiency virus mnd(GB-1) strain uses CXCR4, not CCR5, as coreceptor for entry in human cells.. *Journal of General Virology* 1998;79(9):2203–2205.

117. Elliott STC et al. Dualtropic CXCR6/CCR5 Simian Immunodeficiency Virus (SIV) Infection of Sooty Mangabey Primary Lymphocytes: Distinct Coreceptor Use in Natural versus Pathogenic Hosts of SIV. *J. Virol.* 2015;89(18):9252–9261.

118. Riddick NE et al. Simian Immunodeficiency Virus SIVagm Efficiently Utilizes Non-CCR5 Entry Pathways in African Green Monkey Lymphocytes: Potential Role for GPR15 and CXCR6 as Viral Coreceptors. *J. Virol.* 2016;90(5):2316–2331.

119. Islam S et al. CCR6 Functions as a New Coreceptor for Limited Primary Human and Simian Immunodeficiency Viruses [Internet]. *PLoS One* 2013;8(8). doi:10.1371/journal.pone.0073116

120. Islam S et al. CKR-L3, a deletion version CCR6-isoform shows coreceptor-activity for limited human and simian immunodeficiency viruses. *BMC Infect Dis* 2014;14:354.

121. Samson M et al. Resistance to HIV-1 infection in Caucasian individuals bearing mutant alleles of the CCR-5 chemokine receptor gene. *Nature* 1996;382(6593):722–725.

122. Chen Z et al. Natural Infection of a Homozygous Δ24 CCR5 Red-capped Mangabey with an R2b-Tropic Simian Immunodeficiency Virus. *J Exp Med* 1998;188(11):2057–2065.

123. Gautam R et al. Simian Immunodeficiency Virus SIVrcm, a Unique CCR2-Tropic Virus, Selectively Depletes Memory CD4+ T Cells in Pigtailed Macaques through Expanded Coreceptor Usage In Vivo. *J Virol* 2009;83(16):7894–7908.

124. Broussard SR et al. Simian Immunodeficiency Virus Replicates to High Levels in Naturally Infected African Green Monkeys without Inducing Immunologic or Neurologic Disease. *J. Virol.* 2001;75(5):2262–2275.

125. Diop OM et al. High Levels of Viral Replication during Primary Simian Immunodeficiency Virus SIVagm Infection Are Rapidly and Strongly Controlled in African Green Monkeys. *J. Virol.* 2000;74(16):7538–7547.

126. Silvestri G et al. Nonpathogenic SIV Infection of Sooty Mangabeys Is Characterized by Limited Bystander Immunopathology Despite Chronic High-Level Viremia. *Immunity* 2003;18(3):441–452.

127. Kornfeld C et al. Antiinflammatory profiles during primary SIV infection in African green monkeys are associated with protection against AIDS. *Journal of Clinical Investigation* 2005;115(4):1082–1091.

128. Rodríguez B, Sethi AK, Cheruvu VK, et al. PRedictive value of plasma hiv rna level on rate of cd4 t-cell decline in untreated hiv infection. *JAMA* 2006;296(12):1498–1506.

129. Mattapallil JJ et al. Massive infection and loss of memory CD4+ T cells in multiple tissues during acute SIV infection. *Nature* 2005;434(7037):1093–1097.

130. Mehandru S et al. Primary HIV-1 Infection Is Associated with Preferential Depletion of CD4+ T Lymphocytes from Effector Sites in the Gastrointestinal Tract. *J Exp Med* 2004;200(6):761–770.

131. Mehandru S et al. Mechanisms of Gastrointestinal CD4+ T-Cell Depletion during Acute and Early Human Immunodeficiency Virus Type 1 Infection. *J. Virol.* 2007;81(2):599–612.

132. Veazey RS et al. Gastrointestinal Tract as a Major Site of CD4+ T Cell Depletion and Viral Replication in SIV Infection. *Science* 1998;280(5362):427–431.

133. Milush JM et al. Virally Induced CD4+ T Cell Depletion Is Not Sufficient to Induce AIDS in a Natural Host. *J Immunol* 2007;179(5):3047–3056.

134. Sumpter B et al. Correlates of Preserved CD4+ T Cell Homeostasis during Natural, Nonpathogenic Simian Immunodeficiency Virus Infection of Sooty Mangabeys: Implications for AIDS Pathogenesis. *J Immunol* 2007;178(3):1680–1691.

135. Beaumier CM et al. CD4 downregulation by memory CD4+ T cells in vivo renders African green monkeys resistant to progressive SIVagm infection. *Nat Med* 2009;15(8):879–885.

136. Vinton C et al. CD4-Like Immunological Function by CD4− T Cells in Multiple Natural Hosts of Simian Immunodeficiency Virus. *J. Virol.* 2011;85(17):8702–8708.

137. Kaiser P et al. Productive Human Immunodeficiency Virus Type 1 Infection in Peripheral Blood Predominantly Takes Place in CD4/CD8 Double-Negative T Lymphocytes. *J. Virol.* 2007;81(18):9693–9706.

138. Wetzel KS et al. CXCR6-Mediated Simian Immunodeficiency Virus SIVagmSab Entry into Sabaeus African Green Monkey Lymphocytes Implicates Widespread Use of Non-CCR5 Pathways in Natural Host Infections [Internet]. *J Virol* 2017;91(4). doi:10.1128/JVI.01626-16

139. Perelson AS. Modelling viral and immune system dynamics. *Nat Rev Immunol* 2002;2(1):28–36.

140. Klatt NR et al. Availability of activated CD4+ T cells dictates the level of viremia in naturally SIV-infected sooty mangabeys. *J Clin Invest* 2008;118(6):2039–2049.

141. Avalos CR et al. Quantitation of Productively Infected Monocytes and Macrophages of SIV-Infected Macaques. *J. Virol.* 2016;JVI.00290-16.

142. Bernard-Stoecklin S et al. Semen CD4+ T Cells and Macrophages Are Productively Infected at All Stages of SIV infection in Macaques. *PLoS Pathogens* 2013;9(12):e1003810.

143. Li Y et al. SIV Infection of Lung Macrophages. *PLoS ONE* 2015;10(5):e0125500.

144. Li SL et al. Monocyte/macrophage giant cell disease in SIV-infected cynomolgus monkeys. *Research in Virology* 1991;142(2):173–182.

145. Brenchley JM et al. CD4+ T Cell Depletion during all Stages of HIV Disease Occurs Predominantly in the Gastrointestinal Tract. *J Exp Med* 2004;200(6):749–759.

146. Smit-McBride Z, Mattapallil JJ, McChesney M, Ferrick D, Dandekar S. Gastrointestinal T Lymphocytes Retain High Potential for Cytokine Responses but Have Severe CD4+ T-Cell Depletion at All Stages of Simian Immunodeficiency Virus Infection Compared to Peripheral Lymphocytes. *J. Virol.* 1998;72(8):6646–6656.

147. Sodora DL et al. Toward an AIDS vaccine: lessons from natural simian immunodeficiency virus infections of African nonhuman primate hosts. *Nature Medicine* 2009;15(8):861–865.

148. McGary CS et al. Increased Stability and Limited Proliferation of CD4+ Central Memory T Cells Differentiate Nonprogressive Simian Immunodeficiency Virus (SIV) Infection of Sooty Mangabeys from Progressive SIV Infection of Rhesus Macaques. *J. Virol.* 2014;88(8):4533–4542.

149. Greenwood EJD et al. Loss of memory CD4+ T-cells in semi-wild mandrills (Mandrillus sphinx) naturally infected with species-specific simian immunodeficiency virus SIVmnd-1. *Journal of General Virology* 2014;95(1):201–212.

150. Cartwright EK et al. Divergent CD4+ T Memory Stem Cell Dynamics in Pathogenic and Nonpathogenic Simian Immunodeficiency Virus Infections. *J Immunol* 2014;192(10):4666–4673.

151. Chahroudi A, Silvestri G, Lichterfeld M. T memory stem cells and HIV: a long-term relationship. *Curr HIV/AIDS Rep* 2015;12(1):33–40.

152. Ploquin MJ-Y et al. Distinct expression profiles of TGF-β1 signaling mediators in pathogenic SIVmac and non-pathogenic SIVagm infections. *Retrovirology* 2006;3:37.

153. Estes JD et al. Early Resolution of Acute Immune Activation and Induction of PD-1 in SIV-Infected Sooty Mangabeys Distinguishes Nonpathogenic from Pathogenic Infection in Rhesus Macaques. *J Immunol* 2008;180(10):6798–6807.

154. Bosinger SE et al. Global genomic analysis reveals rapid control of a robust innate response in SIV-infected sooty mangabeys. *J Clin Invest* 2009;119(12):3556–3572.

155. Bosinger SE, Sodora DL, Silvestri G. Generalized immune activation and innate immune responses in SIV infection. *Curr Opin HIV AIDS* 2011;6(5):411–418.

156. Jacquelin B et al. Nonpathogenic SIV infection of African green monkeys induces a strong but rapidly controlled type I IFN response [Internet]. *Journal of Clinical Investigation* [published online ahead of print: November 23, 2009]; doi:10.1172/JCI40093

157. Harris LD et al. Downregulation of Robust Acute Type I Interferon Responses Distinguishes Nonpathogenic Simian Immunodeficiency Virus (SIV) Infection of Natural Hosts from Pathogenic SIV Infection of Rhesus Macaques. *Journal of Virology* 2010;84(15):7886–7891.

158. Muthukumar A et al. Timely triggering of homeostatic mechanisms involved in the regulation of T-cell levels in SIVsm-infected sooty mangabeys. *Blood* 2005;106(12):3839–3845.

159. Chakrabarti LA et al. Normal T-Cell Turnover in Sooty Mangabeys Harboring Active Simian Immunodeficiency Virus Infection. *J. Virol.* 2000;74(3):1209–1223.

160. Kaur A et al. Dynamics of T- and B-Lymphocyte Turnover in a Natural Host of Simian Immunodeficiency Virus. *J. Virol.* 2008;82(3):1084–1093.

161. Grossman Z, Meier-Schellersheim M, Paul WE, Picker LJ. Pathogenesis of HIV infection: what the virus spares is as important as what it destroys. *Nat Med* 2006;12(3):289–295.

162. Picker LJ et al. Insufficient Production and Tissue Delivery of CD4+Memory T Cells in Rapidly Progressive Simian Immunodeficiency Virus Infection. *J Exp Med* 2004;200(10):1299–1314.

163. Lederer S et al. Transcriptional Profiling in Pathogenic and Non-Pathogenic SIV Infections Reveals Significant Distinctions in Kinetics and Tissue Compartmentalization. *PLOS Pathog* 2009;5(2):e1000296.

164. Jacquelin B et al. Innate Immune Responses and Rapid Control of Inflammation in African Green Monkeys Treated or Not with Interferon-Alpha during Primary SIVagm Infection. *PLOS Pathog* 2014;10(7):e1004241.

165. Reina J-ML et al. Gag p27-Specific B- and T-Cell Responses in Simian Immunodeficiency Virus SIVagm-Infected African Green Monkeys. *J. Virol.* 2009;83(6):2770–2777.

166. Schmitz JE et al. Inhibition of Adaptive Immune Responses Leads to a Fatal Clinical Outcome in SIV-Infected Pigtailed Macaques but Not Vervet African Green Monkeys. *PLOS Pathog* 2009;5(12):e1000691.

167. Zahn RC et al. Simian Immunodeficiency Virus (SIV)-Specific CD8+ T-Cell Responses in Vervet African Green Monkeys Chronically Infected with SIVagm. *Journal of Virology* 2008;82(23):11577–11588.

168. Zahn RC et al. Suppression of adaptive immune responses during primary SIV infection of sabaeus African green monkeys delays partial containment of viremia but does not induce disease. *Blood* 2010;115(15):3070–3078.

169. Jin X et al. Dramatic Rise in Plasma Viremia after CD8+ T Cell Depletion in Simian Immunodeficiency Virus–infected Macaques. *J Exp Med* 1999;189(6):991–998.

170. Schmitz JE et al. Control of Viremia in Simian Immunodeficiency Virus Infection by CD8+ Lymphocytes. *Science* 1999;283(5403):857–860.

171. Barry AP et al. Depletion of CD8+ Cells in Sooty Mangabey Monkeys Naturally Infected with Simian Immunodeficiency Virus Reveals Limited Role for Immune Control of Virus Replication in a Natural Host Species. *J Immunol* 2007;178(12):8002–8012.

172. Wang Z, Metcalf B, Ribeiro RM, McClure H, Kaur A. Th-1-Type Cytotoxic CD8+ T-Lymphocyte Responses to Simian Immunodeficiency Virus (SIV) Are a Consistent Feature of Natural SIV Infection in Sooty Mangabeys. *J. Virol.* 2006;80(6):2771–2783.

173. Kaur A et al. Emergence of cytotoxic T lymphocyte escape mutations in nonpathogenic simian immunodeficiency virus infection. *Eur. J. Immunol.* 2001;31(11):3207–3217.

174. Gaufin T et al. Experimental depletion of CD8+ cells in acutely SIVagm-Infected African Green Monkeys results in increased viral replication. *Retrovirology* 2010;7(1):42.

175. Okoye A et al. Profound CD4+/CCR5+ T cell expansion is induced by CD8+ lymphocyte depletion but does not account for accelerated SIV pathogenesis. *J Exp Med* 2009;206(7):1575–1588.

176. Brenchley JM, Price DA, Douek DC. HIV disease: fallout from a mucosal catastrophe?. *Nat Immunol* 2006;7(3):235–239.

177. Favre D et al. Critical Loss of the Balance between Th17 and T Regulatory Cell Populations in Pathogenic SIV Infection. *PLoS Pathogens* 2009;5(2):e1000295.

178. Brenchley JM et al. Differential Th17 CD4 T-cell depletion in pathogenic and nonpathogenic lentiviral infections. *Blood* 2008;112(7):2826–2835.

179. Xu H, Wang X, Veazey RS. Th17 Cells Coordinate with Th22 Cells in Maintaining Homeostasis of Intestinal Tissues and both are Depleted in SIV-Infected Macaques. *J AIDS Clin Res* 2014;5(5). doi:10.4172/2155-6113.1000302

180. Wijewardana V et al. Kinetics of Myeloid Dendritic Cell Trafficking and Activation: Impact on Progressive, Nonprogressive and Controlled SIV Infections. *PLoS Pathogens* 2013;9(10):e1003600.

181. Barratt-Boyes SM, Wijewardana V. A divergent myeloid dendritic cell response at virus set-point predicts disease outcome in SIV-infected rhesus macaques. *J Med Primatol* 2011;40(4):206–213.

182. Wang X et al. Profound loss of intestinal Tregs in acutely SIV-infected neonatal macaques. *J Leukoc Biol* 2015;97(2):391–400.

183. Vantourout P, Hayday A. Six-of-the-best: unique contributions of γδ T cells to immunology. *Nat Rev Immunol* 2013;13(2):88–100.

184. Kosub DA et al. Gamma/Delta T-Cell Functional Responses Differ after Pathogenic Human Immunodeficiency Virus and Nonpathogenic Simian Immunodeficiency Virus Infections. *J. Virol.* 2008;82(3):1155–1165.

185. Martini F et al. Acute Human Immunodeficiency Virus Replication Causes a Rapid and Persistent Impairment of Vγ9Vδ2 T Cells in Chronically Infected Patients Undergoing Structured Treatment Interruption. *J Infect Dis.* 2002;186(6):847–850.

186. Poggi A et al. Migration of Vδ1 and Vδ2 T cells in response to CXCR3 and CXCR4 ligands in healthy donors and HIV-1–infected patients: competition by HIV-1 Tat. *Blood* 2004;103(6):2205–2213.

187. Gaufin T et al. Effect of B-Cell Depletion on Viral Replication and Clinical Outcome of Simian Immunodeficiency Virus Infection in a Natural Host. *J. Virol.* 2009;83(20):10347–10357.

188. Gicheru MM et al. Neutralizing antibody responses in Africa green monkeys naturally infected with simian immunodeficiency virus (SIVagm). *Journal of Medical Primatology* 1999;28(3):97–104.

189. Hirsch VM. What can natural infection of African monkeys with simian immunodeficiency virus tell us about the pathogenesis of AIDS?. *AIDS Rev* 2004;6(1):40–53.

190. Mohan M et al. Focused Examination of the Intestinal Epithelium Reveals Transcriptional Signatures Consistent with Disturbances in Enterocyte Maturation and Differentiation during the Course of SIV Infection [Internet]. *PLoS One* 2013;8(4). doi:10.1371/journal.pone.0060122

191. Brenchley JM et al. Microbial translocation is a cause of systemic immune activation in chronic HIV infection. *Nat Med* 2006;12(12):1365–1371.

192. Brenchley JM, Douek DC. Microbial Translocation Across the GI Tract. *Annu Rev Immunol* 2012;30:149–173.

193. Pandrea I et al. Cutting Edge: Experimentally Induced Immune Activation in Natural Hosts of Simian Immunodeficiency Virus Induces Significant Increases in Viral Replication and CD4+ T Cell Depletion. *J Immunol* 2008;181(10):6687–6691.

194. Pandrea I et al. Coagulation biomarkers predict disease progression in SIV-infected nonhuman primates. *Blood* 2012;120(7):1357–1366.

195. Hao XP et al. Experimental colitis in SIV-uninfected rhesus macaques recapitulates important features of pathogenic SIV infection. *Nat Commun* 2015;6:8020.

196. Kristoff J et al. Early microbial translocation blockade reduces SIV-mediated inflammation and viral replication. *J Clin Invest* 2014;124(6):2802–2806.

197. Cumont M-C et al. Early Divergence in Lymphoid Tissue Apoptosis between Pathogenic and Nonpathogenic Simian Immunodeficiency Virus Infections of Nonhuman Primates. *Journal of Virology* 2008;82(3):1175–1184.

198. Estaquier J et al. Programmed cell death and AIDS: significance of T-cell apoptosis in pathogenic and nonpathogenic primate lentiviral infections.. *Proc Natl Acad Sci U S A* 1994;91(20):9431–9435.

199. Hurtrel B et al. Apoptosis in SIV infection. *Cell Death Differ* 2005;12(S1):979–990.

200. Meythaler M et al. Differential CD4+ T-Lymphocyte Apoptosis and Bystander T-Cell Activation in Rhesus Macaques and Sooty Mangabeys during Acute Simian Immunodeficiency Virus Infection. *J. Virol.* 2009;83(2):572–583.

201. Mandl JN et al. Divergent TLR7 and TLR9 signaling and type I interferon production distinguish pathogenic and nonpathogenic AIDS virus infections. *Nat Med* 2008;14(10):1077–1087.

202. Diop OM et al. Plasmacytoid Dendritic Cell Dynamics and Alpha Interferon Production during Simian Immunodeficiency Virus Infection with a Nonpathogenic Outcome. *Journal of Virology* 2008;82(11):5145–5152.

203. Hirao LA et al. Early Mucosal Sensing of SIV Infection by Paneth Cells Induces IL-1β Production and Initiates Gut Epithelial Disruption [Internet]. *PLoS Pathog* 2014;10(8). doi:10.1371/journal.ppat.1004311

204. Lu W et al. Virus-Host Mucosal Interactions During Early SIV Rectal Transmission. *Virology* 2014;464–465:406–414.

205. Pan D et al. Lack of Interleukin-10-Mediated Anti-Inflammatory Signals and Upregulated Interferon Gamma Production Are Linked to Increased Intestinal Epithelial Cell Apoptosis in Pathogenic Simian Immunodeficiency Virus Infection. *J. Virol.* 2014;88(22):13015–13028.

206. Miller CJ, Abel K. Immune mechanisms associated with protection from vaginal SIV challenge in rhesus monkeys infected with virulence-attenuated SHIV 89.6. *Journal of Medical Primatology* 2005;34(5–6):271–281.

207. Reynolds MR et al. CD8+ T-Lymphocyte Response to Major Immunodominant Epitopes after Vaginal Exposure to Simian Immunodeficiency Virus: Too Late and Too Little. *Journal of Virology* 2005;79(14):9228–9235.

208. Weiler AM et al. Genital Ulcers Facilitate Rapid Viral Entry and Dissemination following Intravaginal Inoculation with Cell-Associated Simian Immunodeficiency Virus SIVmac239. *Journal of Virology* 2008;82(8):4154–4158.

209. Henning TR, McNicholl JM, Vishwanathan SA, Kersh EN. Macaque models of enhanced susceptibility to HIV [Internet]. *Virol J* 2015;12. doi:10.1186/s12985-015-0320-6

210. Li Q et al. Glycerol monolaurate prevents mucosal SIV transmission. *Nature* 2009;458(7241):1034–1038.

211. Wang Y et al. The Toll-Like Receptor 7 (TLR7) Agonist, Imiquimod, and the TLR9 Agonist, CpG ODN, Induce Antiviral Cytokines and Chemokines but Do Not Prevent Vaginal Transmission of Simian Immunodeficiency Virus When Applied Intravaginally to Rhesus Macaques. *Journal of Virology* 2005;79(22):14355–14370.

212. Ribeiro Dos Santos P et al. Rapid dissemination of SIV follows multisite entry after rectal inoculation. *PLoS ONE* 2011;6(5):e19493.

213. Smedley J et al. Tracking the Luminal Exposure and Lymphatic Drainage Pathways of Intravaginal and Intrarectal Inocula Used in Nonhuman Primate Models of HIV Transmission. *PLOS ONE* 2014;9(3):e92830.

214. Keele BF, Estes JD. Barriers to mucosal transmission of immunodeficiency viruses. *Blood* 2011;118(4):839–846.

215. Salazar-Gonzalez JF et al. Genetic identity, biological phenotype, and evolutionary pathways of transmitted/founder viruses in acute and early HIV-1 infection. *Journal of Experimental Medicine* 2009;206(6):1273–1289.

216. Gnanadurai CW et al. Genetic Identity and Biological Phenotype of a Transmitted/Founder Virus Representative of Nonpathogenic Simian Immunodeficiency Virus Infection in African Green Monkeys. *Journal of Virology* 2010;84(23):12245–12254.

217. Pandrea I et al. Simian immunodeficiency virus SIVagm.sab infection of Caribbean African green monkeys: a new model for the study of SIV pathogenesis in natural hosts. *J. Virol.* 2006;80(10):4858–4867.

218. National Research Council (US) Committee for the Update of the Guide for the Care and Use of Laboratory Animals. *Guide for the Care and Use of Laboratory Animals [Internet]*. Washington (DC): National Academies Press (US); 2011:

219. Regulations AW. Animal Welfare Act2013;

220. Sir David Weatherall Working Group. The Weatherall report on the use of non-human primates in research. A working group report chaired by Sir David Weatherall FRS FMedSci [Internet]2006;https://royalsociety.org/topics-policy/publications/2006/weatherall-report/. cited February 12, 2018

221. Aarnink A et al. MHC polymorphism in Caribbean African green monkeys. *Immunogenetics* 2014;66(6):353–360.

222. Ma Z-M et al. High Specific Infectivity of Plasma Virus from the Pre-Ramp-Up and Ramp-Up Stages of Acute Simian Immunodeficiency Virus Infection. *J. Virol.* 2009;83(7):3288–3297.

223. He T et al. Critical Role for the Adenosine Pathway in Controlling Simian Immunodeficiency Virus-Related Immune Activation and Inflammation in Gut Mucosal Tissues. *J. Virol.* 2015;89(18):9616–9630.

224. Ma D et al. Simian Immunodeficiency Virus SIVsab Infection of Rhesus Macaques as a Model of Complete Immunological Suppression with Persistent Reservoirs of Replication-Competent Virus: Implications for Cure Research. *J Virol* 2015;89(11):6155–6160.

225. Policicchio BB et al. Multi-dose Romidepsin Reactivates Replication Competent SIV in Post-antiretroviral Rhesus Macaque Controllers. *PLOS Pathogens* 2016;12(9):e1005879.

226. Hilldorfer BB, Cillo AR, Besson GJ, Bedison MA, Mellors JW. New Tools for Quantifying HIV-1 Reservoirs: Plasma RNA Single Copy Assays and Beyond. *Curr HIV/AIDS Rep* 2012;9(1):91–100.

227. Ma Z-M et al. SIVmac251 Is Inefficiently Transmitted to Rhesus Macaques by Penile Inoculation with a Single SIVenv Variant Found in Ramp-up Phase Plasma. *AIDS Res Hum Retroviruses* 2011;27(12):1259–1269.

228. Lopker MJ et al. Derivation and Characterization of Pathogenic Transmitted/Founder Molecular Clones from Simian Immunodeficiency Virus SIVsmE660 and SIVmac251 following Mucosal Infection. *J. Virol.* 2016;90(19):8435–8453.

229. Wang F et al. RNAscope: A Novel in Situ RNA Analysis Platform for Formalin-Fixed, Paraffin-Embedded Tissues. *The Journal of Molecular Diagnostics* 2012;14(1):22–29.

230. Micci L et al. CD4 Depletion in SIV-Infected Macaques Results in Macrophage and Microglia Infection with Rapid Turnover of Infected Cells. *PLOS Pathogens* 2014;10(10):e1004467.

231. Mandy FF, Nicholson JKA, McDougal JS, CDC. Guidelines for performing single-platform absolute CD4+ T-cell determinations with CD45 gating for persons infected with human immunodeficiency virus. Centers for Disease Control and Prevention. *MMWR Recomm Rep* 2003;52(RR-2):1–13.

232. Liu J et al. Comparative Analysis of Immune Activation Markers of CD8+ T Cells in Lymph Nodes of Different Origins in SIV-Infected Chinese Rhesus Macaques [Internet]. *Front. Immunol.* 2016;7. doi:10.3389/fimmu.2016.00371

233. Canestri A et al. Discordance Between Cerebral Spinal Fluid and Plasma HIV Replication in Patients with Neurological Symptoms Who Are Receiving Suppressive Antiretroviral Therapy. *Clin Infect Dis* 2010;50(5):773–778.

234. Zink MC et al. High Viral Load in the Cerebrospinal Fluid and Brain Correlates with Severity of Simian Immunodeficiency Virus Encephalitis. *J Virol* 1999;73(12):10480–10488.

235. Bissel SJ et al. Cerebrospinal Fluid Biomarkers of Simian Immunodeficiency Virus Encephalitis. *J Neuroimmune Pharmacol* 2016;11(2):332–347.

236. Sui Y et al. Early SIV Dissemination After Intrarectal SIVmac251 Challenge Was Associated With Proliferating Virus-Susceptible Cells in the Colorectum:. *JAIDS Journal of Acquired Immune Deficiency Syndromes* 2016;71(4):353–358.

237. Milush JM et al. Rapid dissemination of SIV following oral inoculation. *AIDS* 2004;18(18):2371–2380.

238. Miller CJ et al. Propagation and Dissemination of Infection after Vaginal Transmission of Simian Immunodeficiency Virus. *J. Virol.* 2005;79(14):9217–9227.

239. Liovat A-S, Jacquelin B, Ploquin MJ, Barré-Sinoussi F, Muller-Trutwin MC. African non human primates infected by SIV-why don't they get sick? Lessons from studies on the early phase of non-pathogenic SIV infection. *Current HIV research* 2009;7(1):39–50.

240. Duncan CJA, Sattentau QJ. Viral Determinants of HIV-1 Macrophage Tropism. *Viruses* 2011;3(11):2255–2279.

241. Isaacman-Beck J et al. Heterosexual Transmission of Human Immunodeficiency Virus Type 1 Subtype C: Macrophage Tropism, Alternative Coreceptor Use, and the Molecular Anatomy of CCR5 Utilization. *Journal of Virology* 2009;83(16):8208–8220.

242. Picker LJ, Hansen SG, Lifson JD. New paradigms for HIV/AIDS vaccine development. *Annu. Rev. Med.* 2012;63:95–111.

243. Holznagel E, Norley S, Holzammer S, Coulibaly C, Kurth R. Immunological changes in simian immunodeficiency virus (SIVagm)-infected African green monkeys (AGM): expanded cytotoxic T lymphocyte, natural killer and B cell subsets in the natural host of SIVagm. *Journal of General Virology* 2002;83(3):631–640.

244. Mir KD, Gasper MA, Sundaravaradan V, Sodora DL. SIV infection in natural hosts: Resolution of immune activation during the acute-to-chronic transition phase. *Microbes Infect* 2011;13(1):14–24.

245. Deeks SG, Tracy R, Douek DC. Systemic Effects of Inflammation on Health during Chronic HIV Infection. *Immunity* 2013;39(4):633–645.

246. Somsouk M et al. Gut epithelial barrier and systemic inflammation during chronic HIV infection. *AIDS* 2015;29(1):43–51.

247. Kuller LH et al. Inflammatory and Coagulation Biomarkers and Mortality in Patients with HIV Infection. *PLOS Medicine* 2008;5(10):e203.

248. Jacquelin B et al. Innate Immune Responses and Rapid Control of Inflammation in African Green Monkeys Treated or Not with Interferon-Alpha during Primary SIVagm Infection. *PLOS Pathogens* 2014;10(7):e1004241.

249. Ericsen AJ et al. Microbial Translocation and Inflammation Occur in Hyperacute Immunodeficiency Virus Infection and Compromise Host Control of Virus Replication. *PLOS Pathogens* 2016;12(12):e1006048.

250. Estes JD et al. Damaged Intestinal Epithelial Integrity Linked to Microbial Translocation in Pathogenic Simian Immunodeficiency Virus Infections [Internet]. *PLoS Pathog* 2010;6(8). doi:10.1371/journal.ppat.1001052

251. Gordon SN et al. Disruption of Intestinal CD4+ T Cell Homeostasis Is a Key Marker of Systemic CD4+ T Cell Activation in HIV-Infected Individuals. *The Journal of Immunology* 2010;185(9):5169–5179.

252. Cassol E et al. Persistent Microbial Translocation and Immune Activation in HIV-1-Infected South Africans Receiving Combination Antiretroviral Therapy. *J Infect Dis* 2010;202(5):723–733.

253. Gandhi RT et al. Levels of HIV-1 persistence on antiretroviral therapy are not associated with markers of inflammation or activation. *PLOS Pathogens* 2017;13(4):e1006285.

254. Klatt NR, Funderburg NT, Brenchley JM. Microbial translocation, immune activation and HIV disease. *Trends Microbiol* 2013;21(1):6–13.

255. Marchetti G, Tincati C, Silvestri G. Microbial Translocation in the Pathogenesis of HIV Infection and AIDS. *Clinical Microbiology Reviews* 2013;26(1):2–18.

256. Pandrea I et al. Using the Pathogenic and Nonpathogenic Nonhuman Primate Model for Studying Non-AIDS Comorbidities. *Curr HIV/AIDS Rep* 2015;12(1):54–67.

257. Pandrea I et al. Antibiotic and Antiinflammatory Therapy Transiently Reduces Inflammation and Hypercoagulation in Acutely SIV-Infected Pigtailed Macaques. *PLOS Pathogens* 2016;12(1):e1005384.

258. Thuijls G et al. Non-invasive markers for early diagnosis and determination of the severity of necrotizing enterocolitis. *Ann. Surg.* 2010;251(6):1174–1180.

259. Halfon P et al. Accuracy of hyaluronic acid level for predicting liver fibrosis stages in patients with hepatitis C virus. *Comp Hepatol* 2005;4:6.

260. Pandrea I et al. Functional Cure of SIVagm Infection in Rhesus Macaques Results in Complete Recovery of CD4+ T Cells and Is Reverted by CD8+ Cell Depletion. *PLoS Pathogens* 2011;7(8):e1002170.

261. Estes JD et al. Antifibrotic Therapy in Simian Immunodeficiency Virus Infection Preserves CD4+ T-Cell Populations and Improves Immune Reconstitution With Antiretroviral Therapy. *J Infect Dis* 2015;211(5):744–754.

262. Schindelin J et al. Fiji: an open-source platform for biological-image analysis. *Nature Methods* 2012;9(7):676–682.

263. Preibisch S, Saalfeld S, Tomancak P. Globally optimal stitching of tiled 3D microscopic image acquisitions. *Bioinformatics* 2009;25(11):1463–1465.

264. Rueden CT et al. ImageJ2: ImageJ for the next generation of scientific image data. *BMC Bioinformatics* 2017;18:529.

265. Fredrik Barrenas et al. African Green Monkeys Control SIV Pathogenesis Through Macorphage Associated Wound Healing. *Nature Communications* 2019;In revision.

266. Brocca-Cofano E et al. Pathogenic Correlates of Simian Immunodeficiency Virus-Associated B Cell Dysfunction. *J. Virol.* 2017;91(23):e01051-17.

267. Lane BR et al. The C-X-C chemokine IP-10 stimulates HIV-1 replication. *Virology* 2003;307(1):122–134.

268. Mandell DT et al. Pathogenic Features Associated with Increased Virulence upon Simian Immunodeficiency Virus Cross-Species Transmission from Natural Hosts. *J. Virol.* 2014;88(12):6778–6792.

269. Giavedoni LD, Velasquillo MC, Parodi LM, Hubbard GB, Hodara VL. Cytokine Expression, Natural Killer Cell Activation, and Phenotypic Changes in Lymphoid Cells from Rhesus Macaques during Acute Infection with Pathogenic Simian Immunodeficiency Virus. *J Virol* 2000;74(4):1648–1657.

270. Klatt NR et al. Compromised gastrointestinal integrity in pigtail macaques is associated with increased microbial translocation, immune activation, and IL-17 production in the absence of SIV infection. *Mucosal Immunol* 2010;3(4):387–398.

271. Sandler NG, Douek DC. Microbial translocation in HIV infection: causes, consequences and treatment opportunities. *Nature Reviews Microbiology* 2012;10(9):655–666.

272. Klebanoff SJ. Myeloperoxidase: friend and foe. *Journal of Leukocyte Biology* 2005;77(5):598–625.

273. Sandler NG et al. Type I interferon responses in rhesus macaques prevent SIV infection and slow disease progression. *Nature* 2014;511(7511):601–605.

274. Verhelst J, Hulpiau P, Saelens X. Mx Proteins: Antiviral Gatekeepers That Restrain the Uninvited. *Microbiol. Mol. Biol. Rev.* 2013;77(4):551–566.

275. Mitson-Salazar A et al. Hematopoietic prostaglandin D synthase defines a proeosinophilic pathogenic effector human TH2 cell subpopulation with enhanced function. *Journal of Allergy and Clinical Immunology* 2016;137(3):907-918.e9.

276. Fukata M et al. The Myeloid Differentiation Factor 88 (MyD88) Is Required for CD4+ T Cell Effector Function in a Murine Model of Inflammatory Bowel Disease. *The Journal of Immunology* 2008;180(3):1886–1894.

277. Huebener P, Schwabe RF. Regulation of Wound Healing and Organ Fibrosis by Toll-like Receptors [Internet]. *Biochim Biophys Acta* 2013;1832(7). doi:10.1016/j.bbadis.2012.11.017

278. Macedo L et al. Wound Healing Is Impaired in MyD88-Deficient Mice. *Am J Pathol* 2007;171(6):1774–1788.

279. Meier M, Tokarz J, Haller F, Mindnich R, Adamski J. Human and zebrafish hydroxysteroid dehydrogenase like 1 (HSDL1) proteins are inactive enzymes but conserved among species. *Chem. Biol. Interact.* 2009;178(1–3):197–205.

280. Lasarte JJ et al. The Extra Domain A from Fibronectin Targets Antigens to TLR4-Expressing Cells and Induces Cytotoxic T Cell Responses In Vivo. *The Journal of Immunology* 2007;178(2):748–756.

281. Oshima H et al. Stat3 is indispensable for damage-induced crypt regeneration but not for Wnt-driven intestinal tumorigenesis. *The FASEB Journal* 2018;33(2):1873–1886.

282. Pickert G et al. STAT3 links IL-22 signaling in intestinal epithelial cells to mucosal wound healing. *Journal of Experimental Medicine* 2009;206(7):1465–1472.

283. Willson TA, Jurickova I, Collins M, Denson LA. Deletion of Intestinal Epithelial Cell STAT3 Promotes T Lymphocyte STAT3 Activation and Chronic Colitis Following Acute Dextran Sodium Sulfate Injury in Mice. *Inflamm Bowel Dis* 2013;19(3):512–525.

284. Reynolds JM et al. Interleukin-17B antagonizes interleukin-25-mediated mucosal inflammation. *Immunity* 2015;42(4):692–703.

285. Estes J et al. Collagen Deposition Limits Immune Reconstitution in the Gut. *J Infect Dis* 2008;198(4):456–464.

286. Li Q et al. Simian Immunodeficiency Virus—Induced Intestinal Cell Apoptosis Is the Underlying Mechanism of the Regenerative Enteropathy of Early Infection. *J Infect Dis* 2008;197(3):420–429.

287. Rieder F, Fiocchi C. Intestinal fibrosis in inflammatory bowel disease — Current knowledge and future perspectives. *Journal of Crohn's and Colitis* 2008;2(4):279–290.

288. Yuan B et al. Changes in the Expression and Distribution of Claudins, Increased Epithelial Apoptosis, and a Mannan-Binding Lectin-Associated Immune Response Lead to Barrier Dysfunction in Dextran Sodium Sulfate-Induced Rat Colitis. *Gut Liver* 2015;9(6):734–740.

289. Ghavami S et al. Apoptosis and cancer: mutations within caspase genes. *Journal of Medical Genetics* 2009;46(8):497–510.

290. Lu Z, Ding L, Lu Q, Chen Y-H. Claudins in intestines [Internet]. *Tissue Barriers* 2013;1(3). doi:10.4161/tisb.24978

291. Funaoka H, Kanda T, Fujii H. [Intestinal fatty acid-binding protein (I-FABP) as a new biomarker for intestinal diseases]. *Rinsho Byori* 2010;58(2):162–168.

292. Estes JD. Pathobiology of HIV/SIV-Associated Changes in Secondary Lymphoid Tissues. *Immunol Rev* 2013;254(1):65–77.

293. Alexander C, Rietschel ET. Bacterial lipopolysaccharides and innate immunity. *J. Endotoxin Res.* 2001;7(3):167–202.

294. Apetrei C et al. Pattern of SIVagm Infection in Patas Monkeys Suggests that Host Adaptation to SIV Infection May Result in Resistance to Infection and Virus Extinction. *J Infect Dis* 2010;202(S3):S371–S376.

295. Raehtz K, Pandrea I, Apetrei C. The well-tempered SIV infection: Pathogenesis of SIV infection in natural hosts in the wild, with emphasis on virus transmission and early events post-infection that may contribute to protection from disease progression. *Infection, Genetics and Evolution* 2016;46:308–323.

296. Sodora DL et al. Toward an AIDS vaccine: lessons from natural simian immunodeficiency virus infections of African nonhuman primate hosts. *Nat Med* 2009;15(8):861–865.

297. Mudd JC, Brenchley JM. Gut Mucosal Barrier Dysfunction, Microbial Dysbiosis, and Their Role in HIV-1 Disease Progression. *J Infect Dis* 2016;214(suppl_2):S58–S66.

298. Wéra O, Lancellotti P, Oury C. The Dual Role of Neutrophils in Inflammatory Bowel Diseases [Internet]. *J Clin Med* 2016;5(12). doi:10.3390/jcm5120118

299. Deleage C et al. Impact of early cART in the gut during acute HIV infection [Internet]. *JCI Insight* 2016;1(10). doi:10.1172/jci.insight.87065

300. Brazil JC, Parkos CA. Pathobiology of neutrophil-epithelial interactions. *Immunol Rev* 2016;273(1):94–111.

301. Wang J. Neutrophils in tissue injury and repair. *Cell Tissue Res* 2018;371(3):531–539.

302. Canary LA et al. Rate of AIDS Progression Is Associated with Gastrointestinal Dysfunction in Simian Immunodeficiency Virus–Infected Pigtail Macaques. *The Journal of Immunology* 2013;190(6):2959–2965.

303. Barrenas F et al. Deep Transcriptional Sequencing of Mucosal Challenge Compartment from Rhesus Macaques Acutely Infected with Simian Immunodeficiency Virus Implicates Loss of Cell Adhesion Preceding Immune Activation. *J. Virol.* 2014;88(14):7962–7972.

304. M Asmuth D et al. Role of Intestinal Myofibroblasts in HIV-Associated Intestinal Collagen Deposition and Immune Reconstitution following Combination Antiretroviral Therapy. *AIDS (London, England)* 2015;29. doi:10.1097/QAD.0000000000000636

305. Estes JD et al. Simian Immunodeficiency virus-Induced Lymphatic Tissue Fibrosis Is Mediated by Transforming Growth Factor β1-positive Regulatory T Cells and Begins in Early Infection. *J Infect Dis* 2007;195(4):551–561.

306. Zeng M et al. Cumulative mechanisms of lymphoid tissue fibrosis and T cell depletion in HIV-1 and SIV infections. *J Clin Invest* 2011;121(3):998–1008.

307. Smythies LE et al. Human intestinal macrophages display profound inflammatory anergy despite avid phagocytic and bacteriocidal activity. *J Clin Invest* 2005;115(1):66–75.

308. Ueda Y et al. Commensal microbiota induce LPS hyporesponsiveness in colonic macrophages via the production of IL-10. *Int Immunol* 2010;22(12):953–962.

309. Palesch D et al. Sooty mangabey genome sequence provides insight into AIDS resistance in a natural SIV host. *Nature* 2018;553(7686):77–81.

310. Choudhary SK et al. Low Immune Activation despite High Levels of Pathogenic Human Immunodeficiency Virus Type 1 Results in Long-Term Asymptomatic Disease. *J. Virol.* 2007;81(16):8838–8842.

311. Klatt NR et al. Limited HIV Infection of Central Memory and Stem Cell Memory CD4+ T Cells Is Associated with Lack of Progression in Viremic Individuals. *PLOS Pathogens* 2014;10(8):e1004345.

312. Hazenberg MD et al. Persistent immune activation in HIV-1 infection is associated with progression to AIDS. *AIDS* 2003;17(13):1881–1888.

313. Riddick NE et al. A Novel CCR5 Mutation Common in Sooty Mangabeys Reveals SIVsmm Infection of CCR5-Null Natural Hosts and Efficient Alternative Coreceptor Use In Vivo. *PLOS Pathog* 2010;6(8):e1001064.

314. Barouch DH et al. Rapid Inflammasome Activation following Mucosal SIV Infection of Rhesus Monkeys. *Cell* 2016;165(3):656–667.

315. Langfelder P, Horvath S. WGCNA: an R package for weighted correlation network analysis. *BMC Bioinformatics* 2008;9(1):559.

316. Pesquita C et al. Metrics for GO based protein semantic similarity: a systematic evaluation. *BMC Bioinformatics* 2008;9(5):S4.

317. Clauset A, Newman MEJ, Moore C. Finding community structure in very large networks. *Phys. Rev. E* 2004;70(6):066111.

318. Sivanandham R et al. Neutrophil extracellular trap production contributes to pathogenesis in SIV-infected nonhuman primates. *J Clin Invest* 128(11):5178–5183.

319. Leoni G, Neumann P-A, Sumagin R, Denning TL, Nusrat A. Wound repair: role of immune-epithelial interactions. *Mucosal Immunol* 2015;8(5):959–968.

320. Park JE, Barbul A. Understanding the role of immune regulation in wound healing. *Am. J. Surg.* 2004;187(5A):11S-16S.

321. Ank N et al. Lambda interferon (IFN-lambda), a type III IFN, is induced by viruses and IFNs and displays potent antiviral activity against select virus infections in vivo. *J. Virol.* 2006;80(9):4501–4509.

322. Parra A et al. Decreased dopaminergic tone and increased basal bioactive prolactin in men with human immunodeficiency virus infection. *Clin. Endocrinol. (Oxf)* 2001;54(6):731–738.

323. Hillyer P et al. Expression profiles of human interferon-alpha and interferon-lambda subtypes are ligand- and cell-dependent. *Immunol. Cell Biol.* 2012;90(8):774–783.

324. Hou W et al. Lambda Interferon Inhibits Human Immunodeficiency Virus Type 1 Infection of Macrophages. *J Virol* 2009;83(8):3834–3842.

325. Denis J-F, Lévesque M, Tran SD, Camarda A-J, Roy S. Axolotl as a Model to Study Scarless Wound Healing in Vertebrates: Role of the Transforming Growth Factor Beta Signaling Pathway. *Adv Wound Care (New Rochelle)* 2013;2(5):250–260.

326. Seifert AW, Monaghan JR, Voss SR, Maden M. Skin Regeneration in Adult Axolotls: A Blueprint for Scar-Free Healing in Vertebrates. *PLOS ONE* 2012;7(4):e32875.

327. Witte MB, Barbul A. General principles of wound healing. *Surg. Clin. North Am.* 1997;77(3):509–528.

328. Ritenour AM, Dickie R. Inhibition of Vascular Endothelial Growth Factor Receptor Decreases Regenerative Angiogenesis in Axolotls. *Anat Rec (Hoboken)* 2017;300(12):2273–2280.

329. Lévesque M, Villiard E, Roy S. Skin wound healing in axolotls: a scarless process. *J. Exp. Zool. B Mol. Dev. Evol.* 2010;314(8):684–697.

330. Krämer A, Green J, Pollard J, Tugendreich S. Causal analysis approaches in Ingenuity Pathway Analysis. *Bioinformatics* 2014;30(4):523–530.

331. Okizaki S et al. Suppressed recruitment of alternatively activated macrophages reduces TGF-β1 and impairs wound healing in streptozotocin-induced diabetic mice. *Biomed. Pharmacother.* 2015;70:317–325.

332. Godwin JW, Pinto AR, Rosenthal NA. Macrophages are required for adult salamander limb regeneration. *Proc. Natl. Acad. Sci. U.S.A.* 2013;110(23):9415–9420.

333. Lévesque M et al. Transforming growth factor: beta signaling is essential for limb regeneration in axolotls. *PLoS ONE* 2007;2(11):e1227.

334. Chen L, Klass C, Woods A. Syndecan-2 regulates transforming growth factor-beta signaling. *J. Biol. Chem.* 2004;279(16):15715–15718.

335. Kawakami Y et al. Wnt/β-catenin signaling regulates vertebrate limb regeneration. *Genes Dev* 2006;20(23):3232–3237.

336. Ramani AK et al. A map of human protein interactions derived from co-expression of human mRNAs and their orthologs. *Mol. Syst. Biol.* 2008;4:180.

337. Soares MP, Teixeira L, Moita LF. Disease tolerance and immunity in host protection against infection. *Nat. Rev. Immunol.* 2017;17(2):83–96.

338. Svardal H et al. Ancient hybridization and strong adaptation to viruses across African vervet monkey populations. *Nature Genetics* 2017;49(12):1705–1713.

339. Neufeld DA, Day FA, Settles HE. Stabilizing role of the basement membrane and dermal fibers during newt limb regeneration. *Anat. Rec.* 1996;245(1):122–127.

340. Yurchenco PD, Patton BL. Developmental and pathogenic mechanisms of basement membrane assembly. *Curr. Pharm. Des.* 2009;15(12):1277–1294.

341. Lee SSJ et al. Structure of the integrin binding fragment from fibrillin-1 gives new insights into microfibril organization. *Structure* 2004;12(4):717–729.

342. Lenselink EA. Role of fibronectin in normal wound healing. *International Wound Journal* 2015;12(3):313–316.

343. Christensen RN, Tassava RA. Apical epithelial cap morphology and fibronectin gene expression in regenerating axolotl limbs. *Dev. Dyn.* 2000;217(2):216–224.

344. Donaldson DJ, Mahan JT, Yang H, Yamada KM. Integrin and phosphotyrosine expression in normal and migrating newt keratinocytes. *Anat. Rec.* 1995;241(1):49–58.

345. Yin H et al. IL-33 accelerates cutaneous wound healing involved in upregulation of alternatively activated macrophages. *Mol. Immunol.* 2013;56(4):347–353.

346. Patel VP et al. Molecular and Functional Characterization of Two Novel Human C-C Chemokines as Inhibitors of Two Distinct Classes of Myeloid Progenitors. *J Exp Med* 1997;185(7):1163–1172.

347. Chevalier MF et al. The Th17/Treg Ratio, IL-1RA and sCD14 Levels in Primary HIV Infection Predict the T-cell Activation Set Point in the Absence of Systemic Microbial Translocation. *PLOS Pathogens* 2013;9(6):e1003453.

348. Rollenhagen C, Asin SN. IL-8 Decreases HIV-1 Transcription in Peripheral Blood Lymphocytes and Ectocervical Tissue Explants:. *JAIDS Journal of Acquired Immune Deficiency Syndromes* 2010;54(5):463–469.

349. Lane BR et al. Interleukin-8 Stimulates Human Immunodeficiency Virus Type 1 Replication and Is a Potential New Target for Antiretroviral Therapy. *J. Virol.* 2001;75(17):8195–8202.

350. Ploquin MJ et al. Elevated Basal Pre-infection CXCL10 in Plasma and in the Small Intestine after Infection Are Associated with More Rapid HIV/SIV Disease Onset. *PLOS Pathogens* 2016;12(8):e1005774.

351. Simmons RP et al. HIV-1 infection induces strong production of IP-10 through TLR7/9-dependent pathways. *AIDS* 2013;27(16):2505–2517.

352. Foley JF et al. Roles for CXC Chemokine Ligands 10 and 11 in Recruiting CD4+ T Cells to HIV-1-Infected Monocyte-Derived Macrophages, Dendritic Cells, and Lymph Nodes. *The Journal of Immunology* 2005;174(8):4892–4900.

353. Deshmane SL, Kremlev S, Amini S, Sawaya BE. Monocyte Chemoattractant Protein-1 (MCP-1): An Overview. *J Interferon Cytokine Res* 2009;29(6):313–326.

354. Delaloye J et al. Increased macrophage migration inhibitory factor (MIF) plasma levels in acute HIV-1 infection. *Cytokine* 2012;60(2):338–340.

355. Regis EG et al. Elevated levels of Macrophage Migration Inhibitory Factor (MIF) in the plasma of HIV-1-infected patients and in HIV-1-infected cell cultures: a relevant role on viral replication. *Virology* 2010;399(1):31–38.

356. Cocchi F et al. Identification of RANTES, MIP-1α, and MIP-1β as the Major HIV-Suppressive Factors Produced by CD8+ T Cells. *Science* 1995;270(5243):1811–1815.

357. Moriuchi H, Moriuchi M, Combadiere C, Murphy PM, Fauci AS. CD8+ T-cell-derived soluble factor(s), but not β-chemokines RANTES, MIP-1α, and MIP-1β, suppress HIV-1 replication in monocyte/macrophages. *Proc Natl Acad Sci U S A* 1996;93(26):15341–15345.

358. Gonzalez-Andrades M et al. Establishment of a novel in vitro model of stratified epithelial wound healing with barrier function [Internet]. *Sci Rep* 2016;6. doi:10.1038/srep19395

359. Ley K. M1 Means Kill; M2 Means Heal. *The Journal of Immunology* 2017;199(7):2191–2193.

360. Rey-Giraud F, Hafner M, Ries CH. In Vitro Generation of Monocyte-Derived Macrophages under Serum-Free Conditions Improves Their Tumor Promoting Functions. *PLOS ONE* 2012;7(8):e42656.

361. Côté CH, Bouchard P, van Rooijen N, Marsolais D, Duchesne E. Monocyte depletion increases local proliferation of macrophage subsets after skeletal muscle injury. *BMC Musculoskeletal Disorders* 2013;14(1):359.

362. Fink K et al. Depletion of macrophages in mice results in higher dengue virus titers and highlights the role of macrophages for virus control. *European Journal of Immunology* 2009;39(10):2809–2821.

363. Burwitz BJ et al. Technical Advance: Liposomal alendronate depletes monocytes and macrophages in the nonhuman primate model of human disease. *J Leukoc Biol* 2014;96(3):491–501.

364. Wen T, Rothenberg ME. The Regulatory Function of Eosinophils [Internet]. *Microbiol Spectr* 2016;4(5). doi:10.1128/microbiolspec.MCHD-0020-2015

365. Lampinen M et al. Eosinophil granulocytes are activated during the remission phase of ulcerative colitis. *Gut* 2005;54(12):1714–1720.

366. Jia Daile et al. Interleukin-35 Promotes Macrophage Survival and Improves Wound Healing After Myocardial Infarction in Mice. *Circulation Research* 2019;124(9):1323–1336.

367. Zhong X et al. Baicalein Inhibits Dextran Sulfate Sodium-induced Mouse Colitis. *J Cancer Prev* 2019;24(2):129–138.

368. Mei Y et al. PAP-1 ameliorates DSS-induced colitis with involvement of NLRP3 inflammasome pathway. *Int. Immunopharmacol.* 2019;75:105776.

369. Fang W, Zhu S, Niu Z, Yin Y. The protective effect of syringic acid on dextran sulfate sodium-induced experimental colitis in BALB/c mice. *Drug Dev. Res.* [published online ahead of print: July 16, 2019]; doi:10.1002/ddr.21524

370. Zhai R et al. Strain-Specific Anti-inflammatory Properties of Two Akkermansia muciniphila Strains on Chronic Colitis in Mice. *Front Cell Infect Microbiol* 2019;9:239.

371. Tabb B et al. Reduced Inflammation and Lymphoid Tissue Immunopathology in Rhesus Macaques Receiving Anti–Tumor Necrosis Factor Treatment During Primary Simian Immunodeficiency Virus Infection. *J Infect Dis* 2013;207(6):880–892.